INTRODUCTION

1.1 General Concepts

A prerequisite for safe and stable operation of an electric power system is the accurate and reliable measurement of the system parameters, in particular, current and voltage. Conventionally, currents and voltages in power plants and substations are measured using instrument transformers (ITs) which are classified into inductive-type current transformers (CTs) and electromagnetic induction-type voltage transformers (VT) or capacitor voltage dividing-type voltage transformers (CVTs).

In a traditional protection system, ITs provide protective relays with a scaled-down replica of the power system currents and voltages. In this system, ITs interface relays through hardwired copper cabling. Besides transforming the signal energy levels between the protective or metering device connected to their secondary side and the power system current and voltage signals connected to their primary side, ITs also provide electric isolation. Furthermore, the magnetic coupling between their primary side and their secondary side may introduce signal distortions that are not present in the power network but are created within the transformer. Saturation of the CTs core is the main cause of distortions for CT.

Numerical relay are sensitive to distortions originated within the IT and could operate incorrectly under certain fault conditions. Conventional instrument transformers output consists of analog signals that are hardwired from the IT's location in the substation switchyard to the relay's location in the substation's control room. Therefore, two complicated problems originate from this traditional protection system using conventional IT and numerical relay with an analog interface, one related to conventional IT design and characteristics and other related to the analog interface.

Research effort into viable alternatives to instrument transformers has been ongoing for many years to reduce the cost, improve the performance of power system protection, and accuracy of this device. This research has accelerated due to the new requirements of the modern metering and protection systems based on electronic and microprocessor devices. This trend in the modern systems has allowed the development of novel transducers where the accuracy, the reliability and the safety has been significantly improved [1].

Technical solutions based on Optical instrument transformer and Hybrid instrument transformer integrates the best advantage of the technology in power system. The optical current transformer and the optical voltage transformer are the optimum solutions proposed. However, mainly due to interface modifications there have been a limited number of industrial applications in power system.

The OFCTs offer electrical isolation, as there is no direct contact with the electrical conductor. The OFCTs possess higher dynamic range over large frequencies, exhibit more linear response with zero hysteresis when compared to the conventional CTs. The OFCTs are light and compact, and consumes very less power for their operation. Therefore, there is no chance of explosion and hence safe. The basic principal used in OFCT is the Faraday Effect. When a light guiding Faraday medium is placed in a magnetic field, which is produced by the current flowing in the conductor around the magnetic core, the plane of polarization of the linearly polarized light is rotated. The angle of rotation is proportional to the magnetic field strength, proportionality constant, and the interaction length. The proportionality constant is the Verdet constant (V) which is dependent on both temperature and wavelength of the light [2],[3],[4]. Opto-electrical methods are used to measure the angle of rotation of the polarization plane. By measuring the angle, the current flowing in the current carrying conductor can be calculated.

1.2 Motivation

The real time measurement of electric parameters is a fundamental requirement to fully characterize the energy flow in power grids and better understand its operation enabling the development of sustainable energy management systems. Instrument transformers in a high voltage environment can easily achieve magnetic saturation, damaged by heat, and short-circuits or atmospheric electrical discharges. Moreover, CIT accuracy is not constant in all operating range. Furthermore, these CIT have high dimensions and weight and cannot be suspended on the electric line. Therefore, in SMART power grid is necessary to improve the instrument transformers technology [5], [6].

The high growth in the optical fiber based technology led to material cost decrease of optical transducers components. These types of optical transducers are quite attractive and have been gaining great interest since they can be light, small, immune to

electromagnetic interference (EMI), presenting good performance in high voltage, having large bandwidth, high sensitivity, environmental ruggedness, and the ability for distributed sensing. Other important aspects are electrical passivity, not needing local electric power, and enabling the possibility of multiplexing of a large number of sensing elements [5].

Optical Fiber transducer technology are maturing as a technology and offer a number of advantages over conventional instrument transformer regimes, including the possession of inherent electrical isolation, chemical inertness, immunity to EMI, and their small size and serial multiplexing capability.

In terms of implementation cost, the proposed sensing regimes are especially attractive for high-voltage applications owing to the inherent immunity to EMI and reduced insulation requirements. Depending on the design of the OFCTs, several turns of fiber can be wound around the conductor to increase the signal to noise ratio of the OFCT. This gain in signal to noise ratio is traded with the ability of the OFCT to measure extremely high fault currents without fringe management algorithms. However, advanced processing techniques such as fringe management techniques can be implemented in OFCTs, and high signal to noise ratios and high fault current measurements can be achieved simultaneously. Therefore, the optical current transformer and the optical voltage transformer are the optimum solutions proposed.

1.3 Objectives of the Research

The main goal of this thesis is to develop new optical fiber current transducers for metering and relaying in power system protection and monitoring.. The main specific and operational objectives of this research are:

- Design, development and characterization of new optical fiber current transformer (OFCT) configurations based on Faraday Effect, in optical fiber for detection of electrical current.
- Design an OFCT that has a good stability, accuracy and has a large dynamic range.
- Exploration of sensing mechanisms such as magneto-optic (Faraday Effect) and electro-optic (Pockel Effect) effects for the sensing head design.

- Development of strategies for interrogation of the developed optical fiber current transformers (OFCTs), including polarizmeteric, and interferometric based.
- Develop a mathematical model to simulate and analyze the optical fiber current transformer (OFCT) and Optical voltage transformer (OVT).
- Study steady state and transient performances of optical fiber current transformers.
- To provide comparisons between an integrated measurement and protection solution based on OFCTs and OVTs and the conventional CTs and VTs connected to the protective numerical relay.
- To compare between OFCTs and conventional CTs in terms of performance used in protection system under faults condition in non-linear region.

In order to verify the mathematical model experimental work are conducted.

1.4 Problem Statement

Current measurements are of fundamental importance in power system. These measurements are inputs to functions for relaying, metering, control and monitoring of power systems. While the conventional copper-wound iron core current transformers have performed on the whole quite well since the late 1800's, performance limitations and catastrophic explosive failures have provided an impetus towards using other methods. In recent years, it has been recognized that there are significant advantages to using optical methods for measuring electrical currents in applications such as high voltage power lines. The optical current measurements are typically done by means of the Faraday magneto-optic effect. Conventionally, a sequence of relays and circuit breakers (CBs) are deployed along power systems. When a fault occurs, the corresponding CTs and VTs send fault current and voltage information to relays at the substation. Based on the current and voltage information and pre-set rules, the relays will then command appropriate breakers to trip. Besides the difficulty of coordinating different protective devices in a large system, the saturation and hysteresis incurred in the CT response during a large surge in fault current is another major challenge faced by the conventional fault detection method. Most protective devices make operating decisions based on rms values of fault

currents. If the CT signal is distorted by saturation, its rms value will be much lower than the actual fault current. This can interfere the coordination among relays. When CT saturation is high, it can even prevent relays from tripping. In recent years, several new techniques like wavelet transform and statistical pattern recognition are also used to improve the fault detection. Recently, an optical fiber based current and voltage measuring system for high-voltage distribution lines has been proposed. The main objective is to develop optical fiber current transformer using Faraday Effect based fault detection and monitoring method that replaces the conventional CT. Conventional instrument transformers utilize an iron core and windings ratio to step down the current measured in the primary to a more manageable current level for secondary devices such as meters and relays. This signal may be distorted due to saturation of the magnetic core. This research discusses the characteristics of optical current transformers, specifically for relaying applications where measurement of fault-level currents is required and compares both steady state and transient performances of conventional magnetic with OFCT.

1.5Methodology

In order to achieve the research objectives the following methodology is used:

1. Optical Fiber Current Transformer Design

Modeling of optical fiber current transformer and simulate the model using MATLAB SIMULINK. The optimal performances of the components can be determined. The obtained results will be analyzed and evaluated.

2. Using OFCT based Fault Detection in Power System Protection model

Evaluate OFCT performance using various fault conditions. The significant surges in magnitude readings of these OFCTs corresponding to faults in certain phases will decide the type of the fault whereas the location of such optical will determine that the fault is towards the downstream line segment from where the OFCTs are installed.

3. SIMULATION

Simulations with the proposed fault detection method to detect and locate different types of faults under various system abnormalities in radial as well as networked systems are discussed. The case studies presented here use the steady state 50 Hz fault currents data generated by MATLAB/SIMULINK software and those fault data are

exported to MATLAB for further signal processing to simulate the reflected signal from an OFCT in case of of overcurrent protection scheme and the signal from an OVT and OFCT for fault detection and clearance procedure.

4. Experimental Investigation

The power system protection will be done experimentally using optical fiber current transformer and using conventional current transformer. The simulation results of the model can be compared with the experimental results. The power system performance will be investigated when the protection and monitoring system are provided with the optical fiber current transformer.

1.5 Thesis Structure

The thesis is organized in seven chapters covering analysis, simulation, and experimental aspects of OFCT used in power system protection.

Chapter two introduces the literature review about Optical Current Transformer and its application in power system monitoring and protection.

Chapter three introduces instrument transformers. Furthermore, it concentrates on the optical current transformer characteristics and configurations in the forms of a polarizometeric and Sagnac interferometer.

Chapter four presents the modeling details of different components of the optical fiber current transformer and numerical protective relay consideration used in the remainder of work. In addition, it presents the model of optical fiber current and optical voltage transformer to determine the performance characteristics including linearity, dynamic range, and frequency response characteristic.

Chapter five presents the simulation and results discussion characteristics of digital output of optical current transformer. In this chapter, power system using optical fiber current transformer model is used to demonstrate the performance of the proposed method in ensuring the accurate and secure operation of the numerical protective relay for different faults condition.

Chapter six describes the experimental work and the associated software and hardware implementation. In order to implement protective numerical relay technique experimentally the software and hardware are implemented on a practical test rig. The system components are described in detail.

Finally, the conclusions of key results are presented in Chapter seven. Future research directions in line with the work are also presented in this final chapter.

1.6 Author's Contributions

This thesis has made the following contributions to the field of numerical power system protection using optical fiber current transformer. The main contributions of this thesis are:

- Detailed view on OFCT accuracy measurement constrains in high voltage applications. Verify that Faraday Effect and Pockel Effect are better alternative for current and voltage measurement for power system protection and monitoring than Conventional instrument transformers.
- Evaluation of influence of instrument transformers on numerical protection system performance.
- Development of optical fiber current transformer model the simulation environment for automated and comprehensive evaluation of the performance Criteria.
- An evaluation of possible algorithms appropriate for OFCT signal processing and requirements on equipment and algorithms used for power system protection and fault detection.
- Criteria and methodology for performance evaluation of a numerical protection system, consisting of novel optical instrument transformers interfaced to numerical relays via an IEC 61850-9-2 digital process bus.
- Practical demonstration based on numerical protection example of how the use of the OFCT for current measurement can change today's practices in steady and transient state current measurement.
- Definition of standard high voltage network with OFCTs and OVTs that allows decoupling of measuring devices engineering aspects from protection and control engineering via process bus.

Chapter Two
Literature Review and Background Study

2.1 Introduction

This chapter details with relevant background and provides a literature review for the performance evaluation of optical instrument transformer used in power system protection. A brief review of the advantages and disadvantages of optical instrument transformer is presented. The literature review covers research related to optical current transformer configuration, sensing material, sensitivity of optical current transformer and frequency response of optical current transformer for power system protection and monitoring.

The literature presents numerous developments, design and testing of Optical Instrument Transformers that can be used for understanding and evaluating the performance of the system behaviors. Since the optical current transformers (OCTs) and optical voltage transformers (OVTs) are the two types of instrument transformers. This literature review explained each transformer separately dealing with the accuracy, transient behavior, bandwidth, comparison of the systems, and flexibility of digital and analog systems.

2.2 Current Measurement and Monitoring Application

The first studies on the optical current transformers (OCT) are published at the end of 1970s and during the 1980s. Those studies mainly concentrated on the feasible of optical transformers application in power system. Most of the studies focused on the development of a Faraday Effect-based low-voltage optical current sensor. In late 1980s and the early 1990s, researchers began to study the applications of optical current transformers in high voltage. Some researchers investigated the transient behaviors of OCTs. From the beginning of the 1990s until today, large numbers of studies dealt with the performance improvement of OCTs that are used for power system protection and monitoring. Different variations of the Faraday Effect and the effect of various environmental conditions are studied. At present, several different

OCTs have been developed and offered for applications in power system protection and monitoring.

Steer, et al [1] presented a comparison between OCTs and conventional CTs in their paper, which describes the design and test of an OCT. They also mention two broad categories of optical fibers that are available: multimode and single mode. Single mode is most appropriate for current sensors. The principle of OCT is the Faraday Effect; the change of polarization angle (azimuth) is proportional to the part of the magnetic field parallel to the propagation direction of the light. If the fiber forms a closed path around a conductor, the change of the polarization angle depends on the number of ampere-turns. Vibration or a change in temperature of the sensing fiber could affect the accuracy of readings [2].

In recent years, optical current and voltage transducers have reached a high degree of maturity and started to compete with conventional instrument transformers. Optical Fiber Transducers are ideally adapted to high voltage environments as they are immune to electromagnetic interference and there is no galvanic connection between the sensor head on high voltage and substation electronics. Many problems of their conventional counterparts are inexistent such as magnetic saturation or danger of catastrophic failure. The wide bandwidth of optical sensors is important for fast protection and power quality monitoring. Optical transducers can be easily installed on/or integrated into existing substation equipment such as circuit breakers or bushings resulting in significant space savings and reduced installation costs. Furthermore, there is no danger of a contamination of the environment due to loss of oil [3].

In the case of OCTs that use the Faraday Effect, a rotation in the angle of polarization of the light propagating in magneto-optic material is induced by an external magnetic field. A short explanation regarding the Faraday Effect, as well as the different interrogation techniques that can be used to interrogate the polarization rotation angle are presented. Then, two different groups of OCTs using this effect are analyzed. Silva et al. [4] study two different groups of optical current transformers using this effect (all fiber optic transformers and bulk optic based transformers). A key aspect of the concept of all fiber optic sensors is that the optical fiber acts both as the sensing element and communication channel, which allows for simple solutions and reduces

the losses in the fiber connections. By winding the optical fiber around the electric conductor, immunity to external currents or magnetic fields, as well as, tunable sensitivity can be easily achieved. As for bulk optic transducers, they usually present higher sensitivity and robustness, which are very important aspects in real applications. In both cases, saturation effects such as the ones that occur in ferromagnetic based transducers are avoided allowing higher measurement ranges.

Leung, et al [5] discussing the principle of the OCT which is to measure the magnetic field caused by a current using optical modulation and demodulation in accordance with the Faraday Effect. In principle, it is possible to measure dc current, and if the material of sensor elements is not ferromagnetic, compact and lightweight CTs free of magnetic saturation can be designed. In addition, the use of light for transmitting signals is advantageous for electrical insulation and control of electromagnetic induction noise. If OCTs are developed by making use of such features, it will enable the dynamic ranges of OCTs to be extended, while achieving a compact and lightweight construction of units.

The OCTs are becoming more commonly available for use in power systems measurement and monitoring. A number of suppliers have developed various kinds of OCTs in the last few decades. Most OCTs have the same basic operational principles, but they may be optimized for different transducer applications. OCTs can offer better accuracy compared to a conventional CT, a better transient response due to the lack of an iron core, and a wider bandwidth for the Faraday effect-based measuring systems. Typically, OCTs are also safer, lighter, and smaller [6]–[9]. The interconnection of OCTs with power system monitoring and protection equipment is usually different from that of the magnetic CTs. OCTs offer three different output signals: digital, low-energy analog and high-energy analog outputs. All outputs represent the secondary output of conventional current transformers [10]–[12].

Several advantages of OCT have been recognized compared with conventional iron-core current transformers. Immunity to EMI, noncontact measurement, high dynamic range, compact design, and impossibility of explosion, and high bandwidth that allows harmonic analysis of current represent the main advantages of OCT from the electrical power industry aspect. The latest optical current sensing techniques can be used to implement an OCT are illustrated in [6]–[13]. The OCTs are commonly

considered to contribute to saving cost and space for installation. The former have the advantage of higher accuracy. For the GIS, the optical fiber CT is desirable for the reasons of low cost and freedom of configuration. The small sized OCT and simple configuration of the GIS can be realized by the optical fiber CTs [32].

The literature shows several studies on OCT improvements [13]–[19]. Most of them aim to demonstrate that the developed OCTs have higher performance, suitable for power system applications, and can replace the conventional CTs. Different comparison methods are used to show the comparability of OCTs with conventional CTs [20]–[23]. Furthermore, a few OCTs have been installed together with conventional CTs at substations, allowing a comparison of the two devices' performances in practical power system conditions. Results are encouraging but have been limited [24]–[27]. Literature reports only a few comprehensive laboratory studies on the comparison of these CTs [28], [29]. Specifically, there are only few studies to analyze the digital output characteristics of OCTs.

There are different types and several techniques can be used to implement an OCT, a bulk OCT which uses a ring-like glass sensing element, all fiber optical fiber current transformer (OFCT) which uses an optical fiber as a sensing element, and fiber bragg gratings (FBGs) are remarkable sensing elements [30],[31]. In addition, they allow the additional flexibility to implement signal-processing techniques for interferometric demodulation, and such characteristic triggered local research oriented to the interrogation of Fabry-Pérot (FP) interferometers.

The FBG based current transducer is secure and immune from interferences. These transducers can be compensated for temperature drift and easily be integrated into an optical sensing network. A broadband light source at a substation scans the change in reflected optical power at a unique frequency band that corresponds to the surge in magnetic field associated with an increased fault current at a certain location. A unique feature of this real-time scheme is that it only requires current information for fault detections in both radial and network systems with various pole structures and line configurations.

A new multiparametric optical fiber current transducer is presented for simultaneous temperature and vibration sensing in high voltage environment. The optical transducer holds three multiplexed fiber Bragg gratings (FBGs) as the sensing

elements. In the transducer, each FBG can simultaneously measure temperature and vibration independent of the other FBGs. All the FBGs used to monitor vibration are able to monitor the frequency of mechanical vibration and electromagnetic vibration. FBGs are able to measure the temperature as well as vibration changes caused by the machine shutdown [32].

A comparison between the performances of flint glass fiber and twisted single mode fiber (usually used before the flint glass) as a Faraday element is presented [32], and showed that the system with the flint glass fiber is more stable than the one with twisted fiber.

A new optical bulk with high refractive index for applications in optical current transducers is reported. The results illustrated optical bulk could have ten times higher Verdet constant and small internal mechanical stress [33].

Jinling, et al. presented in a comparative method for the development of an OCT in [34]. A permanent magnet is used as a reference source, and the OCT is designed accordingly. Performance of the new designed is tested, and results are satisfactory.

A major problem in developing all fiber OFCT is that the performance of the fiber is distorted by linear or circular birefringence and the level of this birefringence is affected by hostile environmental noises, such as vibration, thermal stress, manufacture imperfections and other effects. The environmental noise problem can be solved by appropriate packaging and the correct mounting of the transducer [36], [37].

The presence of linear birefringence significantly reduces the transducer sensitivity due to the polarization state degeneration. However, an effective alternative is to include a Mirror Faraday Rotator (MFR) into the all fiber OFCT. This results in a MFR-OFCT, which can greatly reduce the effect of perturbations due to vibrations. Although some experimental results exist, published reports on the performance of MFR- OFCTs are severely limited. Consequently, detailed technical analysis and performance evaluation of an MFR-OFCT is essential, before they can be considered for use with protection relays. Computer simulations can provide the flexibility to iteratively change the various parameters associated with the MFR-OFCT. Some methods for linear birefringence compensation using reflected light propagation have been presented, such as Faraday rotating mirrors [38] and fiber polarization rotators

[39] which also double the sensitivity for the same fiber length. The use of a twisted single mode fiber to impose a circular birefringence in the fiber has been demonstrated in [40]. A similar approach is to use spun high birefringence fibers [41]. Linear birefringence can also be reduced by fiber annealing process [42], [43]. Theoretical models and experimental measurements for the Verdet constant dispersion in annealed fibers have been presented in [44].

Moghadas, et al. [45] studied a real OFCT system which is built and the signals acquired from the photodetectors are processed by the Faraday's Laws formulas and the ANN method, giving measurement results for both signal processing strategies. The coil temperature measurements are also included in the ANN signal processing. In order to compare these results, a current measuring instrument standard is used together with a metrological calibration procedure. Preliminary results from a variable temperature experiment illustrates the higher accuracy, better than 0.2% of maximum error, of the ANN methodology, resulting in a quick and robust method to hands with OFCT difficulties on of non-idealities compensation.

Petricevic et al. [46] studied the harmonic measurements using portable OFCT, modified for current harmonic measurement in high voltage electric power systems. The improved sensing head is designed to allow accurate sensing of the current harmonic levels over the entire frequency range of interest.

The response of OCTs placed in high electric field environments, such as gas-insulated systems (GIS), can be influenced by the Electro-optic (EO) Kerr effect. The EO Kerr effect is an electric-field-induced linear birefringence that arises when an electric field changes the polarizability of the glass molecules. Linear birefringence, from either stress, bending, waveguide form, or the EO Kerr effect, alters the response of a Faraday Effect current transducer. Optical fiber current transducers have several economic and performance advantages over conventional current transducers in fault detection and metering. The bandwidth and high dynamic range of these Optical transducers provide the power utility engineer with a diagnostic tool for evaluating generators and the transmission grid [47]. Due to their all-dielectric design, installation costs are significantly lower, and transducers failure does not pose a threat to power utility personnel or equipment [48].

The GIS environment or other high voltage applications are where OITs have the greatest economic advantage, but no study of the EO Kerr effect on these transducers has been made. Over the last two decades, there have been field tests of optical current transducers in GIS environments [48]. However, the EO Kerr effect on these transducers is not noted or detected. Some reasons for not detecting the EO Kerr effect in these current transducers are low or non-uniform electric fields, short optical path, and polarizer alignment.

The simultaneous measurement of voltage and current using the EO Kerr effect or Pockels effect has been shown in [49] this scheme is secure and immune from interferences. They use fast and compact magnet transducers instead of current or potential transformers to translate current induced magnetic field into optical signal. These sensors can be compensated for temperature drift and easily be integrated into an optical sensing network. A broadband light source at a substation scans the change in reflected optical power at a unique frequency band that corresponds to the surge in magnetic field associated with an increased fault current at a certain location. A unique feature of this real-time scheme is that it only requires current information for fault detections in both radial and network systems with various pole structures and line configurations. It can easily coordinate with other protective devices and is free from any time-current coordination curves.

The OCT has many essential advantages over a conventional current transformer consisting of an iron core and copper winding. For example, the OCT shows no saturation effects, excellent electric isolation and requires no flammable materials such as oil. Therefore, introducing the OCT to the electric power system will launch a new generation of GIS.

The reliability performance of the NxtPhase developed OCT is defined by Nicholson in [50]. The importance of dependability, reliability, maintainability, and interchangeability brought attention to this study. It provided a structure for the development of a reliability program. Therefore, a reliability performance of the system must be implemented during the theoretical design.

Kucuksari [51] studied the OFCT calibration technique for NxtPhase products. The aim of the calibration is to prove the accuracy of an OFCT in which the optical sensor must have better than 0.2% accuracy. The OFCT accuracy depended on the current

level, and each output type had to be calibrated. Generally, at low, current the accuracy decreased. Consequently, the calibration is performed in two levels: low current level (LEA) (less than 100 A) and high current levels (HEA) (100 to 3600 A). Each output is calibrated with these two levels using a high precision CT.

Rahmatian, et al. [52] described the NxtPhase produced (according to the IEC 60044-7, 60044-8, IEEE C57.13, IEEE C37.92 standards) 550 kV class three-phase combined optical voltage and current transducer (NXVCT). Dielectric performance and the effect of temperature and vibration on the accuracy are tested in HV laboratory. The device met the accuracy requirements of IEC 0.1% class voltage transformers when the temperature is in the range of –40 ^{o}C to +60 ^{o}C. The device also maintained 0.1% class accuracy when subjected to vibration. Blake and Rose, are tested a NxtPhase produced OCT and OVT with a Landis-Gyr class 2 MAXsys 2510 power meter in the current is varied between 0.01% to 150% of the CT rated current, and the voltage is kept constant. The thermal rating of the OCT is tested using 63 kA for a few cycles. The mechanical integrity of the OCT is tested using 171 kA peak dynamic current. The accuracy test is performed according to the method described by Blake in [16]. The results show that NxtPhase products had better accuracy than described in the standards.

In order to satisfy the high measurement requirements for the high power grid, advanced packing techniques for the sensing fiber coil is required, in order to avoid birefringence problems. To achieve a more stable performance, the sensing fiber must be placed without coating and inside a capillary filled with silicone oil to avoid internal friction during handling. A thin strip of fiber-reinforced epoxy serves as a robust protection of the capillary tube [53], [54].

Some optical fiber current transducers are already commercially available from ABB, Alstom Grid (previous NXTphase) and Artche to measure electrical current on electrical potentials up to 800 kV. The ABB Company assures a range of operation up to 500 kA and ±0.1 % accuracy in DC measurements [54]. Another sensor from the same company named MOCT from ABB, it also has a dynamic range from 1 A to 4 kA with accuracy performances that exceed IEC Class 0.2 S and ANSI Class 0.15 S for metering applications. The system provides accurate waveform reproduction up to 100 kA. Different sensor weights, for different voltage rated are also supplied [55].

The sensor NXCT from NxtPhase (bought by Alstom) for 362 kV has a dynamic range from 1 A to 4 kA with performances that exceeds the IEC Class 0.2S and IEEE Class 0.3 accuracy (0.15 %) for metering applications. The OFCT is also able to measure up to 63 kA RMS for short-time current and accurate waveform reproduction up to 6 kHz. Different OFCT weights are supplied. The weight discrepancy is due to the isolation required and it has been showed the OFCT can operate in a temperature range between -40 ºC to +55 ºC [56].

The latter company, Arteche, provides an all-fiber OFCT named SDO OCT for operation in the 100 ARMS to 5000 ARMS range, satisfying IEC class 0.2/0.2S this sensor works within a temperature range of -40 ºC to +55 ºC [57].

2.3 Voltage Measurement and Monitoring Application

Optical voltage transformers (OVTs) are designed based on Pockels effect. The Pockels effect is the electrical field-produced birefringence of polarized lights in crystals that are placed in an electrical field. Different types of crystals exist and have been used for the OVT applications. The Pockels effect is similar to the Kerr effect, which is observed mainly in liquids; both are described in [58]. Many publications present the development of Pockels effect-based optical sensors. Most of them are focused on crystal sensor development and the material aspect of crystals, as well as the problem of the temperature sensitivity of these crystals [59].

The optical voltage transformers are usually combined with OCT applications. This literature review presents the studies on power system applications of the Pockels effect and the studies of OVTs for high voltage applications. The Pockels effect is similar to the Kerr effect generally. Excluding the difference is that the birefringence is proportional to the electric field in the case of Pockels effect, and it is quadratic in case of the Kerr effect. The EO Kerr effect has been used for many years to measure high voltages and electric fields. In fibers, the EO Kerr effect has been used for voltage sensing and modulating the polarization state. This literature review summarizes the power system applications of the Pockels effect and publications related to the OVT.

Cease, et al. [60] developed an OVT using the current sensing method. This current sensing method has been used before to develop a magneto-optic current transducer

(MOCT) for SCADA and protection systems [61]. The tests of MOCT proved that it is stable, reliable, and accurate. The main difficulty with using this current transformer for the voltage sensing is that the MOCT is sensitive only to magnetic fields, not electric fields. However, voltage measurements need OVTs that are sensitive to electric fields. The technique used in this study is used to measure the current flowing through the series connected capacitors proportional to the voltage to be measured. The output of the MOCT is proportional with the voltage. This yields an optical transducer, which provides the benefits of optical sensing and test results are compared with the magnetic VT, and 0.8% deviation is observed.

The principle of the OVT is to measure voltages using optical modulation and demodulation in accordance with the Pockels effect is proposed by Sawa et al. [2]. With the OVTs, the input impedance into the sensing elements can be raised by reducing the size of OVT elements. This enables designing a voltage-measuring system smaller than a conventional VT by combining an OVT with a capacitor voltage divider (CCVT). The OVT is not affected by surge noise, permitting the response frequency band to be extended to a required value.

Kurosawa, et al [61] developed and tested an OVT for DC voltage measurement. They had studied the development of OVT for AC voltage measurement in gas-insulated switchgears earlier. The Pockels effect did not work properly for DC measurements, so they developed a method that overcomes this problem. In the later study, the developed DC voltage measurement system is described and a series of tests that examined ratio error and temperature characteristics is presented. Field tests of the equipment are also presented. Results obtained are agree with the desired values and proved that the designed transformer is appropriate for control and protection of DC power systems.

Li and Cui [62] presented a new optical voltage and current transducer with an electrically switchable quarter wave-plate. A Bi4Ge3O12 (BGO) crystal is used as a transducer. The study described the principles of system operation, which included a new application of polarization multiplexing technology for the measurement of multiple variables. Sensitivity and measurement ranges are tested for both AC and DC. The presented experimental results proved the variability of the proposed combined optical current and voltage transducers.

Rahmatian, et al. [52] presented 138 kV and 345 kV OVT designs and their high voltage test results. The Pockels effect is used for the voltage measurements. A quadrature method is applied to obtain voltage from electric field measurements by placing three miniature optical field sensors placed inside the column. This method defined the needed number of sensors, as well as their positions. A novel shielding technique and multi-sensor quadrature method is used to reduce the stray field-caused errors. It is known that OVTs had wide bandwidth; however, due to the difficulties of generating high-voltage high-frequency signals. A standard capacitive divider and a step-up power transformer are used as harmonic sources to test the bandwidth. In order to test the accuracy of transformers under severe contamination, fog pollution tests are conducted. The pollution test proved that pollution does not affect the accuracy. Insulation performances of the OVTs are tested and a 650 kV peak lightning impulse test as well as 750 kV peak chopped impulse test are applied to the 138 kV class OVTs. A 345 kV OVT is also tested with a switching impulse under wet conditions. Partial discharge tests are performed as well on both OVTs. All units performed satisfactorily under tests. The accuracy of optical voltage transducers under pollution and other field distributions is tested. Resistive shielding is used in OVTs in order to avoid any impact on accuracy. In this study, a series of tests are conducted to test the performance of the shielding [48], Two OVTs are placed very close to each other. The sensing head of one of the OVTs is grounded and the other OVT is energized with 50 kV. This situation represented the worst-case scenario in a substation. The output voltage of the grounded transformer is zero. The result obtained shows that the neighboring 50 kV-produced electric field did not affect the grounded transformer output and accuracy.

Bohnert, et al. [63] of ABB in Switzerland developed OCTs and OVTs for high-voltage substations. The electro-optic voltage transducer (EOVT) is based on the Pockels effect and additional temperature sensor is used to compensate for the temperature dependence of the Pockels effect. The insulator supporting the EOVT is filled with a soft polyurethane resin instead of the usual SF6 gas. Different applications of the equipment are described and tested according to the standards. Results proved that the designed optical voltage transformers are suitable for high voltage applications.

2.4 Protection Scheme Application

The accurate measurement of electric energy is a fundamental aspect in the development of sustainable energy management systems. In this context, OCTs are vital tools nowadays as they allow accurate measurement of consumption and fast identification of failures on power systems [64]. In a high voltage environment, conventional CTs can be easily damaged by heat, short-circuits or atmospheric electrical discharges and it is essential to employ protection circuits and insulation, which requires constant maintenance and surveillance. However, standard CTs used presently in the electric power industry for metering and protection applications have many associated limitations [65]. For instance, due to their high dimension and weight, some of these devices cannot be suspended on the electric line and imply high installation cost [66], [67]. Conventional CTs for metering and protection applications in high power grids are usually heavy parts of instrumentation with high costs associated to installation and maintenance since they are susceptible to damage. Furthermore, their intrinsic transduction mechanism is prone to saturation effects and often a tight sensitivity/bandwidth compromise is required resulting in the need to use distinct devices according to the particular application.

The measurement of the electric current through optical methods is appealing for applications in high power systems because it has several advantages over traditional methods, such as the high bandwidth, high electrical insulation, immunity to EMI, multiplexing ability, lightweight, and compatibility with the technology of optical fiber communication. In this context, OFCTs are becoming a very attractive tool for a new generation of smart grids allowing accurate measurement of power consumption and rapid identification of faults in power systems [65]. They can provide large bandwidth, sensitivity, large dynamic range, and immunity to electromagnetic interferences. Comparatively to conventional transformer they can be much lighter and compact and since they are intrinsically dielectric, they can be more easily insulated.

The nominal output of a conventional CT is usually 5 A; 1 A is also used. A large value of secondary current is chosen, almost a century ago, to give noise immunity, and to provide sufficient energy to operate electromechanical relays or meters. For OCTs, alternative low energy outputs (typically a few volts or a few mA) have been

preferred [68]. The design of the power supply become problematical if a large current has to be supplied without distortion. In any case, adequate isolation from interference is provided by the optics, and modem metering and relaying devices do not require much energy to operate. Given that, a low energy output will be used. The designers of a digital Type 1 system have solved the problem by designing the equipment at the other side of the interface. One manufacturer of a Type 3 system has reached agreement with a meter company on a 10 mA signal. This amounts to a choice of scale factor (mA out for Ampres in). Bearing in mind all the other important parameters that must be specified to define system performance, scale factor seems like a rather minor decision. In fact, for the analog systems, it makes little difference whether the output is a small current or a small voltage. The choice has not been standardized and is at present decided by the user.

Kondo and Kurosawa are studying the sensing technology is the application to the protective relaying systems of the electric power facility [69], [70]. The first application for the OCT is in protection systems for series capacitor banks [71]. The OCTs are used in a protection system based on single board computers with different relay functions implemented as software algorithms. The interface between the OCT and the relay is a parallel digital data bus. The OCTs are of two types, with measuring ranges of 4-640 A, and 200-32000 A. Within each of these ranges, the accuracy is better than ± 1% of measured current. The sampling speed is limited to 800 Hz.

The interfacing of the OCT with the existing measuring devices and relays is one of the essential differences. OCTs are inherently, different by the conventional CTs. They measure the primary current based on the optical effect of the electric current and so, offer a numeric image of the current. This signal must be then converted in the continuous form, possible to be amplified. They can note slight performances of the measuring devices, especially at small primary currents. The slight performances and their dependency on the OCT's design are due to the noise contained by the output signal and the method used by the different numeric devices to compute certain parameters. It is important that the signal/noise ratio (SNR) to be as high as possible, because the measuring devices could indicate wrong measurements or high harmonic distortion factor. In what concerns the positive economic benefits of using

the new OITs, they can be quantified in time, taking into account the low costs for installation and minimal maintenance costs [72], [73].

Interfacing the OFCT with conventional meters and relays requires a new approach. Bull, et al [51] studied interfacing of optical current transformers with the existing meters and relays in a substation The OCT output is an inherently digital signal in an NxtPhase produced OCT. This digital signal is converted to an analog voltage signal and to analog current signal. The device had three types of output: digital, low-energy-analog (LEA) (e.g., 4 V represents rated current) and high-energy-analog (HEA). The low energy analog (LEA) output is designed for either metering or digital relaying. High-energy analog (HEA) output allows for use of OCTs in substations with conventional relays and meters. The NxtPhase OCT output had an inherent noise that can affect the sensitivity of both meters and relays. These incorrect readings appeared at low current levels. One effective method of reducing the SNR is wrapping the conductor with multiple turns of fiber. This method increased the sensitivity of the OFCT and reduced noise to an insignificant level.

Mladen, et al [74] is measured the influence of OIT characteristics on the performance of numerical protection relays. The defined indices for protection functions have been presented in [75]–[77]. Power quality performance indices used to evaluate the difference in performance between the conventional protection systems, which are used conventional ITs and the digital protection system that used OVTs and OCTs. Results show that the use of OCTs and OVTs are expected to positively influence the performance of protection. Furthermore, it is possible to use the same set of optical transducers for protective relay, revenue metering and power quality metering applications without degrading the overall performance of the system.

2.4.1 Faults Detection and Overcurrent Protection Scheme

The CT dynamic response is one of the most important specifications of the CT in electric power system. A mandatory test by the norm IEC 60044-8 is the precision ones, which is the main objective of designers to obtain waveforms without distortion. The main defect of the traditional CT is its transient responses cannot

satisfy the measuring and protection requirement of the larger short circuit current with the high-speed development of recent power industry [78].

During faults, the current magnitude may be much larger than the rated CT current. The fault current might also have substantial amount of DC components as well as there could be remanent flux in the CT [79]. All these factors contribute to CT saturation. A saturated CT may compromise the reliability of power system protection since inaccurate values of the current are transferred from the secondary side to the IED and leading to false tripping of the power system. Therefore, CT saturation is required to detect quickly so that the IED can perform necessary adjustment or correction in the protection function.

Several methods to detect CT saturation phenomena have been developed in [78] – [82], all of them have their own advantages and disadvantages. Majority of the methods that have been developed are usually based on the protection function they are associated with. However, limited work has been done on a standalone method to detect CT saturation exclusively using the CT measurements.

Lastly, OFCT can replace the conventional CTs since OFCT does not experience saturation phenomenon. However, OFCT technology is still developing and studies show that long term operation stability of OFCT is questionable [83]. Furthermore, majority of the industries still use conventional CTs for relaying. Hence, algorithms to detect CT saturation within an IED are developed.

Ibrahim and Nabil [84] are investigated the influence of CT saturation on over-current digital relays, in distribution systems where loads are relatively small and connected to switch-gears with high short circuit levels. A study is performed to verify the operations of instantaneous and time-delayed over-current digital relays to ensure coordination with other devices and safe isolations of faults. It is shown that instantaneous digital relays will perform properly with a relatively small CT's. A criterion for selecting CT's for instantaneous digital over-current relays operations is presented. However, time-delayed over-current relays will be significantly impacted by CT's saturation and special care shall be taken to achieve coordination with other devices.

Chen et al, [20] presented a developed OCT using a Rogowski coil to detect and measure the line current. The developed OCT is compared with convectional CT for

steady state and transient measurements. The results show that the developed OCT could serve better than the magnetic CT for overcurrent protection, differential protection, and distance protection schemes.

In a power transmission system in which underground cable (UGC) lines are intermingled with overhead lines (OHL) and when a fault occurs, fault section locating systems are necessary to detect a fault in the cable section or in the overhead line sections and to make output signal to the protection relays to lock the reclosing operation of CBs. For this purpose, a fault section locating system using the novel OFCT is developed. The OFCT is developed to detect the fault and to decide the location whether it is in the cable section or in the overhead line sections [85], [86].

Nasukawa [87] described development of a novel OFCT and development of a fault section locating system and a fault point locating system using the OFCTs. Practical applications of the developed systems are also reported. By using the new sensing technology devices, stable detection of current is possible by only encircling the OFCT around the cable. The OFCT has other strong points such as immunity from electromagnetic noise, capable of long distance signal transmission, fast response, ease of electric insulation. When a fault occurs, each of the OFCT detects the surge current that arrives from the fault point, and transmits the signal to the local station. Then, each of the local stations measures arrival time of the surge current precisely with GPS clock and sent the data to the master station. The master station decides the fault point from difference of the arrival time data sent from the local stations. The velocity of surges is nearly 50% - 60% of speed of light in the space. As a results, such strong points are utilized in the new systems for fault section location and fault point location applied in the underground power lines.

Kurosawa, et al [88] are carried out the new sensing technology, “fault section” and “fault point” locating systems for underground transmission lines, this developed sensing device can be installed easily to the existing power apparatus by winding the flexible sensing fiber around the current conductor, and also, it has stable measurement characteristics.

In certain network locations, hybrid lines exist, comprising a mixture of OHL and UGC. From a protection point of view, it is desirable to attempt reclosure of the breaker after the fault has cleared if the fault lies on the overhead line, but not if the

fault lies on the underground section. In conventional protection schemes, it is not possible to discriminate which section of a hybrid line is subject to the fault and to install additional measurement and protection devices at the cable terminals is costly and can be impractical. Based on this, an optical fiber multidifferential relay could be developed that would provide passive current measurement at multiple locations along the hybrid line, including at cable terminals. In this way, the relay would be able to determine, with a high level of discrimination, which section of the line is faulted and could initiate reclosure accordingly [89].

Dhilju [90] is developed sensing network. These magnetostrictive-based OFCTs with FBGs are passive and provide a fast and effective method for real-time monitoring of line currents various locations simultaneously. For protection purpose, they can replace conventional VTs and CTs that are susceptible to saturation and hysteresis. The FBGs based OFCT fiber based sensing network enables the development of new fault detection and location schemes and flexible coordinating strategies among protective devices without relying on any time-current coordination curves. By careful deployment of FBG based OFCT, they can detect all faults irrespective of types and locations and are robust against fault impedances, high harmonic contents in line currents, OFCT vibration noise or OFCT malfunctions.

2.4.2 Differential Protection Scheme

Conventional differential protection schemes rely on a protection relay and a pair of CTs that measure current phasors separately at the boundaries of the protected zone. The scheme requires a separate, often optical communications channel for the sharing of measurement information to enable the timely identification of reaction to internal faults [91].

The performance of the protection devices such as differential and impedance relays is mainly based on the operating condition of the CTs. Distorted secondary currents due to CT saturation depending on the magnitude of the fault current and a remnant flux in the iron core can cause mal-operation or operating time delay of protective relays. Therefore, protective relay engineers have to take account of the CT saturation problem when they design a protective relay, especially such as current differential relay.

There are several traditional techniques provide secure operation during conditions, such as CT saturation, magnetizing inrush current, core saturation, any mismatch between CTs and zero-sequence current. Moreover, this techniques offer features, such as speed and selectivity.

Khan and Sidhu [92] are proposed new directional comparison-based internal/external fault detection and discrimination technique for the protection of all commonly used phase-shifting transformer (PST) types. Moreover, unlike the differential solutions, the proposed technique solves the problem of nonstandard varying phase shift without tracking the tap-changer position. Performance evaluation of the proposed technique shows that it provides the best overall protection solution for commonly used single/two-core symmetrical/asymmetrical PSTs. Further, addresses and solves various challenges that can influence the overall performance of the algorithm.

Nasir, et al [93] are demonstrate through simulations the evaluation of a novel, all-optical differential current protection scheme employing low voltage piezoelectric transducers, FBG transducers and Rogowski coils is presented. The optical power reflected from the FBG is monitored by means of a single photodetector, whereas a simple optoelectronic threshold detector detects fault occurrence. An immediate response to an increase in differential current can be achieved even at low voltage levels such as these generated by Rogowski coils providing a low-cost and fast-acting fault detection system.

The performance of feeder differential protection [94] is evaluated on an EMTP/ATP simulated power network where the current transducers are MFR-FOCTs. Results are describe the response of the protection to an external solid phase to ground fault at the Received end and an internal solid phase to ground fault solid fault at Send end. The external and internal fault measured by the MFR-OFCTs. The scaling of the MFR-OFCT output signals have been calibrated to match the output of the CTs. However, when considering the operating response of the protection, the differential currents derived the MFR-OFCT outputs are significantly above the biased operating characteristic. Consequently, the protection has no problem in recognizing, in either case, that the fault is internal to the protected unit, it can easily discriminate between an internal and external fault, even when the measured signals are limited by the MFR-OFCT measurement range [95].

Moghadas, et al [96] are proposed and successfully implemented approach to differential protection using two identical FBG based OFCT. Since the approach does not require the use of interrogators the cost of the measurement system is significantly reduced. By monitoring the reflected optical power modulation and comparing it to set threshold fault detection has been demonstrated. The new technique has the potential to enable very fast-acting and inexpensive all-optical unit protection. In a practical deployment the OFCTs may be at different temperatures due to their distant locations along a transmission line. The FBG peak shifts due to temperature may then introduce errors in fault detection and false tripping. Therefore, this temperature related issues and suitable temperature compensation methods will be developed to ensure reliable fault detection over varying environmental conditions with a minimum of fault positives.

FBG based OFCT is described the design and testing of an all-optical power systems protection network in differential protection configuration and demonstrated its high performance over a range of fault scenarios and resistances. Further development of the technology will lead to field-ready packaged devices with reduced size and improved performance in terms of reduced noise and increased sensitivity [97].

Differential protection for UHV transformers (involving primary, secondary and tertiary windings) is extensive and complex due to the requirement for multiple measurement points [98]. As an example, UHV transformers may incorporate 40–50 transducers (CTs and VTs) which must deliver measurements to the protection relays. The use of smaller, dielectric transducers for this purpose is desirable. In particular, the optical scheme's flexibility to multiplex all transducers on a single or multiple fibers would be highly convenient. Additionally, FBG based transducers are capable of measuring current other parameters such as temperature, vibration, and pressure [99], and these measurements are therefore compatible with any chosen FBG interrogation and multiplexing scheme. A single "protection and monitoring" scheme could therefore be developed on this basis, delivering full electrical and mechanical coverage of these large, valuable items of plant.

Philip et al [100] is detail a FBG transducers based solution to wide area measurement of current and voltage for protection applications. Experimentally demonstrated the performance of the protection scheme in differential current

configuration, and thereafter discuss novel protection applications of the system. The system functioned correctly for all applied internal and external faults over a total distance of 18.5 km between measuring points. Even though the full potential and limitations of this technology is yet to be systematically quantified considering a number of protection performance influencing factors.

2.4.3 Distance Protection Scheme

Conventional distance protection schemes require accurate representations of current and voltage as inputs. Communication between relay locations is used to enhance the speed and selectivity of such schemes. From the measurement data, the impedance of the transmission line is calculated up to a predefined point, known as the reach point. For short circuit faults up to this reach point, assuming a "solid" short circuit, then the calculated impedance will be less than the impedance of the line up to this point. Such schemes often employ a separate, commonly optical, communications channel for the exchange of status and logic data to enable the timely identification of and reaction to faults at various locations on the system [101].

Distance relays are used for protection of high voltage transmission line as they provide more secure, faster, and reliable protection. Fault rate is usually much higher in transmission lines as compared to other components of the power system. The occurrence of the different types of the faults produces very large currents in the power system. Conventional CT utilize an iron core and winding ratio to step down these currents to a more manageable level for the secondary devices such as protective relays and meters [102] – [104]. The signal fed to relays and meters is distorted due to saturation of iron core. Therefore, the CT will not be capable for supplying and reproducing the primary component to secondary side until it comes out of saturation. The inaccurate secondary current, the less information is given to a distance relay, which causes it either to under reach or overreach. Possible conventional solutions of these problems are detailed in [105], [106].

Additionally, when either the number of relays or the distance between relays is increased, timing problems can arise due to the limited bandwidth, speed, and changeable latencies of the communication channels and the increased computation requirements.

Sarwade et al [107] is studied the replacing conventional CT by Rogowski coil. Influence of secondary burden of CT is investigated and it proved that not considering this factor could cause a CT to produce a highly distorted secondary current. Rogowski coil with integrator produces exact replication of primary current without distorting it with any amount of load burden and able to overcome under reaching issue of the distance relay.

Both established OCTs and OVTs rely on interferometric or polarimetric measurement techniques and thus the distance from interrogator to measurement point cannot be greater than around 100 metres in most cases. Additionally, as with conventional electrical transducers, it is not possible to discriminate between superimposed sensor responses and thus serial multiplexing is not possible. For these reasons, wide-area coverage, measurement over long distances and high numbers of transducers not presently achieved by conventional current or voltage measurement schemes. Therefore, present commercial optical transducers for the power industry offer gains in measurement quality, that is, accuracy, rate, and immunity to interference, but cannot contribute to the development of novel protection architectures or applications.

The optical transducers are physically small and are able to be multiplexed, thus overcoming limitations in existing conventional schemes and allowing the implementation of novel protection architectures that are not achievable either with present electrical or optical measurement techniques in the power industry. Such an approach has the potential to address the limitations of standard protection architectures by presenting at a single location, data relating to voltage and/or current from multiple widespread locations on a network [108], [109].

The capability of the technology to measure both current and voltage over extended distances has clear application in distributed distance protection and in other novel methods for protection of power networks, particularly future networks where high numbers of distributed generation sources may be connected to the network [110].

Philip, et al, [111] are proposed and successfully a prototype FBG based optical transducers based distance protection scheme using distributed measurement of current and voltage waveforms has been demonstrated, with three different fault scenarios modeled and tested. The results are providing an enhancement, or an

alternative to conventional distance protection methods. The availability of simultaneous measurement data from local and remote locations presents opportunities for more accurate impedance calculations and removes the need for a dedicated communication channel between the measurement points for scheme logic, such as acceleration or blocking. Moreover, accurate discrimination of fault location can be achieved from the distributed measurement data being available; this could be used to modify conventional zone settings. The availability of measurement data from local and remote ends could also be used to improve fault location accuracy, which is a further benefit of the proposed technique.

Due to their capability for long-distance (>100 km) interrogation, FBGs based transducer schemes will be highly suitable for the wide-area backup protection of multiple circuits on a large network. Monitoring and protection based on current and voltage measurements taken at multiple locations will be possible from a single central location.

Presently, phasor measurement units (PMUs) require use of the GPS network to accurately time-stamp current or voltage measurements for direct comparison of phasors at diverse locations on the network [112]. Access to the GPS clock is required primarily because otherwise it is not possible to synchronize measurements that are taken by a variety of different schemes at different locations. Alternatively, the precision time protocol, which has been developed as an alternative to the GPS mechanism [113], may be applied to synchronize clocks on a network, but this requires infrastructure for continuous communication between all measurement devices.

Use of the long-distance OVTs and/or OCTs network could facilitate synchrophasor measurement without the use of GPS, since in the optical scheme the relative delay between measurement points is measurable. A constant delay of approximately 4.9 μs/km (9.8 μs/km round trip) will exist between FBG based reflections arriving at the interrogation unit, which can be corrected at the central interrogator/relay. Since FBG interrogators can make measurements across a span of 100 km or more, there is potential for centralized wide-area synchrophasor coverage without a requirement for absolute time-stamping or access to the GPS network [114].

The requirement in present protection architectures for the continual communication of measured values or Boolean flags between co-operating relays is most evident in multi-terminal networks, since each relay is measuring independently, their tripping states must be communicated to all other relays for effective operation of the overall protection scheme. Compared to the centralized, passive optical approach, this architecture is expensive and convoluted, requiring many relays and dedicated communication channels. There is clear justification in this instance for development of a centralized protection by FBGs based OFCT. Therefore, Niewczas et al [115] proposed that established optical fiber measurement technology has excellent potential in improving present power system protection systems and meeting the protection demands of future networks.

Ferry, et al [116], are investigated the performance of distance protection with conventional CT device and OFCT. Various factors contributing to the secondary current distortion, e.g., CT saturation and OFCT current clipping has been evaluated. These phenomena do not exist in OFCT. The OFCT current clipping will only occurs if the fault current magnitude higher than the OFCT maximum detectable setting current. CT saturation results in a reduction of the current magnitude and a phase shifting in the current. The reduction of the current magnitude may result in the distance relay under-reaching or slower relay operation. Meanwhile, the phase shifting in the current may result in the distance relay over-reaching. On the other hand, the OFCT clipping will only result in a reduction of the current magnitude, but will not result in a phase shifting in the current. Hence, the OFCT current clipping will not cause the distance relay over-reaching. The facts that CT may cause both under-reaching and overreaching, meanwhile OFCT may cause under-reaching only, and it is easier to prevent OFCT current clipping than CT saturation, indicate that the modern OFCT can provide the distance protection better security than the conventional CT.

2.5 Summary

In this chapter, there has been a review of research of optical current transformer. Some initial implementations are summarized and the benefits and challenges related to power system protection using optical instrument transformer are discussed.

Recent publications describes the development and practical application of a optical fiber current sensing technique such as developed schematic configuration of the optical fiber current sensing device and developing of sensing element material. The literature on both optical voltage and optical current transformers presents many studies. All of the works aim to prove that the developed Optical Instrument Transformers (OITs) have higher performance, are suitable for power system applications and can replace the conventional ITs. Different comparison methods are used to show the compatibility of optical ITs with conventional ITs. Furthermore, few optical ITs have been installed in addition to encouraging limited conventional ITs at substations, which would allow a comparison of the two devices' performances in practical power system conditions. The literature reports only a few comprehensive laboratory studies on the power system protection based optical transducer. Specifically, there is no study to analyze the digital output characteristics of OFCTs in different protection schemes. However, models for optical instrument transformers are not very well presented. A few modeling studies have been performed only on optical elements of the OFCTs in order to improve the accuracy, but a complete model that considers the optics and the electronics together has not been presented. Consequently, there are no simulation results and methods presented due to the lack of complete model existence. Therefore, the literature review shows that OFCT used in power system protection and monitoring has attracted little research effort.

Chapter Three
Instrument Transformers

3.1 Introduction

In the measuring, counting, control and protection (relaying) field of power supply, it is well known the need of monitoring the electrical potential and current in the conductors of the transmission lines and the conductors connected to substation power transformers. These measurements are transmitted to a central station for the control, protection and monitoring of the entire power system to assist the dispatch operator and other bulk network functions depending on the so-called Power Control Centre [46]. Making use of the excellent features of the sensing technique, various current and voltage monitoring devices and systems are developed, applied practically for the protection, and monitoring in the electric power facility. This chapter provides theoretical background on various instrument transformer designs, performance characteristics, and their impacts on output signals. In addition, to describes the development and applications of instrument transformers and different measuring techniques used in power system. The problem faced the conventional instrument transformer are introduced first. After that, the design and performance of the optical instrument transformer and their types and configurations are discussed.

3.2 Instrument Transformers Function

Systems for the monitoring and the management of electricity networks are composed of four sub-systems. Figure 3.1 depicts the insulating function that the instrument transformer provides between the High Voltage (HV) portions of the network versus the secondary plant equipment in the control room. Instrument transformers are used with measuring and protective equipment in order to monitor electrical parameters such as current and voltage or to use these parameters to activate protection schemes. Thus, they are used with ammeters, voltmeters, energy meters, power factor meters, wattmeters, etc., for the measurement of current and voltage, and with protective relays for tripping circuit breakers in the event of faults

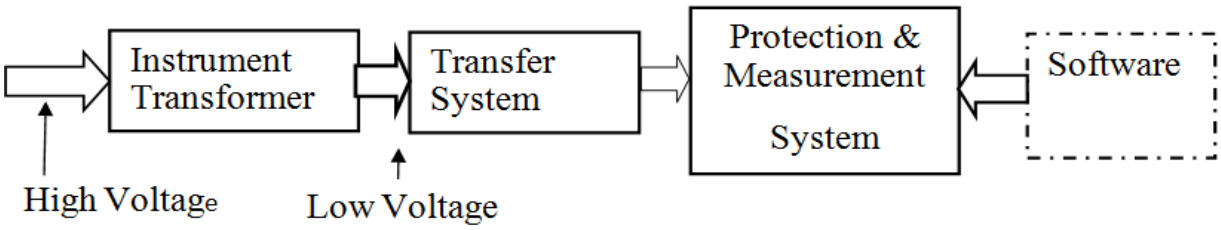

Figure 3.1 Instrument Transformers Functional Diagram

Their role in electrical systems is primary importance for various reasons concerning to safety, accuracy, and standardization. The main role of instrument transformer is shown in Figure 3.2.

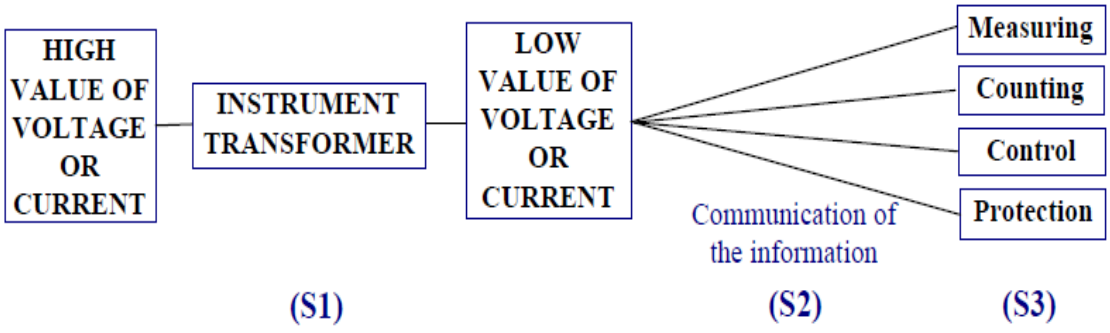

Figure 3.2 Role of the instrument transformer in electrical systems

In order to develop an interface between secondary equipment and process bus another interface between high-tension side and merging unit is required. This interface will transform high voltages and currents to low value voltages and currents. Instrument transformers consist of current transformers and voltage transformers. The purpose of instrument transformers is to convert the high voltages and currents to the low values of currents and voltages in a power system. The rapid and reliable operation of the power system protection and control is dependent on reasonably accurate measurements of electrical signals associated with controlled elements of the power system. The values of currents and voltages from instrument transformers during large and small disturbances in the power system are of great importance with respect to their accuracy of measurement [47]. The protection systems are dependent totally on the measurements from the instrument transformers, so accurate performance evaluation of CTs/VTs are very importance.

3.3 Conventional Instrument Transformers

Conventional instrument transformers are also known as the electromagnetic transformers. The name instrument transformer (ITs) is a general classification applied to current and voltage devices used to change currents and voltages from one magnitude to another or to perform an isolating function, that is, to isolate the utilization current or voltage from the supply voltage for safety to both the operator and the end device in use. The main purpose of the ITs is to produce a proportional secondary signal of currents and voltages from the incoming primary currents and voltages. ITs are used commonly in metering and protective relaying in the electrical power systems. They facilitate the safe measurement of large current value and large voltage value from high voltage lines. The primary winding is connected with the source of currents or voltages to be measured and the secondary winding is normally connected to a meter, relay, or a burden resistor to develop a low-level voltage that is well-suited for metering, control and protection purpose. The Current transformer (CT) can be represented by the equivalent circuit of Figure 3.3 where all quantities are referred to the secondary side.

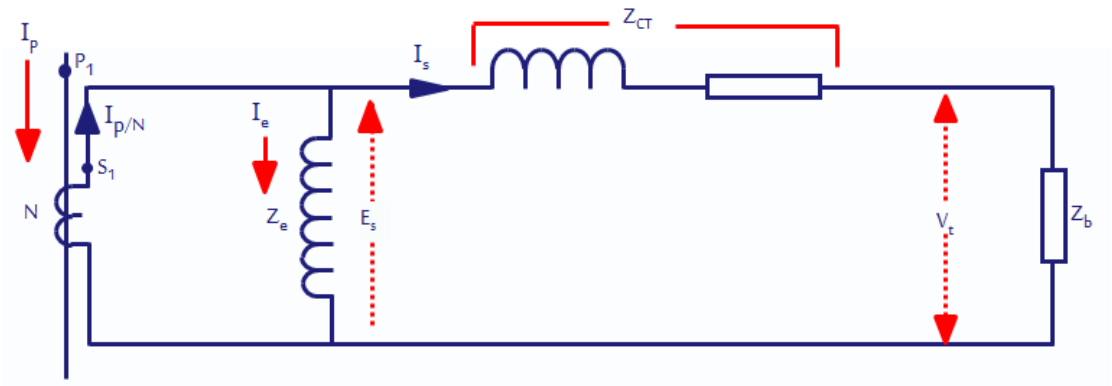

Figure 3.3 Equivalent Circuit for CT

3.3.1 Voltage Transformers

The inductive voltage transformers (VTs) (sometimes referred to as potential transformers) are the dominant sources of the voltage output signals for measurement and protective devices and relays in medium and high voltage networks due to their simple construction and low costs.

Voltage transformers (VTs) are operate under the same principle as power transformers, but specially designed to provide high accuracy over a specified range

dependant on whether it is used for metering or protection purposes. The standards establishing the performances of the voltage transformer define it as an instrument transformer in which the secondary voltage is substantially proportional to the primary voltage and differs in phase from it by an angle, which is approximately zero for appropriate direction of the connections. There are two main types of conventional voltage transformers:

1. Electromagnetic Voltage Transformers (VTs)
2. Coupling Capacitor Voltage Transformers (CVTs).

The CVTs are work basically as capacitance potential dividers and they are preferred over VTs for high voltage applications due to their reduced size and cost when compared to VTs. The equivalent circuit for the CVT is illustrated in Figure 3.4.

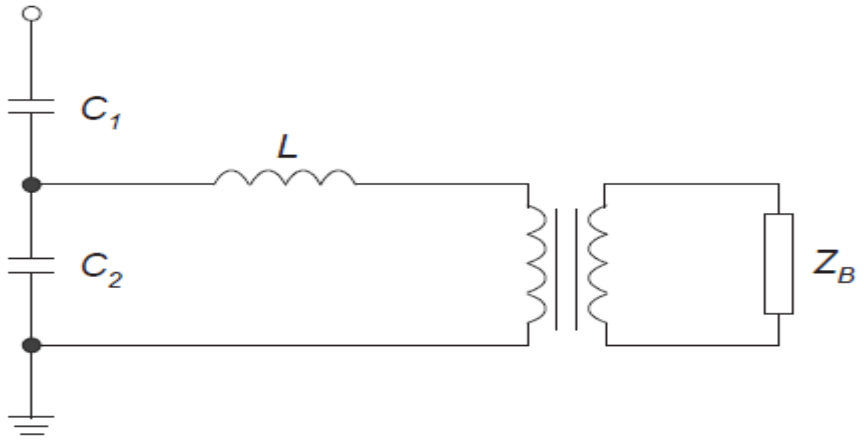

Figure 3.4 Equivalent Circuit for CVT

For a long time, winding type voltage transformers (VT) have been used to measure voltage for the control and the protection of electric power systems. However, with the recent demand for larger capacity in electric power systems, transmission voltage becomes higher, and hence the distance of insulation increases. This leads to an increase in size of VTs. On the other hand, burden of VTs can be reduced due to the shift in technology as following is briefly commented in the two points (IEC Standard 185, 186 [48].

The accuracy of VT depends on the leakage reactance and the winding resistances, which determine how the errors vary as the burden on the secondary increases. The permeability and the power dissipation of the core affect the exciting current and hence the errors at zero burden. The core material used affects the physical size of the

transformer with a smaller size being possible if cold-rolled grain-oriented steels are used as opposed to hot rolled steels. If cut cores are used, the saturation flux density is much higher. Standards for voltage transformers specify errors that must not be exceeded for various classes of accuracy. Limitation in errors leads to limits of watt loss and magnetizing current. The effect of this is to reduce the working flux density of the voltage transformer as compared to the power transformer. Care must also be taken in designing the winding, as the winding resistance and reactance affect errors.

In extra high voltage systems, due to cost reasons it would be disadvantageous to build such transformers for higher voltages. Therefore, CVTs are used. They consist of a capacitive voltage divider that has an output in the kV-range. A magnetically coupled core type voltage transformer is then connected in series with the capacitive divider, providing an output of reasonable magnitude for use with secondary equipment such as protection equipment. An inductor is also connected in series with the capacitor voltage divider and the magnetic voltage transformer [49]. However, the output voltage is affected by the burden, at the tapping point and as the burden current becomes larger, the error of division could be prohibitive. This means that the secondary voltage decreases and a phase error are introduced. Compensation for these errors is introduced in the form of an inductance, which is connected in series with the burden. The value of the inductance is such as to cause resonance with the capacitance value of both the capacitors at the supply frequency.

A higher output could be obtained by choosing a higher tapping voltage for a given value of high voltage capacitor. Later, this voltage can be transformed using an intermediate instrument voltage transformer, which also reduces the burden current flowing in the capacitor transformer. As for the magnetic voltage transformer, the behavior of the CVTs at frequencies other than the power frequency is not specified by the standards.

3.3.2 Current Transformers

The current transformer (CT) is an instrument transformer in which the secondary current, in normal conditions, is substantially proportional to the primary current and differs in phase from it by an angle, which is approximately zero for an appropriate direction of the connections.

Conventional current transducers are transformers (CTs) with copper wire windings and iron cores, are now widely used in power systems. For high-voltage applications, porcelain insulators and oil-impregnated materials have to be used to provide insulation between the primary bus and the secondary windings. The insulation structure has to be designed carefully to avoid electric field stresses, which could eventually cause insulation breakdown. The electric current path of the primary bus has to be designed properly to minimize the mechanical forces on the primary conductors for through faults. The reliability of conventional high-voltage CTs has been questioned by engineers at some utility companies who have been experienced violent destructive failures of these CTs that caused fires and impact damage to adjacent apparatus in the switch yard, electric damage to relays, and power service disruptions [50].

With the short circuit capacities of power systems getting larger and the voltage levels going higher, the conventional CT becomes more and more massive and costly. Although the introduction of SF6 insulated CTs in recent years has improved reliability, it has not reduced the cost of this type of CT.

In addition to the concerns mentioned above, other performance limitations of the conventional CT have raised more concerns [51]. The saturation of the iron core under fault current and the low frequency response of the conventional CT make it difficult to obtain accurate current signals under power system transient conditions. This is specially so for those currents with transient DC components, which aid a remanent flux condition in the core and may cause inappropriate functioning of relays. The saturation of the iron core also reduces the dynamic range of the CT. In power systems, the electric current is much smaller under normal operating conditions than under fault conditions. Because of the small dynamic range of conventional CTs, more than one CT is needed at one location to cover the requirement of metering and relaying.

Microprocessor based control techniques and numerical protection relays being introduced into power systems, conventional CTs have caused further difficulties, as they are likely to introduce electromagnetic interference through the ground loop into the digital systems.

Furthermore, the standard 5A or 1A low burden secondary configuration is not compatible with the new technology that uses analogue to digital converters requiring low voltage input at the front end.

3.4 Conventional Instrument Transformers Performance Problems

The current transformers are the key components as they produce the access to the high currents in a power system through reduced replica on the secondary side. It enables the protection function to detect the faults within time limits and isolate them. Therefore, the protection devices are totally dependent on the measurement values coming from the instrument transformers. Unfortunately, there is a problem of saturation in the CTs core. The CT cores have the problem of nonlinear excitation when exposed to high fault currents. Therefore, the nonlinear excitation forces the nonlinear saturation in the core material of the current transformer. When the nonlinear saturation phenomena occurs the measured value of CTs on the secondary side is no more according to the turn's ratio, which leads to the triggering of wrong event. On the other hand, the new replacements for the conventional instrument transformers are the non conventional instrument transformers also known as optical current transformers (OCTs) and optical voltage transformers (OVT). The OCT plays an important part in the smart substation, it uses the electronic technology to measure the voltage and current of power system and supplies these data to relay protection and control system. Compared with traditional electromagnetic current transformer, the OCT has many advantages, such as simple insulation structure, immunity to electromagnetic interference, no saturation effect, no flammable materials such as oil.

3.5 Conventional Instrument Transformers Correction Performance

Most Conventional Instrument Transformers currently in use are electromagnetic devices that suffer from magnetic saturation effects, residual field effects, and electromagnetic interference. Moreover, with the super increase in voltages (several hundred kV) in power transmission systems, the insulation of the Conventional Instrument Transformers becomes more difficult and expensive. In addition to protection relaying systems, the deregulation and growth of independent power producers and regional transmission companies have created a need for many new

high voltage revenue-metering points [52]. Therefore, there is no need to make special arrangements, which would correct the errors.

3.5.1 Correction of Voltage Transformers Performance

Inductive voltage transformers, if selected in a proper way, do not introduce errors, which could affect operation of protective devices. It is so in both steady state and during transients. Therefore, there is no need to make special arrangements that would correct the errors.

However, in case of capacitive voltage transformers it is otherwise. Since the CVTs are equipped with the compensating inductance and the ferroresonance suppressing circuits, they may introduce substantial errors if there is a sudden change of the primary voltage. The errors may cause maloperation of protective devices, particularly if there is a sudden drop of primary voltage. Therefore, correction of expected errors may be advantageous.

The equivalent circuit of a CVT is presented in Figure 3.5. The ferroresonance suppressing circuit is represented by the elements R_f, L_f, C_f.

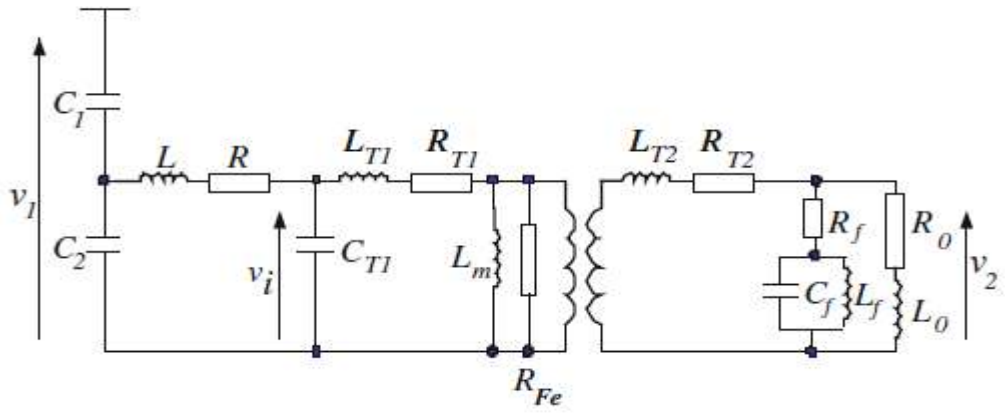

Figure 3.5 Equivalent circuit of a capacitive voltage transformer

The entire circuit may be considered linear, therefore, one may write the following Laplace transform relation as in (3.1).

$$\frac{V_2}{V_1} = N_u F(s) \tag{3.1}$$

where, N_u is a transformation ratio of the CVT, F(s) is a Laplace transfer function of the circuit, and V_1; V_2 are primary and secondary CVT voltages.

The correction ought to process the secondary voltage by a transfer function, which is equal to inverse of the CVT transfer function. Therefore, the corrected secondary voltage V_{2c} becomes as in (3.2).

$$V_{2c} = V_2 \,.\, F(s) \approx N_u . V_1 \tag{3.2}$$

where, F1(s) = 1/F(s)

3.5.2 Correction of Current Transformer Errors

The errors of current transformers are much greater than the ones of voltage transformers. It is so because:

1. Errors of the CTs are much more damaging for proper operation of digital devices,
2. Current transformers are strongly non-linear, because of the non-linear magnetizing characteristic of the cores, therefore their errors are much more difficult to calculate and correct,
3. Due to the hysteresis loop of the magnetization characteristic of the core it is hardly possible to establish the starting value of the core flux,
4. Range of levels of primary currents and the time constants of their DC components are great.

If during the steady state operation the primary current levels of the transformer are within the accuracy range (they are below the rated level multiplied by the accuracy limit factor) the errors of transformation do not affect operation of protective relays. However, if the primary currents are larger it is otherwise.

Typical wave-shapes of primary and secondary currents in case of a CT saturation with purely resistive burden are presented in Figure 3.6.

Obviously, magnitude of protection criterion values calculated on the basis of saturated CT secondary signal may fall quite distantly from their correct values, which might have been determined if the CT primary unsaturated signal was available. Erroneous measurement may in consequence lead to false decisions and protection maloperation. Therefore, the CT saturation phenomenon may impair protection system reliability if appropriate algorithms for saturation detection and/or correction are not applied to eliminate the problem.

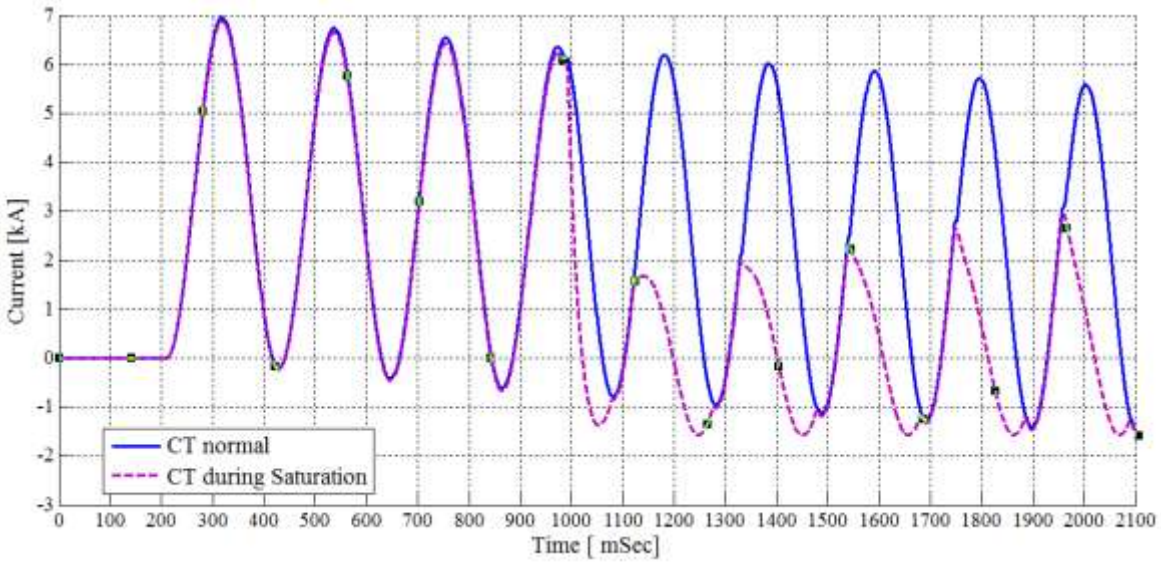

Figure 3.6 Steady state errors of the CT due to large input signal

There are three ways of overcoming the problem and make correct operation of the protective devices possible. They are:

1. Application of the CTs with larger accuracy limit factor, i.e., CTs that do not saturate during steady state operation,
2. Application of the relay algorithms, which are insensitive to the errors, for example they make measurements only in the fraction of periods, when the transformation is correct, or they introduce large restraint.
3. Calculation of the primary current on the ground of the secondary, corrupted wave shape.

The first way is obvious, but in some cases it requires the CTs with the cores of very large cross-sections. The second and third ways do not require very large cross-sections, but they demand identification of the fraction of periods, when the CT is not saturated.

The large number of journal and conference papers, which dealt with the CT saturation detection and correction issue, may be divided into three groups:

1. No CT current correction is performed, but the information on CT saturation is used for other purpose, e.g. for adaptation of protection settings or performing calculations during CT unsaturated periods only.

2. Correction performed is based on the information extracted from the secondary current during the saturation interval, which reproduces the primary current wave shape.
3. Correction is based on information extracted from the secondary current during the non-saturation interval, which aims at determination of the fundamental and DC component of the primary current.

The first step of all the correction procedures is to determine the beginning and end of each saturation span. It is not a simple task; however, a few approaches may be applied to solve it. Among the algorithms for CT correction the ones based on algorithmic approach as well as novel Artificial Intelligence schemes are proposed.

3.6 Instrument Transformer Problem in Power System Protection

Conventional instrument transformers are coupling between power network on the primary side, and protective devices on the secondary side. Inherent to this coupling are signal distortions in various forms. These distortions are, in a sense, artificial: they do not originate from the power network, but are inserted by the coupling within the instrument transformers. Protective devices may be sensitive to signal distortions, regardless of their source. As a result may lead to catastrophic mal-operation in power system protection. Thus, protection system performance is strongly dependent on performance of instrument transformers.

Conventional instrument transformers output consists of analog signals that are hardwired from the IT's location in the substation switchyard to the relay's location in the substation's control room. Therefore, two types of problems originate from this traditional protection system using conventional ITs and IEDs with an analog interface. One related to conventional ITs design and characteristics and other related to analog interfacing [53].

3.6.1 Design and Characteristics Problems

Signals distortions created by ITs may cause protection IED to malfunction due to inherent to their design, therefore, their effect can only be minimized but not completely suppressed. Saturation in the case of CTs and subsidence transients in the case of CCVTs are the two most common signal distortions. The input signal

accuracy requirement of protection relays are different from power quality metering devices. Consequently, there is usually a need for different instrument transformers to provide high accuracy metering of certain power system parameters and/or conditions and different ones for relaying.

3.6.2 Interfacing Problems

The errors in ratio and phase angle depend on the impedance connected to the secondary of the transformer. This impedance is commonly referred to as burden. Long cabling will cause a higher burden to be connected on the secondary side of the instrument transformer. The value of the secondary burden may create a distorted secondary current under maximum fault conditions [54].

The cost of parallel copper wiring used to connect three phase signals between instrument transformers at the process level (switchyard) and protection IED at the control room represents a considerable portion of the total installation cost. It also eliminates the need for auxiliary transformers in protective relays, which are required to convert high power signals coming from conventional ITs.

3.7 Non-Conventional Instrument Transformers

To overcome problems related to Conventional Instrument Transformers, two main approaches can be identified; Either improvement of protective relays, to make them less sensitive to distortions or development of a new instrument transformers, to make them more accurate in delivering signal replicas.

Recently, non-conventional instrument transformers (NCITs) have been developed and tested. Furthermore, NCIT have achieved high performance regarding power system protection and automation. Non-conventional instrument transformers are also known as optical current transducer OCTs and optical voltage transducer OVTs. Since their transformation of the measured current and voltage quantities are based on optical methods which need an electronic interface for its operation. The general structure of an optical Instrument Transformer system is shown in Figure 3.7. It consists of an optical source (Laser, LED, Laser diode etc.), optical fiber (single or multimode), doped fibers, and/or bulk materials are employed as the transducer (sensor heart). At the output of the sensor system, a photodetector is used to detect the

variation in the optical signal that is caused by the physical perturbation of the system and signal processing electronics. In the optical fiber sensors systems, the optical parameters that can be modulated are the amplitude, phase, color (spectral signal), and state of polarization.

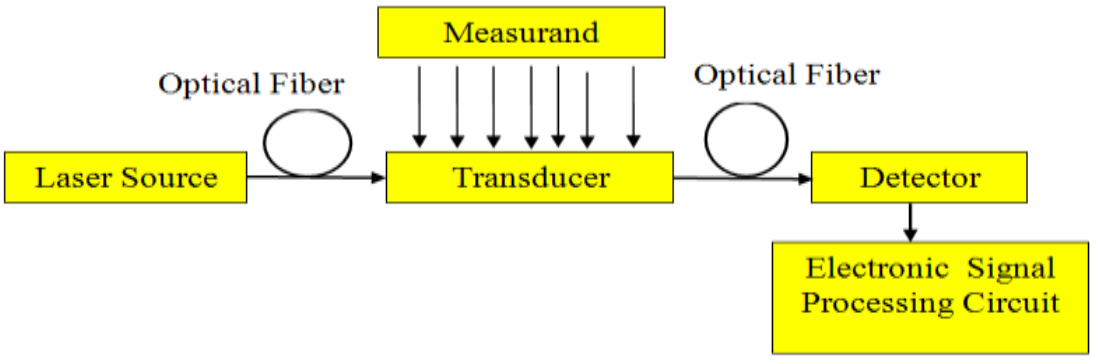

Figure 3.7 Basic components of an optical fiber Instrument Transformer

One of the key advantages of optical instrument transformers is the possibility of supplying digital current and voltage samples to numerical protection relay. Moreover, there are promise to deliver accurate signal replicas of currents and voltages to relaying, metering and power quality IED. A digital interface that replaces the copper wiring with a single fiber optic communication bus means a significant reduction in engineering and material cost. Optical instrument transformers (OITs) with compact dimensions and digital outputs have found a suitable place in the modern digital substation. In addition, their performance satisfies the protection and metering requirements under most worst conditions of temperature, mechanical vibrations, and electromagnetic compatibility [38]. The OCTs and OVTs play a sensing and digitizing role for current and voltage information with the processing capabilities of digital electronics.

The designs of digital output interface of OCTs and OVTs are based on IEC/IEEE standards. The sensed current and voltage measurements are transmitted to them as optical digital signals. Therefore, the primary equipment and substation system wiring can be simplified due to extensive use of optical fiber for communication of current and voltage information and operating commands [41].

3.7.1 Hybrid Current Transformers

At present, this type of device tries to explore the combination of the optical fiber current transformers and the conventional current transformers. The main advantage is that as the insulation is provided by the optical fiber itself, and the cost of the insulation needed for a conventional current transducer would be greatly reduced [42]. Electronic current transformers (ECTs) with a Rogowski coil have been developed, which bring simple insulation structures and excellent dynamic performances to electronic instrument transformers.

The ECT is based on the principle of a Rogowski coil by taking into account of saturation free characteristics and economical efficiency. The Rogowski coil is a coil distributed uniformly in a non magnetic core that surrounds the conductor carrying the current to be measured. The sensing coil consists of the wire group wound and internal return wire loop in the opposite direction. This arrangement ensures excellent suppression of external magnetic fields.

Compared with the traditional CTs, Rogowski coil current transducers (RCCTs) have many merits because the absence of a ferromagnetic core virtually eliminates circuit loading and saturation concerns. Therefore, these transducers have been researched and designed to replace the traditional CTs [43–45]. They have an excellent transient response capability. Moreover, Rogowski coils can produce a safe low voltage (LV) output eliminating the hazards associated with misalignment and open secondary windings. In addition the variety of diameters and current ranges available allows the user to carry only one lightweight probe for a wide range of applications. Therefore, their use has increased very recently in applications of power electronics relay protection, and power quality measurements or transients. As for the electronic voltage transformer EVT, a capacitive voltage divider of high reliability and simple insulated construction is applied. The sensing units are arranged near the Rogowski coil and the capacitive voltage divider to each bay and one Merging Unit (MU) is provided to get the secondary information. The interface between sensing unit and MU is provided by the optical fiber connection. The MU is connected to the process bus via optical fiber. Optical fibers are well suited for transmission in HV environments by virtue of their all dielectric construction. They are highly resistant to electrical break-down and electromagnetic interference. Due to the working in HV

environment, the ECT is designed as two standalone units mutually interconnected only via the optical fiber. The real-time data is sampled at the HV side unit and transferred through the optical fiber to the MU. The principal diagram of the ECT is shown in Figure 3.8.

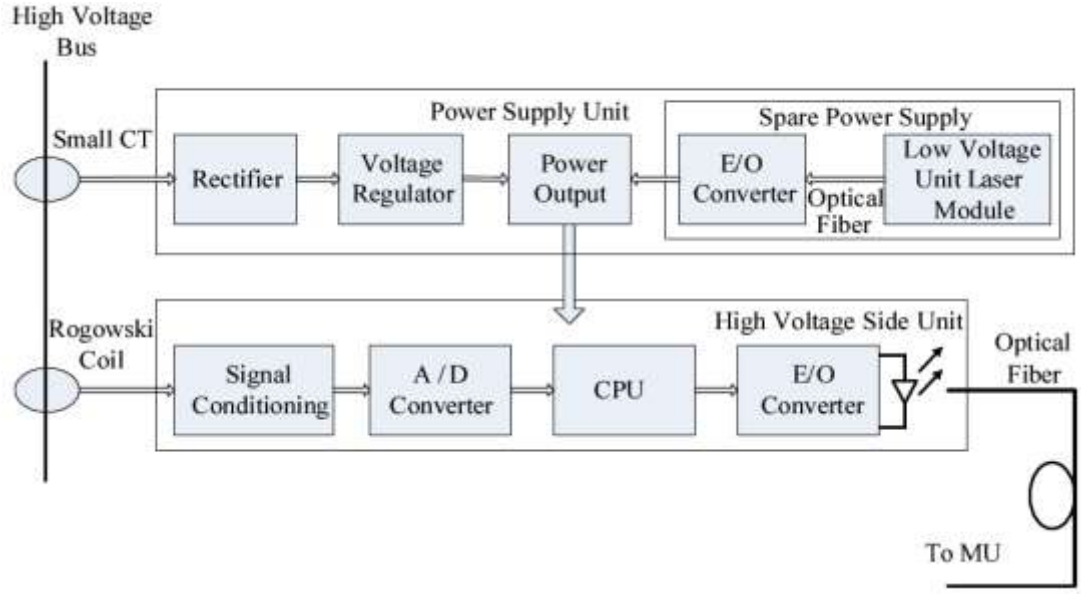

Figure 3.8 Schematic diagram of the ECT with a Rogowski coil

3.7.2 Optical Voltage Transformer

Voltage transformers (VTs) and capacitive voltage transformers (CVTs) are commonly used in high-voltage and extra-high-voltage grids. However, VTs are confronted with problems like large volume, ferroresonance phenomena, and increasing insulation difficulty as voltage grade increases [37].

However, such transformers have the fundamental disadvantage that saw tooth oscillations tend to appear and the suppression of these oscillations requires additional devices that entail rather considerable additional cost. Moreover, compared with VTs, CVTs have more advantages due to their simple insulation structure and high performance-price ratio.

Nevertheless, CVTs have poor transient responses because they contain coupling capacitances, intermediate transformers, compensation reactors, and other energy storage elements. Moreover, high-frequency oscillation caused through ferroresonance easily occurs on the secondary side, which will threaten the safe operation of the apparatus [56]. The optical voltage transformer (OVTs) based on electro-optic effect utilize the knowledge that linearly polarized light which passes

through materials that are situated in strong electric or magnetic fields, is rotated in its polarization plane with respect to the field. OVTs are based on the Pockels Effect have numerous advantages, such as high measuring accuracy, good safety, and avoidance of electromagnetic field interference.

The basic principal of the OVTs is to modulate the irradiance of the light directed to the OVT by an optical fiber according to the potential difference between the HV-line and the ground potential. The modulation of the light is accomplished by placing a material that has an optical property, which is sensitive to the electrical field strength (Pockels effect) inside the OVT. The basic principle of OVT is illustrated in Figure 3.9. The OVT consists of three lenses, a polarizer, a quarter-wave plate, a Pockels cell and an analyzer. The measuring principle is based in the so-called Pockels effect.

A high voltage is applied between the upper and bottom electrodes of the Pockels cell. These voltage is selected by a capacitor divider. Then a light, which intersect perpendicularly the applied voltage, is conducted through the Pockels cell.

The light beam is emitted from laser with a constant intensity and it is collimated with the lens and linearly polarized through the polarizer. The quarter-wave plate changes the linearly polarized light to a circular one. Then the circular polarized light is change to an elliptically light in the Pockels cell by the linear electro-optic effect which is called the Pockels effect.

Then the circular polarized light change to a elliptically light in the Pockels cell by the linear electro-optic effect which is called the Pockels effect. This ellipticity of the elliptically polarized light is split into two components polarized perpendicular to each other by the analyzer, the optical axis of which makes an angle of 90^{o} with that of the polarizer, the light beams split into two components are guided to two photo detectors through lenses and optical fibers.

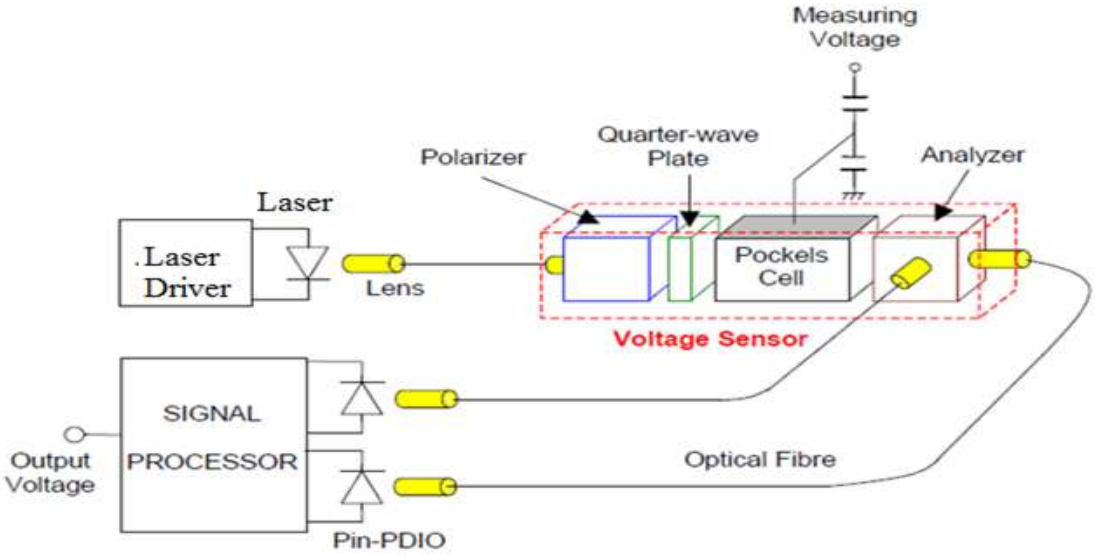

Figure 3.9 Schematic Configuration for Optical Voltage Transformer

Assuming that the ellipticity is much smaller than one, intensity I_1 and I_2 of the light beams measured with two photo detectors is given as follows in (3.3) and (3.3.4).

$$I_1 = \frac{I_o}{2}(1 + m_v \,.\sin(\omega.t) \tag{3.3}$$

$$I_2 = \frac{I_o}{2}(1 - m_v \,.\sin(\omega.t) \tag{3.4}$$

where, I_o is light beam intensity in front of the analyzer and ω is angular frequency of the applied voltage . The modulation depth of component light m_v is given by (3.5)

$$m_v = \frac{2\pi.n_o^3\gamma_{41}.l.V_{in}}{2\lambda.d} \tag{3.5}$$

Where, n_0 is refractive index of Pockels cell without applied voltage

V_{in} is amplitude of applied voltage,

γ_{41} is electro-optical coefficient of the Pockels cell

l is optical path length of Pockels cell

d is distance between electrodes

Both signals are driving to the signal processor unit where the following calculation is carried out and the output voltage V_{out} is obtained by (3.6).

$$V_{out} = \frac{I_1 - \bar{I}_2}{\bar{I}_2} - \frac{I_2 - \bar{I}_2}{\bar{I}_2} = k.V_{in}.\sin(\omega.t) \tag{3.6}$$

Then the applied voltage $V_{in}.\sin(\omega t)$ can be measured by detecting the output voltage *Vout*.

The optical voltage transformer comprises crystal, the distribution of refractive index of which depends on electrical field, wires for leading the electric field onto the surface of the crystal. The polarizers aligned on both sides of crystal, and phase shift phase to detect changes in the distribution of the refractive index, and optical fibers for routing light through the construction formed by polarizers and the crystal. The inner cavity surrounding crystal of the sensor is filled with a transparent material that has low extinction coefficient and dielectric constant, such as silicone [57].

3.7.3 Optical Fiber Current Transformers

Electrical current measurements are of fundamental importance in power networks and particularly where they are used for relaying, metering, control, and monitoring purposes. While the conventional CTs have performed on the whole is quite well since the late 1800's. Nevertheless, their performance limitations and other failures have provided an impetus towards using other methods.

Recent demands for higher voltage electric power systems have led to an increase in the size and cost of the conventional CTs. The saturation of the iron core tinder fault current and the low frequency response of the conventional CTs make it difficult to obtain accurate current signals under transient conditions and it also reduces the dynamic range of the CT. Moreover, with digital control and numerical protection relay being introduced into power systems. The conventional CTs have caused further difficulties, as they are likely to introduce electromagnetic interference (EMI) through the ground loop into the digital systems. The elimination of EMI in the current measuring system is therefore required.

With this growth in the capacity of electric power systems, the role of a superior performance protection relaying systems are becoming more significant. Such a system can immediately recognize any sudden failures, such as a surge, and disconnect the failure parts from the power systems.

Moreover, with the super increase in voltages (several hundred kV) in power transmission systems, the insulation of the CTs becomes more difficult and

expensive. Hence, optical current transformers (OCTs) that do not suffer from electromagnetic interference are good substitutes for conventional CTs.

In addition to protection relaying systems, the deregulation and growth of independent power producers and regional transmission companies have created a need for many new high voltage revenue-metering points [8].

Hence the potential use of optical CTs that provide high accuracy is promising and their concept is quite old [9]. Optical CTs are based on the Faraday rotation effect, which states that the polarization of light waves is rotated with the propagation of the light along (or opposite to) a magnetic field inside some material. Optical Fiber Current Transformers (OFCTs) are not the only optical CTs. Bulk-optic CTs such as flint glass closed-loop type and crystal based (Faraday cell) CTs have also been extensively studied and tested.

The sensitivity of OFCTs is depending on Verdet constant, which indicates the rotation angle of the polarization per unit magnetic field per unit propagation length. Compared with the bulk devices, the Verdet constant of optical fibers is quite small, but the optical path length can be increased to compensate for it by winding the fiber around a current conducting element a large number of turns. Although, the bulk-optic CTs provide better mechanical stability and smaller sizes, OFCTs provide ease in forming a closed-loop (to make the transformer respond only to the enclosed current), adjustability of the sensitivity and dynamic range, less insertion loss, and a higher signal-to-noise ratio (SNR). In OFCTs, linearly polarized optical waves are input to the optical fiber coil. The linear polarization can be expressed mathematically as a superposition of two circular polarizations (right-hand and left-hand). The magnetic field induced around a current carrying element induces a circular birefringence inside the optical fiber coil. Hence, after passing through the coil, a relative phase difference between two circular polarization components is generated, which results in the rotation of the linear polarization angle in proportion to the enclosed current and the number of fiber turns. Although the concept is quite simple, in actual implementation, several difficulties that limit the resolution of the sensor systems are encountered. Optical fibers have some linear birefringence due to the imperfection of the core shape, which may distort the output signals of OFCTs. Linear birefringence of the optical fiber caused by bend and packaging is a problem

that has plagued OFCT utilizing the Faraday Effect. It causes a reduction in the measured Faraday rotation due to the non-zero differential phase between the eigenmodes of the birefringent fiber. Annealing can reduce this linear birefringence considerably [38]. Nevertheless, it has a difficulty in practice because the annealing is generally done after the winding process of the fiber coil. An inevitable linear birefringence, induced by bending of optical fiber around the current-carrying element, exists. Moreover, the effects of vibration, mechanical stress or strain and temperature variation on the linear birefringence are also critical. Several techniques have been proposed to cope with these problems.

Through the progress of researches and developments of optical fiber current transformers for a long time, the stability of performances, simplification of structures, and reduction of manufacturing costs have been recognized as common subjects for the widespread of the practical application of the technology. In the developed sensing technology, these subjects are achieved using special fiber type as a sensing element that is used to improve the stability of optical system and simplicity signal processing approaches.

Nowadays there is a great diversity of optical current transformers, taking into account the sensing mechanism employed and the materials used, OCTs can be organized in four main groups as follows:

1. All-fiber Current Transformer (OFCTs): The fiber itself acts as a transducer mechanism. The magneto-optical effect (or Faraday Effect) is used to induce a rotation in the angle of polarization of the light propagating in the fiber, which is proportional to the magnetic field. Usually, the fiber is coiled around the electrical conductor, making it immune to external currents and magnetic fields.
2. Bulk optic Current Transformer: These sensors use a piece of glass or crystal with high Verdet constant as the transducer, which is placed near (or around) the electrical conductor. The magnetic field is also measured using the magneto-optical effect. These sensors are usually cheap, robust and more sensitive.
3. Magnetic force Current Transformer: In an analogous process to the piezoelectric elements, when a magnetic field is applied to a magnetostrictive

element it induces mechanical changes in the material. These changes can be again measured by attaching a Fiber Bragg Grating (FBG) to the magnetostrictive element.

4. Hybrid Current Transformer these type employ some of the standard electromagnetic technology already existent and some of optical technology. In this case, the first current transducer is done with conventional electromagnetic technology (such as, a Rogowski coil) but its interrogation and information transportation is done by an optical fiber system. The objective of these sensors is to construct an interrogation system that takes advantages of the high level of electrical isolation offered by optical fibers and avoids difficulties associated with birefringence.

3.7.3.1 Optical Fiber Current Transformers Principles

The Faraday Effect was the first magneto-optical effect to be proposed and demonstrated in optical current transformers. The Faraday Effect sometime referred to as Faraday rotation which is based on interaction between the external magnetic field and the oscillation of the electrons in the medium. The Faraday Rotation Effect which states that the polarization of light waves is rotated with the propagation of the light along (or opposite to) a magnetic field inside some material is optical fiber current transformer principles.

Assume that a linearly polarized wave, which can be considered as superposition of one left-hand circularly polarized wave and one right hand circularly polarized wave, enters a medium. Circularly polarized light will cause the electrons to rotate around their respective nucleus and the charge polarization will be proportional to the radius of this circle [20]. That the angle of rotation of linearly polarized light is proportional to the strength of the magnetic field and the cosine of the angle between the field and the propagation direction of the light wave. This rotation can be expressed mathematically by (3.7).

$$\varphi = \int_{L} V\vec{B} \,.\, dl \tag{3.7}$$

where, φ is the angle of state of polarization, $\boldsymbol{V}$ is the material Verdet constant, which is both dispersive and temperature dependent [18], $\boldsymbol{B}$ is the magnetic flux density vector and *dl* is the differential vector along the direction of propagation. This effect is called the Faraday Effect or linear magneto-optic effect and can be used to build optical current sensors. Figure 3.10 illustrates the polarization rotation due to a parallel external magnetic field on a magneto-optical material, such as, glass.

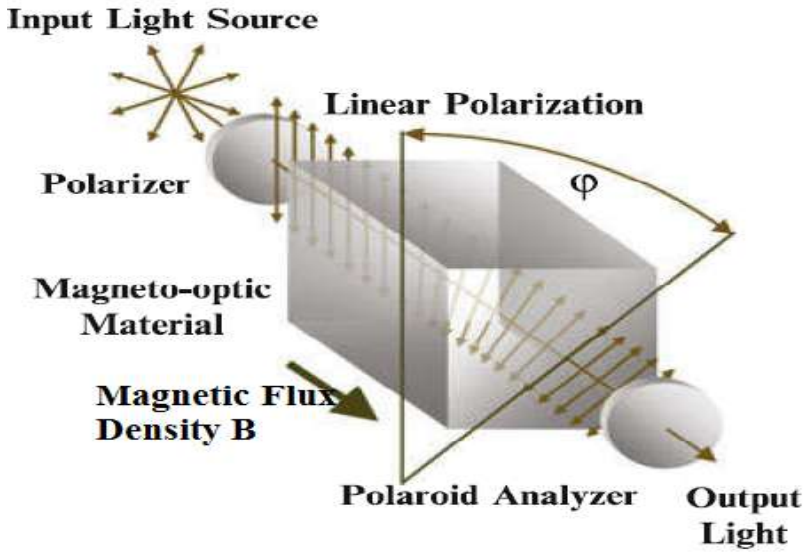

Figure 3.10 Faraday Effect in linearly polarized light

The Faraday Effect is distinct from the inherent circular birefringence that appears in some materials, in that its sign depends on the direction of the magnetic field with the respect to the direction of propagation of the light [59]. The Faraday Effect occurs in many solids, liquids, and gases. The magnitude of the rotation depends upon the strength of the magnetic field, the nature of the transmitting substance, and Verdet constant, which is a property of the transmitting substance, its temperature, and the frequency of the light. The direction of rotation is the same as the direction of current flow in the wire of the electromagnet, and therefore if the same beam of light is reflected back and forth through the medium, its rotation is increased each time [14]. The Faraday Effects is non-reciprocal. Therefore, if the same light passes through the same medium, but with opposite propagation direction, the rotation of polarization will be cumulative The Faraday Effect is present, to some extent, in all materials and its characteristics are related to the other magnetic properties of the material. It varies with temperature, much more in paramagnetic and ferromagnetic than in diamagnetic

materials. It is linear with magnetic field in diamagnetic materials but saturates in ferromagnetic materials, and its magnitude generally diminishes with increasing wavelength.

The sensitivity of OFCTs depends on Verdet constant. This constant is an optical constant that describes the strength of the Faraday Effect for a particular material. The Verdet constant indicates the rotation angle of the polarization per unit magnetic field per unit propagation length. The Verdet constant characterizes the capability of a transparent medium to rotating the sensitivity to magnetic fields tend to have the greatest temperature dependence polarization plane in a magnetic field. The Verdet constant is also wavelength dependent and will be affected by temperature. In order to keep high sensitivity for the sensor a stable Verdet constant is required which in turn will put certain requirement on both the material and the wavelength of operation. The value of the Verdet constant is determined by some coefficients of the optical medium and the input wavelength.

The Verdet constant determines magneto-optic properties of medium in which light beam propagates. It depends on the wavelength (λ) which can be described by (3.8).

$$V = -\frac{e\lambda}{2mc}\left(\frac{d\mathrm{n}}{d\lambda}\right) \tag{3.8}$$

Where, $\left(\frac{d\mathrm{n}}{d\lambda}\right)$is the dispersion of intrinsic index which indicates that the Verdet constant is linearly proportional to the dispersion of the material and *e* and *m* are charge and mass of an electron respectively, *c* is the speed of light in vacuum. The refractive index (n) of the medium depends on wavelength (λ) according to Cauchy's equation [60] and is given by (3.9).

$$n = a + \left(\frac{b}{\lambda^2}\right) \tag{3.9}$$

Where, *a* and *b* are constants. Combining equation (3.8) and (3.9), yield the Verdet constant as a function of wavelength is given by (3.10).

$$V(\lambda) = \frac{K_1}{\lambda^2} \tag{3.10}$$

Where, $K_1 = e.b/m.c$ is the constant

Therefore, the Verdet constant is inversely proportional to the wavelength squared as shown in (3.10).

3.7.3.2 Optical Fiber Current Transformer Configurations

Several different configurations have been proposed in order to detect the Faraday Effect. Generally, they are two main detection schemes that can be employed:

1. Basic Polarimetric Detection Configurations.
2. Dual Quadrature Polarimetric Detection Configuration.
3. Interferometric Configurations.

These two configurations will be described as well as the components and their unique qualities, followed by an outline of the birefringence problem and noise sources, and ending with a review of novel materials.

1. Basic Polarimetric Detection Configuration

Different signal analysis techniques can be used to quantify the Faraday rotation of the azimuth of the output light from an optical current sensor. One way to detect this rotation is by using a polarimetric detection scheme, which consists of two polarizers, one at the input of the sensor acting as polarizer and the other at the output acting as analyzer. Where the angle offset between the transmission axes of the polarizer and analyzer is aligned at 45° by a polarization controller (PC). The arrangement of the basic detection scheme is illustrated in Figure 3.11. The first polarizer has the objective of defining the initial polarization state of the light wave and the second polarizer is used to adjust the sensor sensitivity and transforms the polarization rotation into a light intensity modulation that can be measured using a photodetector [61].

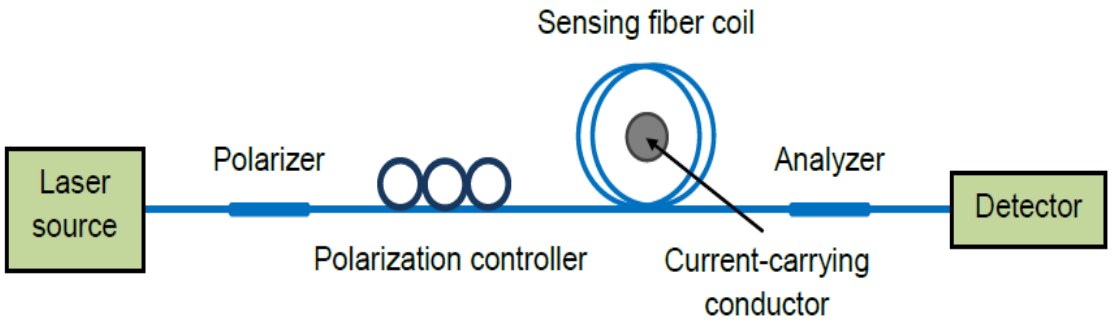

Figure 3.11 Polarimetric Detection Scheme

According to Malus law, when two polarizers are in such arrangement, the intensity of the output light is given by (3.11).

$$I_{out} = I_{P1}.\cos^2(\varphi) \quad (3.11)$$

Where, I_{P1} is the light intensity after the first polarizer and where φ is the angle of state of polarization is the relative angle between the transmission axes of the polarizers. The maximum sensitivity is achieved when this angle is 45°. This means that with the polarizers having a relative angle of 45°, any small change in the plane of polarization of the light, in the path between the two polarizer's, induced by an external magnetic field, will be transformed in a larger change of intensity at the output. Adjusting the polarizers for the maximum sensitivity, the OFCT transfer function is expressed as in (3.12) [61].

$$I_{out} = \frac{I_{in}}{2}[I_{P1}.\sin(2\varphi)] \quad (3.12)$$

In order to eliminate the dependence of the sensor response to the input laser source intensity fluctuations, the final processed output signal can be obtained by normalized the AC component by the DC component that is expressed as in (3.13).

$$S_{AC} = \sin(2\varphi) \quad (3.13)$$

The basic polarimeter would require calibration when the sensing fiber coil contains non-negligible linear birefringence. The polarized light propagates along both axes of the birefringent fiber due to a possible interface angle-offset and Faraday rotation. Unless the transmission axes of the polarizer is aligned at 45° to that of the birefringent fiber axes such that one of the fiber axes is aligned with that of the analyzer, the two beams with different phase delays may produce unwanted interference effects at the analyzer.

2. Dual Quadrature Detection Configuration

Another improvement of polarimetric detection scheme is the Dual Quadrature Scheme, this configuration is represented in Figure 3.12. Linearly polarized light propagates through the fiber as sensor element. While propagating through the fiber coil, the plane of polarization of the light rotates in the presence of a magnetic field. At the output end of the polarizer beam splitter (Wollston Prism), that separates two orthogonal polarizations in two distinct outputs, S_1 and S_2. These two signals are detected by two independent photodetectors and processed by an analog circuit that computes the output signal ***S***, given by (3.14). To obtain maximum sensitivity, the relative orientation between the polarizer and the input polarization has been adjusted to 45°.

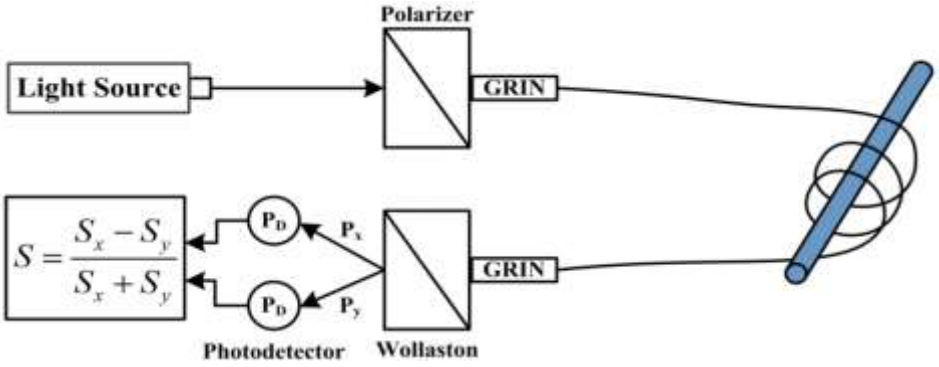

Figure 3.12 Schematic of the dual-quadrature polarimetric

Instead of using a Wollaston prism, it is possible to use a fiber coupler to divide the signal into two polarized states at ±45° with respect to the input polarizer, and allowing the generation of two output signals with opposite phase. This dual quadrature scheme offers enhanced common noise rejection than the previous one. When the Faraday rotation is relatively small and the linear birefringence (β) effect is included in the sensing element, and then the output signal can be calculated using (3.14).

$$S = \frac{S_1 - S_2}{S_1 + S_2} = \sin(4\varphi) \tag{3.14}$$

The two methods presented above do not take into account the linear birefringence effect, which as can be seen from (3.14), can greatly reduce the sensitivity of the sensor. Furthermore, because the linear birefringence (β) is usually temperature dependent, severe measurement errors can be introduced. In order to account for linear birefringence, it is necessary to introduce other detection methods that requires more sophisticated signal processing strategies.

3. Interferometric Detection Schemes

In the polarimetric detection scheme, the rotation of the plane of polarization of linear polarized light is analyzed. This rotation can also be analyzed in terms of circular polarization, corresponding to a phase difference between the two circular orthogonal modes (left-handed and right-handed circular polarization). This can be performed using an interferometric detection scheme where a modulation frequency carrier is generated, and the optical phase variation that is modulated by time delay induced between arms of the interferometer, will contain the electric current information. This phase carrier can be generated using an unbalanced Michelson or Mach-Zehnder

interferometer, or other interferometric configuration, such as Sagnac interferometer [8]. Figure 3.5 shows a Sagnac interferometer configured for the Faraday Effect, which is commonly used in gyroscopes and it is sensitive to non-reciprocal effects [62]. This interferometer is interrogated using a heterodyne detection scheme.

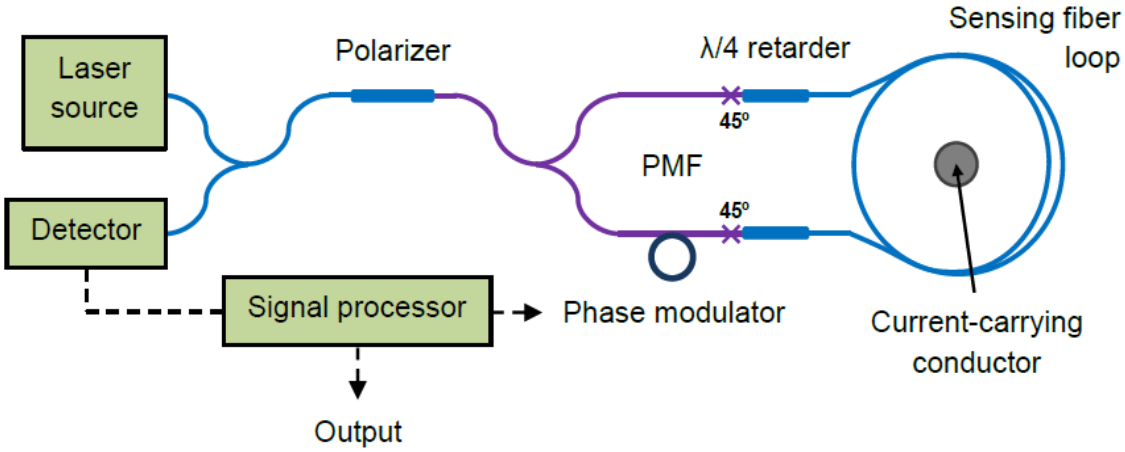

Figure 3.13 Sagnac loop interferometer current transformer

In this particular application, light from an optical broadband source, is linearly polarized with a fiber polarizer and is injected into the Sagnac loop with crossed λ/4-wave plates mounted at an angle of 45° and −45° relative to the plane of polarization of the linearly polarized inputs, for the upper and lower plate, respectively. In this configuration each of the counter propagating waves are converted to orthogonal circular states. These two counter propagating waves travel the Sagnac loop with different velocities, due to the external magnetic field induced circular birefringence. After crossing the loop, they are converted again into linear polarization modes and interfere after crossing the output linear polarizer. Finally, the two beams combine in the Polarizer Maintaining Fiber (PMF) to produce an optical power modulation at the polarizer.

$$P = \frac{P_o}{2}.(1 + \cos(\Delta\varphi)) \qquad (3.15$$

Using either Pseudo-Heterodyne or Heterodyne processing schemes, the relative phase accumulated in the Sagnac loop, which is proportional to the magnetic field generated by the electric current on the conductor, can be recovered. Some disadvantages of using this type of interferometer include temperature and vibration dependent sensitivities.

To enhance Sagnac loop interferometer current transformer operational performance characteristics the reflection configuration is proposed for linear birefringence compensation, using reflected light propagation have been presented, such as Faraday rotating mirrors which also doubles the sensitivity for the same fiber length. This proposed configuration is shown in Figure 3.14, a fiber polarizer is set at 45° with respect to the axes of the Polarization Maintaining Fiber (PMF). As a result, orthogonal linear polarizations along the two axes co-propagate towards the optical fiber coil. Prior to entering the optical fiber coil, the linear polarizations are converted into left- and right-circular polarizations by a quarter-wave retarder. At the end of the optical fiber coil, light is reflected by a Faraday rotator mirror (FRM) and passes through the optical fiber coil a second time. The quarter-wave retarder converts the returning circular polarizations back to orthogonal linear polarizations, which are also interchanged. Due to reflection configuration, the states of polarization swaps and each polarization component travels the optical path made by the other polarization. At the end, both polarization pass through the same optical path and compensate all reciprocal effects, but still maintaining a phase difference proportional to the electric current to be measured. This makes the configuration highly immune to external perturbations, as reciprocal phase noise and polarization dependent loss (PDL) tend to cancel themselves [63]. According, the double pass through the optical fiber coil, the current-induced non-reciprocal differential phase change is twice as large as that of the Sagnac configuration expressed by (3.16).

$$\Delta\varphi = 4\theta \tag{3.16}$$

In fact working with interferometers, means it is necessary to use a stable optical source, in addition to the modulation despite granting certain immunity to low frequency noise, limiting the system bandwidth. Another crucial problem is due to the phase difference introduced by the λ/4-wave plate that can have small deviations and as a result change the system sensibility [64].

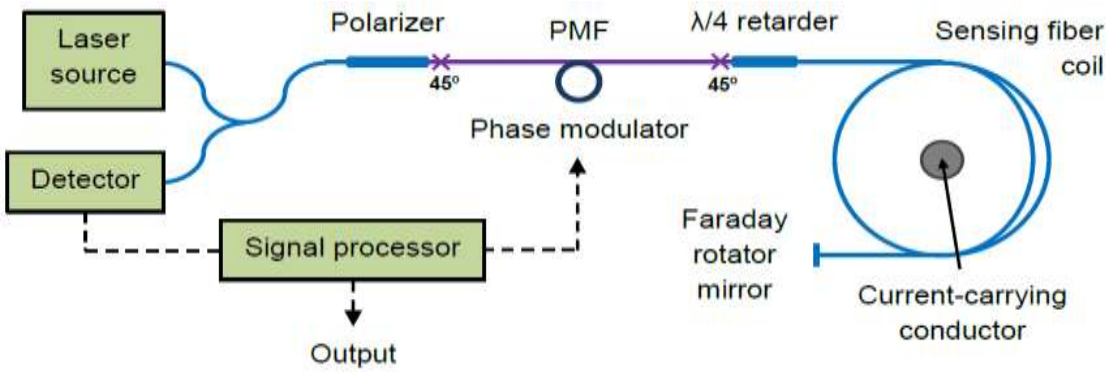

Figure 3.14 In-line interferometer current transformers

3.8 Summary

This chapter describes the basic theory of instrument transformers namely, the typical conventional instrument transformers designs, their characteristics and their impacts on signals distortions. Typical current transformer designs, as well as typical VT/CCVT designs were described from the stand-point of protection system. The problems associated with conventional instrument transformers on the power system protection were addressed. Main source of distortions with CTs is the saturation and main source of distortions with VTs/CCVTs is the subsidence transient and ferroresonance. Causes and mechanisms of mentioned distortions are discussed. Means of lessening their impact are also addressed. The conclusion is that impact of instrument transformer designs and characteristics on distortions may be significant. When the power system conditions are adequate, output signal can be significantly different from the scaled-down version of input signal. This presents motivation to investigate influence of distortions on protective devices and use of a novel measurement technique. The improvement needed is facilitated by emerging novel instrument transformer designs such as optical instrument transformers. The novel designs should be verified for correct supply of current and voltage signal replicas before being commissioned. The optical instrument transformer has been briefly reviewed. Further, a complete description of the OFCTs has been given, showing advantages and disadvantages of each detection configuration. In power system protection, configurations employing bulk materials and particularly Optical Fiber Current Transformers are the only ones commercially available for high power systems, providing better performances and depending on the configuration, immunity to external magnetic fields. The OFCTs based on the Faraday Effect which

is the most common optical effect used in current sensing, were evaluated using polarimetric detection schemes and interferometric detection configuration.

Optical instrument transformers have unique advantages such as high sensitivity, immunity to EMI, small size, lightweight, robustness, and the ability to provide multiplexed or distributed sensing.

Chapter Four
Modeling and Design

4.1 Introduction

Instrument Transformers are essential equipment in the chain of protection of the electrical power system. Their specification, usage, and placement must be optimized to eliminate failures during operation. Electrical networks involve complex designs that must incorporate safety of people, security, and availability of power supply.

This chapter aims to drive a mathematical model of the optical fiber Current Transformer from its principles of operation indicating the various detection configurations. Various optical components that make up the OFCT are modeled. The models, which are used to represent OFCTs, make certain approximations such as the birefringence induced in sensing fiber are neglected, optical power fluctuation and propagation loss are assumed to be neglected. These approximations arise partly out of a wish to determine the dynamic performance of OFCTs. Accordingly, it is desirable to reduce the complexity of the OFCTs model whilst maintaining an acceptable level of accuracy.

To eliminate linear birefringence that is induced by mechanical stress, thermal stress, manufacture imperfections, and other effects the OFCT with Faraday Rotation Mirror are redesigned using Jonse Matrix.

After that, the model of numerical relays are developed practically overcurrent and distance relays are also modeled, including algorithms of fault detection and decision making.

4.2 Optical fiber Current Transformer Modeling

The basic principal used in modeling and designing an optical current Transformer (OCT) is based on Faraday Effect. Generally OCT consists of an optoelectronic (OE) module which positioned in low voltage side mainly in control room, sensor head which is lay in high voltage side, and standard fiber cables in between. The schematic diagram of optical fiber current transformer, which employed dual polarimetric schematic detection configuration, is illustrated in Figure 4.1.

The optoelectronic module performs the tasks including sends polarized light to the sensor coil and receives the reflecting polarized light from the sensor coil. In addition, optoelectronic module compares intensity component of the polarized light in proportion to the magnetic field that induced by primary current and converts the resultant electrical signal into compatible form which digital devices.

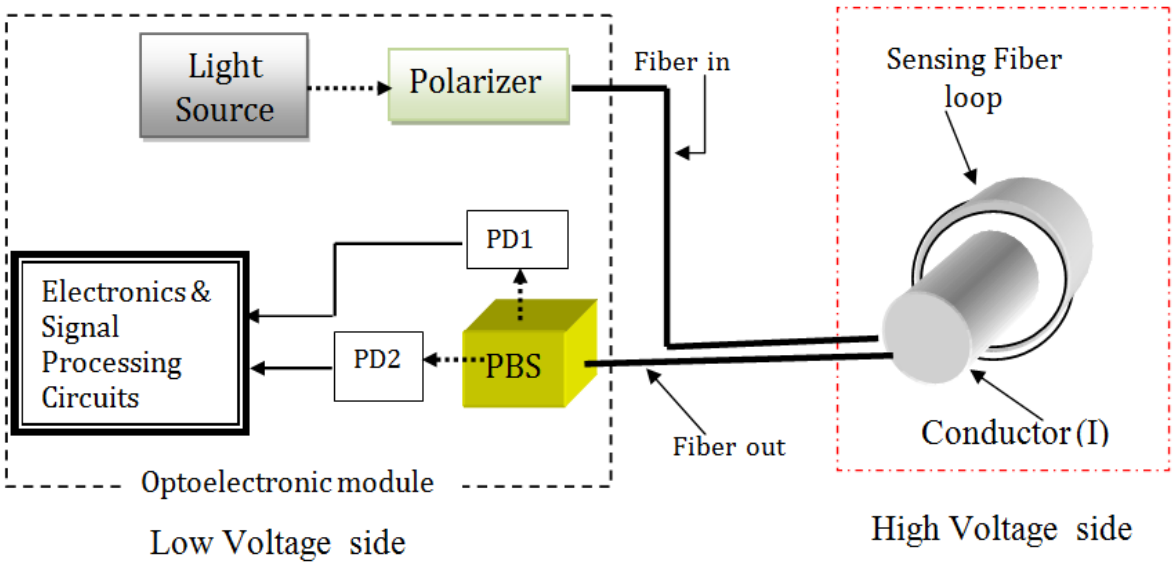

Figure 4.1 schematic diagram of Optical Fiber Current Transformer

The operation of optical current sensors based on rotation of polarization direction by the magnetic field paralleling with the direction of the optical beams. When the optical path is closed, the rotation angle of the polarization plane is in proportion to the product of the Verdet constant of the sensing materials and the current generating the magnetic field. For Optical Fiber Current Transformer, a magnetic field will be built up round the current-carrying Conductor, satisfying Ampere's circuital law. Therefore, the rotation angle φ in the fiber is expressed as in (4.1) [65].

$$\varphi = \oint Hdl = N_F V I_{elec} \quad (4.1)$$

where, N_F the number of turns of sensing optical fiber loop, I_{elec} is the electrical current in conductor and V is Verdant constant.

A laser beam is passing through polarizer to produces linearly polarized light. This linearly polarized light coupled into fiber sensing element, before passing through the Polarizer Beam Splitter (PBS), which converts the laser light into separate orthogonal linearly polarized light component. The electromagnet produces the magnetic field

proportional to current in the conductor. Accordingly, magnetic field rotates the linearly polarized light by an angle (φ) due to the Faraday rotation. Subsequently, PBS analyzer will send the horizontal component to the first photodetector (PD1) and the other vertical component of the optical power to the second photodetector (PD2). The photodetectors convert the light signal into an electrical signal. These signals are fed to an electronic signal processing circuits, depending on incident signals the output has been calculated [66] -[67].

Theoretically, Optical fiber current transformer consists of six operational subsystems: Laser Source, Polarizer, Fiber Sensing Turns, Polarizer Beam Splitter, and Signal Processing Circuit. In order to design and investigate appropriate operation performance each subsystem must be modeled individually.

4.2.1 Laser Source Model

Light source is a very important component in fiber optic system because its characteristics give an intense impact on the structure and performance of the whole systems. In optical fiber system, the common used laser sources are semiconductor laser diodes [68]. The electrical signal stimulates the laser diode emit correspondent optical signal transmitted through a fiber. It is very important to specify and determine the working condition of laser diode, specially the linear region of the laser diode because before and after the linear region laser diode response is nonlinear to the input signal.

The analysis of laser diode in an Optical Fiber System is focused mainly on the relationship between optical output power and the diode drive current, which has been dictated by rate equations. Due to the variety in the category of laser diode and mathematical models, many different forms of laser diode rate equations is found throughout the literature.

For optical fiber current transformer, the mathematical rate equations of laser diode are used as mathematical model for laser diode that is expressed as in (4.2), (4.3) and (4.4) [69].

$$\frac{dN(t)}{dt} = \frac{i(t)}{qV_a} - g_0 \frac{[N(t) - N_o]S(t)}{1 - \varepsilon S(t)} - \frac{N(t)}{\tau_n} \tag{4.2}$$

$$\frac{dS(t)}{dt} = \Gamma g_0 \frac{[N(t) - N_o]S(t)}{1 - \varepsilon S(t)} - \frac{S(t)}{\tau_p} + \frac{\Gamma\beta}{\tau_n} N(t) \quad (4.3)$$

$$\frac{d\phi(t)}{dt} = \frac{1}{2}\alpha_L \left[\Gamma g_0 [N(t) - N_o] - \frac{1}{\tau_p}\right] \quad (4.4)$$

Where, *i(t)* is laser current [mA], S(t) is photon density [m^{-3}], Γis optical confinement factor, g_o is slope gain[cm^{-3}/s], N(t) is carrier density [m^{-3}], $N_o$is carrier density at transparency[cm^{-3}], ε is gain saturation parameter [cm^3], τ_p is photon lifetime[s],β is spontaneous emission factor , $\tau_n$is carrier lifetime, V_a is volume of the active region[cm^3], α_L is line width enhancement factor, q is electron charge and $\phi(t)$ is phase of the laser electric field.

The Laser diode optical output power is expressed mathematically as in (4.5) [70].

$$P(t) = \frac{V_a \eta h\upsilon}{2\Gamma \tau_p} S(t) \quad (4.5)$$

Where, η is total quantum efficiency, υ is frequency of the laser [s^{-1}] and h is phase of the laser electric field [J.s]

The polarization of a given wave is determined by the electrical field. Laser Light is electromagnetic radiation and consists of both an electric field and a magnetic field. Laser light output can be express as the electric field as in (4.6) [71].

$$E_{laser}(t) = \sqrt{P(t)}.\, e^{i\phi(t)} \quad (4.6)$$

Light can be modeled in terms of transverse electromagnetic waves and its polarization corresponds to the variation of the electric field as a function of time, in a determined point of space, in the direction of propagation. Considering polarized light propagating in the z direction, the electric field can be represented as two orthogonal fields as in (4.7).

$$\vec{E}(Z,t) = \vec{E}_x(z,t) + \vec{E}_y(z,t) \quad (4.7)$$

4.2.2 Polarizer Model

Light can be either linearly, elliptically, circularly or randomly polarized. For linear polarized light, the orthogonal electric field components have same amplitude and a relative phase that is zero or multiple of π. A polarizer is a device that transforms natural light into polarized light. There are several devices that produce this effect, and they can be based on dichroism or selective absorption, reflection, scattering, and

birefringence or double refraction. As a common characteristic, they all have some form of asymmetry associated to the process of light propagation.

In optics, polarized light can be effectively described in an extremely compact mathematical form using Jones calculus. It can be viewed as simplified version of Mueller Calculus, which uses a full description of light by Stokes vectors. Thus, Stokes vectors can be used for the analysis of partially polarized or unpolarized light. However, in most cases the main interest is to analyze the propagation of polarized light, which is typical situation for the laser beam propagation. Then any arbitrary state of polarization *E* is written as a linear superposition of these two states has been expressed as in (4.8).

$$\boldsymbol{E} = \begin{pmatrix} E_x e^{i\phi_x} \\ E_y e^{i\phi_y} \end{pmatrix} \tag{4.8}$$

In optical fiber current transformer the laser beam x and y directions is ideally linear polarized. As a result, polarizer mathematical model is expressed as in (4.8) [72].

$$\boldsymbol{E}_{polarizer} = \frac{1}{\sqrt{2}} \begin{bmatrix} 1 \\ 1 \end{bmatrix} . \boldsymbol{E}_{laser} \tag{4.9}$$

4.2.3 Sensing Fiber Model

Figure 4.2 illustrates the sensor head used to detects the current via fiber optic cable. The refractive index of core fiber optic cable, Verdet constant, Faraday Effect, attenuation, and delay are taken into consideration during the modeling of sensing fiber head.

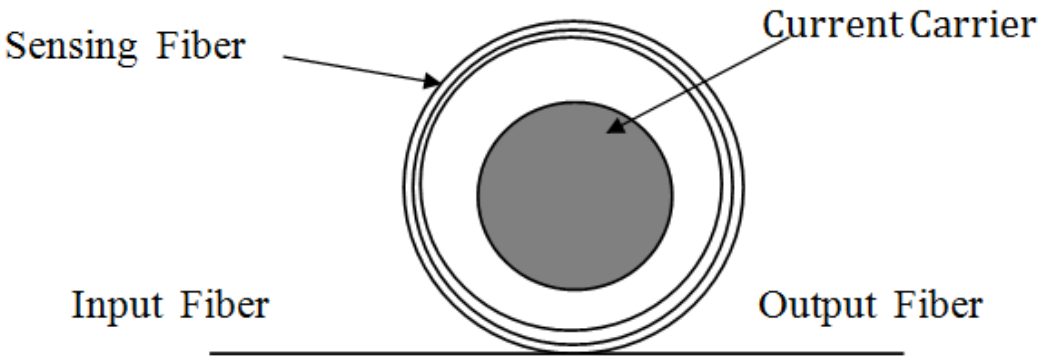

Figure 4.2 Sensing Fiber Turns

The rotation of the polarization azimuth angle $\boldsymbol{\varphi}$ induced by a magnetic flux density $\boldsymbol{B}$ that is produced by current through conductor is given by (4.10).

$$\varphi = \mu_o \oint_c B dl = \mu_o V N_F I_{elec} \tag{4.10}$$

Where, N_F is the number of turns of coil-shaped optical fiber sensor and $\boldsymbol{V}$ is Verdet constant, and $\boldsymbol{I_{elec}}$ is electrical current through conductor.

The fiber optic sensor with several turns around the conductor makes possible use of a sensitive sensor based on optical fiber with low Verdet constant [73].

The attenuation coefficient of the fiber is a function of fiber length at specific optical power of the laser is then given by (4.11).

$$\alpha(L) \approx \frac{1}{L} \log\left(\frac{P_{in}}{P_{out}}\right) \tag{4.11}$$

Where, $L = 2\pi N$ is the length of fiber [m] and $\alpha(L)$ is attenuation [dB/km]

Scattering losses in fiber depends on the material refractive index and the wavelength. Variation of the wavelength causes Rayleigh-type Scattering. The attenuation coefficient due to Rayleigh scattering, which is a function of the wavelength, is expressed as in (4.12) [60]

$$\alpha(\lambda) \approx 7.81 * 10^{11} * \mathrm{e}^{-\left(\frac{48.48}{\lambda}\right)} + \left(\frac{1}{\lambda^4}\right) \tag{4.12}$$

The attenuation of the electric field in the fiber it could be expressed as in (4.14)

$$\boldsymbol{E}_{alfa} = \boldsymbol{E}_{polarize} \cdot \sqrt{10^{-\frac{\alpha L}{10}}} \tag{4.13}$$

The refractive index of optical medium (n) is depends on the beam wavelength (λ) that mathematically represented by (4.14).

$$n = \sqrt{\left(1 + \frac{K}{1 - (\lambda_o/\lambda)^2}\right)} \tag{4.14}$$

where, *K* is wave vector [rad/m] and λ_o is wavelength in vacuum [m].

A classical electrodynamics approach gives an expression for Verdet constant, which is expressed as function of the wavelength of laser used and the change in index of refraction per change in wavelength. The Verdet constant (V) is calculated from (4.15) [60].

$$V(\lambda) = \frac{\pi}{\lambda}\frac{n^2(\lambda) - 1}{n(\lambda)}\left(A + \frac{B}{\lambda^2 - \lambda_o^2}\right) \quad (4.15)$$

where, A and B are constants which depend on type of optical material used in sensing head, $n(\lambda)$ is index of refraction at a given wavelength, and $\lambda_o$is initial wavelength.

The Jones matrix (M) is used to model the optical fiber loop and rotation of the plan of the polarized light by an angle φ is given by (4.16) [74].

$$M = \begin{bmatrix} cos\varphi & -sin\varphi \\ sin\varphi & cos\varphi \end{bmatrix} \quad (4.16)$$

4.2.4 Analyzer Model

An optical polarizer beam splitter cube is a device that is used to split a beam of light into two orthogonal components depending on polarization state. When a light beam inters the beam splitter, the beam splits into two components. These are the transmit radiation polarized type, which is referred-to by type "P", and the reflect radiation polarized type, which is referred-to by type "S". While the electric field intensity vector of type "P" is parallel to the plane of incidence beam that of type "S" is perpendicular.

The beam splitter is completely characterized by a unitary (2 × 2) matrix (***M)*** that describes how the device transforms the incident modes into the outgoing modes in the Heisenberg picture [75]. Neglecting linear birefringence in the fiber, Faraday Effect is similar to what is expressed in (4.16).

Small changes of optical rotation can be detected using a polarizer beam splitter that is called Wollaston Prism (WP). WP separates the magneto-optically rotated electric field vector E of the emergent light into two orthogonal components.

Depending on the photodetector input-output characteristics, the photodetector (PD_1, PD_2) outputs are proportional to square of the amplitude of electric field E^2 vector directed in the X-direction component E_{XR}^2 and the Y-direction component E_{YR}^2 respectively. In order to obtain maximum sensitivity the polarizer must be attuned at 45° clockwise with respect to X-axis of the polarized input light beam, the intensity (I_X , I_Y) of the components are expressed as (4.17).

$$I_X = \frac{1}{4}E_o^2 \cos(45^0 + \varphi) \quad (4.17a)$$

$$I_Y = \frac{1}{4}E_o^2 \cos(45^0 - \varphi) \quad (4.17b)$$

If both reflection and transmission output change is recorded synchronously, and heterodyne data processing is performed, the angle of state of polarization is given in (4.18) [49].

$$S = \left[\frac{I_X - I_Y}{I_X + I_Y}\right] = \sin(2\varphi) \quad (4.18)$$

4.2.5 Photodetector Optical Model

Silicon photodetectors are semiconductor devices responsive to high energy particles and photons. Photodiodes operate by absorption of photons or charged particles and generate a flow of current in an external circuit, proportional to the incident power**.** During the model of photodiode the responsivity and Low Pass Filter are taken into consideration. The responsivity of a silicon photodiode is a measure of the sensitivity to light, and it is defined as the ratio of the photocurrent $\boldsymbol{I_P}$ to the incident optical power $\boldsymbol{P}$ at a given wavelength which is expressed in (4.20) [76].

$$\mathcal{R}(\lambda) = \frac{I_P}{P} \quad (4.19)$$

In other words, it is a measure of the effectiveness of the conversion of the optical power into electrical current. It varies with the wavelength of the incident light as well as applied reverse bias and temperature. The optical power of light is expressed in (4.20).

$$I_{X,Y} = \mathcal{R}\left|E_{X,Y}\right|^2 \quad (4.20)$$

Where $I_{X,Y}$ photodiode current and $\mathcal{R}$ is responsivity of photodiodes [A/W]. Optical model of silicon photodiode is obtained by $\mathcal{R}$ (λ) replacement [77].

The output photodiode current of the receiver is directly proportional to the optical power reaching the PIN photodiode. By measuring the photodiode output voltage, the electric current through a conductor can be found. The optical power of these two light beams is converted into electrical voltage signals as in (4.21)

$$V_X = \mathcal{R}_X\left(\frac{1}{2}P_0\cos(45^0+\varphi)\right) \quad (4.21a)$$

$$V_Y = \mathcal{R}_Y\left(\frac{1}{2}P_0\cos(45^0+\varphi)\right) \quad (4.21b)$$

Where, $\mathcal{R}_X$ and $\mathcal{R}_Y$ are constants, which include all optical losses and the gain of the optical-electrical conversion. Photodiodes outputs must be normalized to obtained accurate electric current pass through conductor. Since, the differences normalized Sum operation (Δ/Σ) allows eliminating sources of noise common into output signals. Particularly, that comes due to instability of the optical source, vibrations and disturbances in the fiber connection. In addition, the power fluctuations of the optical source will be canceled out, whereas still yielding the information about the state of polarization rotation induced by the electrical current. The angle of polarization rotation is reconstructed by (4.22).

$$\varphi_{out}(V_X, V_Y) = \frac{1}{2}\arcsin\left(\frac{V_X - V_Y}{V_X + V_Y}\right) \quad (4.22)$$

Accordingly, the electrical current can be obtained by (4.23)

$$I_{elec} = \frac{1}{2VN}\arcsin\left(\frac{V_X - V_Y}{V_X + V_Y}\right) \quad (4.23)$$

One major error source is noisy input voltage signals V_X and V_Y. Hence, a sensitivity analysis is required to estimate the impact of noisy signals on φ .

4.3 Reflection Configuration Fiber Optical Current Transformer

The most critical problem of using the fiber as the sensing element in optical current transformer is the effect of the linear birefringence that is induced by mechanical stress, thermal stress, manufacture imperfections, and other effects. The presence of linear birefringence significantly reduces the sensor sensitivity due to the polarization state degeneration. Winding a fiber in loops leads unfortunately to mechanical stress and consecutively to linear birefringence formation in the fiber core. This linear polarization of coupled light wave transforms into elliptical polarization and OFCT sensitivity is decreased.

Some methods for linear birefringence suppression based on diverse principles have been published. The basic method utilizes a twisted single mode fiber [78]. The

twisting imposes a circular birefringence into a fiber. That means the rate of circular birefringence exceeds the rate of linear birefringence. For that reason, the OFCTs can be constructed with back light propagation for the birefringence compensation.

This approach exploits the non-reciprocity of Faraday Effect and the reciprocity of linear birefringence. In the real case, the power losses in the fiber and by the light reflection lead to the presence of residual linear birefringence, which can decrease the sensitivity. The orthoconjugate retroreflector (OCR) is used for the light reflection and polarization rotation, which is canceled out the undesirable linear birefringence in the sensing coil. The common term for this component is Faraday Rotator Mirrors (FRM) at the end of the sensing coil, which will rotate the polarization state with an angle of 90° and doubles the sensitivity for the same fiber length [78].

The schematic diagram of reflection structure fiber optical current transformer is shown in Figure 4.3. Then the mathematical model is established and effect of Faraday Rotation Mirror is analyzed using Junes Matrix.

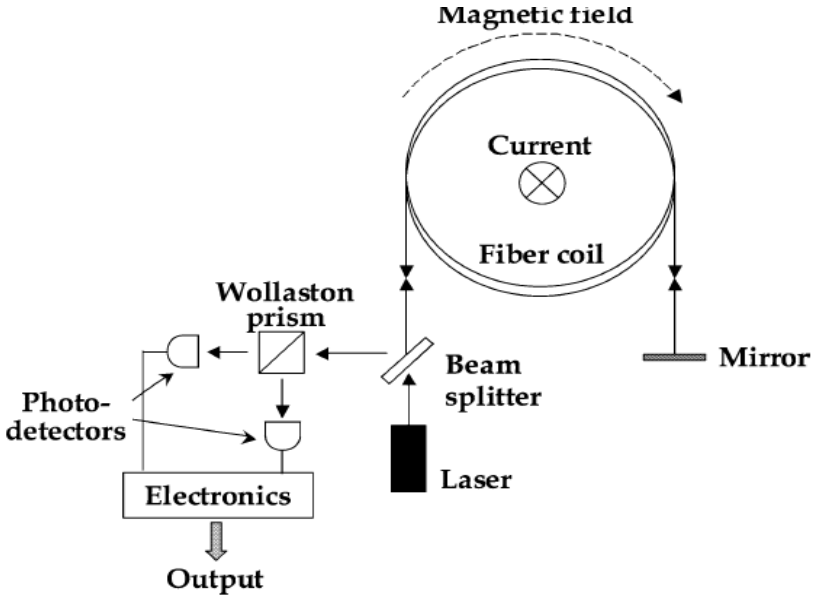

Figure 4.3 Schematics of Reflection Structure of OFCT

4.3.1 Faraday Rotation Mirror Model

In conventional fiber current transformer, the optical signal travels across the sensing head just once a time, whereas in a reflective fiber current sensor, it travels twice the distance because of the presence of a reflecting mirror, which reduces the linear birefringence. However, conventional silica fiber has a very low Verdet constant. In order to obtain a higher current sensitivity, a longer fiber is necessary for the

aforementioned structures; however, this increases the birefringence in the fiber core and reduces the actual sensitivity of the OFCT.

The Jones calculus is used to model optical fiber current transformer with FRM as shown in Figure 4.4. For the simplification, model does not take into account power losses in fiber and on the other optical components. In addition, it is assumed that the single mode fiber which is being analyzed is free from intrinsic linear birefringence [79]. This can be fulfilled for available fibers.

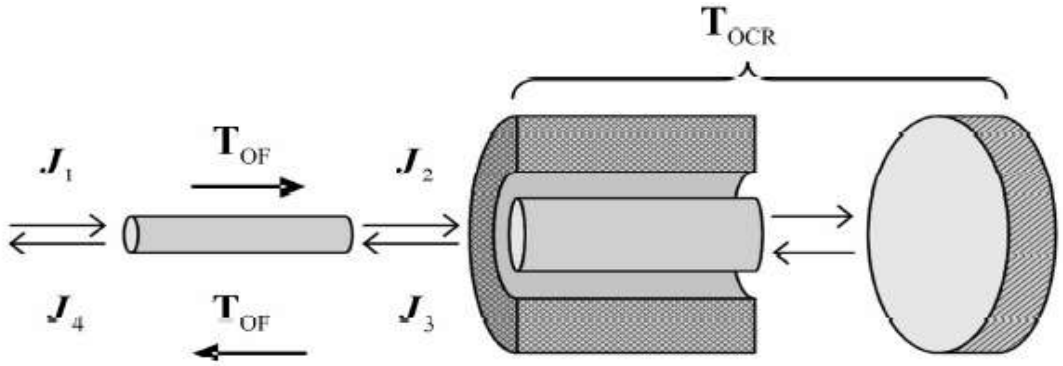

Figure 4.4 The Jones calculus Description of OFCT setup.

The Jones vector describes the light wave on the input of optical fiber is referredJ_1. Consider the polarization angle φ is equal to 45° compared to vertical. Then, the light wave passes the fiber loop described by the matrix T_{OF} and its polarization state is changed. Therefore, (4.24) and (4.25) give the resultant vector.

$$J_2 = T_{OF}.J_1 = \frac{1}{\sqrt{2}}\begin{bmatrix}\alpha + jB & -\gamma \\ \gamma & \alpha - jB\end{bmatrix}.\begin{bmatrix}1\\1\end{bmatrix}$$

$$= \frac{1}{\sqrt{2}}\begin{bmatrix}cos\left(\Delta + j\frac{\delta}{2}\frac{sin\Delta}{\Delta}\right) & -\phi\frac{sin\Delta}{\Delta} \\ \phi\frac{sin\Delta}{\Delta} & cos\left(\Delta - j\frac{\delta}{2}\frac{sin\Delta}{\Delta}\right)\end{bmatrix}.\begin{bmatrix}1\\1\end{bmatrix}$$

$$= \frac{1}{\sqrt{2}}\begin{bmatrix}\alpha + j\beta - \gamma \\ \alpha - j\beta + \gamma\end{bmatrix} \quad (4.24)$$

Where, $\Delta = \sqrt{\phi^2 + (\delta/2)^2}$ (4.25)

Δ is a geometric mean of phase shifts ϕ and δ which are imposed by the circular and unwanted linear birefringence [80]. The light wave J_2 has generally elliptical

polarization state and enters the OCR (T_{OCR}). The light wave passes the fiber in back direction then and on its close end. As a result (4.26) is yield.

$$J_4 = T_{OF}.T_{OCR}.J_2\ \varphi = \frac{1}{\sqrt{2}}\begin{bmatrix}\alpha+j\beta & -\gamma \\ \gamma & \alpha-j\beta\end{bmatrix}.\begin{bmatrix}0 & 1\\ -1 & 0\end{bmatrix}.\begin{bmatrix}\alpha+j\beta-\gamma\\ \alpha-j\beta+\gamma\end{bmatrix}$$

$$= \frac{1}{\sqrt{2}}\begin{bmatrix}\alpha^2+\beta^2+\gamma^2+2\alpha\gamma\ +j2\beta\gamma\\ -\alpha^2-\beta^2+\gamma^2+2\alpha\gamma-j2\beta\gamma\end{bmatrix} \qquad (4.26)$$

The resultant vector (4.24) is relatively difficult to analyze regarding to the investigation of birefringence. For the solution of this problem, the separate instances can be analyzed when only the linear or only the circular birefringence is present. The resultant polarization state is given by their superposition. Consider the presence of linear birefringence δ only ($\phi = 0$).

It is possible to modify the relation (4.26) and the resultant vector can be express as in (4.27)

$$J'_2 = T_{OF}.J_1 = \frac{1}{\sqrt{2}}\begin{bmatrix}\cos(\delta/2)+jsin(\delta/2) & 0\\ 0 & \cos(\delta/2)+jsin(\delta/2)\end{bmatrix}.\begin{bmatrix}1\\1\end{bmatrix}$$

$$= \frac{1}{\sqrt{2}}\begin{bmatrix}\alpha'+j\beta'\\ \alpha'-j\beta'\end{bmatrix} \qquad (4.27)$$

The back propagation of the light wave in the fiber is described by the vector J'_4as given in (4.28)

$$J'_4 = T_{OF}.T_{OCR}.J'_2 = \frac{1}{\sqrt{2}}\begin{bmatrix}\alpha'+j\beta' & 0\\ 0 & \alpha'+j\beta'\end{bmatrix}.\begin{bmatrix}\alpha'-j\beta'\\ -\alpha'-j\beta'\end{bmatrix}$$

$$= \frac{1}{\sqrt{2}}\begin{bmatrix}\alpha'^2+j\beta'^2\\ -(\alpha'^2+j\beta'^2)\end{bmatrix} = \frac{1}{\sqrt{2}}\begin{bmatrix}\cos^2(\delta/2)\ +\sin^2(\delta/2)\\ -(\cos^2(\delta/2)\ +\sin^2(\delta/2))\end{bmatrix}$$

$$= \frac{1}{\sqrt{2}}\begin{bmatrix}1\\-1\end{bmatrix} \qquad (4.28)$$

Thus, a linearly polarized wave at the close end of the fiber is obtained. The polarization state is rotated with an angle ϕ is equal to 90°. The influence of linear birefringence has disappeared. In the second instance, consider the presence of circular birefringence ϕ only (δ = 0) which is induce by the measured magnetic field. (4.29) describe the light wave at the far end of fiber.

$$J''_2 = T_{OF}.J_1 = \frac{1}{\sqrt{2}}\begin{bmatrix}\cos(\phi) & -sin(\phi)\\ -sin(\phi) & \cos(\phi)\end{bmatrix}.\begin{bmatrix}1\\1\end{bmatrix}$$

$$= \frac{1}{\sqrt{2}}\begin{bmatrix}\alpha'' + j\gamma''\\ \alpha'' - j\gamma''\end{bmatrix} \quad (4.29)$$

The back propagation of the light wave in the fiber is described by the vector in (4.30)

$$J''_4 = T_{OF}.T_{OCR}.J''_2 = \frac{1}{\sqrt{2}}\begin{bmatrix}\alpha'' & \gamma''\\ \gamma'' & \alpha''\end{bmatrix}.\begin{bmatrix}\alpha'' + \gamma''\\ -\alpha'' - \gamma''\end{bmatrix}$$

$$= \frac{1}{\sqrt{2}}\begin{bmatrix}\alpha''^2 + \gamma''^2 + 2\alpha''\gamma''\\ -\left(\alpha''^2 + \gamma''^2 + 2\alpha''\gamma''\right)\end{bmatrix}$$

$$= \frac{1}{\sqrt{2}}\begin{bmatrix}(\cos^2\phi - \sin^2\phi + \sin 2\phi)\\ -(\cos^2\phi - \sin^2\phi + \sin 2\phi)\end{bmatrix} \quad (4.30)$$

The terms $\sin 2\phi$ in (4.30) represents phase shift due to the circular birefringence induced by the magnetic field. The light wave travels through the fiber is twice experiencing a double rotation 2ϕ. On the output of the fiber, the polarization state can be evaluated by means of dual quadrature polarimetry.

Both components of vector J_4 can be detected using polarizer beam splitter. Optical power intensities of the waves and the voltages on detector's output are proportional to the square of electric field intensities in both channels. Consequently, the characteristics linear for a small rotation angles can be found.

4.3.2 Model of Reflection structure Fiber Optical Current Transformer

Considering the Jones matrices of the optical elements in Optical Fiber Current Transformer, the system transfer matrices that represent the final states of electric field of the light wave orthogonal components can be written as in (4.31).

$$E_{Xout} = M_P^X . M_Q^B . M_F^B . M_m . M_F^f . M_Q^f . E_{Yin}$$

$$E_{Yout} = M_P^Y . M_Q^B . M_F^B . M_m . M_F^f . M_Q^f . E_{Xin} \quad (4.31)$$

Where, E_{Yin} and E_{Xin} are inputs electric field of lights and E_{Xout} and E_{Yout} are the final states of the return electric field of light wave Jones vectors. M_Q^f and M_Q^B are quarter wave (circular polarizer) matrices for forward and backward travels respectively.

An additional multiplication factor (phase shifter) of $e^{j\left(\frac{\pi}{2}\right)}$ is added to matrices in order to make the calculations appropriate. M_m is the matrix for the mirror, M_F^f and M_F^B are Faraday Rotator matrices for the forward and backward travels respectively. M_P^X and M_P^Y are the reduced polarizer matrices from 2x2 to 1x2 where the zeros are eliminated to make calculations appropriate. The input light electric field and output electric field of each component using the Jones matrix representation can be expressed as in (4.32) and (4.33)[81].

.

$$E_{Xout} = [1 \quad 0]\frac{1}{\sqrt{2}}\begin{bmatrix}1 & j\\ j & 1\end{bmatrix}.e^{j(\pi/2)}.\begin{bmatrix}\cos(\varphi) & \sin(\varphi\\ -\sin(\varphi & \cos(\varphi\end{bmatrix}.\begin{bmatrix}-1 & 0\\ 0 & 1\end{bmatrix}.\begin{bmatrix}\cos(\varphi) & -\sin(\varphi\\ \sin(\varphi & \cos(\varphi\end{bmatrix}.\frac{1}{\sqrt{2}}\begin{bmatrix}1 & -j\\ -j & 1\end{bmatrix}.e^{j(\pi/2)}.\begin{bmatrix}0\\ 1\end{bmatrix} \quad (4.32)$$

$$E_{Yout} = [0 \quad 1]\frac{1}{\sqrt{2}}\begin{bmatrix}1 & j\\ j & 1\end{bmatrix}.e^{j(\pi/2)}.\begin{bmatrix}\cos(\varphi) & \sin(\varphi\\ -\sin(\varphi & \cos(\varphi\end{bmatrix}.\begin{bmatrix}-1 & 0\\ 0 & 1\end{bmatrix}.\begin{bmatrix}\cos(\varphi) & -\sin(\varphi\\ \sin(\varphi & \cos(\varphi\end{bmatrix}.\frac{1}{\sqrt{2}}\begin{bmatrix}1 & -j\\ -j & 1\end{bmatrix}.e^{j(\pi/2)}.\begin{bmatrix}1\\ 0\end{bmatrix} \quad (4.33)$$

In order to calculate the measured current the angle of the polarization ellipse is calculated using system transfer function in (4.32) and (4.33). Then, the intensity transmitted is proportional to the square of the amplitude of electric field and is thus given by (4.34).

$$I_{Xout} = \frac{1}{2}E_{Xout}^2[1+\cos(2\varphi+\phi_1-\phi_2] \quad (4.34)$$

Where, ϕ_i represents phase shift due to the circular birefringence induced by the magnetic field. The corresponding intensities of optical power (I_{out}) can be obtained [82], [83].

$$\begin{bmatrix}I_{Xout}\\ I_{Yout}\end{bmatrix} = \begin{bmatrix}sin^2 2\varphi.(E_{Xin})^2 + cos^2 2\varphi.(E_{Yin})^2 + 2sin2\varphi.cos2\varphi.(E_{Xin}.E_{Yin})\\ cos^2 2\varphi.(E_{Xin})^2 + sin^2 2\varphi.(E_{Yin})^2 - 2sin2\varphi.cos2\varphi.(E_{Xin}.E_{Yin})\end{bmatrix} \quad (4.35)$$

Formula (4.35) is mathematical model of reflection configuration fiber optical current transformer, it can be seen that the response of reflection structure fiber optical current transformer is proportional to the 2φ of the phase difference ϕ_i, since the phase difference is usually very small, in order to improve the measurement accuracy,

it typically use the phase bias and modulation. The signal processing is the ratio of the difference of the two polarization components to their sum gives in (4.36).

$$S = \frac{I_{Xout} - I_{Yout}}{I_{Xout} + I_{Yout}} \tag{4.36}$$

4.4 Electronic Signal Processing

The electronic signal processing system in the optical fiber essentially consists of the optoelectronic conversion circuitry, the signal demodulation scheme and the display. The optoelectronic interface is responsible for the faithful conversion of the optical signal into electrical form.

Electronic signal processing offers various critical advantages particularly in the ease of implementation. Techniques like amplification and filtering are easily applied if the signal is in electrical domain and improve system performance.

The most common semiconductor photodetector is the PIN photodiode, which is generating electrical current when they absorb photons. The amount of electrical current depends on wavelength of the light, size of the photodiode active area and responsivity of the photodiode. The current flowing through the diode is directly proportional to the intensity of the optical input. Low input current and offset voltage levels are the most important requirements on the operational amplifiers used in such sensitive photodiode applications [84].

The detection process begins with optical to electrical conversion and pre-amplification of the received signal. A diagram of a generic transimpedance amplifier for photodiode with its associated noise sources is illustrated in Figure 4.5.

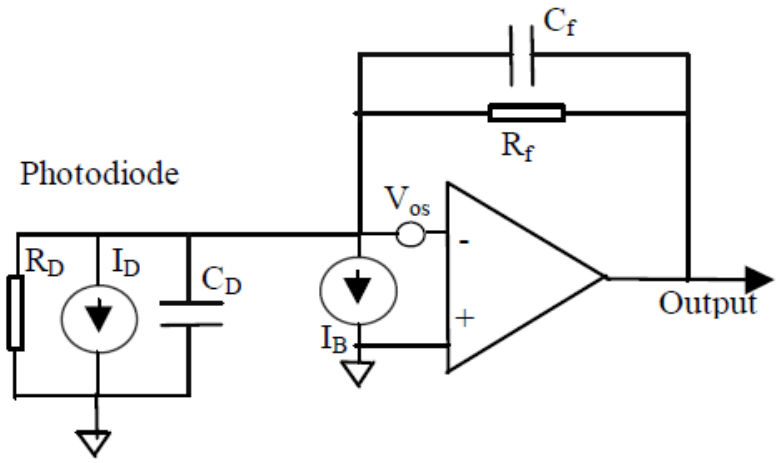

Figure 4.5 Equivalent Circuit of Photodiode Model with DC Error Sources

The fundamental limit of minimum current that can be detected is determined by the total noise in the system. All noise components are combined and equated with a noiseless signal. An expression for the minimum detectable current is then derived. Therefore, this will be used to determine the best case fundamental accuracy limit of OFCT. The total noise signal current is modeled as shown in (4.37)

$$i_n = \sqrt{i_{Sh}^2 + i_t R_f^2 + i_{na}^2 + (e_{na}/R_f)^2} \tag{4.37}$$

Where,

where,

$i_{Sh} = \sqrt{2qP_{AV}\mathcal{R}}$ is shot noise of detector.

$i_t R_f = \sqrt{4kT/\mathcal{R}}$ is thermal noise of feedback resistor.

i_{na} is input noise current of amplifier

e_{na} is input voltage noise of amplifier

q is electronic charge [$1.6 * 10^{-19}$ C]

k is Boltzmann's constant [$1.38 * 10^{-23}$J/°K]

T is Temperature [°K]

P_{AV} is average optical power striking detector [W]

$\mathcal{R}$ is Responsivity of detector [A/W]

The signal current generated in the detector and the incremental change in the signal as a result of the current being measured is expressed in (4.38).

$$\frac{dS}{dI} = \mathcal{R}\frac{P_0}{2}\left(2\varphi\frac{\sin\delta}{\delta}\right) \tag{4.38}$$

The minimum detectable current of the optical OFCT is dictated by the present noise at the detector output that is expressed in (4.39).

$$I_{noise} = \frac{\sqrt{i_{Sh}^2 + i_t R_f^2 + i_{na}^2 + (e_{na}/R_f)^2}}{\mathcal{R}P_o\mu V N_F \sin\delta/\delta} \tag{4.39}$$

The processing explained previously can be electronically implemented either in analog electronic circuit or by microprocessor Based System in order to obtain signals compatible with digital relay and metering circuits.

Using a microprocessor based signal processing scheme in optical fiber current transformer offer benefits such as increasing the signal processing accuracy and eliminates noise effects as well as enhancement of the system reliability and flexibility.

Figure 4.6 shows the electronic setup for the data acquisition (DAQ) of the optical current transformer response signals. The photodiodes convert the optical signal to an electric current. Each electric signal consists of two components:

1. An alternating current (AC) component, due to the effect of magnetic field in the fiber sensing loop
2. Direct current (DC) component, due to the light rectification.

Both components are amplified using a low input bias current operational amplifier. Reference voltage (V_{REF}) and high the resistance (R) value are used to enhance the amplifier gain to compensate DC component of the light, furthermore to accommodate the electric signal to the analog to digital converter (ADC) when the high current passes through the conductor.

The amplified signal is then filtered to avoid aliasing effects. Afterwards, the signal is sampled using a fast 16 bits ADC. The samples are processed using a digital signal processing algorithm on a FPGA device, which calculates Discrete Fourier Transform (DFT) of the current signal for each cycle the 50 Hz AC component and DC component .The DFT values are stored and used to generate suitable output signal for relaying or metering circuit [85].

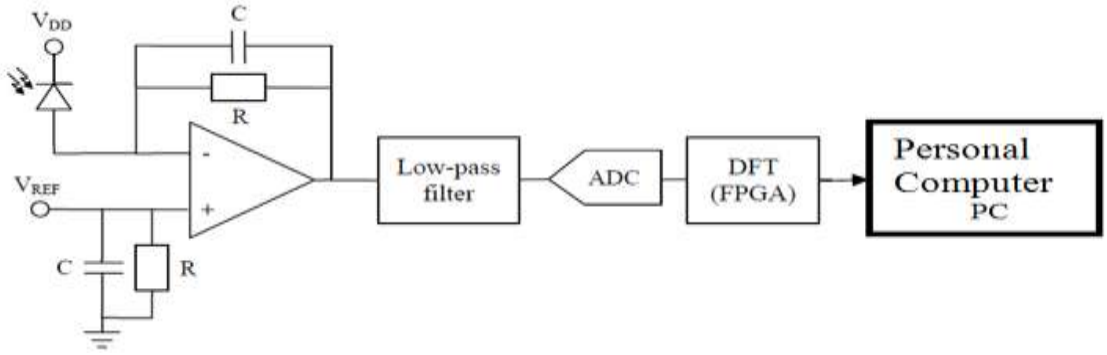

Figure 4.6 Data Acquisition of Optical Current Transformer Signals

4.5 Optical Fiber Current Transformer Bandwidth

Bandwidth of an OFCT is limited by the lowest bandwidth of its components. For the OFCT component, it is limited by the light transit time in the interaction length of the

fiber. Bandwidth limitation to ensure that the total transit time is much faster than the signal change rate. The fiber interaction length in the bandwidth consideration includes the roundtrip length around the conductor and includes the length to and from the OFCT based Faraday Effect [86], [87].

For the purpose of analysis the optical behavior that sets an upper limit on the detection bandwidth BW and an infinite electrical bandwidth of the current signal is assumed. The measurement bandwidth of OFCT based Faraday Effect with bulk glass or fiber coil sensing is limited by the transit time of the light in the sensing element then the bandwidth is nominally taken near the –3dB level of response and it is expressed as in (4.40)

$$BW_{3dB} = \frac{0.44}{\tau} = 0.44.\frac{C}{n}.\frac{1}{2\pi r}.\frac{1}{N_F} \tag{4.40}$$

where τ is transit time, *c* is the speed of light in free space, *n* is the index of refraction in fiber material, N_F is the number of turns in the fiber coil and *r* is the radius of the fiber oil [88].

The bandwidth limit of Faraday Effect current transformers, in most applications, is determined by the light transit time through the sensing coil [63]. Neglecting the effects of linear retardance and assuming pure Faraday rotation in the sensing element, the bandwidth response can be derived. The bandwidth of such a coil is limited by the propagation speed of light inside the material. The transfer-function of an optical fiber sensing coil is illustrated in (4.41) [89].

$$\varphi(\omega) = \varphi_0 \left[\frac{1 - e^{-j\omega\tau}}{j\omega\tau}\right] e^{j\omega\tau} \tag{4.41}$$

Where, τ is an optical fiber sensing coil transit time of optical signal.

The bracketed term is a damping factor which attenuates the zero modulation Faraday rotation φ_0. It can be shown that the magnitude of this function is given in (4.42)

$$\left|\frac{\varphi(\omega)}{\varphi_0}\right| = \left|\frac{\sin(\omega\tau/2)}{(\omega\tau/2)}\right| \tag{4.42}$$

When $(\omega\tau/2)$ = 886 the response is down to $0.707\varphi_0$, this can be defined as a theoretical 3dB of the sensing coil in hertz. For typical values of fiber core index, the frequency of the sensing coil is calculated by (4.43)

$$F_{3dB} = \frac{2.81 * 10^7}{D_C * N_F} \quad (4.43)$$

Where N_F number of is turns and D_C is diameter of the sensing coil [m].

4.6 Optical Voltage Transformer Model

Most optical voltage sensors are based on an electro-optic (EO) crystal and longitudinal Pockel effect. The problem in this case is the sensitivity of EO crystal, which is usually too high in comparison with the measured voltage. The conventional solution is to use capacitive dividers to obtain a small part of the total voltage on the optical voltage transformer [57]. However, the method limits the performance of the optical measurement technology due to the high cost and the stability problem of the capacitive dividers. Another method is to use the multi-segmented sensor, which consists of crystal slices and spacers of dielectric material [90]. The half wave voltage of the multi-segmented sensor is far larger than a single EO crystal in longitudinal modulation.

The orientation of Pockel cell used in the OVT is shown in Figure 4.7 when an electric field is applied on the of Pockel cell along the direction, the principle indexes of refraction are given by (4.44).

$$n_x = n_0 - \frac{1}{2} n_o^3 \gamma_{41} E \quad (4.44a)$$

$$n_Z = n_0 - \frac{1}{2} n_o^3 \gamma_{41} E \quad (4.44b)$$

Where, n_o is the refraction index of the ordinary ray, γ_{41} is the electro-optic coefficient and *E* is the value of the applied electric field strength.

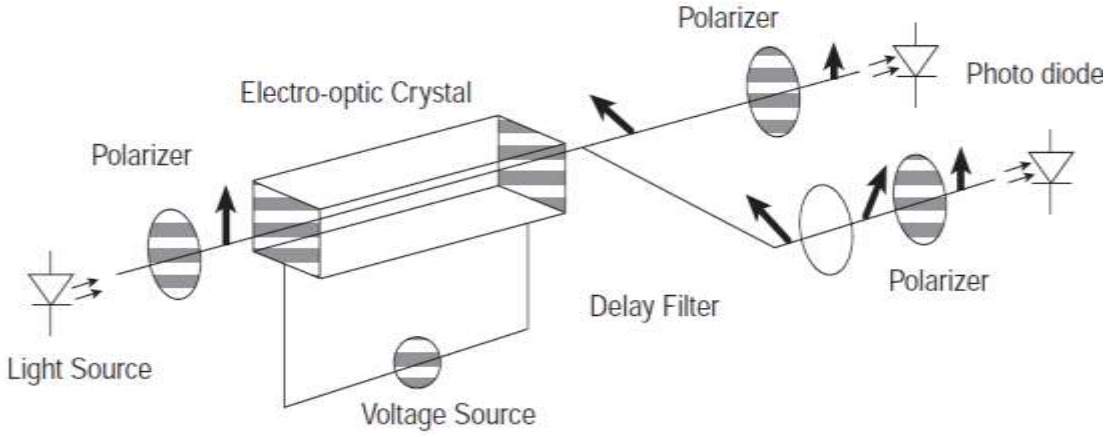

Figure 4.7 Optical Voltage Transformer Components

When a linearly polarized light enters into the Pockel crystal along the *Z* axis, it can be treated as two orthogonally linearly polarized lights along the *X* -axis and *Y* -axis, separately. As the two lights propagate within the crystal, they will experience different phase delays, which can be related to the optical path length difference. (4.45) give the phase delay.

$$\delta_x = (n_0 - n_x)\frac{2\pi}{\lambda}.l = \frac{\pi}{\lambda} n_o^3 \gamma_{22} E \quad (4.45)$$

Where, λ is the light wavelength and *l* is the length of the crystal along the light propagation direction.

If the electric field is obtained by applying a voltage *V* on the two faces of the pockel crystal, the induced phase retardation is expressed as in (4.45)

$$\delta_V = \frac{\pi}{\lambda} n_o^3 \gamma_{22} l.\frac{V}{d} = \frac{\pi V}{V_\pi} \quad (4.45)$$

Where, n_o^3 is refractive index, γ_{22} is electro-optic coefficient, *V* is electric field/voltage V_π is half-wave electric field/voltage and λ_o is free space optical wavelength.

The voltage V is calculated as the voltage across the crystals. The locations of the crystals in the inner tube and the voltages that the crystals are subject to are calculated according to their locations and used as the weighting factor.

The phase rotation angle of δ is in radian and should be less than 0.1 radian. In order to increase the OVT sensitivity, a constant is chosen properly as a multiplication factor [36]. For simulations, 10^{-4} is used as a constant.

4.6.1 Complete Optical Voltage Transformer Model

The model for optical VT is developed in the same way as the method used for developing the OCT model. The optical elements, polarizer, and three Pockel's cells are modeled using the Jones calculus method.

A Pockel's cell can be considered as a rotator, and the Jones matrix of 45 degree-rotated Pockel's cell can be derived as in (4.46) [91].

$$\begin{bmatrix} \cos\left(\frac{\delta}{2}\right) & j\sin\left(\frac{\delta}{2}\right) \\ j\sin\left(\frac{\delta}{2}\right) & \cos\left(\frac{\delta}{2}\right) \end{bmatrix} \tag{4.46}$$

Where, δ is the rotation angle of the wave after passing the Pockels cell.

Based on the operational principle of the optical voltage transformer, the OVT output states are calculated using the Jones matrixes of the optical elements as (4.47).

$$E_1 = M_{pockel1}.E_c \tag{4.47a}$$

$$E_2 = M_{pockel2}.E_c \tag{4.47b}$$

$$E_3 = M_{pockel3}.E_c \tag{4.47c}$$

Where, E_1, E_2 , and E_3 are the final states of each OVT's output, E_C is circular polarized light vector, and $M_{pockel1}$, $M_{pockel2}$ and $M_{pockel1}$ are the Pockels matrixes of each crystal that depend upon the voltage across each crystal.

In order to model of transmitted intensity through the complete optical voltage transformer based on John's calculus is used [21]. The matrices of optical component are used for the calculations, which are performed by (4.48).

$$E_1 = \begin{bmatrix} \cos\left(\frac{\delta_1}{2}\right) & j\sin\left(\frac{\delta_1}{2}\right) \\ j\sin\left(\frac{\delta_1}{2}\right) & \cos\left(\frac{\delta_1}{2}\right) \end{bmatrix} \frac{1}{\sqrt{2}} \begin{bmatrix} 1 \\ j \end{bmatrix} \tag{4.48a}$$

$$E_2 = \begin{bmatrix} \cos\left(\frac{\delta_2}{2}\right) & j\sin\left(\frac{\delta_2}{2}\right) \\ j\sin\left(\frac{\delta_2}{2}\right) & \cos\left(\frac{\delta_2}{2}\right) \end{bmatrix} \frac{1}{\sqrt{2}} \begin{bmatrix} 1 \\ j \end{bmatrix} \tag{4.48b}$$

$$E_3 = \begin{bmatrix} \cos\left(\frac{\delta_3}{2}\right) & j\sin\left(\frac{\delta_3}{2}\right) \\ j\sin\left(\frac{\delta_3}{2}\right) & \cos\left(\frac{\delta_3}{2}\right) \end{bmatrix} \frac{1}{\sqrt{2}} \begin{bmatrix} 1 \\ j \end{bmatrix} \tag{4.48c}$$

The transmitted intensity through the whole OVT is given by (4.49).

$$E_{out} = \frac{\sqrt{2}}{4} \begin{bmatrix} 1 & \mp e^{-j(\delta_V+(\pi/2)} \\ \mp 1 + & e^{-j(\delta_V+(\pi/2)} \end{bmatrix} E_{in} \tag{4.49}$$

The resulting states of the light are analyzed by calculating the intensity of light. The Wollaston principle which is extracted the light into two orthogonal components is

used to simulate photo detectors. By using the Hermitian, calculation the emergent light intensity is given in (4.51).

$$I_{out} = E^*_{out}.E_{out} = \frac{1}{2} I_{in}(1 \pm sin\delta_V) \quad (4.51)$$

Where, $I_{in} = E^2_{in}$ is the incident light intensity.

In the proposed Optical voltage transformer, the sensed signal must be calculated from the measured light intensity that comes out of the sensing element. Considering the crystals class exhibit unwanted linear birefringence due to strain, stress or precipitates [30], [92].

According to the quadratic method used for voltage calculation, the total intensity of the light can be presented as the minus of summation of the three intensities for three phase electrical source are given by (4.52).

$$I_{out1} = \frac{(E^*_{outX1}.E_{outX1}) - (E^*_{outY1}.E_{outY1})}{(E^*_{outX1}.E_{outX1}) + (E^*_{outY1}.E_{outY1})} = \frac{I_{outX1} - I_{outY1}}{I_{outX1} + I_{outY1}} \quad (4.52a)$$

$$I_{out2} = \frac{(E^*_{outX2}.E_{outX2}) - (E^*_{outY2}.E_{outY2})}{(E^*_{outX2}.E_{outX1}) + (E^*_{outY2}.E_{outY2})} = \frac{I_{outX2} - I_{outY2}}{I_{outX2} + I_{outY2}} \quad (4.52b)$$

$$I_{out3} = \frac{(E^*_{outX3}.E_{outX3}) - (E^*_{outY3}.E_{outY3})}{(E^*_{outX3}.E_{outX1}) + (E^*_{outY3}.E_{outY3})} = \frac{I_{outX3} - I_{outY3}}{I_{outX3} + I_{outY3}} \quad (4.52c)$$

$$\boldsymbol{I_T} = -(I_{out1} + I_{out2} + I_{out3}) \quad (4.52d)$$

4.6.2 The Signal Processing Circuit of OVT

The schematic diagram of the signal processing circuit is shown in Figure 4.8. The photocurrent signals are converted into voltages and amplified by the analog amplifiers. High pass (HP) filters and low pass (LP) filters were utilized to acquire the AC and DC components of the sensing signals from two light paths. The AC and DC components are simultaneously sampled by analog to digital converters (ADC). The ADC converters operate at 4 kHz with 16 bits of resolution [85], [92], [93].

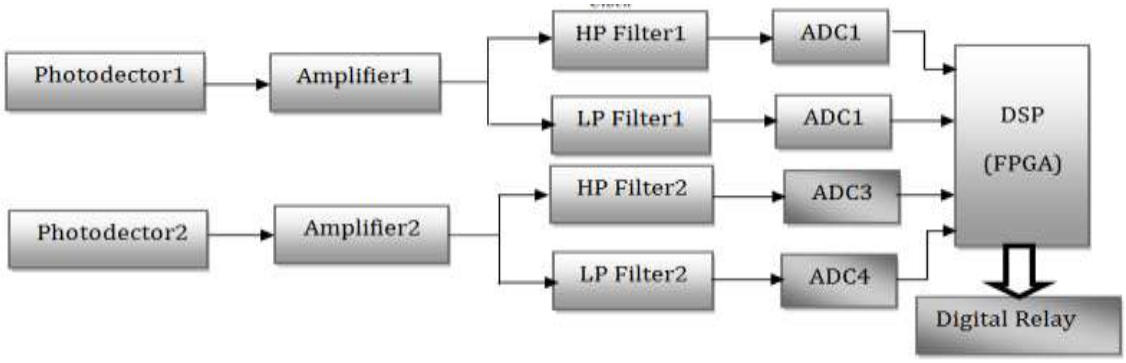

Figure 4.8 Block Diagram of Signal Processing Circuit of OVT

In order to eliminate eliminate the noise in the signal dividing the AC component by the DC one in the Field-Programmable Gate Array (FPGA), the ratios was obtain as in (4.53).

$$\frac{V_{AC1}}{V_{DC1}} = k_1 \frac{-\delta_V}{1 - \delta_U} \approx -k_1 \delta_V (1 - \delta_U) \quad (4.53a)$$

$$\frac{V_{AC2}}{V_{DC2}} = k_2 \frac{-\delta_V}{1 - \delta_U} \approx -k_1 \delta_V (1 - \delta_U) \quad (4.53b)$$

where, k_2 and k_2 are the constants associated with the photodiodes responsivities and electronic mismatches.

When $k_1 \approx k_2$, the output signal of the sensor system is obtained as in (4.54)

$$V_{out} = \frac{1}{\sqrt{2}} \left(\frac{V_{AC2}}{V_{DC2}} - \frac{V_{AC1}}{V_{DC1}} \right) = k_1 \delta_V = k_2 \delta_V \quad (4.45)$$

4.7 Numerical Protective Relays Model

Designing and modeling of digital relay require establishing a generalized relay structure, which is composed of more relevant and common internal modules employed for typical relays. The functionality of each of the internal modules of the generalized numerical relay, namely signal conditioning and sampling module, analog anti-aliasing filtering module, analog-to-digital conversion module, DFT algorithm and relay trip logic, are the essential step adopted [94]– [96].

The operational security of the power system depends upon the successful performance of the thousands of relays that protect equipments and hence protect the whole system from cascading failures. Thus, the failure of a relay to operate as intended may jeopardize the stability of the entire system and equipment in it. The

mal-operation of this relay is generally due to unnecessary tripping that reduces the security of such system and hence its reliability. In order to avoid the unnecessary tripping, many techniques have are developed such as digital filter.

The purpose for which a relay model is to be used to determine the amount of detail required in the representation of the actual relay. Based on this, digital and numerical relay models can be divided into two categories.

1. The models of the first category consider only the fundamental frequency components of voltages and currents. Phasor based models are the first to be widely used to design and apply relays.
2. The models of the second category take into consideration the high frequency and decaying DC components of voltage and current signals in addition to the fundamental frequency components [97], [98]. These models are called transient models of relays.

The generalized phasor-based numerical relay concept consists of a minimum set of hardware modules and software functions [99], [100].

A digital relay design may be simplified by three major functional elements as shown in Figure 4.9.

Figure 4.9 Functional Elements of Protective Digital Relay

Data Acquisition unit constitutes the front-end of the relay and links the digital processing segment of the relay with its analog inputs. In addition, it is performs filtering, sampling and digitalization of the analog input current and voltage signals. The Data Acquisition unit functioning requires the sampling theorem, analysis of the error of signal representation as a function of the sampling frequency, explanation of the concept of the aliasing frequency, an introduction to analog filtering together with common approximations of Analog Filters (AFs), and representation of the horizontal resolution of the Analog to Digital converter (ADC) [101].

The front end of a digital relay consists of four elements as shown in Figure 4.10:

1. Input transducer, which is matches the standard secondary voltage and current with the input signal level appropriate for a numerical protective relays.
2. The signal conditioner which is scales the signals down to match the input range of the subsequent signal processing elements.
3. The analog anti-aliasing Filter (AF) provides necessary, usually low-pass, anti-aliasing filtering. It passes all the signal components that are used by the relaying algorithm, and it stops all the remaining components assumed a noise. Depending on the operating principle of a given relay, different signal components may be considered as the information and noise.
4. The Sample and Hold (S/H) element samples its input signal usually at regular time intervals and the ADC converts the samples into their numerical representation.

Figure 4.10 Functional Subsystems of Numerical Protective Relay

Measurement unit extracts desired quantities and estimates certain parameters of the input signals, such as current and voltage phasors, magnitude, phase angle, resistance, and reactance, active and reactive power, etc. The Decision-making unit uses selected relaying basic operating principles by comparing the signal parameters from the measuring unit with given settings (thresholds). It also uses time delays and logic functions in order to drive the trip and alarm signals.

Different sets of performance indices are defined to evaluate performance of the measuring algorithm and performance of the decision-making algorithm. For example, accurate and fast measurement of the voltage and current phasors of the fundamental components is very important to the distance relay that may be investigated by an integrated Phasor Measurement Unit (PMU). Furthermore, in digital relay system, discrete Fourier transform (DFT) is the most widely used filter algorithm [102], [103] for computing the fundamental phasors and their symmetrical components.

4.7.1 Overcurrent Relay Model

The over-current relay is the most common protective device found inside a protective scheme. This type of relay protects a single or multiple components against over-currents that could be caused by overload or a short circuit. This type of relay only requires a current transformer to determine if the system is operating in abnormal working condition. Over-current relays are normally equipped with a definite or inverse time switching characteristic. The definite time over-current relay operates instantaneously or with a user defined set delay time when the current magnitude surpasses a predetermined value (pick-up current) for a specific period of time. The over-current relay of inverse definite minimum time (IDMT) type is adopted in the system. The over-current relay of IDMT is the relay that starts to operate after the intended time delay. The time delay is also known as operation time. The advantage of the IDMT relay is that the greater the fault currents, the shorter are their operating time [104], [105].

The tripping curves of inverse time relay are defined by the standard IEC 60255 with (4.56). Different types of inverse characteristics which are standard inverse, very inverse, extremely inverse and long inverse can be obtained by varying α and *k*. The constants for these curves are given in table (4.1).

$$t = TMS\left(\frac{k}{\left(\frac{I}{I_s}\right)^{\alpha} - 1}\right) \tag{4.56}$$

where, t is operating time for constant current I (sec),TMS is time multiplier setting, I is energizing current (A), I_s is overcurrent setting (A),and k, α are constants defining the applied curve.

Table 4.1 Parameters for Different Types of Inverse Characteristics

Relay Characteristics Type	α	k
Standard inverse	0.02	0.14
Very inverse	1	13.5
Extremely inverse	2	80
Long inverse	1	120

The main features of the over-current relay are including 3-phase directional instantaneous over-current protection as primary protection, 3-phase time over-current protection as backup protection and residual time over-current protection[107], [108].

The over-current relay as shown in Figure 4.11 consists of following components:

1. Measuring algorithm unit used to extracts current and voltage phasors from the input signals supplied by instrument transformers. Extraction is performed based on Fourier analysis of input signals.
2. Over-current unit that is consists of three sub-elements. The sub-elements are:
   a. Time over-current protection uses inverse-time characteristic to determine operating time.
   b. Residual time over-current protection active only for detection of fault involving ground.
   c. Directional protection determines direction of the flow of the power to determine whether a potential fault is in the direction of protected zone. It restrains assertion of trip command in case of faults in direction opposite to protected zone.
3. Logic element performs certain logic functions to derive trip asserting or trip blocking command at the output of the relay model. The logic is implemented to improve security and dependability of the model.

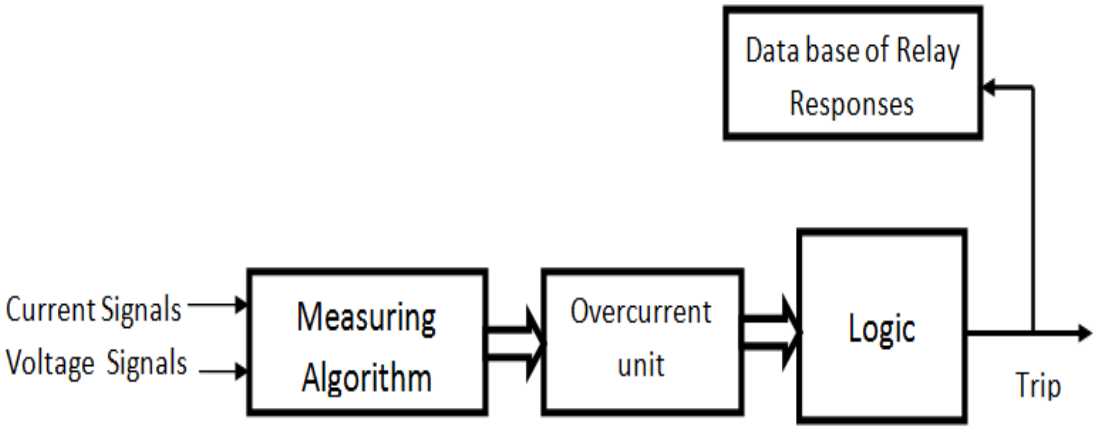

Figure 4.11 Elements of Over-current Relay Model

Output signals of the over-current relay model (trip decision and trip time) are recorded and stored in the database of relay responses. After filtration of fundamental components, current signal of frequency *(f)* is converted into the dc value. This dc

value of current is compared with the pickup value of the relay. By measuring the slope at the zero crossing of the current signal, the peak value (I_{peak}) is given as in (4.57).

$$I(t) = I_{peak} . \sin(2\pi f t) \tag{4.57}$$

The slope m at the zero crossing is expressed in (4.58).

$$m = \frac{dI(t)}{dt} = I_{peak} . 2. \pi \cos(2\pi f t) = I_{peak} . 2. \pi f \tag{4.58}$$

The peak value of current (I_{peak}) obtained is then compared with the pre-set constant value of pickup current ($I_{pick\ up}$) setting of the relay using the comparator block which allows I_{peak} when $I_{peak}\ is\ grater\ than\ I_{pick\ up}$.

The value of I_{peak} is then raised to a suitable power of n to achieve desired relay curve and then integrated as shown in (4.59)

$$constant = \int {I_{peak}}^{\alpha} . dt \tag{4.59}$$

If the value of peak current as determined from slope detection is greater than the pre-set value of severe short-circuit current level then the relay sends zero as a trip command signal to its associated Circuit Breaker after a fixed delay time. The overall digital relay output is the logical multiplication (AND) of instantaneous element and inverse characteristic element outputs, as shown in block diagram Figure 4.12.

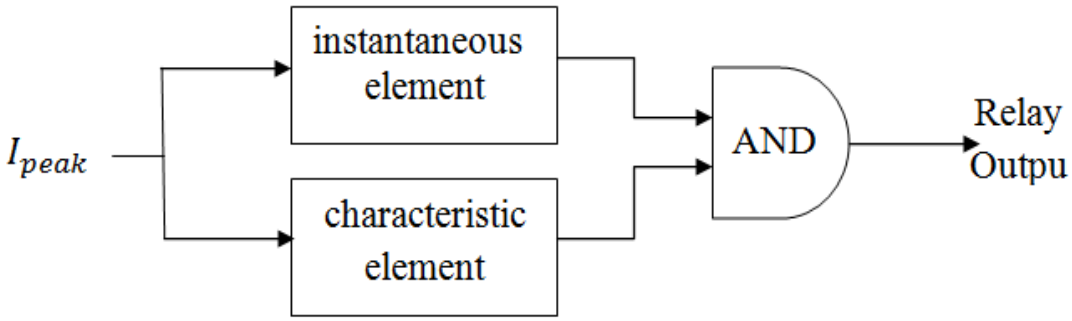

Figure 4.12 Block Diagram for Implementing a Digital Over-Current Relay

The flow chart for model and design- the inverse characteristics of the relay is shown in Figure 4.13.

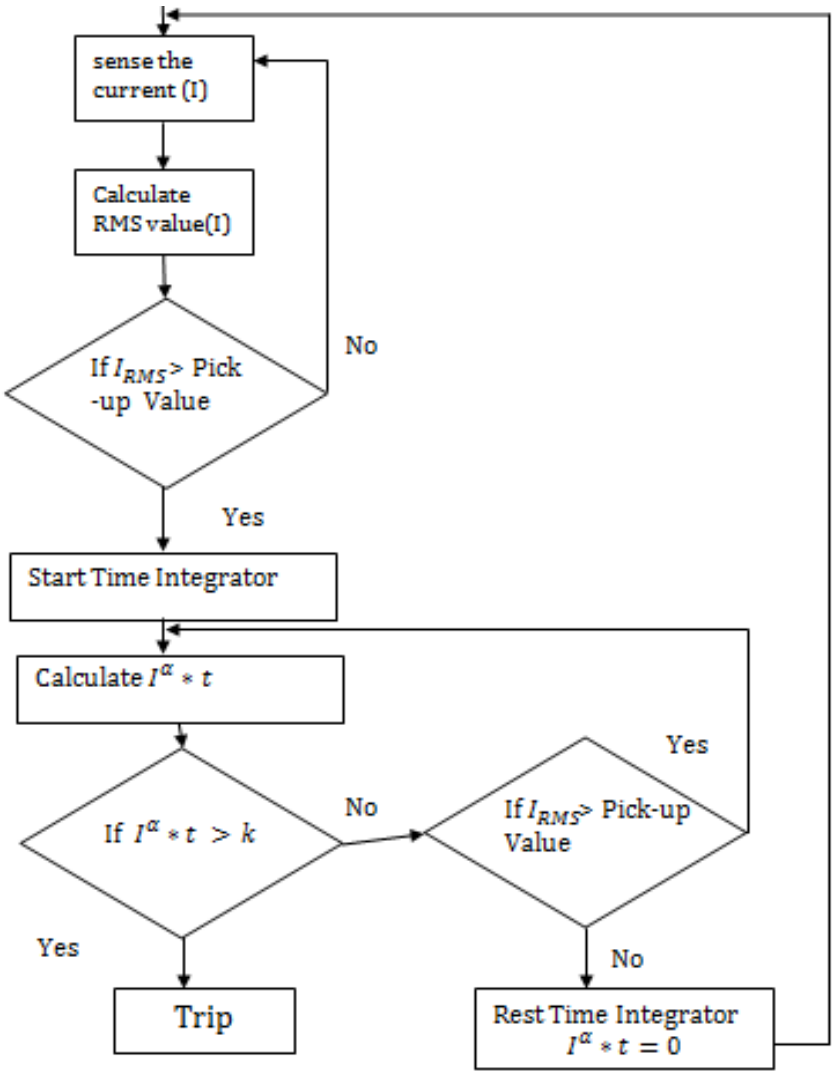

Figure 4.13 Numerical over-current relay Algorithm

4.7.2 Distance Relay Model

Distance relay is the most widely protection relay used to protect transmission lines because of its reliability, selectivity, simplicity, suitability and economy [109]. The distance relay uses the impedance between the relay point and the fault location to determine operation. The apparent impedance of the protected line is calculated using voltages and currents signals. The calculated impedance is compared to the predetermined impedance that is called reach of the relay. When the measured apparent impedance is less than the impedance-reach, the relay issues a trip command to the appropriate circuit breaker. The measuring element of the distance relay is principally laid out such that for each fault type the line impedance of the fault loop is determined. In three phase system zone-one of the relay will have six elements responsible for detecting both phase and earth faults. In order, to compensate error in

measured distance and correct operation the residual factor (k) should be considered. Table 4.2 shows the different algorithm used to measure the fault impedance for different types of fault [110].

Basic distance protection will comprise instantaneous directional Zone one protection and one or more time delayed zones. Numerical distance relays may have up to five zones, some set to measure in the reverse direction. Numerical relays usually have a reach setting of up to 85% of the protected line impedance for instantaneous Zone one protection.

Table 4.2 Fault Impedance Calculation on Difference Faults

Fault type	Algorithm
AG	$V_{an}/(I_a + KI_o)$
BG	$V_{bn}/(I_b + KI_o)$
CG	$V_{cn}/(I_a + KI_o)$
AB/ABG	$(V_{an} - V_{bn})$ / $(I_a - I_b)$
AC/ACG	$(V_{an} - V_{cn})/(I_a - I_c)$
BC/BCG	$(V_{bn} - V_{cn})$ / $(I_b - I_c)$
ABC/ABCG	(V_{an}/I_a) OR (V_{bn}/I_b) OR(V_{cn}/I_c)

Where, A, B, C indicates faulty phase, G indicates Ground, I_a, I_b, I_c indicates current phases, V_{an}, V_{bn}, V_{cn} indicates voltage phases

$K = \frac{(Z_O - Z_1)}{3Z_1}$ is Residual compensation factor, $I_0 = \frac{(I_a + I_b + I_c)}{3}$ is Zero-sequence current, and Z_O , Z_1 are Zero-sequence and positive-sequence impedance respectively.

The parameters of the composite signals in a comparator determine the shape, size, and position of the operating characteristic in the impedance plane. The operating characteristics of distance relays are usually geometric figures, such as circles, straight lines or their combinations. However, in numerical relays it is possible to design operating characteristics of almost any shape. The most common operating characteristics employed by distance relays are impedance, offset impedance, mho,

mho polarized, reactance, and quadrilateral characteristics [111], [112]. The block diagram of numerical distance relay model is shown in Figure 4.14

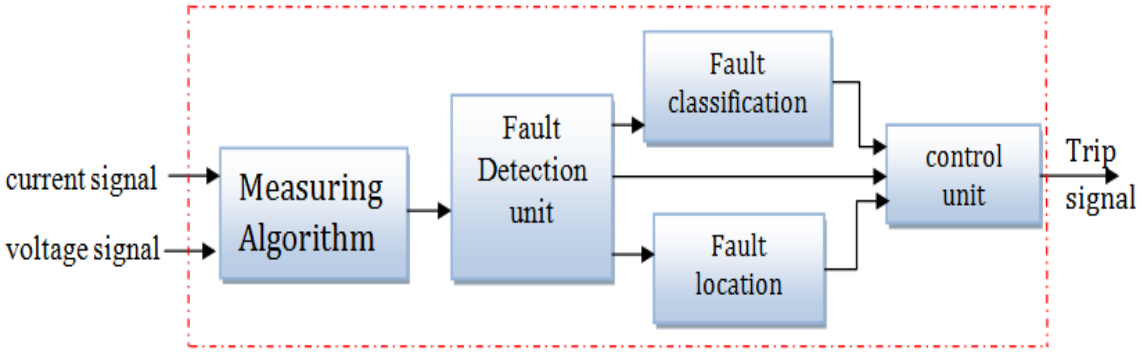

Figure 4.14 Elements of Numerical Distance Relay Model

When fault occur in transmission line, the Fault Detection unit identifies the occurrence of the fault and subsequently activates the Fault Classification and Fault location units. The Fault Classification unit will interpret the faults' values of the voltage and the current signals and according to them; it will be capable of determining the fault type. On the other hand, the Fault location unit will also take the faults' values of the voltage and the current signals and according to them, it will be able to estimate the location of the fault from the relaying point. Finally, the control unit will receive the decisions from the three units in which the output of the fault detection unit will open the circuit breaker at the fault instance through the control circuit.

During faults in a transmission, the voltage signals and current signals contain decaying dc components, higher order frequency components and lower order frequency components. This may affects the performance of digital relay. Therefore, low pass anti-aliasing filters with appropriate cut-off frequency is used to eliminate the higher order frequency components. However, the anti-aliasing filters cannot remove decaying dc components and rejects lower order frequency components. For that reason, the Discrete Fourier transform is usually used to remove the dc-offset components [113], [114]. Figure 4.15 illustrates flowchart algorithm of developed numerical distance relay.

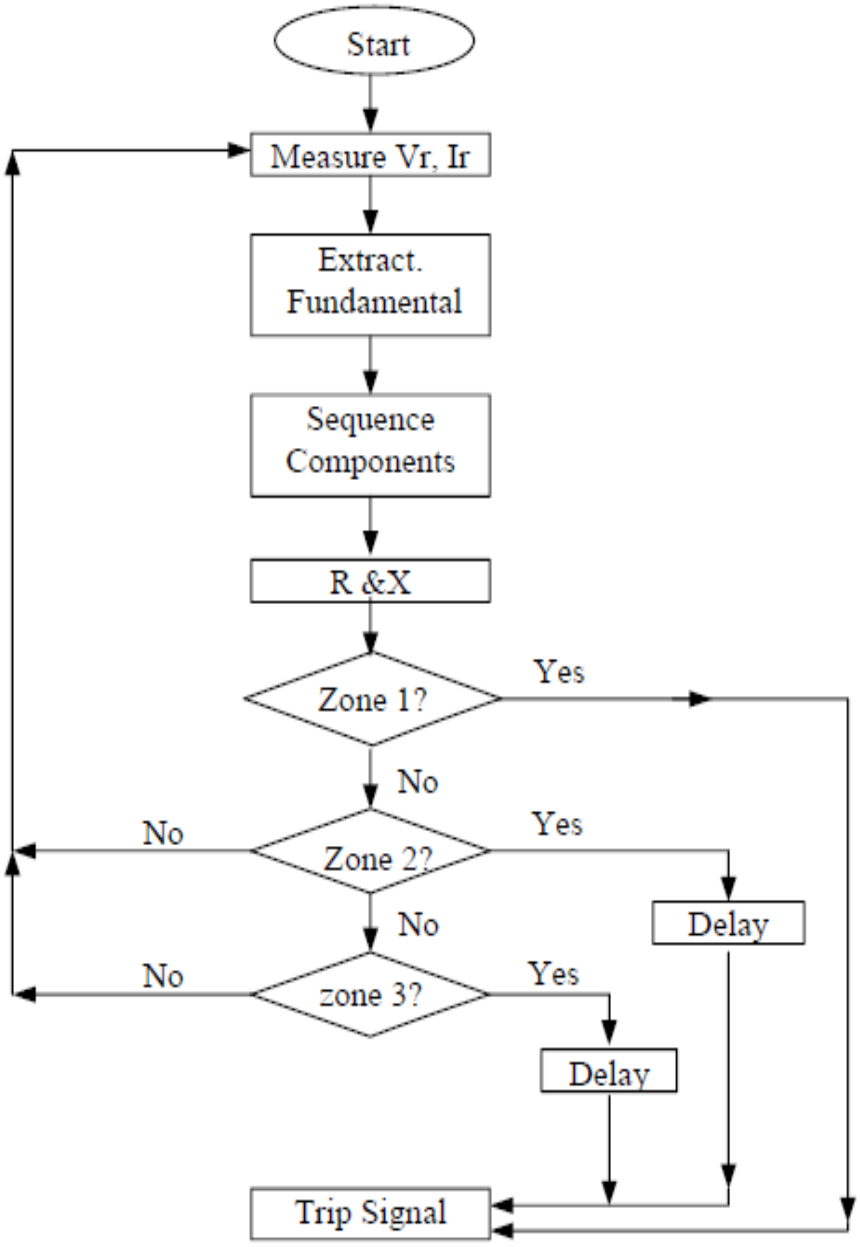

Figure 4.15 Numerical Distance Relay Characteristic Algorithm

4.8 Summary

This chapter reviews typical OFCT designs, some of their characteristics and their available interface options with numerical protection relay. Typical OFCT designs using Faraday Effect and OVT designs using Pockels cell and numerical relays were modeled from the standpoint of protection system applications. This chapter describes the development of mathematical model and design of an optical fiber current sensing technique with the stable properties and compact, simple, and flexible structure of the sensing device. The special characteristics of the OFCTs were achieved by use of the special low birefringence fiber as the Faraday-effect sensing element and were also

achieved with creation of sensing schemes which matched with the features of the fiber. Making use of the excellent features of the sensing technique, various current monitoring devices and systems were developed and applied practically for the control and protection in the electric power facility. In this chapter, the design and performance of the OFCTs are introduced first. The developed equations are used to simulate and evaluate the dual quadrature polarimetric detection configuration in chapter three with signal processing circuit under time domain conditions and frequency domain. After that, the model of numerical relays are developed practically overcurrent and distance relays are also modeled, including algorithms of fault detection and decision making. The mathematical rated equations constants for laser source and detailed Jonse Matrix for Polarizer, Polarizer Beam Splitter, Optical Fiber, and Faraday Rotation Mirror synchronous are detailed in Appendix A**.**

Chapter Five

Simulation and Results

5.1 Introduction

The deployment of Intelligent Electronic Devices (IED), such as nonconventional instrument transformers (OCTs and OVTs), and numerical relays, has facilitated the implementation of next-generation protection systems. The digital output signals of OITs work as the input signals for the digital relays through a process bus based on IEC 61850 standard. Protection performance testing plays an important role in electric power system engineering, because it ensures that protection functions implemented in relays of different types are going to operate as designed and ensure the fastest possible fault clearing. This chapter will simulate the features of testing for Numerical protection relays and discuss the impact of Optical instrument transformer on relay testing. Optical fiber instrument transformers with digital output signals represent important component in protection system based on digital system. The accurate operation of digital protection system required robust instrument transformers.

Performance characteristics for the OFCT and numerical protection relays are presented and discussed. First section provides the performance indices for the OFCT. Second section illustrates different types of test performance indices obtained for the protection system. The discussion of simulation results is given in both previously mentioned sections.

5.2 Configuration of Study System Simulation

The objective of simulation is to examine the performance of optical instrument transformers and numerical protective relays. Various power system events are simulated, influence of instrument transformer models on numerical protective relay behavior can be evaluated. In order to examine the effects of OFCT based power system protection and monitoring on a distribution network the program; MATLAB/SIMULINK is used to simulate the models. Several steps are taken in order to ensure that the desired objectives are achieved. Figure 5.1 illustrates the

procedure for evaluating the performance of power system protection using OFCT and the results are carried-out based on MATLAB/Simulink^{TM} for several scenarios.

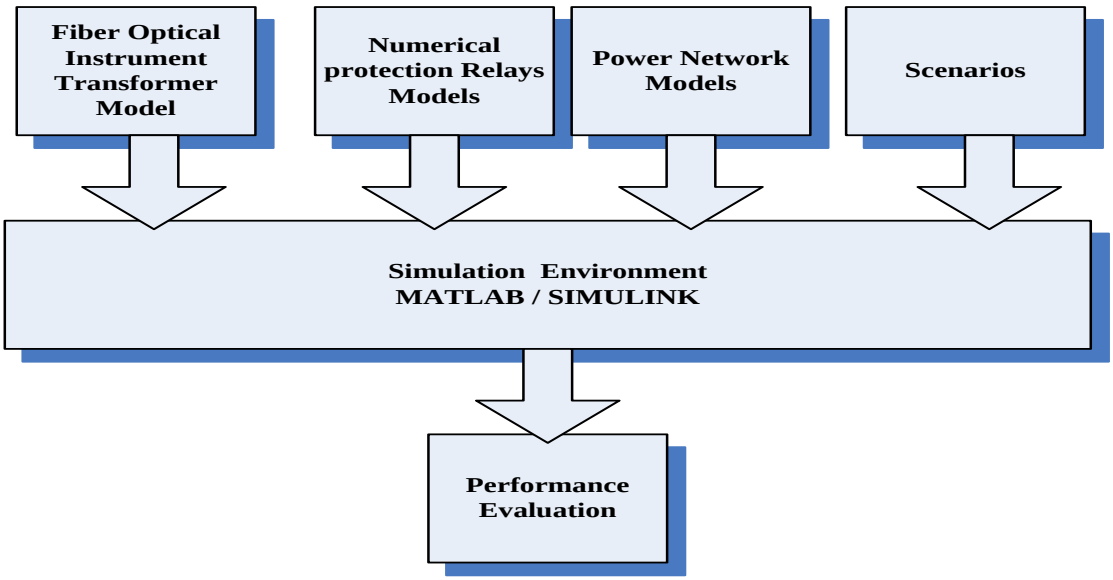

Figure 5.1 Block Diagram of Digital Protection System using OFCT Simulation

The complete simulation system of digital protection system in SIMULINK environment is composed of several modules such as power network, Optical Instrument Transformers, and numerical protective relay.

5.3 Optical Fiber Current Transformer Simulation

Building of optical fiber current transformer (OFCT) software model is very important in order to determine the performance characteristic of OFCT such as sensitivity, linearity, bandwidth, and transient response (These feature are discussed in detail in chapter four).

Figure 5.2 shows the block diagram of OFCT built in Simulink environment. The block diagram model in Figure 5.2 contains five different subsystems:

1. Light source subsystem.
2. Polarizer subsystem.
3. Sensing head subsystem.
4. Photo-detector subsystem.
5. Electronic signal processing subsystem.

The simulation of optical fiber current transformer is based on mathematical modeling derived in chapter 4. The operation of the system started as the light wave travelling through the fiber that is wound around the current carrying conductor experiences changes in the angle of state of polarization due to the Faradays effect corresponding to the magnetic field. The waves are linearly polarized before entering the fiber loop and then with the help of quarter wave plates. For a generic polarization state, which can be described as a combination of two orthogonal circular modes (left and right), the application of the magnetic field, translates into the accumulation of a relative phase between the two modes, proportional to the magnetic field. For linearly polarized light, this relative phase, results in a rotation of the polarization plane. These waves exiting the fiber loop are again linearly polarized and the intensity of optical power is measured to know the change in electric current that is proportional to the rotation of state of polarization.

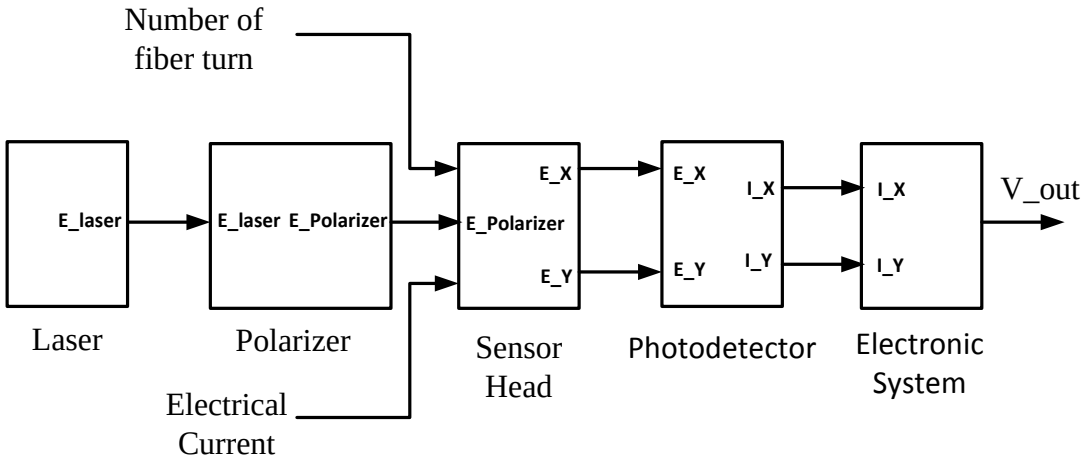

Figure 5.2 Simulink Layouts for Optical Fiber Current Transformer

5.3.1 Light Source Simulation

Laser acts as light source and optical transmitter in optical fiber current transformer. The information needed to be transferred is sent from source to transmitter via electrical signal. The function of light source is to convert the electrical signal into optical form and launch or emit this resulting signal into the optical fiber.

The block represents the light source model is built based on equation (4.25) in chapter four. The complete representation of light source model is shown in Figure 5.3. The simulink model was employed to find numerical solutions for the optimal

operating points, given a constant pumping current. Two bias points above threshold were computed.

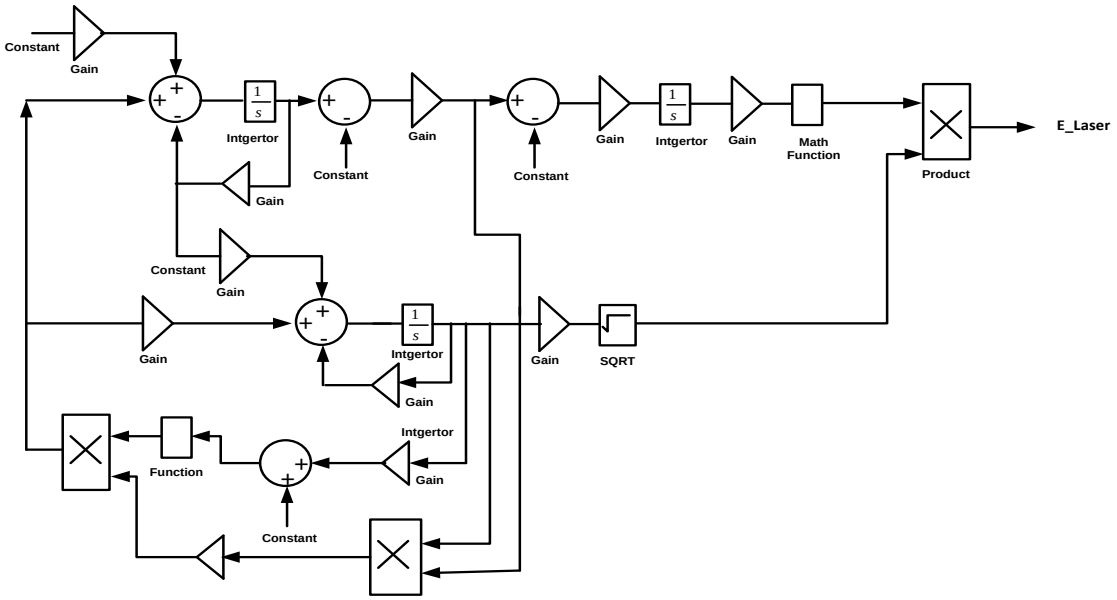

Figure 5.3 Simulink Model of Laser Source

The operation of light source model is evaluated and the simulation is run for period of 2ns pulse of 1mA above the operating point. Figures 5.3 and 5.4 show the obtained results of different bias point of 10mA and 15mA models, respectively. It is clear from the Figure 5.4 the light source response is oscillatory and not stable. The situation get worse when bias current is increased, therefore only the 10mA model was tried with a 1ns pulse of 1mA.

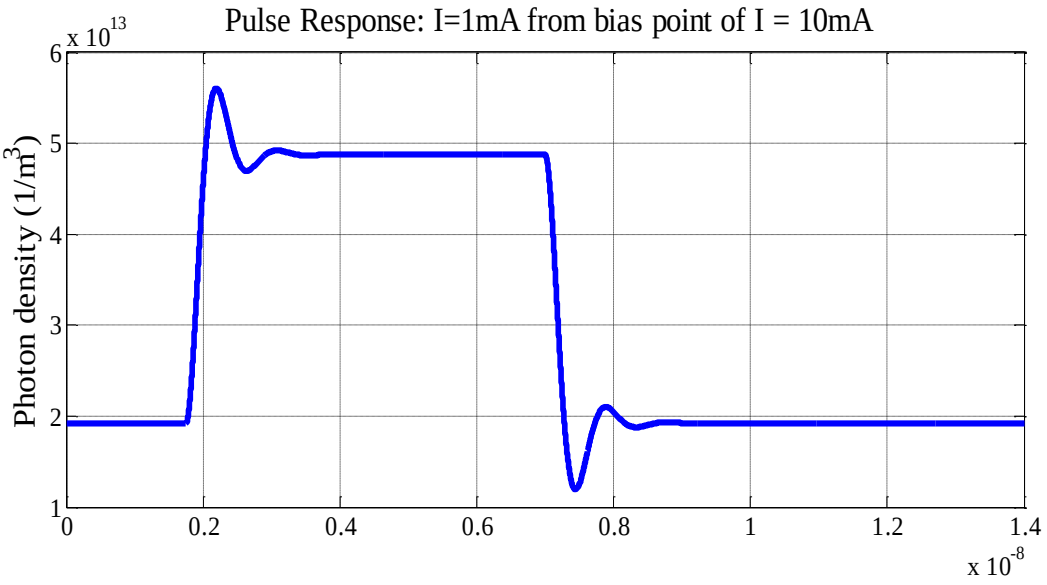

Figure 5.4 Laser Model Response to 2ns, 1mA Pulse for 10mA

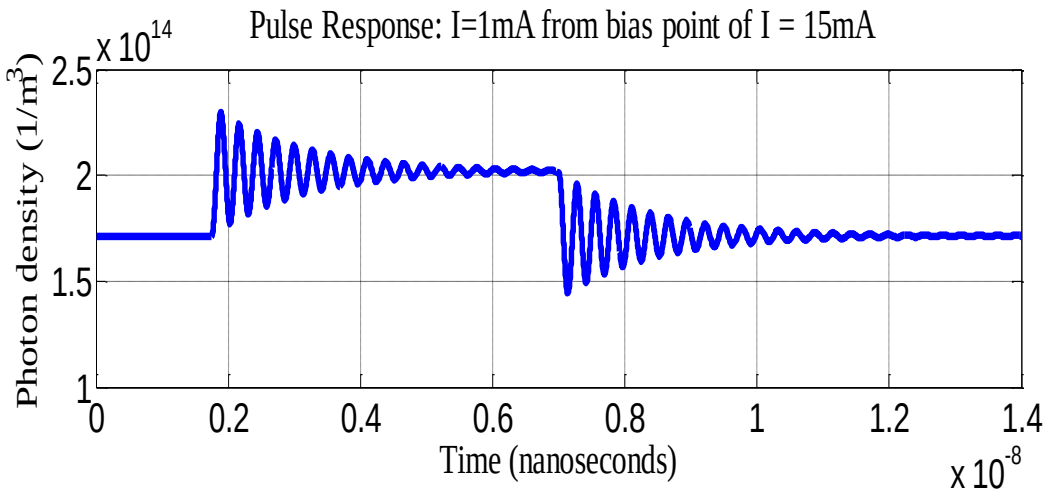

Figure 5.5 Laser Model Response to 2ns, 1mA Pulse for 15mA

A model was constructed to find the threshold current of the diode, and to identify a relatively linear region above threshold for operating point selection. The model also proveds a useful tool for finding numerical solutions for the steady-state values of electron and photon densities for currents above threshold. This model was shown to be an aid in determining the frequency response and eliminating fluctuation in optical power of light source by using optimal driving current.

5.3.2 Polarizer Simulation

The optical power generated from the source model is to be fed to the fiber coil for transmission. Before that, the random polarized light from the laser diode is linearly polarized first and then fed into two fiber sensing head using a polarizer. The implementation of polarizer using simulink illustrated in Figure 5.6.

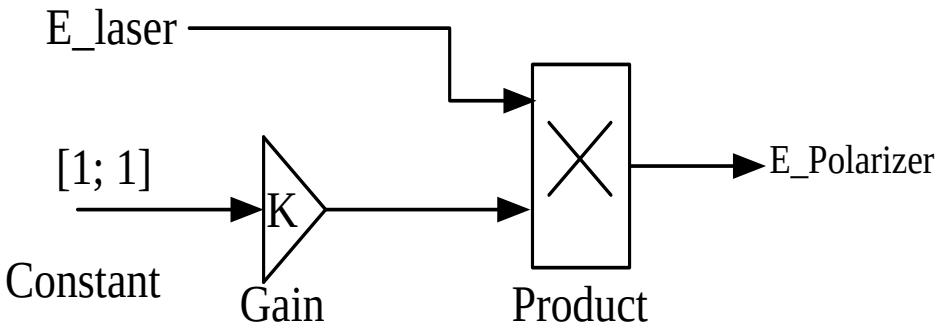

Figure 5.6 Simulink Model of Polarizer

5.3.3 Sensing Head Subsystem

A sensor head is a single mode optical fiber cable used to detect the current through a conductor. The correct selection of core fiber optic cable Refractive index, Verdet constant, Faraday effect, attenuation, and fiber length are take in consideration when modeling the head sensor. The correct selection of parameters affects the OFCT performance characteristics. OFCT sensitivity, linearity, and the major cause of distortion, are mainly dependent on the wavelength of light source, Verdet constant and number of fiber turns. Figure 5.7 shows simulink block diagram of sensing head.

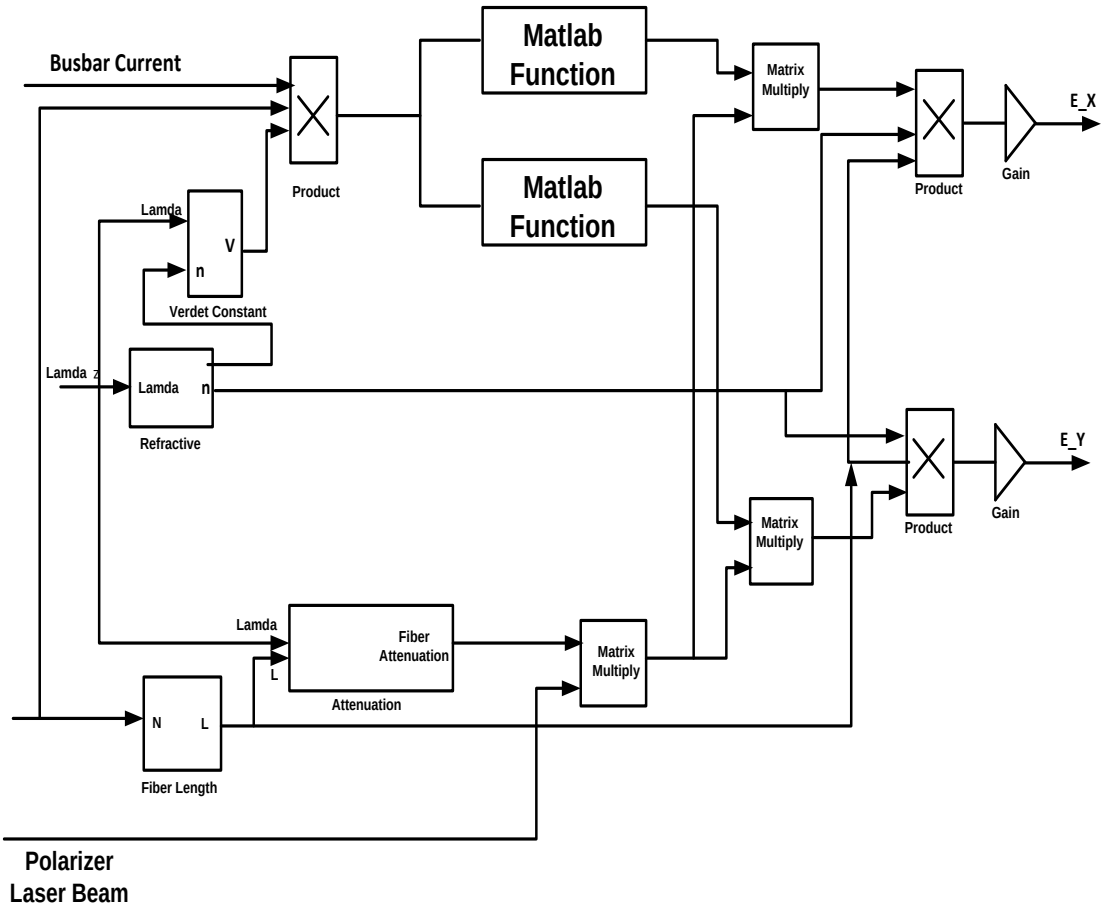

Figure 5.7 Simulink Block Diagrams of Sensing Head

5.3.4 Electronic Processing Subsystem

This subsystem consists of two main parts, a photodetector which converts an optical power to electrical signal, and an electronic circuit which used to extract the state of polarization. Figures 5.8 and 5.9 show the block diagram of photo-detector and the electronic circuit respectively. Building of these block diagrams based on mathematical models described in chapter Four ((4.5) and (4.6)). The parameters

setting of the various components of electronic processing subsystem model are chosen to obtain optimal operation conditions. In order to evaluate the model of electronic processing and ensure the accurate operation, each subsystem is tested individually and if each subsystem operates correctly in stand-alone mod then the whole system will operate correctly.

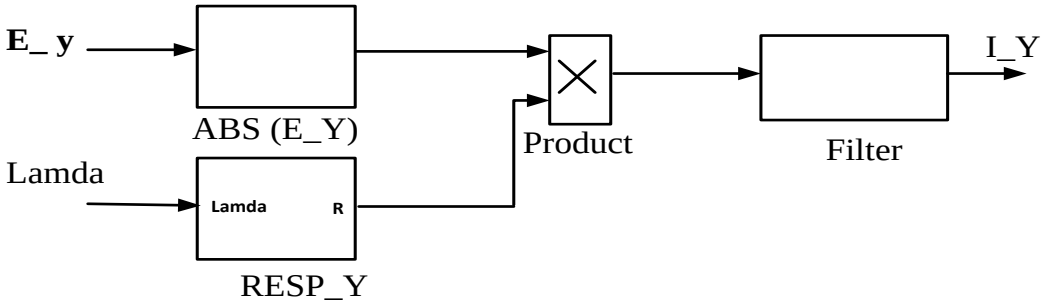

Figure 5.8 Simulink Model of Photodetector

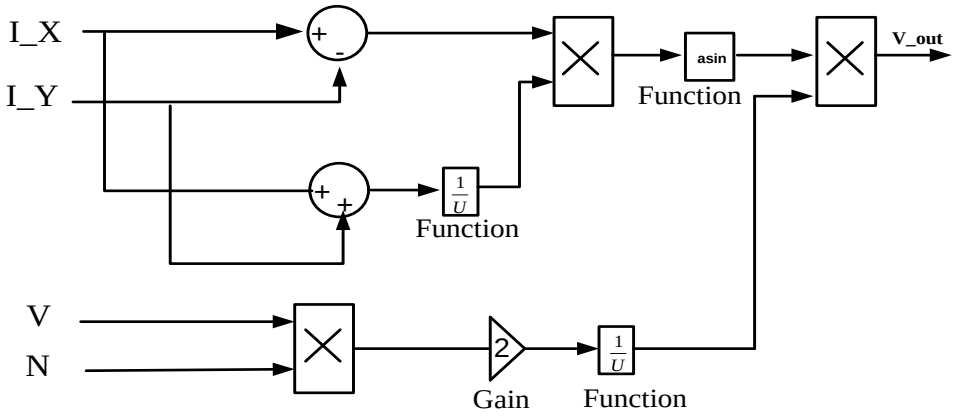

Figure 5.9 Simulink Model of Electronic Signal Processing

5.4 Performance Evaluation of OFCT

The operation characteristics of OFCT such as sensitivity, saturation and linearity are evaluated using AC current of various amplitudes and frequencies. The accurate operation of OFCT significantly affects the operation of digital relay system. OFCT is used to supply the relay with accurate signals from the protected area and relay monitor these signals to detect the abnormal conditions.

The output of OFCT flows through the fiber loop is directly proportional to the applied electrical current. Since the Verdet constant in fused silica fiber is very small, the presence of bending induced birefringence further reduces the system sensitivity,

it is essential to choose the appropriate configuration in which maximum sensitivity is obtained.

Figure 5.10 shows the output voltage signal as a function of applied electrical current measured OFCT with single fiber turn diameter of 20 cm in the range between 20 and 4 kA as well as the deviation of the data from linearity.

By increasing the number of fiber turns of OFCT the sensitivity can be further improved, nevertheless at the expense of a correspondingly reduction in the maximum detectable electrical current.

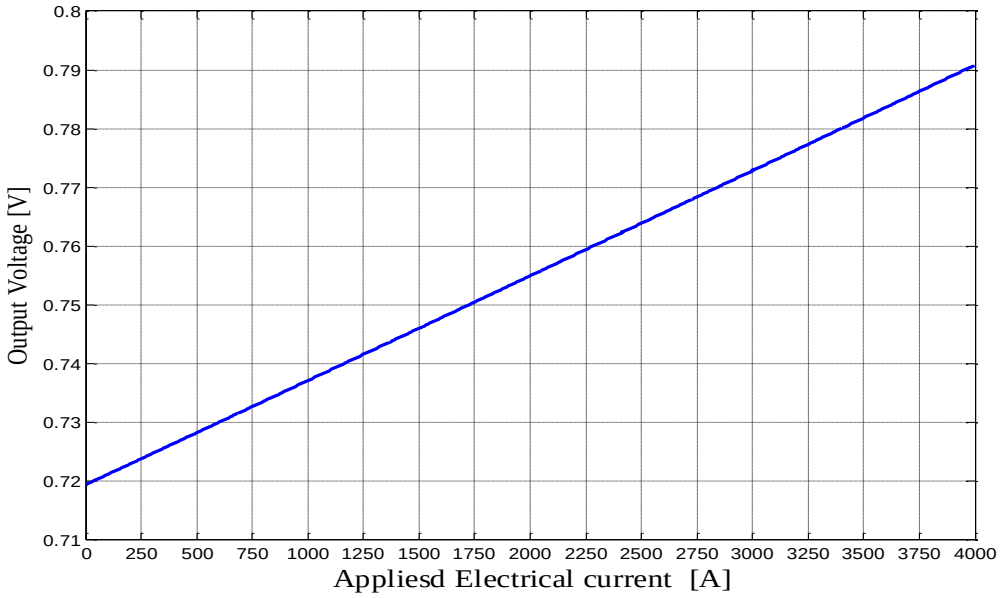

Figure 5.10 The OFCT output Voltage versus Applied Electrical Current

Based on simulation results in Figure 5.10 and analytic calculations, the OFCT is capable to measure low current and detect minimum current by the ever present noise at the detector output.

In OFCT design, the dominant noise component is the source noise which lies -120 dB/Hz below the DC output level. The result is $0.03\ A/\sqrt{Hz}$, i.e. 20 A for our OFCT configured for a 400 KHz bandwidth . At wavelength of 632 nm and with a single loop of fiber a phase shift of 5 μrad corresponds to a current of 20 A. One interesting feature of the OFCT is that the dynamic range can be scaled to fit any application by changing the number of fiber turns on the sensing head.

The linearity of the OFCT and the effect of number of fiber turns on sensor linearity and sensitivity are evaluated as shown in Figure 5.11. The applied electrical current was ranging from 20 A RMS up to 2000 A RMS and the output voltage at wavelength of 633 nm was recorded at different number of fiber turns. Based on obtained results the number of optical fiber coil turns is directly effects on the OFCT sensitivity and linearity and it is closely related to the measurement accuracy of the OFCT.

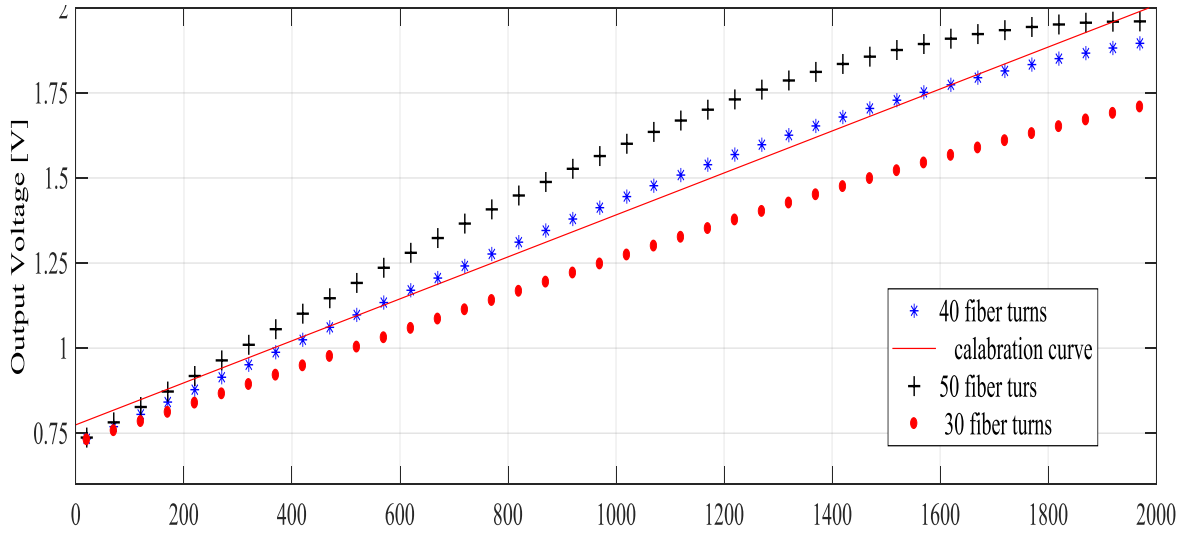

Figure 5.11 Effect of Number of Sensing Fiber Turns on OFCT@ wavelength of 632 nm

From the obtained simulation results, it is clear that the linearity decreases with the increase of the number of fiber turns. The OFCT sensitivity also varies with the number of fiber. OFCTs with higher number of turns make it possible to use optical fiber with lower Verdet constant. Decrease in Verdet constant always followed by increase of wavelength. Therefore, wrong selection of the number of fiber turns has a negative impact on the measurement of the OFCT.

The sensitivity of the OFCT can be optimized for different rated currents by appropriately choosing of the number of fiber loops. Considering that the design of the fiber coil is optimized, it is concluded that the number of fiber turns is set within the range of 30~50. Figure 5.12 shows the combined results of all tests showing a very good linear response and independent of the signal frequency.

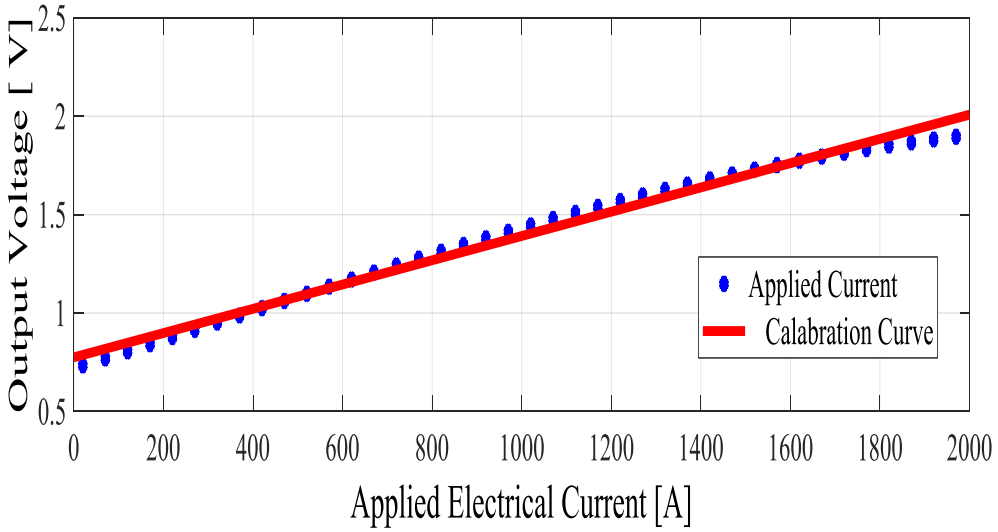

Figure 5.12 Calibration Curve of OFCT Responding to the Applied Electrical Current

In order to evaluate sensitivity, resolution and the possibility of using OFCT configuration at different wavelengths, the OFCT tested with different wavelengths sources of 632 nm, 830 nm, 1330 and 1550 nm.

The OFCT resolution is calculated as two times the standard deviation value of each incremental step, divided by the slope of the calibration curve. With this procedure, it was possible to obtain the OFCT response and respective calibration curves while operating at different wavelengths. With this data, an estimate of the system sensitivity is preformed in all cases.

Figure 5.13 shows a comparison of the results obtained with each optical source, where it is shown the normalized sensitivity as function of wavelength. Sensing head of 630 nm exhibited high most of the optical power attenuation but had high normalized sensitivity compare with optical fiber windows. As a result, the available optical signal reaching the photo-detectors is relatively small leading to a degradation of the signal to noise ratio, requiring high gain amplification and filtering and imposing some limitations on the bandwidth.

As expected, the sensitivity rapidly decreases with the increase of the wavelength, due to the decrease of the Verdet constant. As mentioned before, the Verdet constant of the fiber material at 650 nm is slightly high compare with at 830 nm, 1330 nm and 1550 nm, respectively.

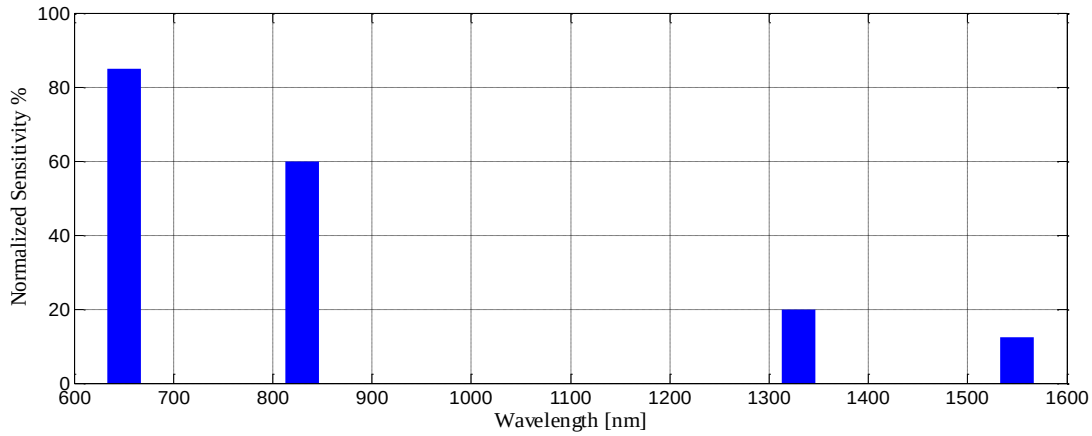

Figure 5.13 OFCT Normalized Sensitivity versus Wavelength

Based on the obtained sensitivities, it was possible to improve the sensitivity of OFCT by increasing the total length and radius of the coil and use as short an optical wavelength as possible. In other words, increasing the number of fiber turns decrease the bandwidth. Therefore, the optimal number of fiber turns must be calculated. To analyze the optical behavior an upper limit on the detection bandwidth (BW) must be set, also an infinite electrical bandwidth of the current signal is assumed.

For OFCT having a coil of 10 cm diameter and number of fiber turns of 35 turn, the theoretical F_{3dB} is 11.24 MHz. Theoretical Optical bandwidth of OFCT of 35 turns 10 cm coil diameter is shown in Figure 5.14. The response, monitored out up to 1MHz, shows negligible attenuation caused by the Electronic signal processing. Obviously, the photo detector and processing circuitry must also possess the desired bandwidth characteristics for the intended application.

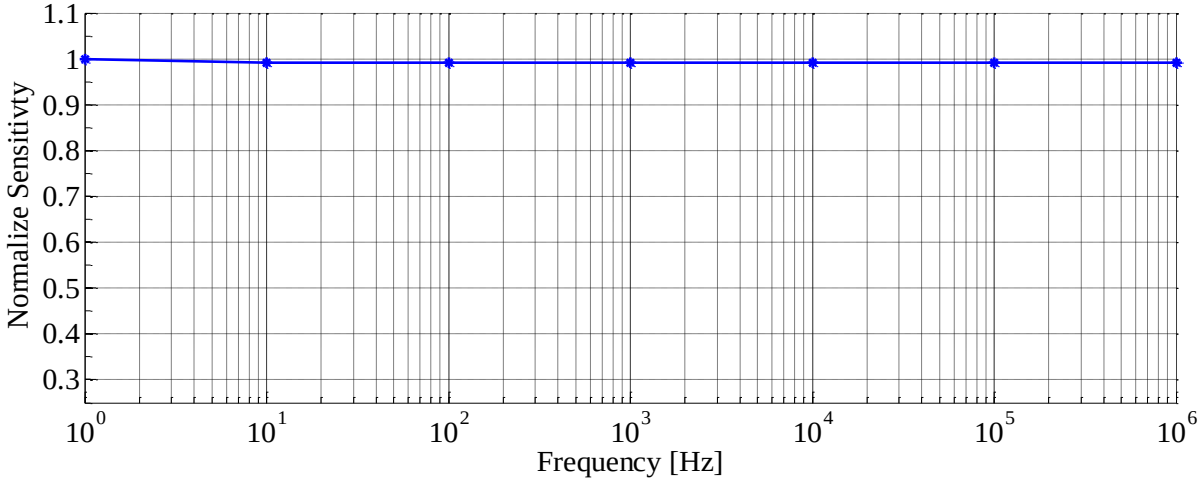

Figure 5.14 Theoretical Optical bandwidth of OFCT

The electronic circuit of FOCT model is very important to determine the response to frequency variation; this is obtained by the equivalent circuit transfer function. The magnitude and phase response of the equivalent circuit is shown in Figure 5.15.

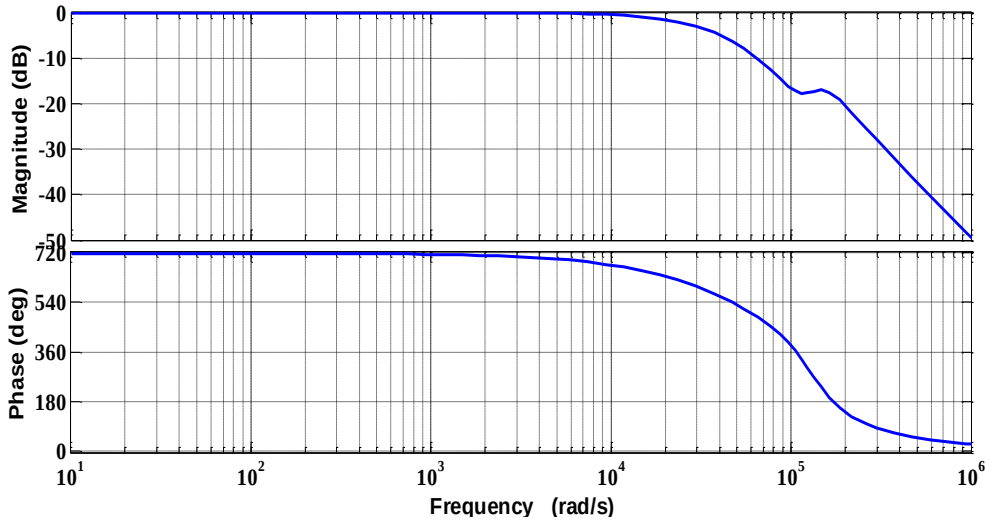

Figure 5.15 Magnitudes and Phase Response of Electronic Circuit

The OFCT bandwidth at different frequencies is investigated by submitting the sensing head to sinusoidal AC current of 50 Hz, 100 Hz, and 250 Hz to 400 kHz in order to observe harmonics and transients. For each frequency, the optical AC response was recorded, while incrementing the electrical current amplitude.

Due to practical limitation of the electronic components, the highest frequency tested was 400 kHz, nevertheless, considering the OFCT intrinsic characteristics, the bandwidth will only be limited by the specification of the detection electronics.

As stated before, Calculating the bandwidth of the OFCT must take into account the limitations of the electronics systems (Photo detectors, Digital Acquisition) and the impact of the available optical power in the signal to noise ratio, and the number of fiber turns the bandwidth of the systems tested was limited. Nevertheless, bandwidth can be increased by using an optical source with higher optical output power that would allow reducing the gain requirements, thus increasing the bandwidth, and also using acquisition boards with better performance. In addition, such value of bandwidth is already adequate for most application of metering and protection.

5.5 Reflection Configuration Simulation

Using Jones formalism it is possible to obtain an analytical expression for the output response of the optical fiber current transformer, by defining a matrix for each component of the optical fiber current transformer.

In a medium having both linear birefringence and circular birefringence induced by Faraday Effect, the corresponding propagation matrix can be found as mentioned in chapter four, by using equation (4.32). The sensing fiber is never strictly free of birefringence, so that the use of a Faraday Rotation Mirror (FRM) cancels the effect of this birefringence and its variations. Furthermore, OFCT response remains independent from of laser source intensity fluctuation and losses.

Depending on the theoretical and analytical studies using Jones Matrix the Reflection Configuration of the FOCT model is built using SIMULINK. A MATLAB program is written to calculate the final states of polarization and to find the final phase shift between the two light wave components according to the input electrical current. This program is then integrated with SIMULINK, it consists of the two main blocks. Each block is built by programming its own S-Function under MATLAB environment. The simulation model used to evaluate the performance of the proposed Optical Fiber Current Transformer is depicted as in Figure 5.16.

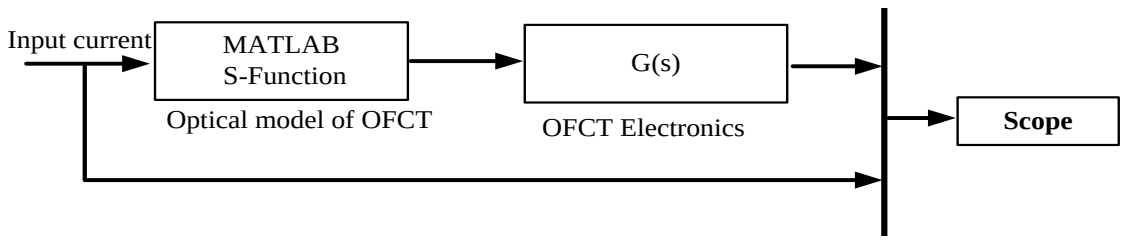

Figure 5.16 Complete Model and its Simulink implementation

A 50 Hz alternating current with different intensity are applied to the fabricated OFCT, and their responding is monitored. The model output voltage phase shift is compared with the input signal electrical current phase is illustrated in Figure 5.17.

From the results obtained, it is observed that, there are no phase difference between the responding signals of the OFCT and applied alternating current signal. Furthermore, the relationships between the amplitude of the OFCT response and the

externally applied current intensity are approximately linear, and no saturation phenomenon is observed in the OFCT response.

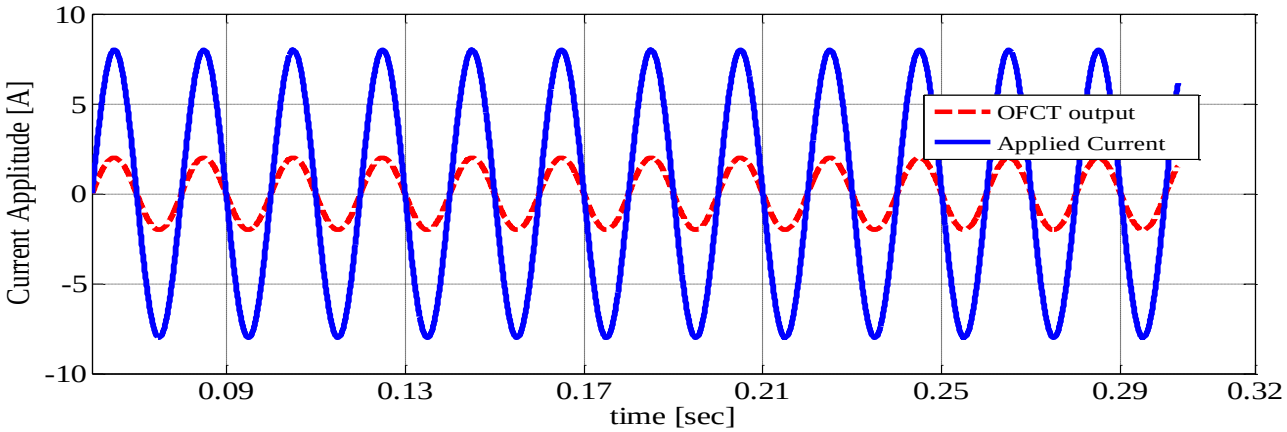

Figure 5.17 Final Phase Shift Variation by Input Current

The results show that the output signal is proportional to the input current signal and has the same phase with different amplitude. The phase shift is normalized with the input current in order to conduct appropriate calculations. Figure 5.18 illustrate the input electrical current and the normalized OFCT's output phase shift plotted together. From Figure 5.18 it is very difficult to see the phase difference between the normalized output signal and the input current signal.

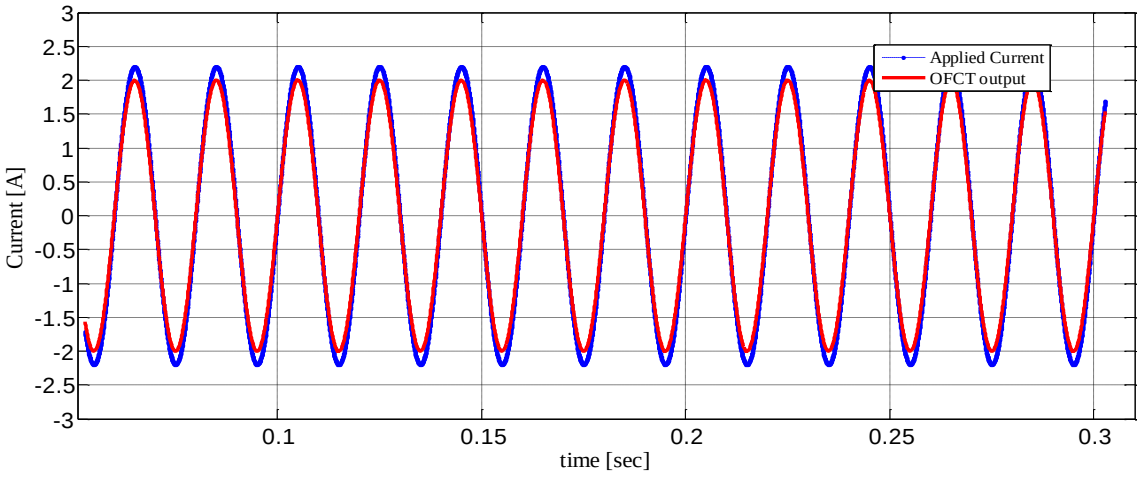

Figure 5.18 Comparisons of Applied Current and OFCT Model Output

The applied electrical Current is sensed by OFCT model and the signal processing circuitry generate an output voltage signal that is compared with the input current signal. The results obtained show that the OFCT model reproduces the input current

successfully. Since the secondary current waveform measured at the output of the OFCT and the primary current waveforms are identical, proving that no saturation occurred and the OFCT replicated the primary current signature accurately throughout dynamic range of the current.

Due to the intrinsic large bandwidth of the OFCT, harmonics and other superfluous noise present in the primary current, within the system bandwidth, can be detected and characterized. Nevertheless, filtering can be applied at the detection stage for measurement of the AC component of the nominal current.

The comparison between OFCT model and Reflection Configuration model based on electronics the normalized amplitude response and phase response characteristics are plotted in Figure 5.19.

The frequency responses of some OFCT configurations have been compared. The results from the simulation show that the OFCT reflection configuration has much better frequency response than non reflection configuration.

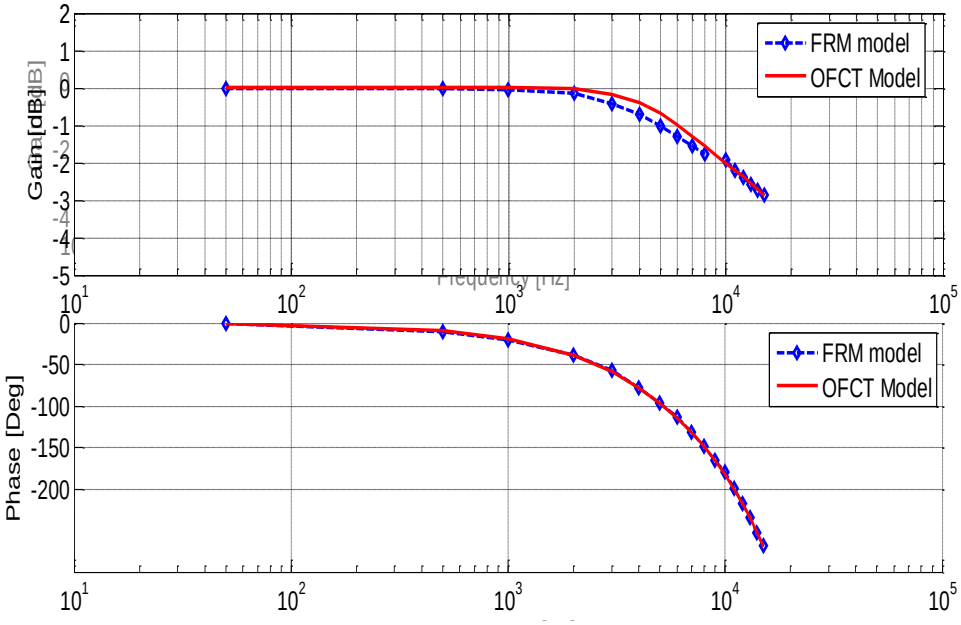

Figure 5.19 Comparisons of Amplitude and Phase Angle Response of OFCT Configurations

The sensitivity of OFCT is dependent on the wavelength of the light source and the number of fiber loop around the current carrying conductor. The OFCTs are capable to measure current with very high accuracy over wide dynamic range with acceptable errors that match the IEC 0.2 class accuracy requirements. This performance eliminates difficulties in conventional instrument transformers. Higher performance

of OFCT can be achieved by precisely designing fiber loop of the sensing head using reflection configuration to eliminate linear birefringence retardations and all possible disturbances in sensing fiber. The FOCT offers attractive features such as improved safety, ease of installation, immunity to electromagnetic interference (EMI), reduced insulation requirement, smaller size, larger dynamic range, and higher accuracy than the conventional CTs and they are less expensive in comparison to conventional CTs. Moreover, OFCT can detect high harmonic current due to high bandwidth without any limitations as in the conventional CT due to magnetic saturation and remnant flux.

As a result, OFCTs deliver within their measurement range a true image of the primary current, also in case of fast transient currents, short circuit currents, and alternating current (AC) with DC offset. Other advantages are enhanced safety no risk from open secondary CT circuits or catastrophic failure and environmental friendliness. Furthermore, OFCTs are providing direct to digital outputs according to the IEC 61850 standard, which are immediately compatible with modern digital substation communication. According to the results obtained, OFCTs has extraordinary features, which is made it more suitable for replacing conventional CTs.

5.6 Power System Protection using Optical Transformer

An experimental power system model is used to examination the dynamic performances and the flexibility of OFCT during normal and abnormal conditions. The experimental model must offer the flexibility to simulate various power system conditions and it has been proven to effectively represent dynamic characteristics of disturbances and faults. The interfacing between OFCT and Numerical relay can be accurately done using either C language or a commercial software package like MATLAB with pre-defined libraries of specialized functions.

The MATLAB/SIMULINK support and Power System Block set (PSB) is utilized to develop customized numerical protective relaying model for testing protective relaying performance. Moreover, add the modeling and simulation to evaluate performance of specific characteristics optical instrument transformers. In MATLAB/SIMULINK environment, optical fiber Instruments and Numerical protective relays are modeled using customize user define function blocks. The

complete system model is structured in a hierarchical manner as shown in Figure 5.20.

Power network model selected for simulations and evaluation of the performance of the power system protection, using optical instrument transformers interconnected by an IEC 61850 process bus, a dedicated test facility is developed as shown in Figure 5. 21.

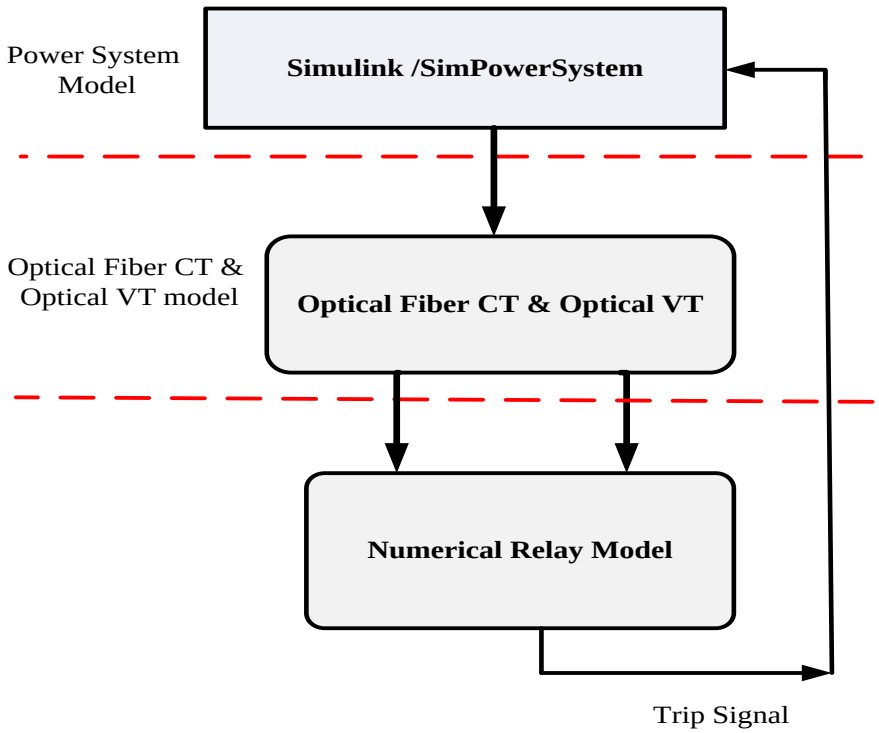

Figure 5.20 The Hierarchical Structure of Complete System Simulation Environment

Figure 5.21 shows the one-line diagram used to test the power system protection which includes optical instrument transformers connected to multifunction numerical relays through an IEC 61850 process bus.

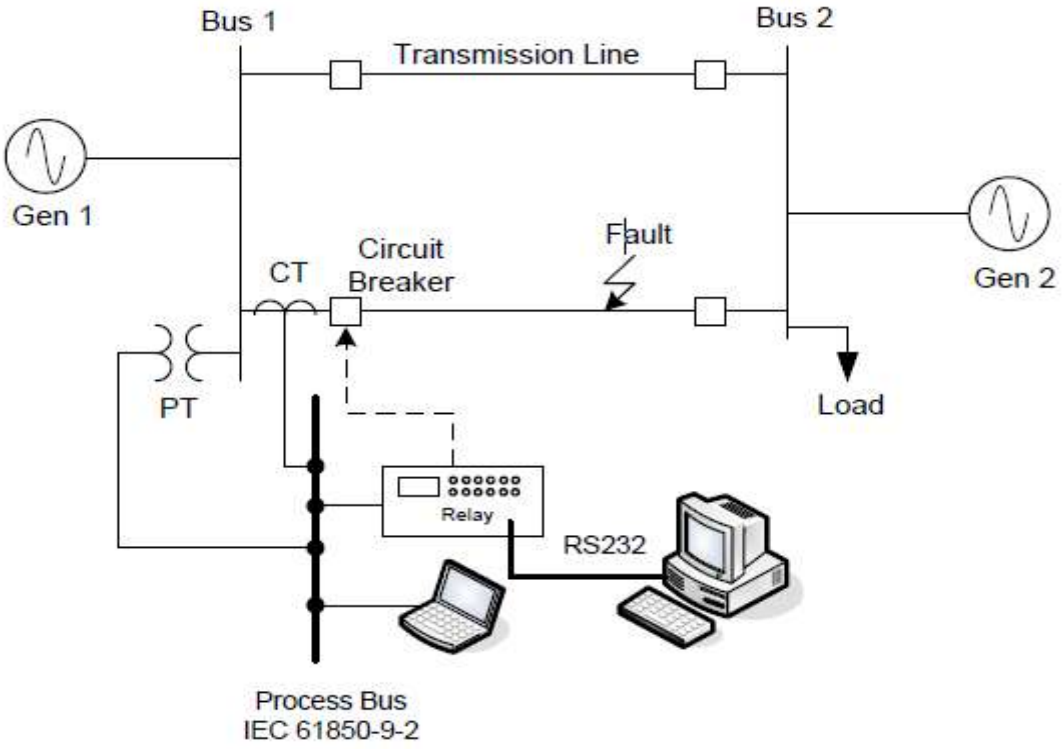

Figure 5.21 Experimental Power System Protection Model

The parameters of power system protection model in Figure 5.21 and their respective settings are discussed in an appendix A.

The power network model and respective parameters are manually setting. In addition, fault conditions of different types at different locations are initiated in order to evaluate the operation power system protection with FOCT. The simulation results, namely the waveforms, fault clearance time and impedance fault are saved to be used later analysis.

5.7 Simulation Scenarios

Several scenarios are created including different types of disturbances to carry-out comprehensive evaluation of the performance of power system protection using FOCT to ensure the robustness of the design and the response during normal and abnormal conditions. The investigation is achieved in MATLAB/SIMULINK environment. In this thesis, two scenarios were simulated:

1. First scenario is selected in situations when we need to emulate the influence of critical conventional instrument transformers operation.

2. Second scenario is selected when we need to reduce the influence of optical instrument transformers (OFCT).

Multifunction Numerical protection relay model with OFCT used to carry-out the scenarios are shown in Figure 5.22. The characteristics of Multifunction Numerical protection relay is selected to operate as over-current relay and distance relay. The distance relay is expected to operate as a primary protection for faults in zone one and backup protection for faults in zone two and zone three.

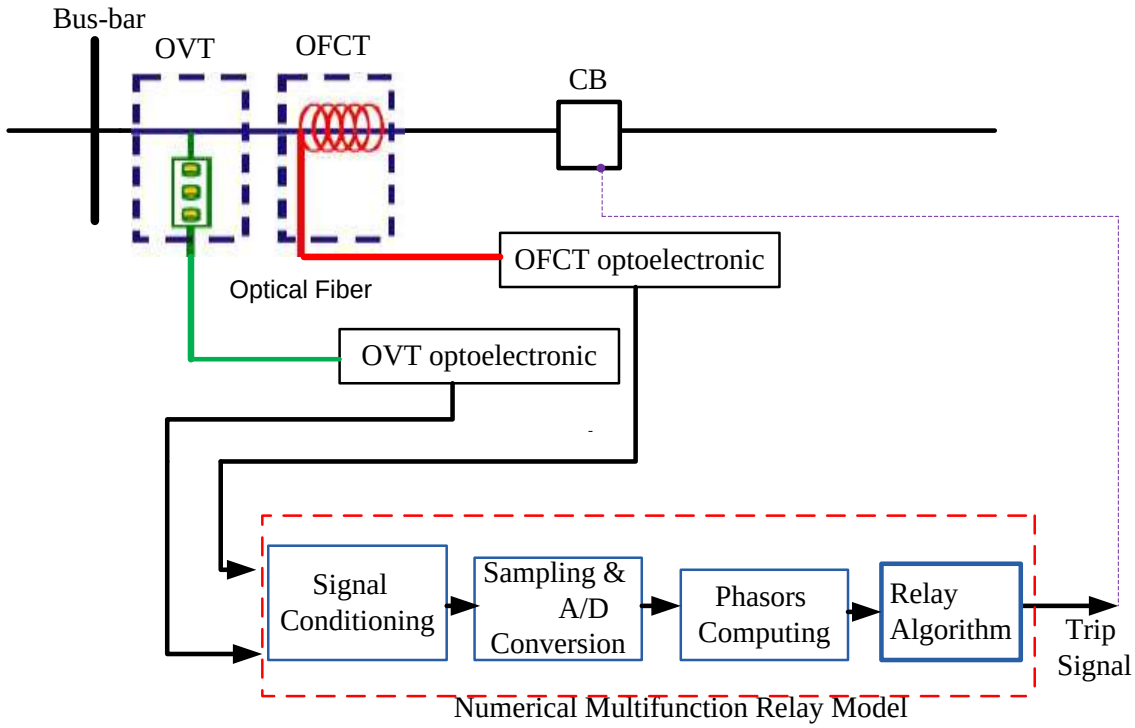

Figure 5.22 General connection diagram of Test System

5.7.1 Overcurrent Protection Scheme

Numerical relay model was set to the overcurrent protection mode using the IEC 60255 standard inverse characteristics. The relay is expected to send a trip signal for faults in the forward zone of protection, while it is expected to restrain from operating for faults in the backward zone of protection. Over-current relay is tested to confirm its correct operation and to ensure the relay will send trip signal at its pick-up setting value, after the definite time delay. The current transformer saturation is one of the major concerns that affect the operation of protection devices.

In order to demonstrate the impact of CT saturation in operation of protection system with conventional CT, the CT on phase-A was intentionally saturated during a fault

simulated. The test scenario represents single-phase-to-ground fault occurs at 50% of the transmission line length.

The general functionality of the Directional Over-current Protection is tested including correct directional sensing and correct phase selection. The voltage measurements are taken from bus 1 and the current measurements are yield from line Bus1 to Bus2. The phase A fault current including a portion of the pre-fault steady state is shown in Figure 5.23 shows the actual current signal and saturated current measurement.

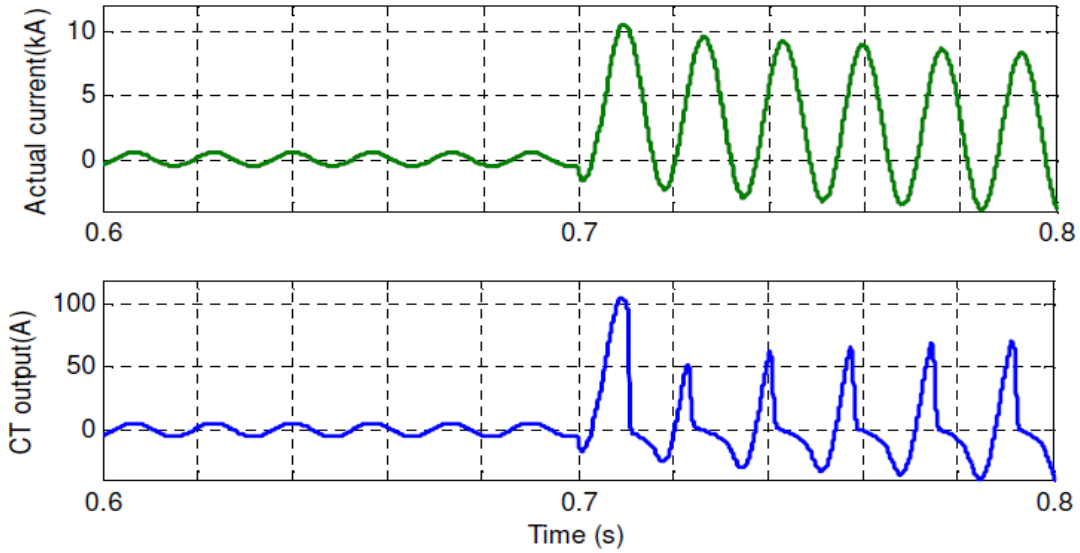

Figure 5.23 Current Waveforms during Conventional CT Saturation

The upper part of Figure 5.24 shows undistorted input signal and distorted input signal by saturation. The dotted line represents the primary current scaled to secondary, while the full line represents the secondary current, which is supplied to the relay model.

Dotted line in lower part of Figure 5.24 presents trip signal for the undistorted input signal, while the full line presents trip signal for input distorted by saturation. The impacts of CT saturation on relay operation as shown in Figure 5.24 appear clearly as time delay of sending tripping signal by more than one cycle. The delay is long enough that it may present mal-operation of the entire power system.

For fair comparison, a protection system over current numerical relay model using OFCT is evaluated during symmetrical and asymmetrical faults at different locations.

First location at backward direction on line (10 %) that faults is simulated for the different cases. In addition, forward locations (10 %, 70 %, and 90 %).

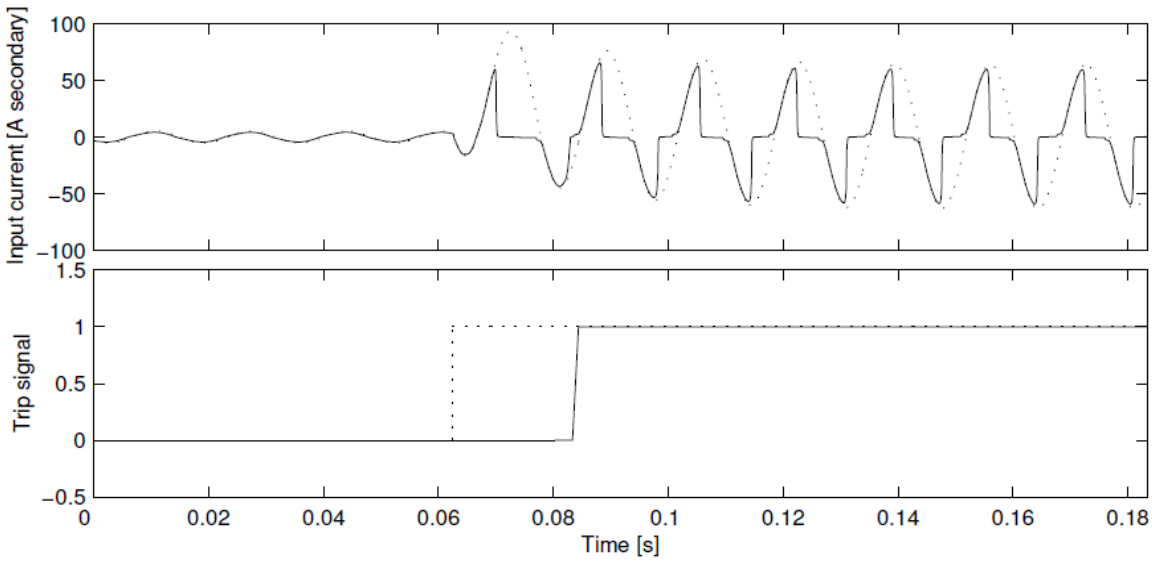

Figure 5.24 Impact of CT saturation on Relay Responses

The trip signal and time response of the relays were recorded and plotted for all selected cases. In both the symmetrical and asymmetrical faults in the power system are accurately detected and fastest isolated. The OFCT output is monitored by tracing peak-to-peak values of the signal and compared to a set threshold. Threshold setting of relay is carefully chosen to ensure that there is a comfortable margin for both sensitivity and stability of the scheme. Additionally, a small stabilizing delay of 0.5 ms has been applied to prevent spurious tripping on random noise. Similarly, different fault conditions are simulated on the system using the proposed OFCT and numerical overcurrent relay algorithm.

Figure 5.25 depicts an operation of overcurrent digital protection system with FOCT and a trip signal generated in response to normal condition. As expected the protection system remain inactive and trip signals are activated.

For verifying protection sensitivity, different fault conditions were used. The simulation results indicated that the Overcurrent relay could detect an occurrence of a fault, which extract current value from OFCT. By passing this current value into simple threshold comparison, the relay generates a trip signal.

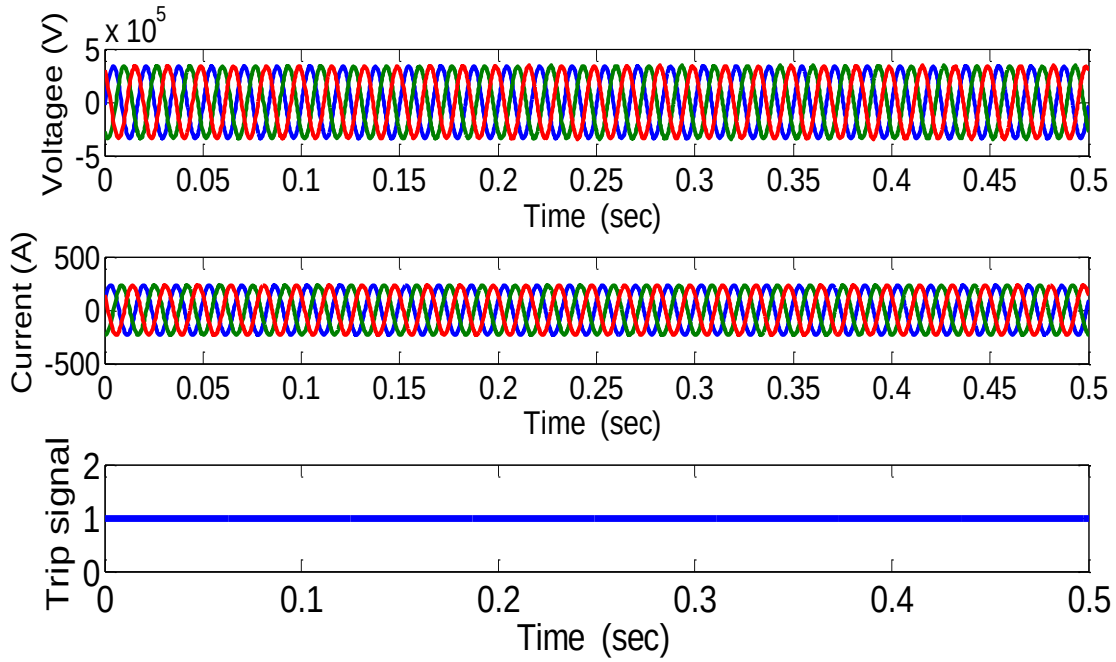

Figure 5.25 Normal Operation Condition and Trip Signal

Firstly, the FOCT is tested during single line to ground fault (SLG) which is the most common faults in the power system. The relay is activated when the SLG fault occur at 0.1 sec and send the trip signal at 0.22 sec with total time delay of 0.12 sec as shown in Figure 5.26 which shows that the relay tripped after around the 6th cycle of the fault, and it ended when the fault current became zero. The simulation results demonstrates the effectiveness of FOCT during SLG fault.

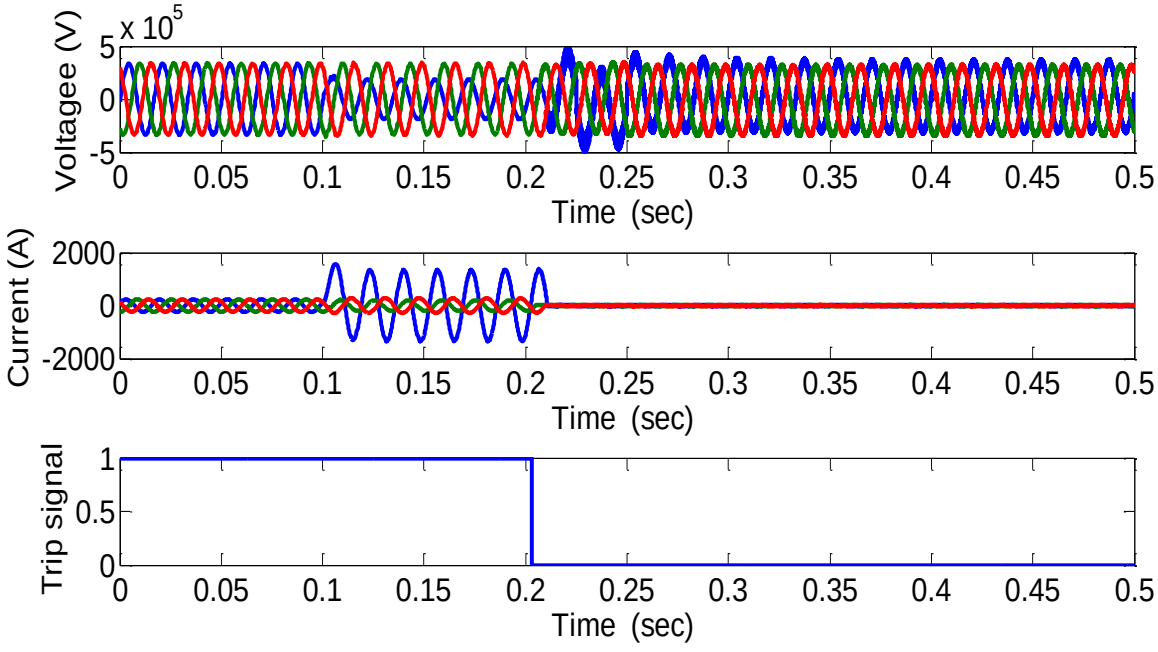

Figure 5.26 Single Line to Ground Fault and Trip Signal

In addition, the FOCT is tested during fault (L-L) for more elaboration and to examine the behavior of voltages, currents, trip signal, and the complete protection system. In this case the relay is activated when the L-L fault occur at 0.25 sec and send the trip signal with delay time of 0.37 sec as shown in Figure 5.27. The simulation result demonstrate the effectiveness of FOCT during L-L fault

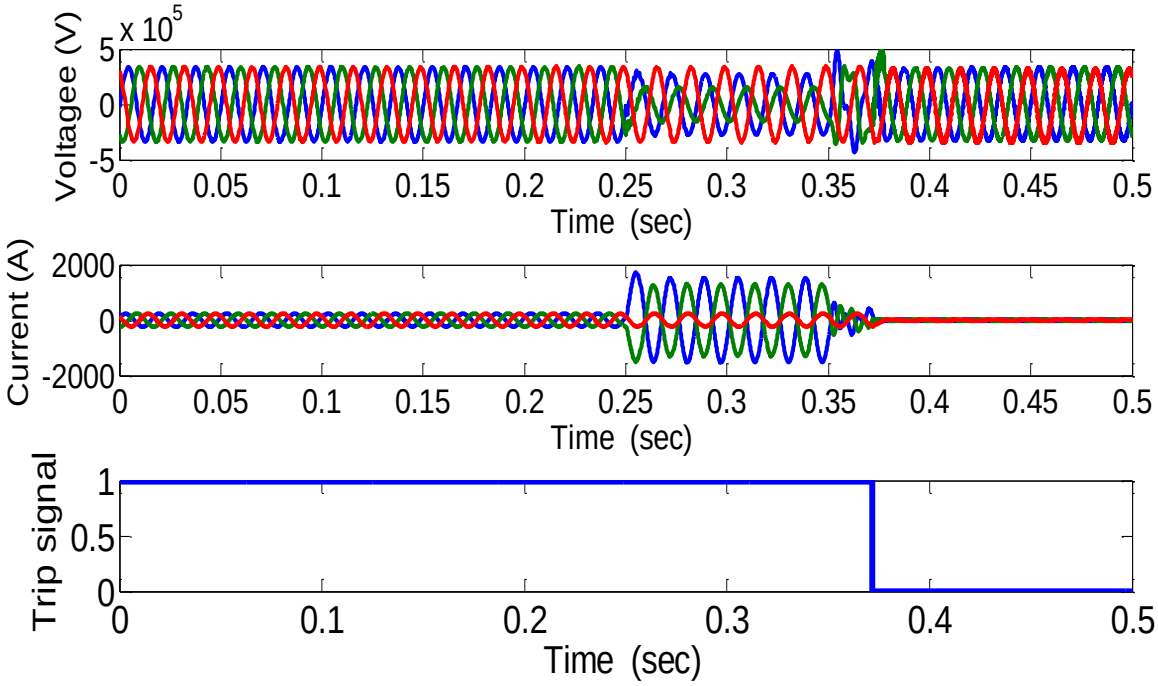

Figure 5.27 Double Lines and Trip Signal

In addition, FOCT is tested during double line to ground fault occur at 0.12 sec as shown in Figure 5.28. The simulation results explain the behavior of three phase input voltages; three phase input currents and the trip signal sent from the numerical relay to the circuit breaker.

Again OFCT is tested during symmetrical three phase fault occurrence at 0.2 sec. The simulation results demonstrate the behavior of the protection system is shown Figure 5.29. Which explains the behavior of sending end voltages and currents with the trip signal. The system responds rapidly and accurately and sends trip signal after a 6th cycle delay.

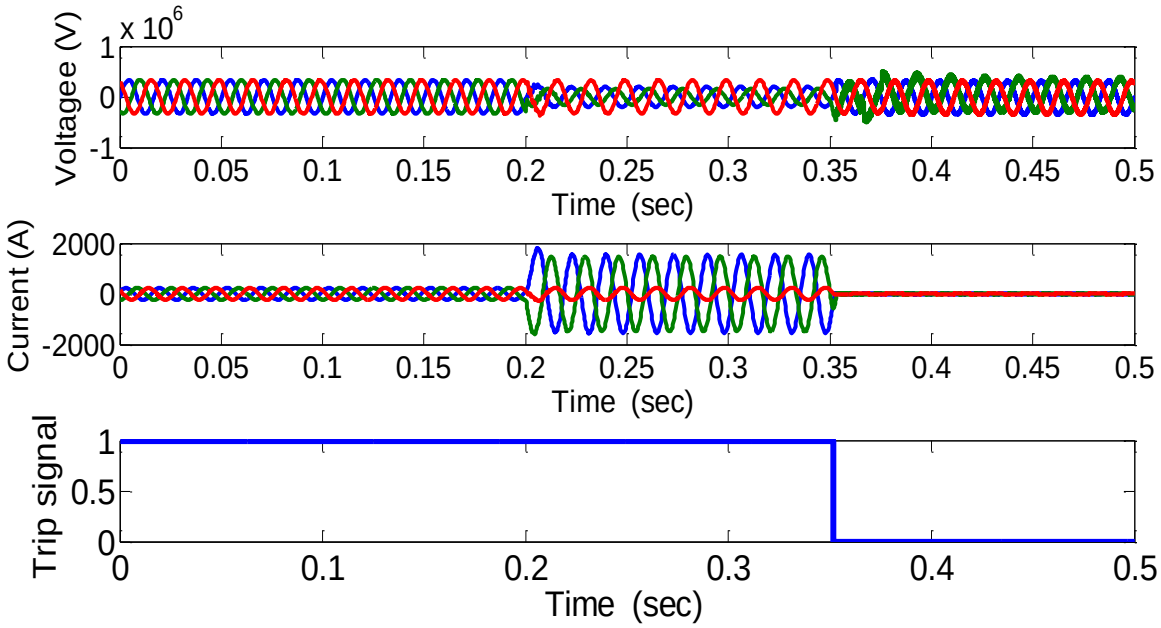

Figure 5.28 Double Lines to Ground Fault and the Trip Signal

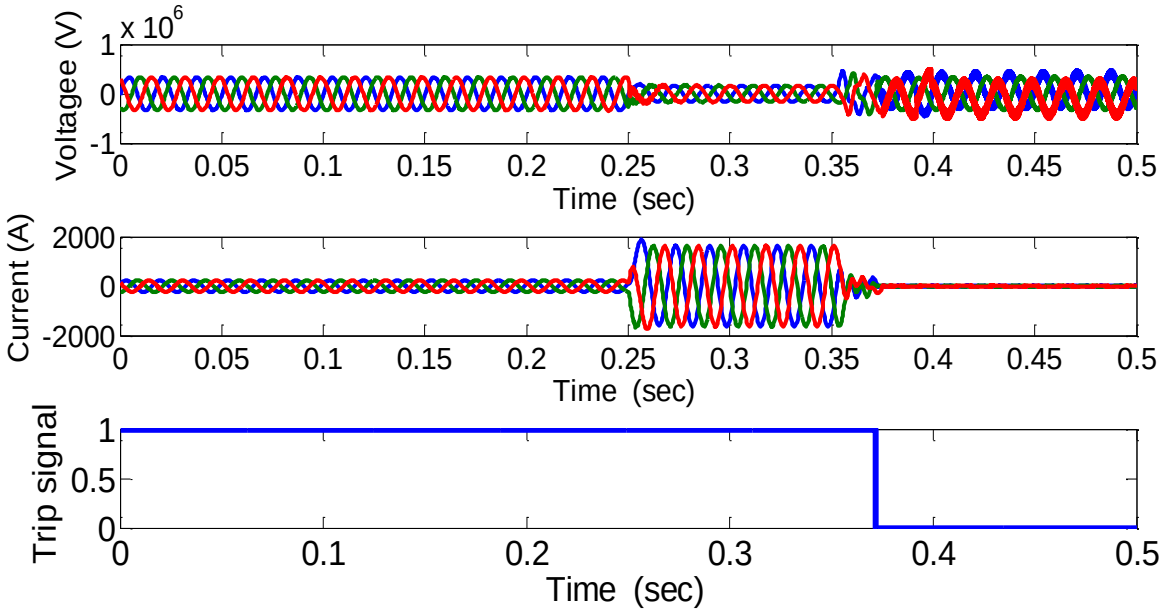

Figure 5.29 Three Phase / Ground Fault, and the Trip Signal

From the developed OFCTs and numerical relay model results shown in figures 5.25 to 5.29, it is clear that, the overcurrent protection functions using OFCT significantly introduce improvement in performance with respect to trip decision and average tripping time. Average operating times for the faults clearance are considerably lower than those of the conventional CT model. Performance of the novel system based on

OFCT can be regarded as excellent when considering simulation results for the overcurrent protection function.

As can be seen from the simulation results obtained, the protection system performance is as expected. However, it could be further improved by better matching of the OFCT to the required current level. The present imperfection in the matching between the operating ranges of the OFCT and the level of noise in the present system. In terms of the current measurement, the measurement error is very small about 2% during the fault. The characteristics of this error are different to those of conventional CTs in that the noise level does not worsen as the input levels rise. Instead, noise levels are constant and percentage current errors will improve post-fault. The present high level of noise in this preliminary implementation can be highly improved by better matching of the operating ranges of the OFCTs to the expected nominal and fault levels. It is anticipated that such refinements could readily reduce measurement errors to less than 1% across the required dynamic range, which easily exceeds existing measurement OFCT standards for protection.

The simulation results show that the OFCT is capable of eliminating the distortion of signal caused by conventional CT and hence greatly improving the reliability of the numerical protection system. Maintained the distortion in acceptable levels will guarantee that performance of protection system is accurate and fast without mal-operation.

5.7.2 Distance Protection Scheme

Distance Numerical Relay always operates in three zones to protect transmission lines. Zone-1 is main protection and other act as back-up protection. The relay performance is tested for both primary and backup zones of protection. The model should be transparent to different types of faults considering the selectivity and the operational time. Every fault type is simulated at different locations along the protected transmission line.

The instantaneous impedance values are calculated based on the voltage and current amplitudes and phases by using conventional instrument transformer.

A typical setting of a mho distance relay uses zone-1 as a primary protection that covers 80% of protected transmission line. Intentional trip time-delay for faults

detected in this zone-1 is set to 0 ms, zone-2 as backup protection which covers remainder 80% through 120% of next protected transmission line time-delay for trip for the faults in this zones is set to 20 power system cycles and zone 3 to protect 100% of immediate line and 150% of next line. If there is more than one next line whether parallel or different feeders, the approach is to use impedance line of the longest line and to assume other lines are out of service, which increases impedance line to have the largest possible protective region.

The zones of protection are set follow, primary zone of protection covers 80% of transmission line with instantaneous operation, and secondly backup zone covers remainder (80% through 100%) of the transmission line. Figure 5.30 depicts the trip signals for all protection zones during normal conditions. The operating characteristics of MHO relay during normal conditions are shown in Figure 5.31.

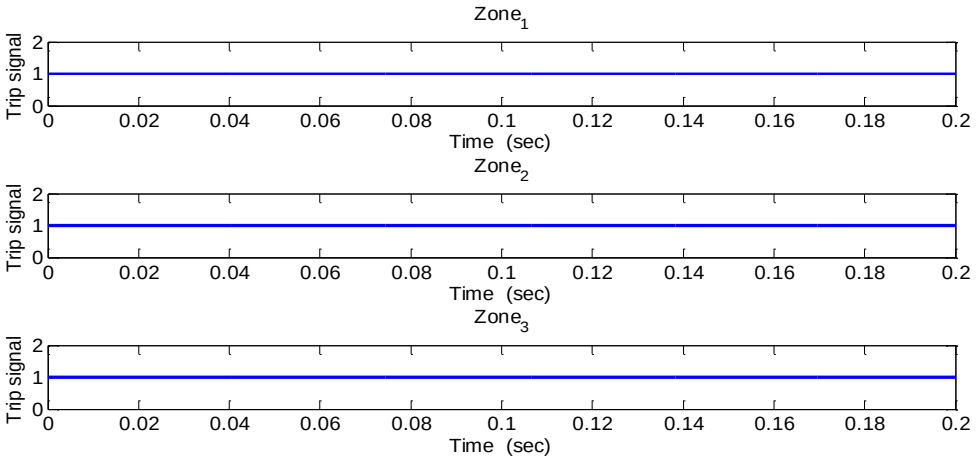

Figure 5.30 The Normal Operating Trip Signal

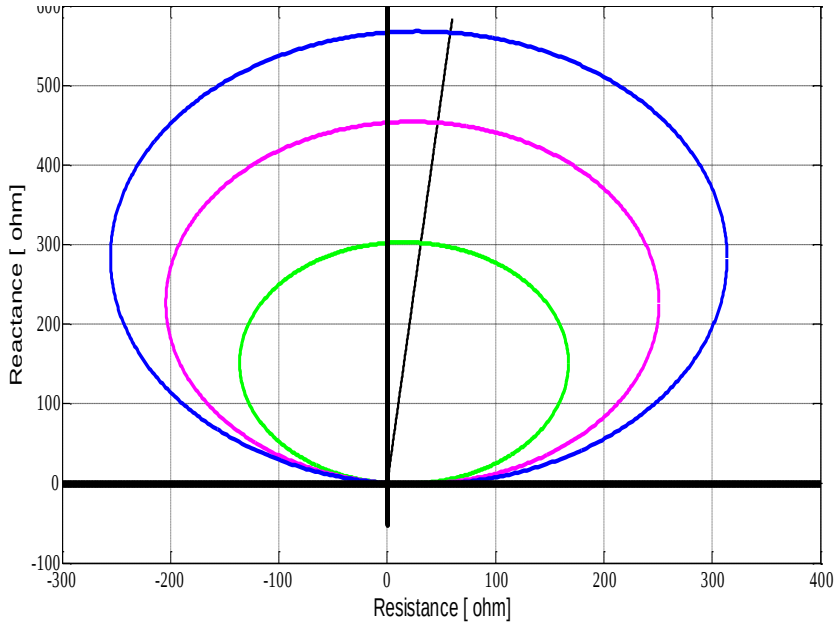

Figure 5.31 the Impedance Trajectories at Normal Operation Condition

The obtained impedance results are illustrated in MHO diagrams to clearly present the reach issues influenced by CT distortion during fault condition. Initially, simulation was carried out to evaluate impact of Current Transformer saturation on fault clearance time.

A phase A-to-Ground (AG) fault is simulated at different location of the transmission line length**.**

Fault impedance is calculated from undistorted and distorted input current and voltage signals. The Fault impedance located in distance relay MHO characteristics, which are determined by the saturated and unsaturated conventional current transformer are shown in Figure 5.32. The obtained results show that fault was identified within zone-1 during the first 50 Hz cycle after the fault inception for undistorted input signals, while the relay model miss-operation by failing to detect a fault in zone-2, and asserted only an intentionally-delayed trip signal (relay acted only as a backup protection) for distorted input signals. The relay model response in this case was unexpected. Such behavior clearly demonstrates negative impact of distortions caused by current transformers (CTs). The dc off-set component in the fault current and remanent flux in the CT, as well as CT secondary total resistance cause the CT to saturate at a lower current magnitude and a phase shifting in the current. The reduction of the current magnitude may result in the distance relay under-reaching or

slower relay operation. Meanwhile, the phase shifting in the current may result in the distance relay overreaching.

in The impact of CT saturation on distance protection scheme based schemes are studied. Saturation of the CT is evaluated for faults near to the relay location and at the reach setting. The impact to reach (underreach or overreach) and operating time are both evaluated.

In order to demonstrate the impact of conventional CT saturation in distance protection scheme, the impact of CT saturation is evaluated for faults near to the relay location and at the reach setting. The impact to reach (under reach or overreach) and operating time are both evaluated. Figure 5.32 depicts the impact of CT on distance relay MHO characteristics. From Figure 5.32 the results show that when the CT is not saturated, the relay would operate appropriately even if the protective reach were lower than the original setting. On the other hand, when the CT undergoes distortion, the measuring algorithm detects the fundamental frequency component of the fault current with a lower value than the actual.

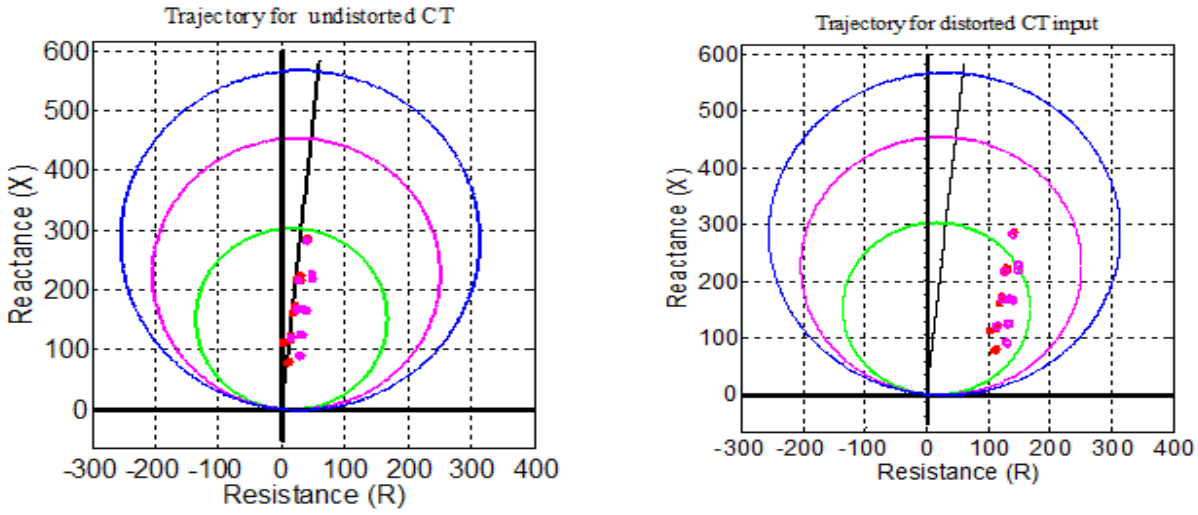

Figure 5.32 Impact of CT on Distance Relay MHO Characteristics

Consequently, they can make the calculated impedance trajectory to enter and exit the zone of protection before the trip signal is asserted, or the calculated trajectory may not enter the zone of protection during the first cycle in which the fault occurred. The relay will believe that the fault is out of its protective zone-1 and thus out of its

responsibilities. Therefore, the effect of the current transformer saturation can cause a delay in issuing a trip signal. It should be noted that if the CT undergoes saturation by the symmetrical fault current, the impedance trajectory calculated by the measuring algorithm may never enter the zone of protection. This is situation in which the relay would not operate appropriately unless the protective reach is increased.

To overcome these problems, the optical fiber current transformer (OFCT) can be used. As well as the same approach and steps used in the previous simulation model through different operational conditions are follows. The conditions are committed to checking the performance of the numerical distance relay during normal operation and abnormal operation. Emphasis replaced conventional instrument transformer by optical ones to obtained voltage and current waveforms along with the developed R-X impedance trajectory for different conditions. The simulation scenarios considered various fault locations, fault types, and different fault inception angles to expose the numerical distance relay model to a realistic range of conditions expected in the field. Similar to the previous scenario, the numerical distance relay model is examined using optical instrument transformer, and different fault types at different locations were applied. In addition to test the effect of fault location on the relay response covered by protection zones. The resulting values were compared with the protection zone boundaries defined for each optical fiber current transformer and optical voltage transformer as 80%, 120 %, and 150% of the line length for Zone-1, zone-2 and zone-3 respectively.

Pre-fault and post-fault voltage and current waveforms are obtained from the simulation tests for the case of a single phase to ground fault at 50% of the line length from relay position are shown in Figure 5.33.

The voltage and current waveforms show the expected response and successful operation of relay model. When the fault occurs, the three-phase bus-bar voltages behind the relays at each end of the line are pulled down until the circuit breakers are opened. The measured voltage is distorted by high frequency components while the current waveforms exhibit exponentially decaying dc components after fault inception. The current waveforms increase in magnitude when the fault is initiated and become zero when the relays operate the circuit breakers to clear the fault.

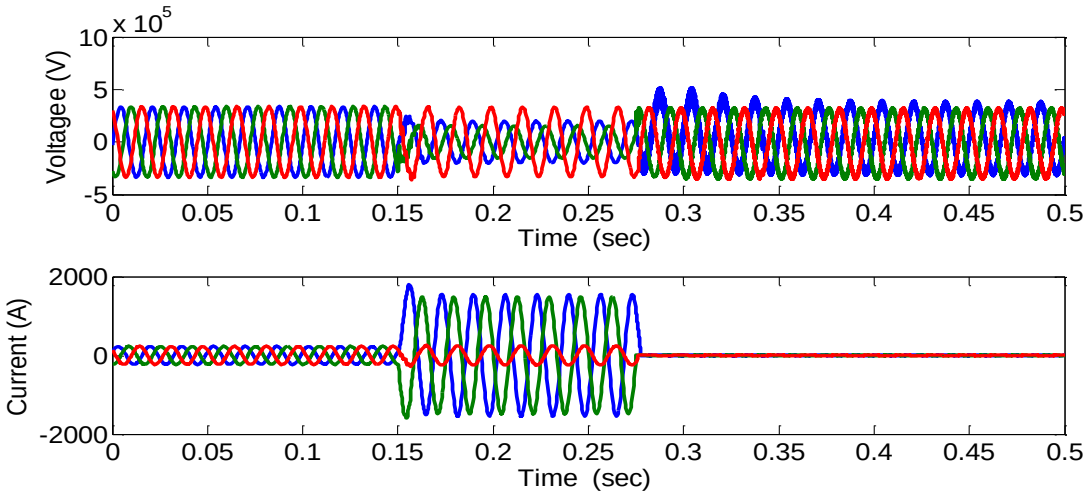

Figure 5.33 Double Lines to Ground Fault and Post-fault Voltage and Current Waveforms

Figure 5.34 shows the fault initiation signal applied within the simulation study, and the trip signals sent by the relays to operate the circuit breakers in the simulation in response to this fault. The results show that relay issued trip signals 0.12 sec after the fault inception. Each circuit breaker opened a few milliseconds later on the next zero crossing of the current waveform in each pole of the breaker.

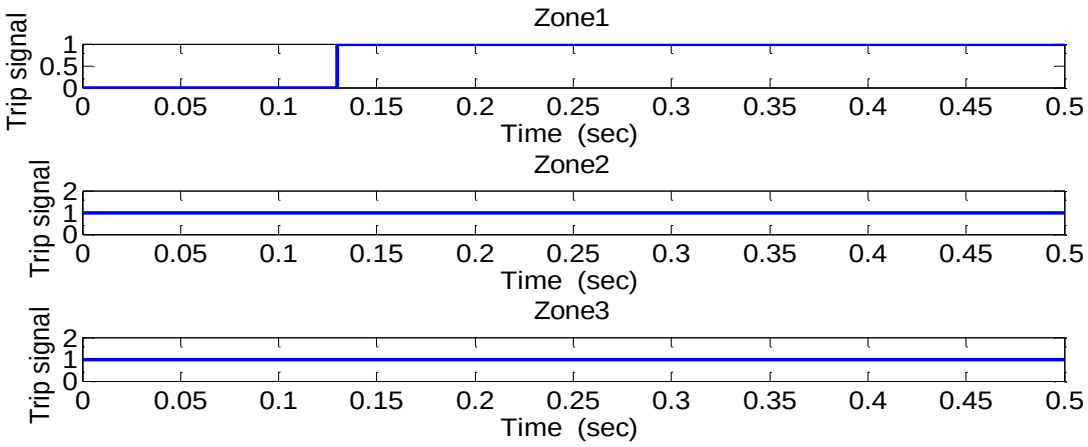

Figure 5.34 The Relay Trip Signals for Single Phase to Ground Fault

Figure 5.35 depicts the measured impedance locus for different phase-to-phase fault locations and for different.

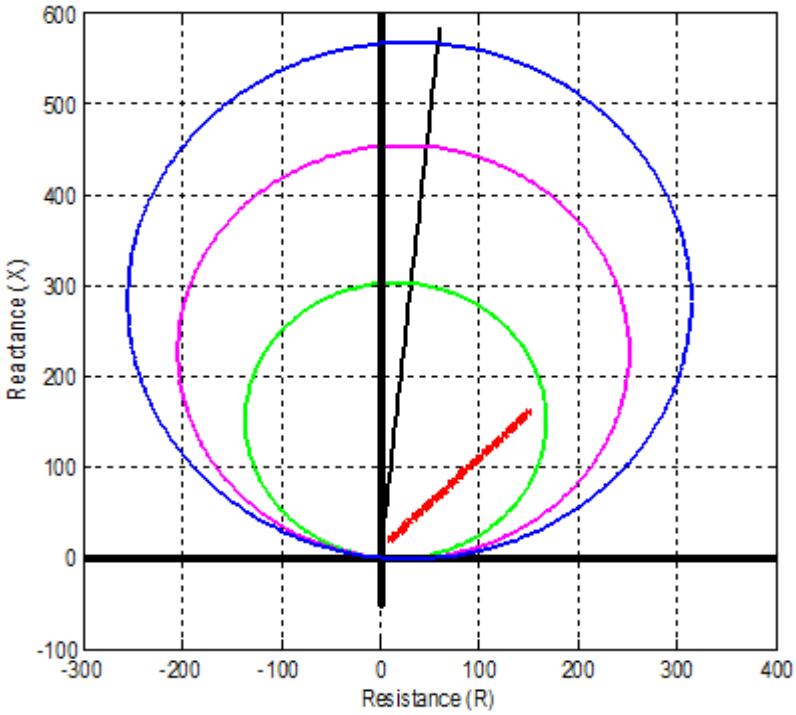

Figure 5.35 Fault Impedance Locus for Fault at Zone-1

From the simulation results, it is noticed that (0% km to 80% km) all faults fall into the primary protection zone-1, the apparent impedance is less than the pre-set value of zone-1 and the relay operate appropriately.

As the same of a previous simulation scenario, a phases and Ground faults applied fall into the backup protection zone. A fault location was covered by zone-2 and zone-3 but it is not covered by zone-1 protections, then relay over reached this fault at the boundary of zone-1 will not trip. As results, distance relay operate at Zone-2 and trip signal was delayed by 20 cycles (0.4 sec). Figure 5.36 shows the relay trip signal Zone-2 tripped 0.4 sec after fault. The three phase to Ground fault impedance trajectory is shown in Figure 5.37. The fault impedance trajectory entered the protection zone-2 characteristic and settled on the protected line. The zone-2 and zone-3 output crossed the trip level after fault occurred. Zone-1 was not because the fault location was out of its reach.

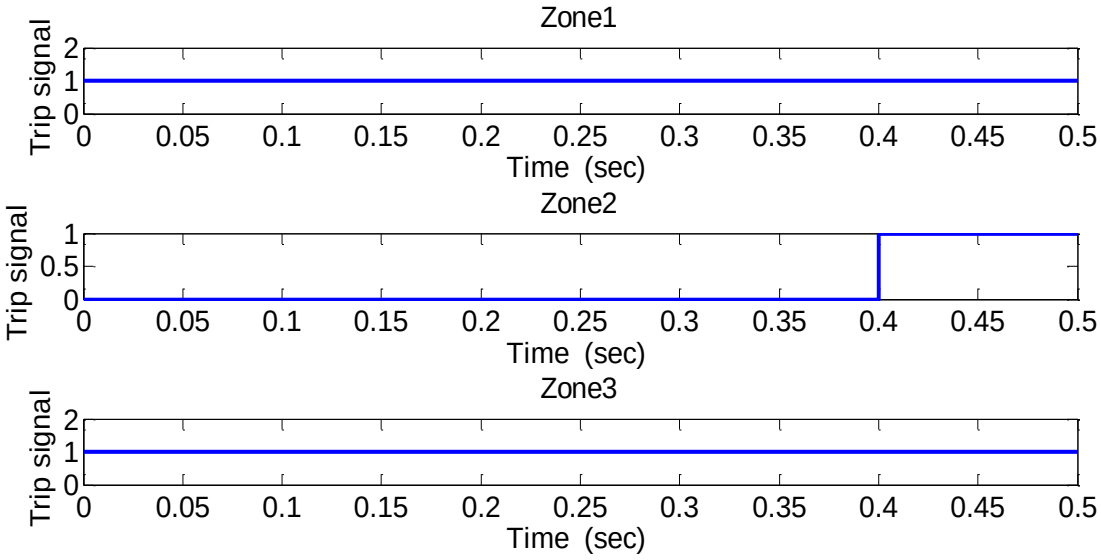

Figure 5.36 the Relay Tripped in Zone-2

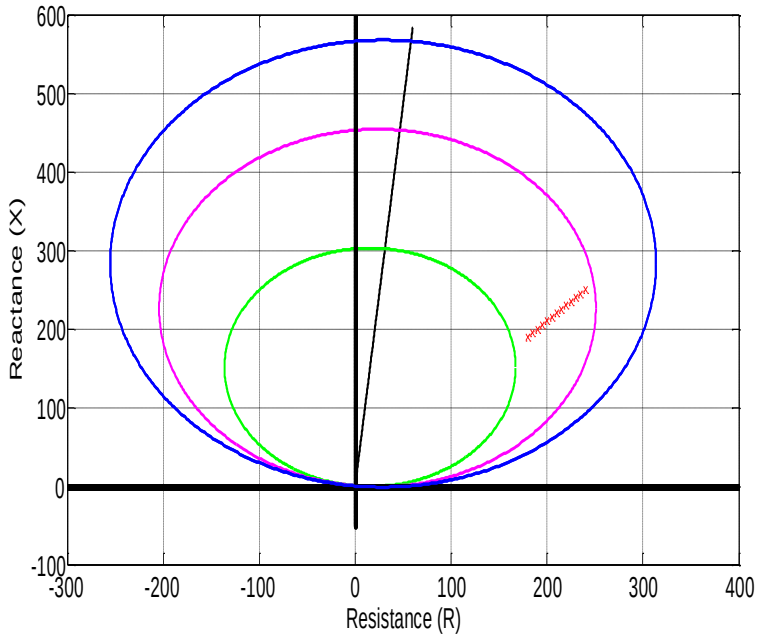

Figure 5.37 Fault Impedance Locus for Fault at Zone-2

In case of the fault was occurred outside of the distance relay's protection zones. Therefore, the based on accurately calculation of the apparent impedance and fault location the relay will determine that the faults are out of its protective region and thus out of its responsibilities. Therefore, there was no tripping in response to this fault. The protection trip signals for fault outside of the numerical distance relay's setting protection zones are illustrated in Figure 5.38. The fault impedance trajectories are shown in Figure 5.39. None of the impedance trajectories entered the protection zones. They all settled on the protected line.

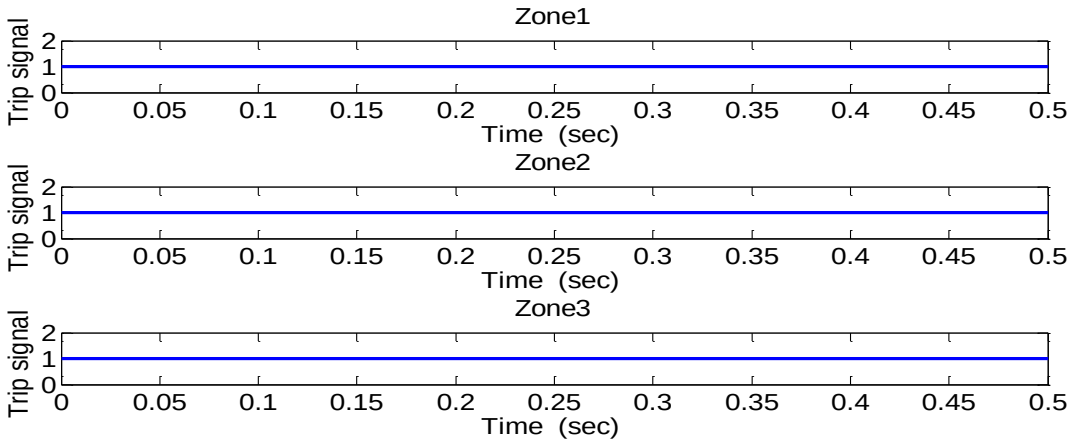

Figure 5.38 Trip Signals for Fault Outside of the Relay Model Setting Zones

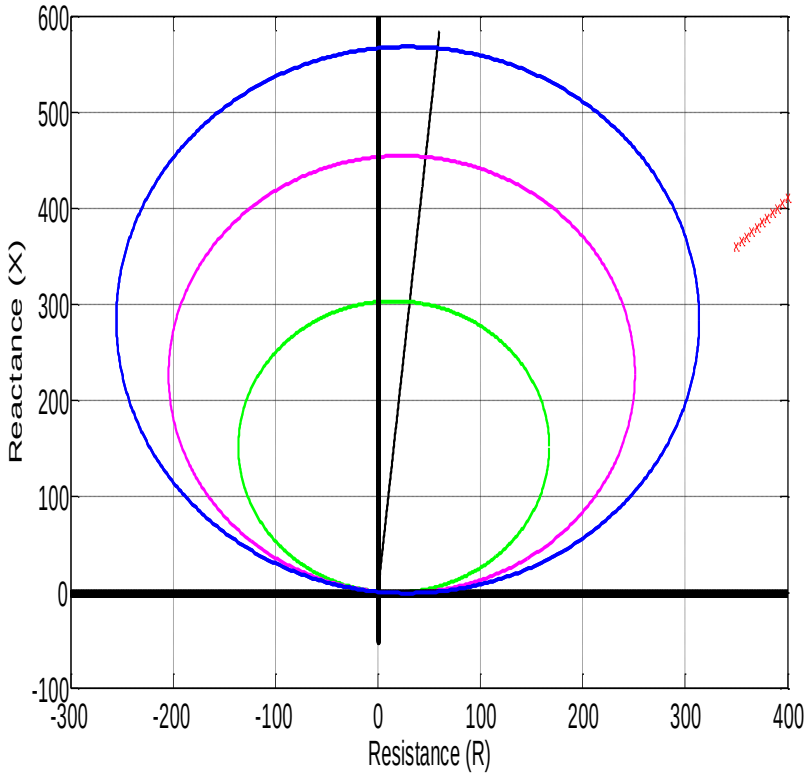

Figure 5.39 Fault Impedance Locus for Fault Outside of Selected Setting Zones

Consider, the previous scenarios, the simulation results were carried out, the apparent impedance is less than the pre-set value and the numerical relay model operate properly. On the other hand, when the apparent impedance is more than the pre-set value and the relay does operate appropriately. Further, it has been shown that, the numerical relay model is issued trip signal if the impedance is within a selected range. Whereas, they did not operate when fault occurred was outside of their protection zones. The impedance locus seen by the relay is clearly visualized and the fault location can also be estimated from the plot. The numerical relay model can also be

verified by comparing the impedance location on the MHO characteristic with the fault location calculation of the numerical relay model under test. The performance of MHO characteristics was schematically evaluated during phases and ground faults.

From simulation results, it is clear that developed model successfully evaluated the performance power system protection using the optical OFCT and OVT for different operational conditions.

The performance of distance protection with conventional CT and OFCT has been investigated. Various factors contributing to the current signal distortion, e.g., CT saturation and OFCT current clipping; has been evaluated. The dc offset component in the fault current and remanent flux in the CT, as well as CT secondary total resistance cause the CT to saturate at a lower current magnitude. These phenomena do not exist in OFCT. The OFCT current clipping will only occurs if the fault current magnitude higher than the OFCT maximum detectable setting current. This indicates that it is easier to prevent OFCT current clipping than the CT saturation, except when the CT is largely over-dimensioned, which is sometimes impractical. CT saturation results in a reduction of the current magnitude and a phase shifting in the current. The reduction of the current magnitude may result in the distance relay under-reaching or slower relay operation. Meanwhile, the phase shifting in the current may result in the distance relay over-reaching. On the other hand, the OFCT clipping will only result in a reduction of the current magnitude, but will not result in a phase shifting in the current. Hence, the OFCT current clipping will not cause the distance relay over-reaching.

The facts that CT may cause both under-reaching and overreaching, meanwhile OFCT may cause under-reaching only, and it is easier to prevent OFCT current clipping than CT saturation, indicate that the modern OFCT can provide the distance protection better security than the conventional CT.

Results obtained carried out, the OFCTs and OVTs, based on new sensing technologies, showed excellent performance for all simulated power system conditions. The performance indices for both, time and frequency domain indicate that OFCT and OVT deliver nearly distortion- free replicas of signals from their primary side. Therefore, they are maintained the distortion in acceptable levels, consequently, it is possible to guarantee that performance of protection system

numerical relay will not be affected or influenced by unacceptable conventional instrument transformer performance.

5.8 Summary

The performance evaluation of numerical protection schemes based on OFCT has been simulated and discussed in this chapter. Specific criteria for OFCT performance are evaluated as well as for the different elements of the protection schemes (optical fiber current transformer, and numerical protection relays). An evaluation methodology was developed and used to perform overcurrent protection and three-zone distance protection simulated according to the different fault types. An optical instrument transformer using protection schemes and conventional instrument transformers with protection schemes were simulated and used to compare the performance indices.

The operating performance of the overcurrent numerical relay fed by OFCT was determined using various simulation scenarios based on operating characteristic, and trip-times. Overall structure of the simulation environment and its software implementation were build in MATLAB M-files for OFCTs simulation, and SIMULINK for Numerical protection relays. This simulation is provided in Appendix C. Results obtained prove that OFCTs are capable to measure current with very high accuracy over wide dynamic range with acceptable errors that match the IEC 0.2 class accuracy requirements. Furthermore, OFCTs are providing direct to digital outputs according to the IEC 61850 standard, these outputs are immediately compatible with modern digital substation communication. According to the results obtained, OFCTs has extraordinary features, which makes it more suitable for replacing conventional CTs.

Results have show that, developed model can successfully evaluate the performance of power system protection using optical fiber current transformer (OFCT) and optical voltage transformer (OVT), for different operational conditions. The results provide a fundamental reference for all participating parties to create a roadmap to achieve the wide deployment of the next generation of the “copper-less” secondary systems based on the Optical instrument transformers and digital Ethernet communications. Optical instrument transformers also provide a solid basis for future

Smart Grid solutions and provide reliable and cost-effective protection and control. The optimal application of an Optical instrument transformer based protection scheme can be achieved by close collaboration between protection specialists in academia and industry. The codes of the MATLAB functions that are used to simulate OFCT, OVT and numerical relay fault detection algorithm are presented in appendix B**.**

Chapter Six
Experimental Work

6.1 Introduction

Measuring electrical currents in high voltage environments using conventional current transformers (CT) is usually an issue that involves a great deal of insulation. Practical solutions are often costly and bulky. The use of optical technology in this field significantly reduces the need for insulation considering its intrinsic dielectric characteristics. Most of the optical sensors used for measuring electrical currents are, in fact, magnetic field sensors based on the magneto-optic Faraday Effect, that is, the induction of circular birefringence in the medium by a magnetic field *H* that causes linear polarized light to rotate its plane of vibration by an angle proportional to the current measured.

This chapter describes the experimental setup and the function of each component used in this work, beside the procedure. In order to verify the optical fiber based power system protection technique experimentally an OFCT is implemented. This chapter details the experimental system and the necessity hardware and software used to perform the OFCT and the performance of power system protection are described. Firstly, the OFCT and its components for measuring the electrical current are demonstrated. Secondly, the electronic signal processing circuit operation is confirmed and then some partial test of the full circuit under load is presented. Due to lacke of some components full power circuit test isn't achieved, so a final simulation of the circuit operation is presented. The relevant features of the Programmable Interrupt Controller (PIC) microcontroller as numerical multifunction relay and its interface circuit are presented.

6.2 System Hardware Components Description

A portable prototype comprises of a lightweight sensing head and a portable interrogation unit connected by fiber optic cable is tested to assess their viability as a versatile meter and protection system in high-power grids. The hardware components

necessary to assemble a basic test OFCT system for measurement and protection system are described as follows:

- Electrical current source (MEGGER PCITS2000/2 Primary Current Injection Test Set made by AVO–MEGGER).
- DC Power Supply.
- Laser source (with wavelength 632 nm) He Ne laser.
- Light Dependent Resistors (LDR).
- Single mode optical fiber and its accessories
- Optical Polarizer and objective lenses.
- Polarizing Beam Splitter as optical analyzer.
- PIC16F877A Microntroller based circuit for OFCT signal processing.
- PIC16F877A Microntroller based circuit for Numerical relays implementation and signal interface circuits.
- Host PC executing software.

These components are integrated together to conduct the optical fiber current transformer based power system protection test. Once all the individual circuit in the system is tested independently and proved to be working, the blocks are put together and tested. The architecture of the hardware to build complete setup used for the experimental test of the experimental model is depicted in Figure 6.1. In order to verify the performance the proposed OFCT experimental setup is shown in Figure 6.2.

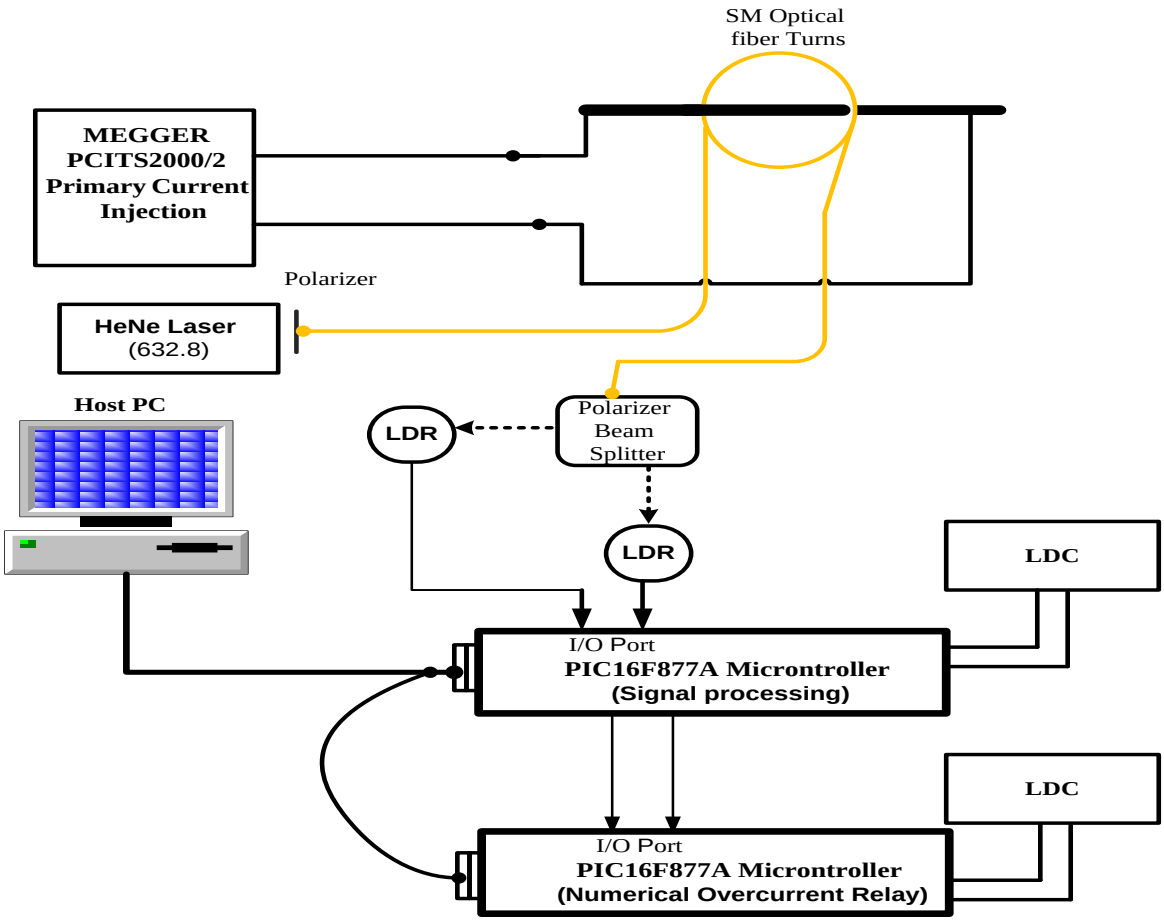

Figure 6.1 Architecture of experiment for the OFCT based protection system

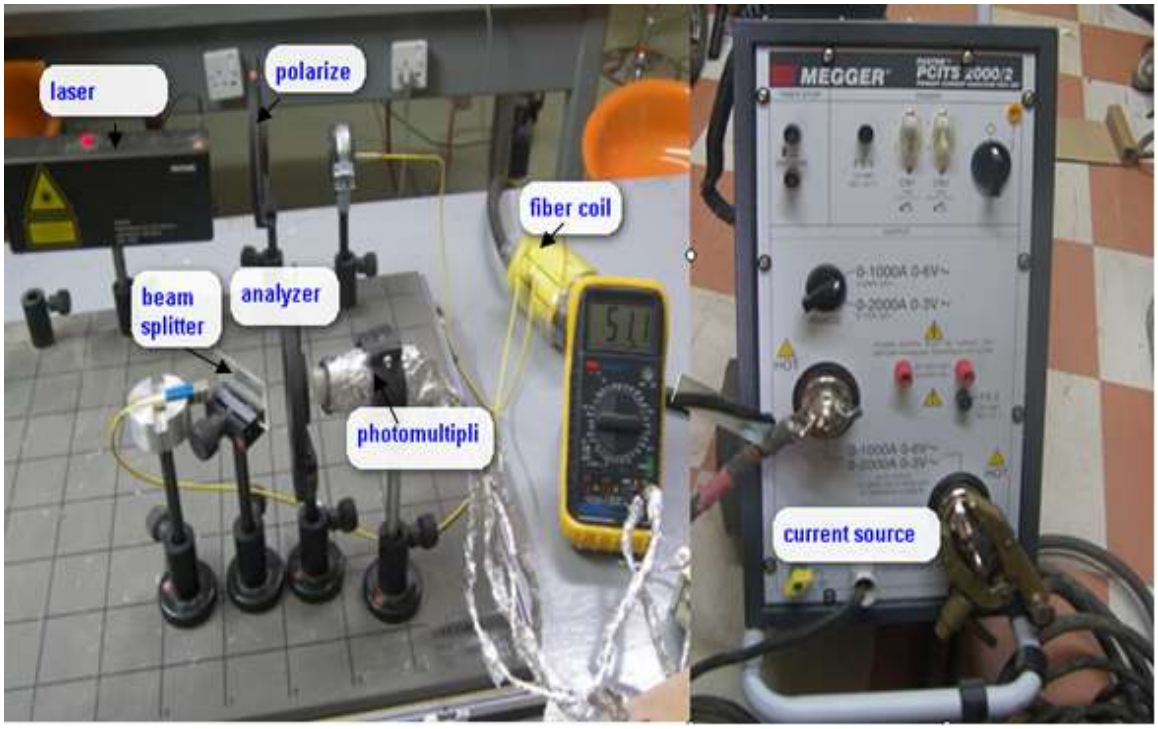

Figure 6.2 Experimental setup

6.3 Readout of Optical Fiber Current Transformer

The Optical Fiber Current Transformer constructed for the aim of this work consists of laser source, polarizer, single mode optical fiber, polarizing beam splitter, and photodetector.

6.3.1 Laser Light Source

The laser source used is a high power HRP050 from PHYWE, which is illustrated in Figure 6.3. It is a red polarized He-Ne laser with a wavelength of 632.8 nm and power outputs up to 1 mW. The Helium Neon laser used because of the following reasons:

- It has low beam divergence (high collimation) provides easy coupling the beam in single mode optical fiber.
- It has suitable wavelength (632.8 nm) to provide high Verdet constant allowed strong Faraday Effect.

Figure 6.3 Helium Neon laser

6.3.2 Polarizer

The polarizer is used to polarize incident light beam (linear polarization) aligned in front of the sensing element (optical fiber). The polarizer used is represented in Figure 6.4, which is made by PHYWE system GmbH.

Figure 6.4 Polarizer

6.3.3 Optical Fiber Sensing Coil and its Accessories

Single Mode cable is a single stand of glass fiber with a diameter of 8.3 to 10 microns that has one mode of transmission. A single Mode Fiber with a relatively narrow diameter, through which only one mode will propagate. The single mode fiber is made by AMP HOLLAND. It has a core /cladding diameter 9/125 µm stamped on the yellow cable jacket and terminated with connectors FC and SC. SC is a push/pull type connector. This connector has emerged as one of the most popular styles. Single mode is used to maintain state of polarization and it is used as a sensing element.

Two aluminum holders are used one to coupling laser beam into the fiber and the other to align beam into photo-detector. Micro lens is used as an optical collimator.

Figure 6.5 is shown the optical fiber sensing coil and its accessories.

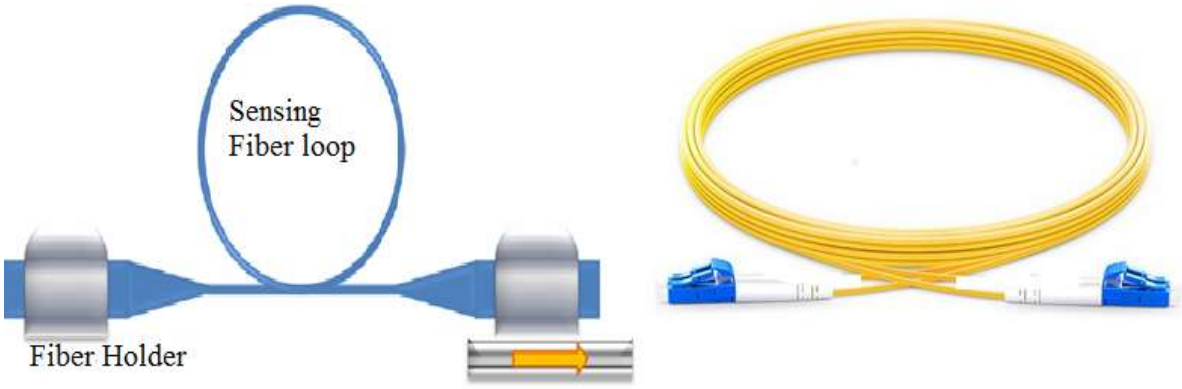

Figure 6.5 Optical Fiber Sensing Coil and its Accessories

6.3.4 Polarizing Beam Splitter

Polarizing Beam splitters (PBS) are available in two forms: plates and cubes. The low polarization dependence of the metallic-dielectric coating allows the transmission and reflection for S- and P-polarization states to be within 3% of each other. This means that they will not change the state of polarization of the incident beam. The PBS that is employed in the experiment is from the Dayoptics. Its wavelength is 633 nm and its dimension is 6.35×6.35×6.35.

6.3.5 Light Dependent Photoresistors

The cadmium sulfide (CdS) or light dependent resistor (LDR) whose resistance is inversely dependent on the amount of light falling on it is known by many names including the photoresistor, photoconductor, photoconductive cell, or simply the

photocell. A typical structure for a photoresistor uses an active semiconductor layer that is deposited on an insulating substrate. The semiconductor is normally lightly doped to enable it to have the required level of conductivity. If light falling on the device is of high enough frequency, photons absorbed by the semiconductor give bound electrons enough energy to jump into the conduction band. The resulting free electrons conduct electricity thereby lowering resistance. The principle of LDR is reducing the element resistance when increasing the intensity of incident light. For the suitable detector circuit connection, a series resistor is necessary for voltage divider and consequently produces an analog voltage range with a certain instantaneous value based on the instantaneous incident light. Providing design engineers with an economical LDR with high quality performance. Token Electronics® now offers commercial grade PGM photo-resistor. Designated the PGM Series, the photo-resistors are available in 5mm, 12mm and 20mm sizes, the conformally epoxy or hermetical package offer high quality performance for applications that require quick response and good characteristic of spectrum. Figure 6.6 shows the physical view of LDR and the detector circuit connection while Figure 6.7 illustrates the LDR as an input to PIC16F877A Microcontroller.

Figure 6.6 Light Dependent Resistor (LDR), (a) Physical view, (b) Wire connection

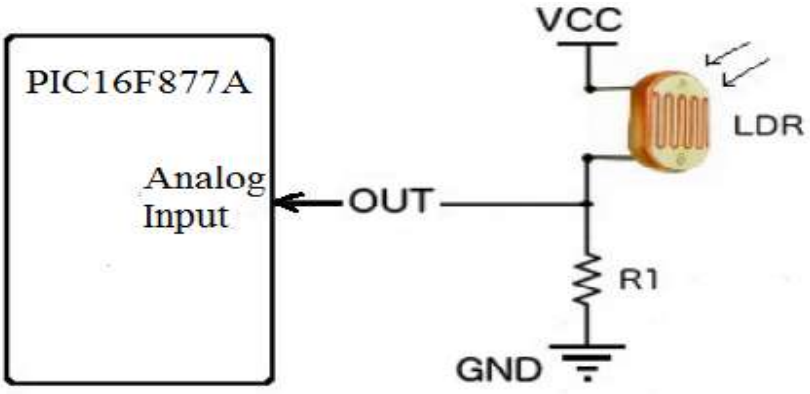

Figure 6.7 Light Dependent Resistor circuit for interface of OFCT to the PIC16F877A Microcontroller DSP ADC input

6.3.6 Signal Processing Electronic Circuit Description

From the perspective of the electronic detection and processing circuitry, optical fiber current transformer present designer with the following challenges:

- Current waveform measured is contained within light in the download fiber. Signal is amplitude modulated on the light carrier and must be converted to voltage if electronic signal processing should take place.
- Light intensity in the receiving fiber is small, typically around 1 nW. When converted by semiconductor light detectors, photocurrent magnitude is in the order of nA. Having in mind portable nature of the device, photomultipliers are not detectors of choice.
- Modulation depth is very small, around 1% for 1 kA rms clamp current.
- Modulating signal should be measured with resolution of 1000:1 and 1% accuracy.
- Fiber motion and laser aging cause both carrier level and signal level shifts.
- Having in mind potential use of this device for measuring harmonic contents of the current, bandwidth of interest is around 2 kHz.

The ultimate objective of this part is to design an electronic signal processing circuitry that uses microcontroller to read light intensities form the OFCT and automatically calculate the corresponding voltage that is proportional to electrical current applied. This design is based on the PIC microcontroller as the main element in the system. The design of this system has been divided into two sections; Hardware design and Software design. A simplified scheme of the implemented electronic signal processing based PIC16F877A Microcontroller as shown in Figure 6.8.

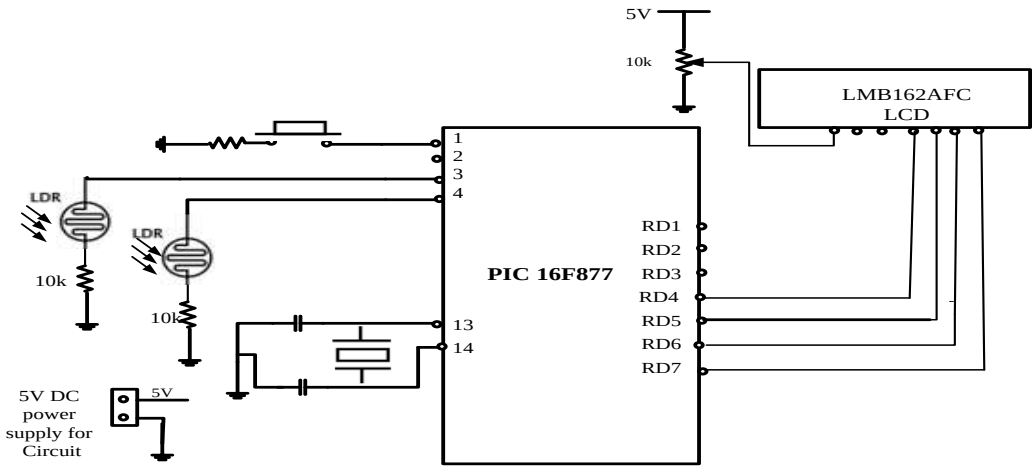

Figure 6.8 The block diagram of the signal processing circuit

6.3.6.1 PIC 16F877A Microcontroller

PIC16F877 is one of the most advanced microcontrollers from Microchip. This controller is widely used for experimental and modern applications because of its low price, wide range of applications, high quality and ease of availability. It is ideal for applications such as machine control applications, measurement devices and study purpose. PIC16F877 has five basic input/output ports. They are usually denoted by PORT A (R A), PORT B (RB), PORT C (RC), PORT D (RD), and PORT E (RE). These ports are used for input/ output interfacing. In this controller, "PORT A" is only 6 bits wide (RA0 to RA7), PORT B, PORT C and PORT D are only 8 bits wide (RB0 to RB7, RC0 to RC7,RD0 to RD7), PORT E has only three bit wide (RE0 to RE7). All these ports are bi-directional. The direction of the port is controlled using TRIS(X) registers, which is used to set the direction of PORT (X). Setting a TRIS(X) bit '1' will set the corresponding PORT(X) bit as input. Clearing a TRIS(X) bit '0' will set the corresponding PORT(X) bit as output.

Based on the number of input/output pins and the other functional features, the PIC16F877A microcontroller has been used as the main device in the development of the electronic detection and processing circuitry. The PIC 16F877A microcontroller is one of the most popular general purpose microcontrollers. It is of 8-bit which means the most available operations are limited to 8-bits. It is a 40-pin IC. The PIC16F877 is contains an ALU which does arithmetic and logic operations, the RAM which is also called the register-file, the program EEPROM (Flash Memory), the data EEPROM and the Working register also called an accumulator. The working register is not a part of the register-file but is a stand-alone. The ALU, the RAM, the Working register and the data EEPROM each manipulate and hold 8-bit-wide data, which ranges in value from zero to 255. The program EEPROM (Flash Memory) works with 14-bit wide words and contains each of the user's instructions.

6.3.6.2 Interfacing LCD to the microcontroller PIC16F877A

Liquid crystal display (LCD) is a type of screen display often used in digital watches, calculators and computers. The LCD display makes use of two layers of polarizing material having solution of liquid crystal between them. When an electric current passes through the liquid crystal, it causes them to align and cause light not to pass

through them. Each crystal acts such as a shutter to either allow or not allow light to pass through. In this research 16 pin LMB162AFC LCD is used to display the readout of optical fiber current transformer. Figure 6.9 shows the LCD pin arrangement.

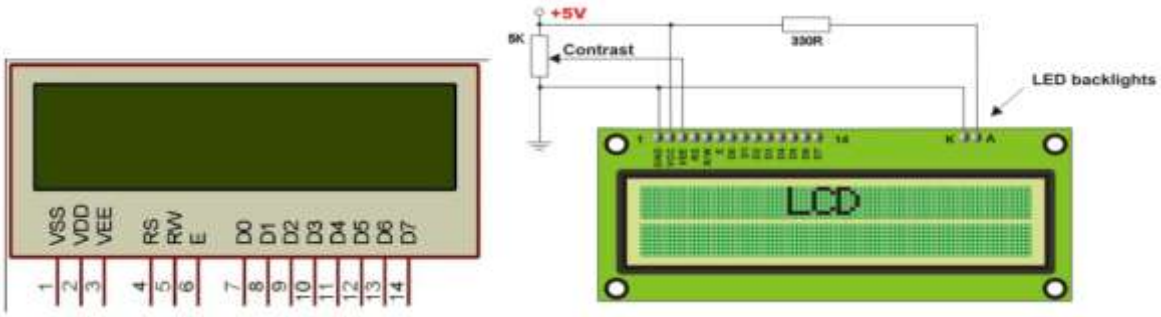

Figure 6.9 LCD pin arrangement

LCD is used to display the readout of optical fiber current transformer. Depending on how many lines are used for connecting an LCD to the microcontroller, there are 8-bit and 4-bit LCD modes. The appropriate mode is selected at the beginning of the operation in the process called initialization. The 8-bit LCD mode uses outputs D0-D7 to transfer data. The main purpose of the 4-bit LCD mode is to save valuable I/O pins of the microcontroller. Only four higher bits (D4 - D7) are used for communication, while others may be left unconnected. Each piece of data is sent to the LCD in two steps-four higher bits are sent first (normally through the lines D4 - D7), and then four lower bits.

Initialization enables the LCD to link and interpret received bits correctly. The standard crystal oscillator gives an accurate frequency and in this case 8MHz crystal is used in microcontroller in order to get internal frequency of 2 MHz. The 8 MHz crystal oscillator is chosen oscillator clock divided by 4 canals to be obtained on OSC2/CLK OUT pin and can be used for testing or synchronizing other logical circuits. Figure 6.10 illustrates LCD interfaced PIC16F877A and crystal oscillator connected to PIC16F877A.

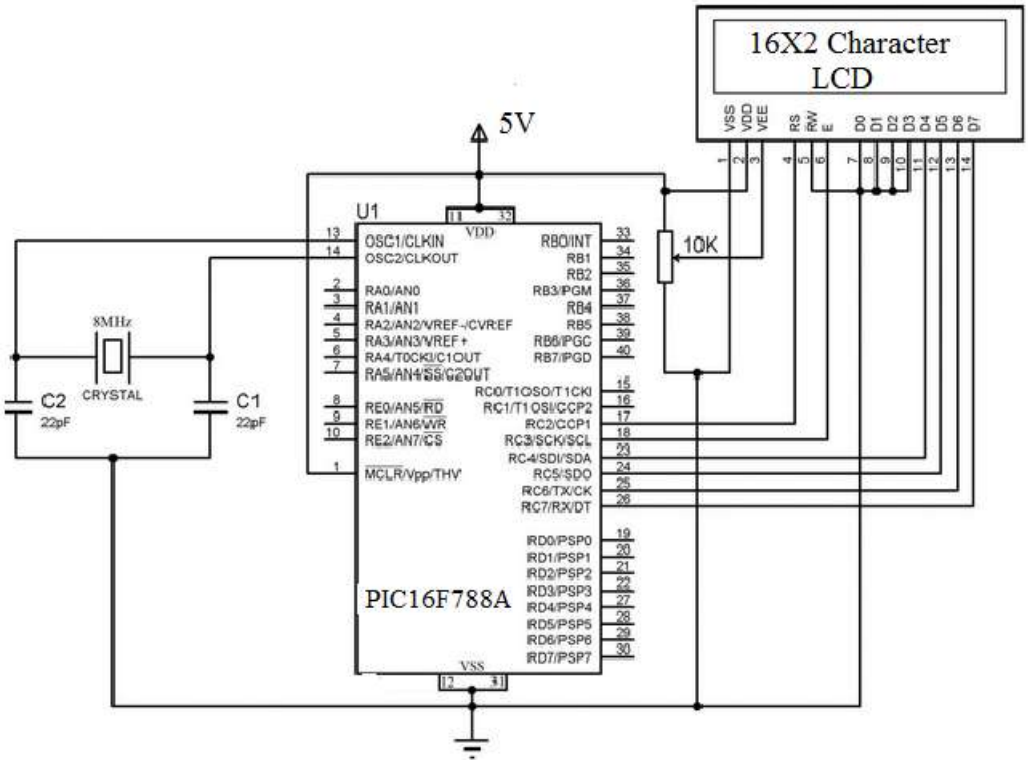

Figure 6.10 Implemented circuit for LCD interfaced and crystal oscillator connected to PIC16F877A

6.3.6.3 Software Description

The mikroC® pro for PIC Compiler allows to write PIC microcontroller applications in C that once compiled have the efficiency and speed of assembly language. Language extensions in the mikroC Compiler give full access to all resources of the PIC microcontroller. The mikroC Compiler translates C source files into relocatable object modules, which contain full symbolic information for debugging with the µVision Debugger or an in-circuit emulator. In addition to the object file, the compiler generates a listing file, which may optionally include symbol table and cross-reference information. PROTEUS® Software; Proteus (**pro**cessor for **te**xt **e**asy to **us**e) is a fully functional, procedural programming language created in 1998 by Simone Zanella. Proteus incorporates many functions derived from several other languages: C, BASIC, Assembly, and Clipper/dBase; it is especially versatile in dealing with strings, having hundreds of dedicated functions; this makes it one of the richest languages for text manipulation.

The Schematic diagram of implementation of signal processing circuit using PIC16F877A microcontroller in PROTEUS® Software environment is shown in Figure 6.11. The detailed circuit diagram and C code in appendix B.

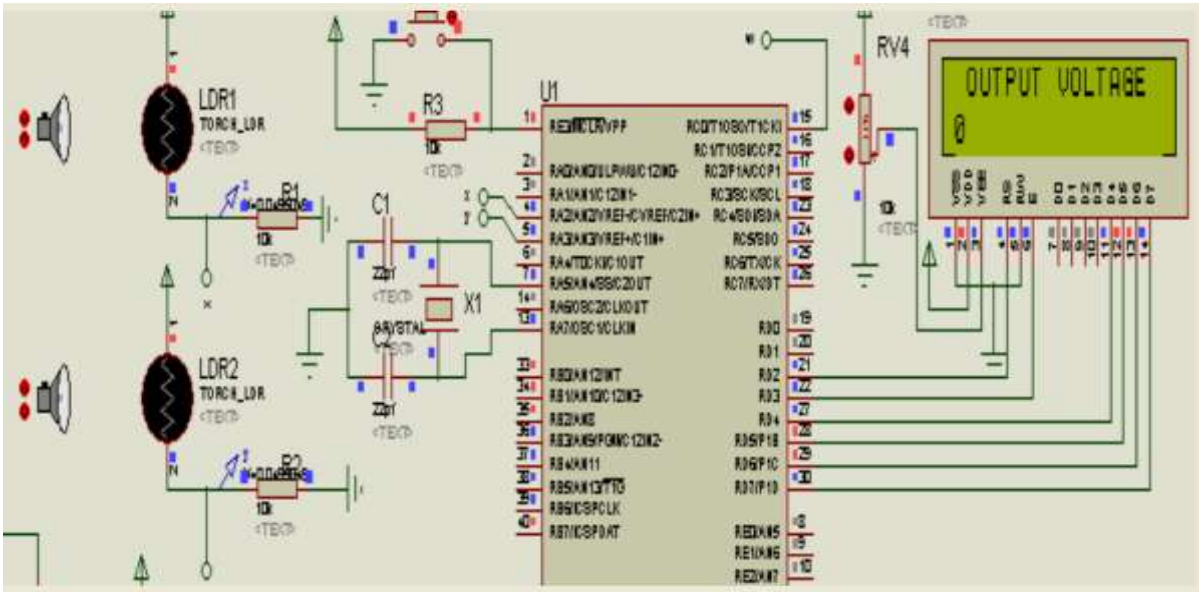

Figure 6.11 Schematic diagram of implementation of signal processing circuit using PIC16F877A microcontroller

6.4 Electrical Current Source

The electrical current source used is MEGGER PCITS2000/2 Primary Current Injection Test Set made by AVO-MEGGER, which is illustrated in Figure 6.12. This Primary Current Injection Test Set is rugged and designed for operation by one person. The PCITS2000/2 is a two-wheeled unit (with a handle). The test set has a separate hand-held controller connected by an expandable cable. This allows the operator to work close to a protective relay while controlling a test. The maximum output current is 2000 A AC at line frequency. By changing the range switch, half the rated output can be obtained at twice the voltage. Additionally, a separate auxiliary voltage output of 250 V, 2 A AC or 125V, 2A AC is available for testing voltage operated relay coils or checking the magnetization characteristics of current transformers. All outputs are fully variable and each test set has a nominal duty cycle when delivering full current and voltage. Continuous operation is possible at 40% of maximum current.

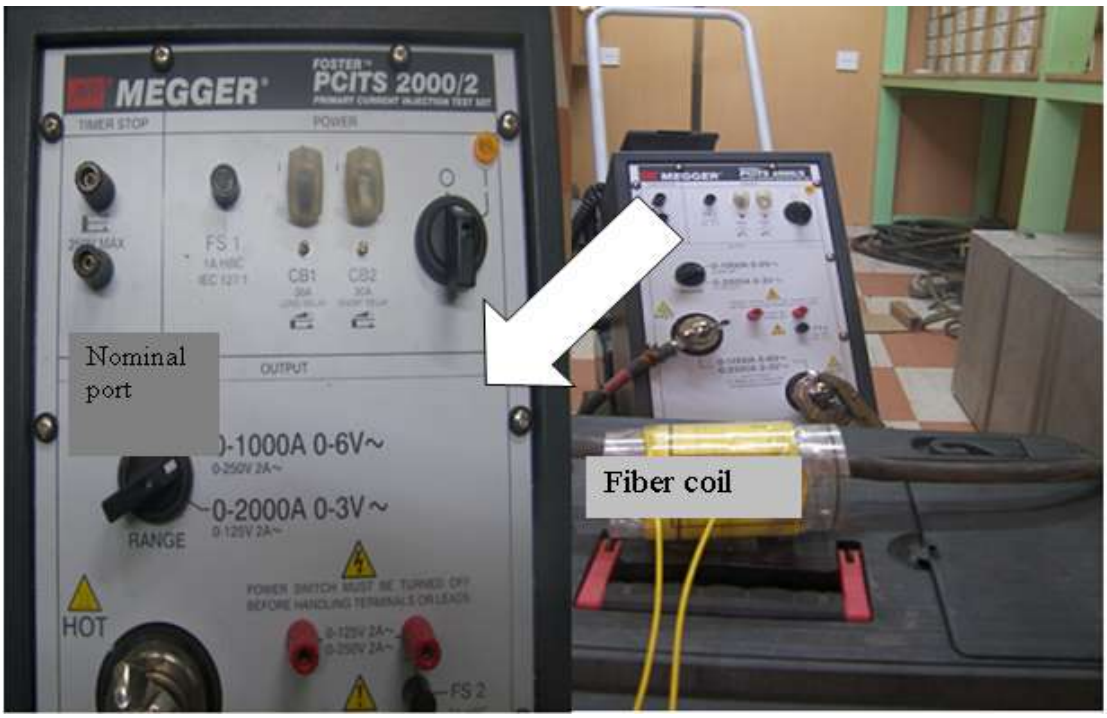

Figure 6.12 a photograph of MEGGER PCITS2000/2 Primary Current Injection Test Set with Optical Fiber coil

6.5 OFCT Experimental Procedures

The single mode optical fiber is winded around the current carrier about 36 turn with diameter of 8 cm. The laser beam is coupled into optical fiber and the emerging beam after collimated micro lens is divided into two components one is transmitted and other reflected by beam splitter and each component is passed through analyzer (at angle of 0° or 90°) and detected by photomultiplier in term of voltage. The two components are detected, one directly at analyzer angle equal to 0° and other by altered output fiber terminal and changed the analyzer angle from 0° to 90°.

The polarizer angle is adjusted until two detected values are equally at no electrical current. Then the electrical current source is started and the current is increased gradually. There is no observed change in each detected values until current reached 20 A. Then the current is increased in step of 20A up to 2000 A and each component is detected and its corresponding voltage value is displayed in LCD. In each step, the intensity of two components is detected using LDRs, which is connected to electronic signal processing circuit. The corresponding voltage value has been calculated and displayed. Figures 6.13 and 6.14 are illustrating the readout of OFCT at no electrical

current path through current carrier conductor while Figures 6.15 and 6.16 are depict the readout of OFCT at maximum electrical current.

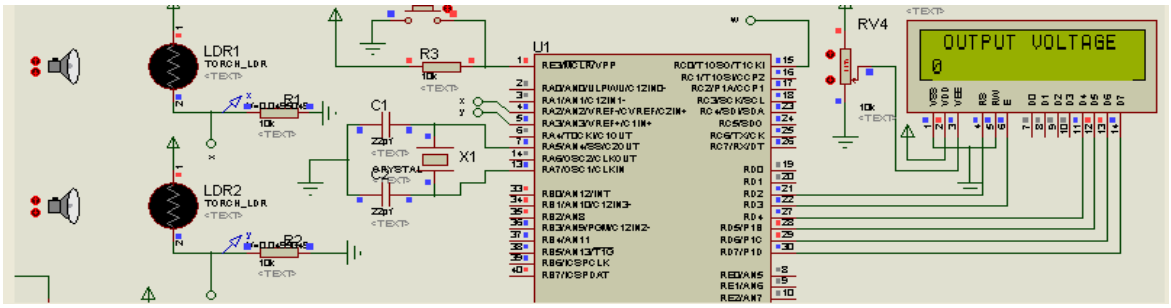

Figure 6.13 The Readout of OFCT at no Electrical Current

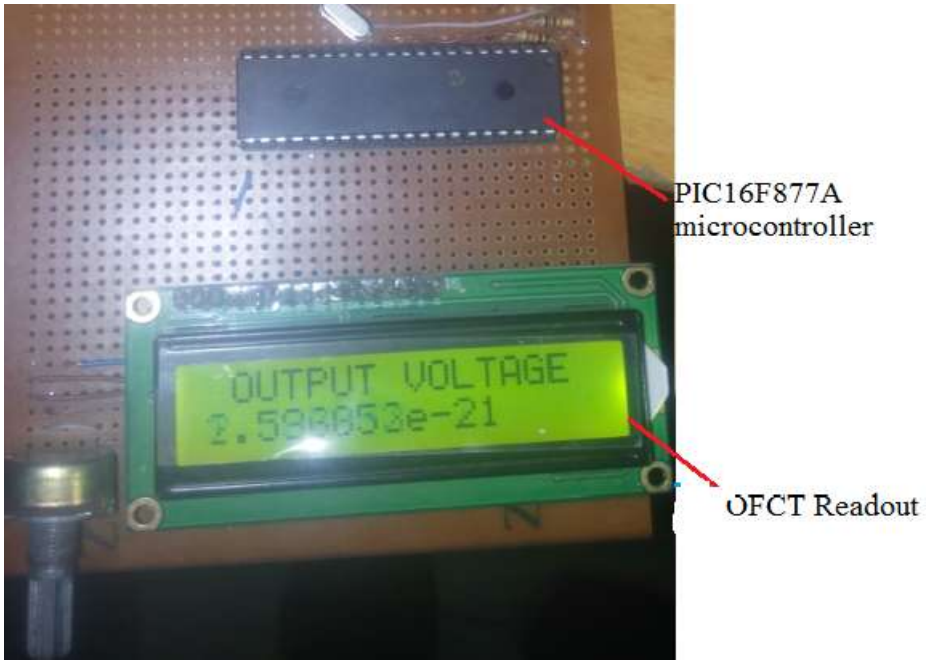

Figure 6.14 Prototype Hardware Readout of OFCT at no Electrical Current

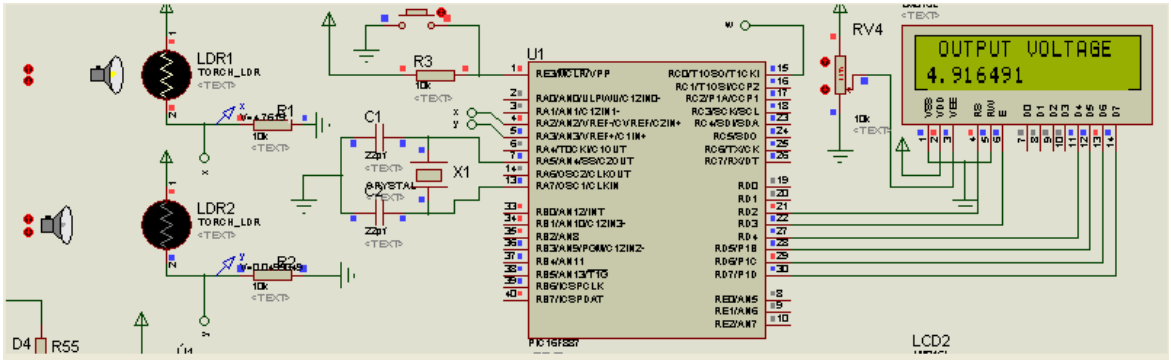

Figure 6.15 Readout of OFCT at Maximum Electrical Current

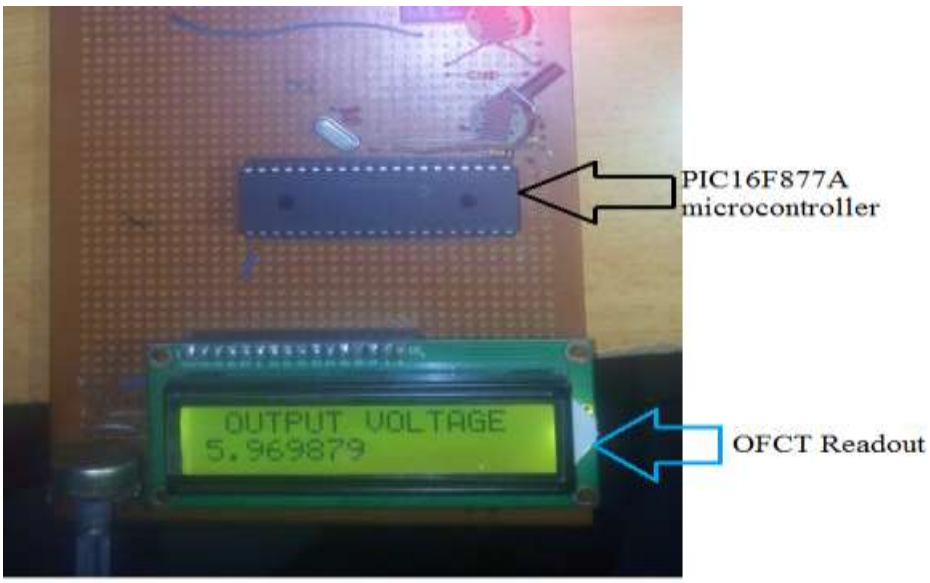

Figure 6.16 Prototype Hardware Readout of OFCT at Maximum Electrical Current

6.6 Numerical Relay for Overcurrent Protection

Microcontroller based Numerical Protective Relays (NPRs) are the latest development in this area. With the development in VLSI Technology, sophisticated and fast microcontrollers are coming up. Their applications to the problems of numerical protective relaying schemes are of current interests to power engineers. The inherit advantages of microcontroller based NPRs over static NPRs with or a very limited range of applications are attractive, flexibility due to their programmable approach. Microcontroller-based NPRs can provide protection at low cost and compete with conventional relays. The present downward trend in the cost of large-scale integrated circuit will encourage wide applications of microcontroller-based applications of microcontroller based NPRs for the protection modern complex power network in the power system.

Overcurrent relay (OCR) provides protection against over currents. This relay uses current inputs from an optical fiber current transformer (OFCT) and compares the measured values with preset values. If the value of input current exceeds the predetermined value, the relay detects an overcurrent and issues a trip signal to the breaker, which opens its contact to disconnect the protected equipment. When the relay detects a fault, the condition is called fault pickup. The relay can send a trip signal instantaneously after picking up the fault in the case of instantaneous over current relay or it can wait for a specific time before sending a trip signal in the case

of time overcurrent relays. This time delay is also known as the operation time of the relay, and is computed by the relay based on the protection algorithm incorporated in PIC microcontroller as DSP.

The implementation for the overcurrent relay consists of PIC16F877A microcontroller, ULN2003A Darlington Transistor, Relay, LCD, LED indicator. The overall block diagram of the proposed overcurrent protection system is shown in Figure 6.17.

A PIC is certain type of microcontroller; a sort of minicomputer that fits on a single chip Integrated Circuit. The controller has a processor core, some memory, and programmable input/output peripherals. The PIC16F877A chip is developed by Microchip Co. US. Since it adopts Reduced Instruction Set Computing (RISC) as kernel structure, it behaves more excellent than the average 8-bit single chip. Meanwhile, it is easy to learn and supports In Circuit Debug (ICD). Voltage and current measuring circuit blocks stand for relative measuring circuits. The measured results are transmitted to corresponding pins of PIC chip through interface circuit, which is designed to interface the measuring circuit and microcontroller.

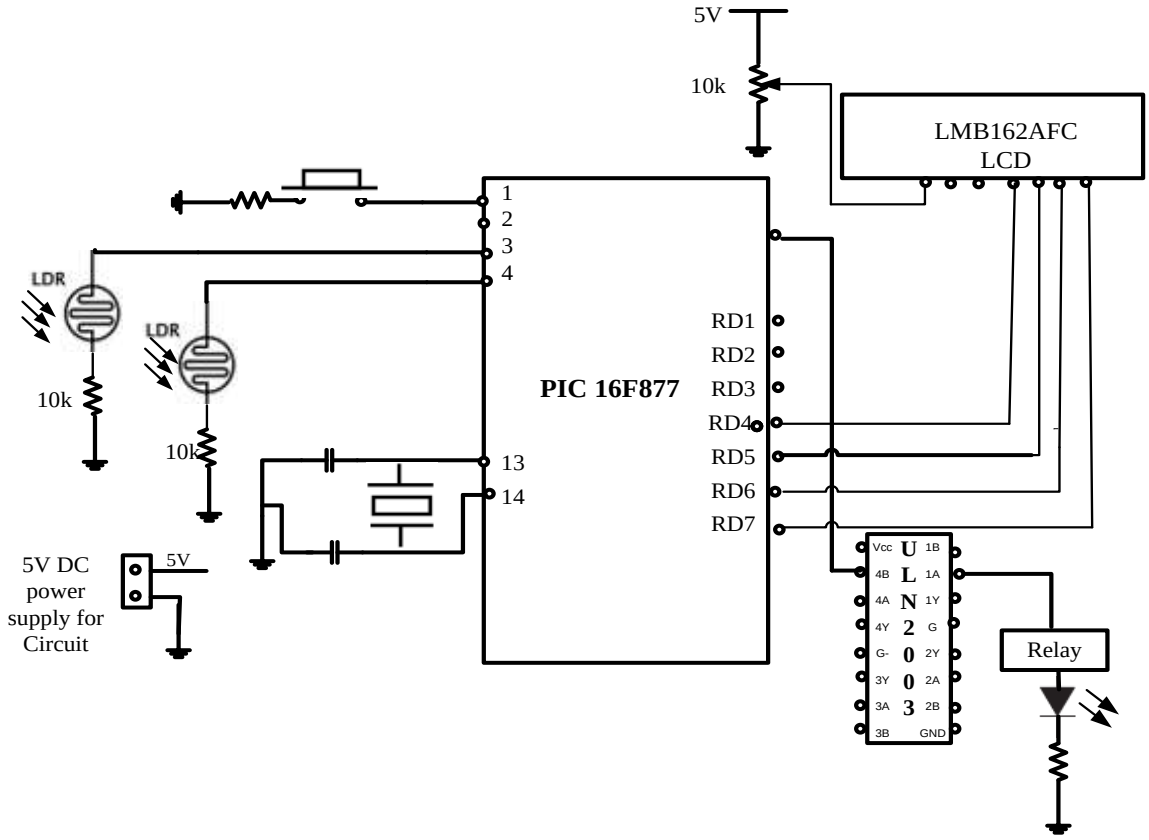

Figure 6.17 Circuit diagram of the Overcurrent Protection Scheme using PIC16F877A microcontroller

6.6.1 Relay

A relay used in this system is a simple electromechanical switch made up of an electromagnet and a set of contacts that is shown in Figure 6.18. Current flow through the coil of the relay creates a magnetic field, which attracts a lever and changes the switch contacts. The coil current can be ON or OFF so relay have two switch positions and they are double throw (changeover) switches. Relays allow one circuit to switch a second circuit that can be completely separate from the first. For example, a low voltage battery circuit can use a relay to switch a 230V AC mains circuit. There is no electrical connection inside the relay between the two circuits; the link is magnetic and mechanical. The coil of a relay passes a relatively large current, typically 30 mA for a 12V relay, but it can be as much as 100 mA for relays designed to operate from lower voltages. Most ICs (chips) cannot provide this current and a transistor is usually used to amplify the small IC current to the larger value required for the relay coil. Relays are usually Single Pole Double Throw (SPDT) or Double Pole Double Throw (DPDT) but they can have many more sets of switch contacts, for example, relays with 4 sets of changeover contacts are readily available.

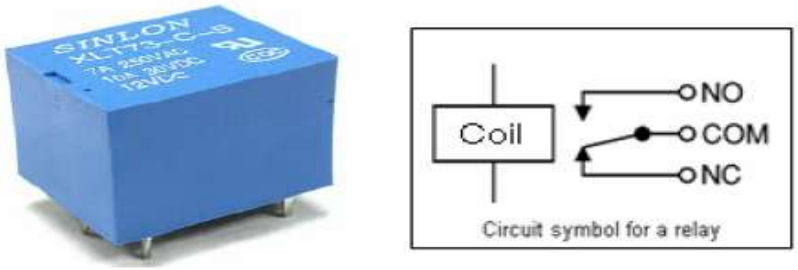

Figure 6.18 Relay

An electromagnetic relay has been employed as a switch to energized circuit breaker in the case of fault occurs. The rating of the relay used in the model system is 5V. Due to the fact that the relay might draw a current of higher value than what the microcontroller can sink or source, therefore, Darlington transistor is used as a logic buffers.

6.6.2 The ULN2003A Buffer

The ULN2003A is a monolithic high voltage and high current Darlington transistor arrays. It consists of seven open collector Darlington pairs with common emitters.

The feature of high voltage outputs with common-cathode clamp diodes is for switching the inductive loads. ULN2003 belongs to the family of ULN200X series of ICs. Different versions of this family interface to different logic families. ULN2003 is for 5V TTL, CMOS logic devices. These ICs are used when driving a wide range of loads and are used as relay drivers, display drivers, line drivers, and logic buffers.

When fault current is detected the RB6 pin of the microcontroller is set high. This produces current that drives the ULN2003A. The ULN2003A in turn completes the relay coil circuit. The relay is energized through the principle of electromagnetic induction. The process is illustrated in Figure 6.19.

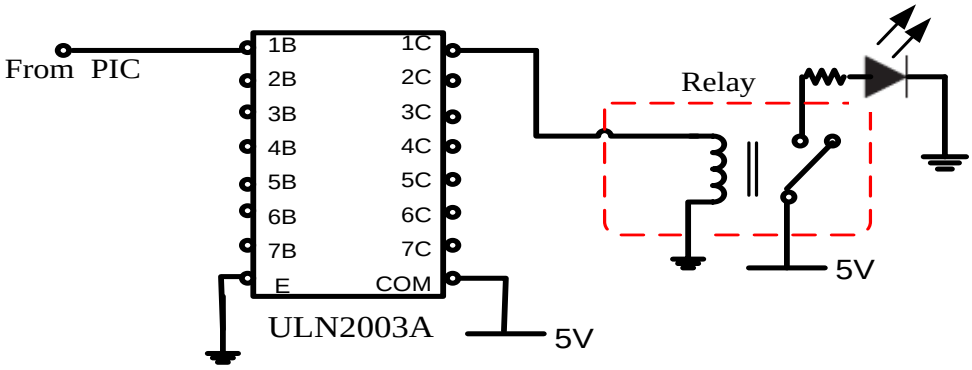

Figure 6.19 Relay energizing through ULN2003

6.6.3 DC Power Supply for the Circuit

Circuit diagram of a typical DC power supply used in this system is shown in Figure 6.20. The transformer steps down the ac voltage to the level of the desired dc output. A diode rectifier then provides a full-wave rectified voltage that is initially filtered by a simple capacitor filter to produce a dc voltage. This resulting dc voltage is given to the LM7805 voltage regulator circuit, which provides a dc voltage with less ripple and constant dc value.

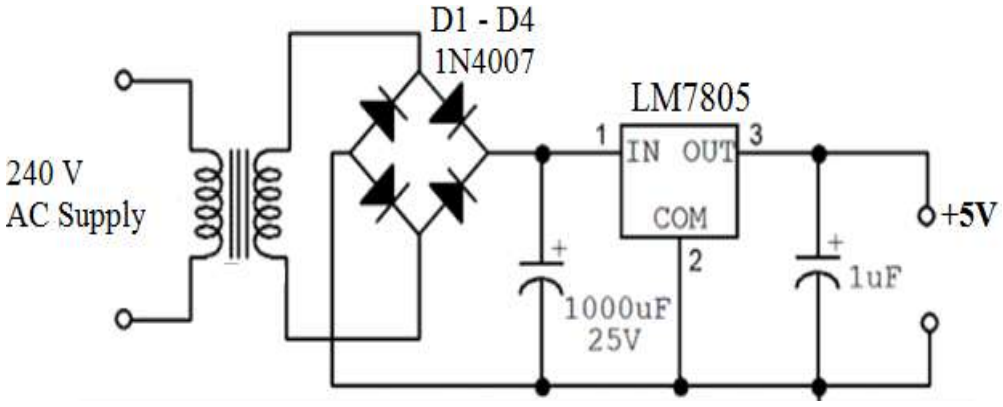

Figure 6.20 DC power supply

6.6.4 Software Algorithm

The algorithm used for developing embedded programming is given by flowchart illustrated in Figure 6.21. The designed algorithm is used to perform the monitoring and protection functions through the proposed system.

Figure 6.21 Flowchart of the proposed monitoring and protection system

6.6.5 Implementation of Overcurrent Relay

The two different implementation methods are used to implement the overcurrent relay on the PIC16F877A microcontroller. Firstly, the overcurrent relay simulation model in Proteus software and determine the value of components. The programming part is performed in mikroC®, a compiler for PIC microcontrollers. The entire program is written in embedded C language. Secondly, PIC16F877A microcontroller circuitry hardware is implemented and programming part for the relay is prepared in mikroC® and directly downloaded into the PIC16F877A microcontroller.

The diagram in Figure 6.22 shows the Proteus schematic diagram of the Overcurrent relay. The microcontroller chosen is PIC16F877A, having 8 ADC ports. In order to use this as an Overcurrent relay for power system protection the multiple ADC ports of microcontroller can be used. The AC current source of 4 KA is taken and is fed OFCT system. An LDR is used in order to change the value of the input analog quantity to the ADC port of microcontroller. From the diagram in Figure 6.23, the relay drive is connected to one of the pins of PORT B of PIC16F877A. The relay coil of 5V is chosen and is connected with the apparatus that is light bulb. The light bulb is energized from a 240V AC voltage source. In order to assure that the relay has

tripped, for visual indication LED's are interfaced with PORT B. When the relay trips the red LED glows to show the tripping action, when the system is stable the green led glows.

In order to realize the overall system, a prototype of the system is developed. The hardware setup based on PIC16F877A microcontroller is shown in Figure 6.23.

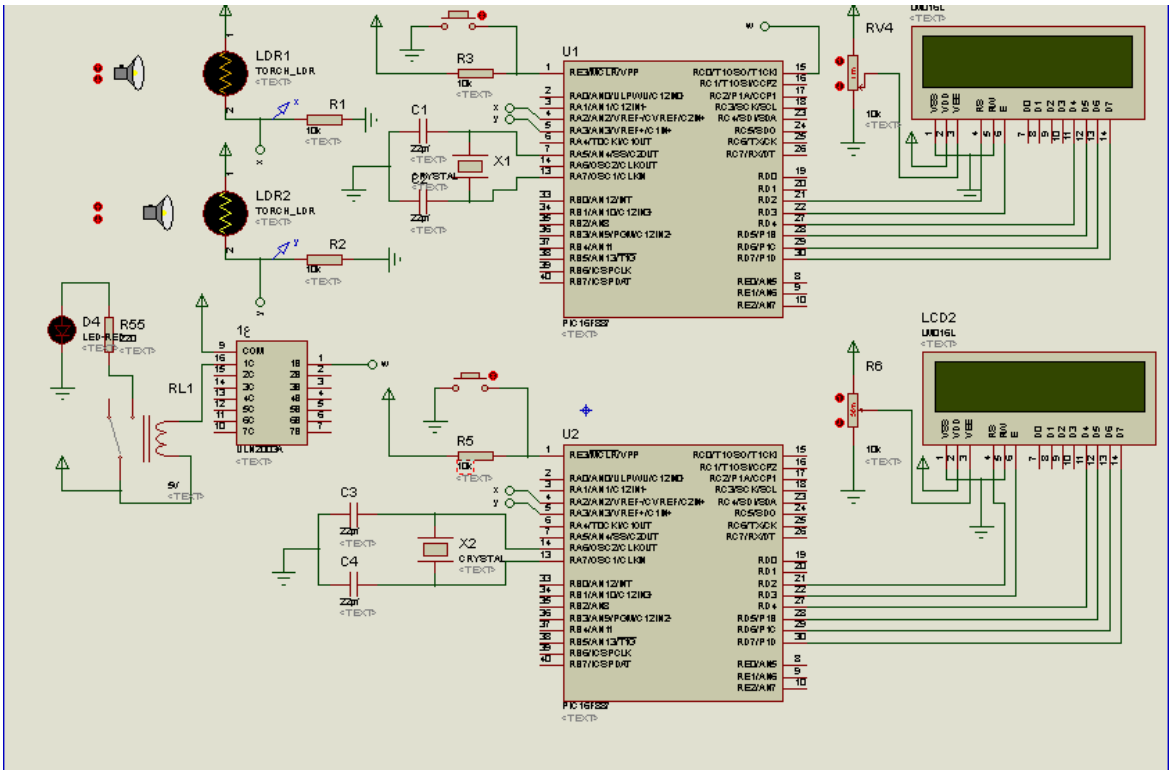

Figure 6.22 Proteus schematic overcurrent relay showing the system status and pickup current value

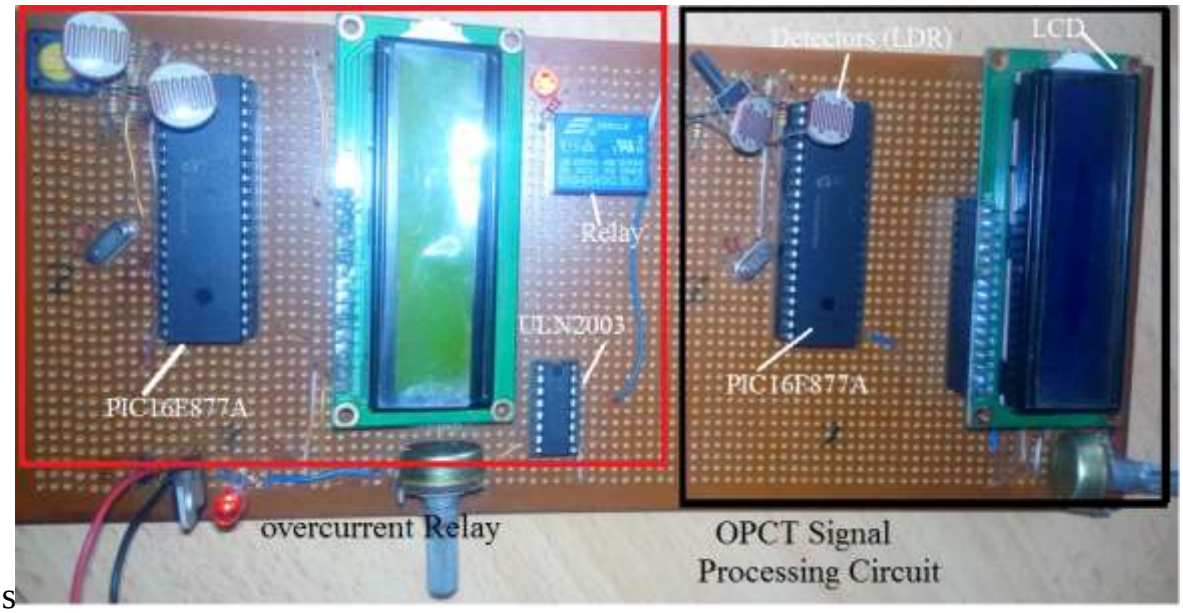

S

Figure 6.23 The hardware of overcurrent and OFCT signal processing

PIC16F877A microcontroller will be used to control and operate the tripping coil in circuit breaker, also to measure and analyze load current from OFCT. Firstly, the load current (energizing current) will be measured using OFCT and converted it from analog voltage to digital using PIC16F877A. Then the load current will display on the LCD and trip circuit breaker using ULN2003A drive.

The over current value is set in the PIC16F877A and when faults (over current) occur, PIC16F877A will energize the ULN2003A drive that will energize the circuit breaker tripping coil which will cause the circuit breaker to trip. The instantaneous and inverse definite minimum time (IDMT) overcurrent relay algorithm is developed. The over current setting may be given by IDMT characteristic.

In order to plot the IDMT characteristics for Overcurrent relay the full load current must be known and taking into consideration 125% overload capacity of the line thermal rating. Therefore, actual operating time is equal to relay operating time plus Circuit Bricker time. The instantaneous overcurrent relay and IDMT relay have been implemented and the LCD shows the system status and the pickup current.

For developing a Experimental model, the hardware is first tested with increase electrical current instead of putting a real fault at the load terminals. The circuit is simulated for normal as well as faulty operation. The pickup value is set to 2.5 A in the program. Using the LDRs, the analog input to the ADC port of the microcontroller is increased and once the current value exceeds, 2.5 A the relay trips the apparatus from the rest of the system and as an observation the light bulb stops glowing with a red LED glowing and LCD displaying the value of pickup current value and status of relay. The normal operation of the overcurrent relay can be realized with the green LED glowing and LCD showing the peak value of line current less than setting value that is shown in Figure 6.24. The overcurrent hardware at normal operation is illustrated in Figure 6.25.

Similarly, the faulty operation in Proteus simulation schematic and experimental model is represented in Figures 6.26 and 6.27 respectively. The LCD displayed the pickup current and system status, which trip has been occurred.

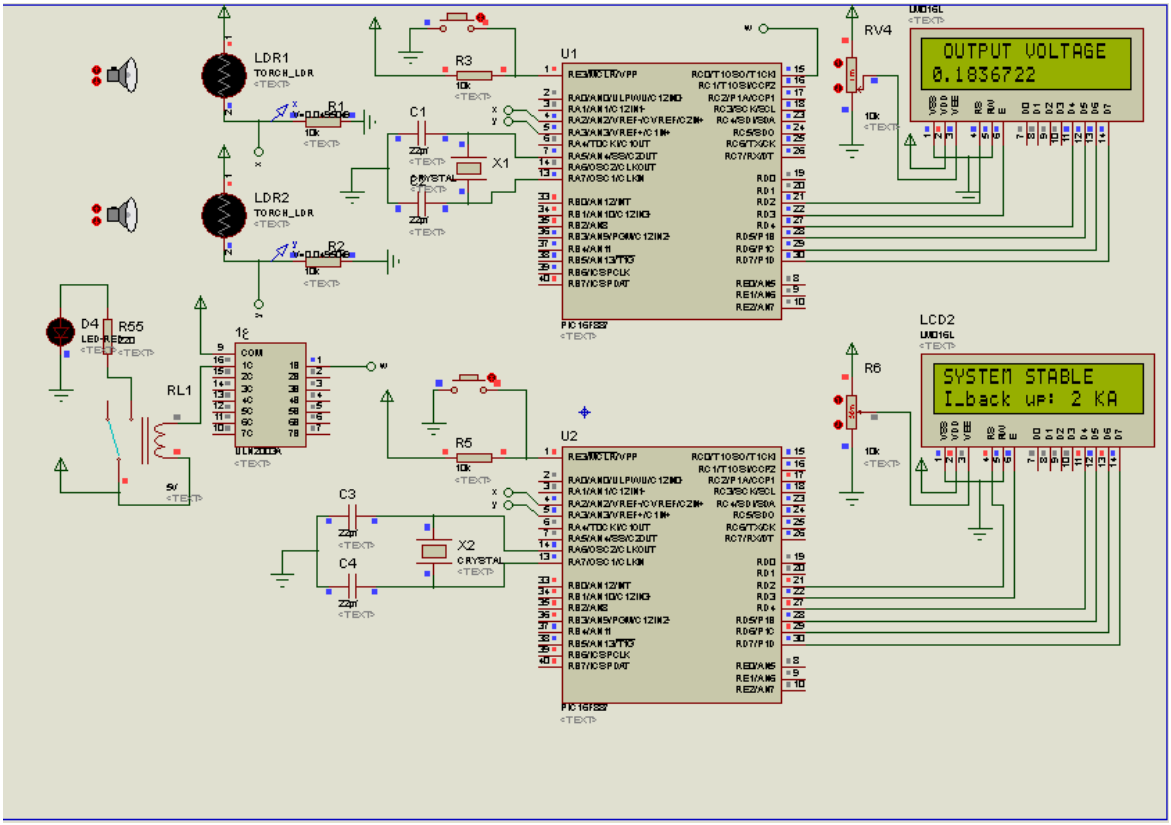

Figure 6.24 Proteus schematic of Microcontroller based overcurrent relay showing the Normal Operation

Figure 6.25 Hardware Overcurrent Relay showing the Normal Operation

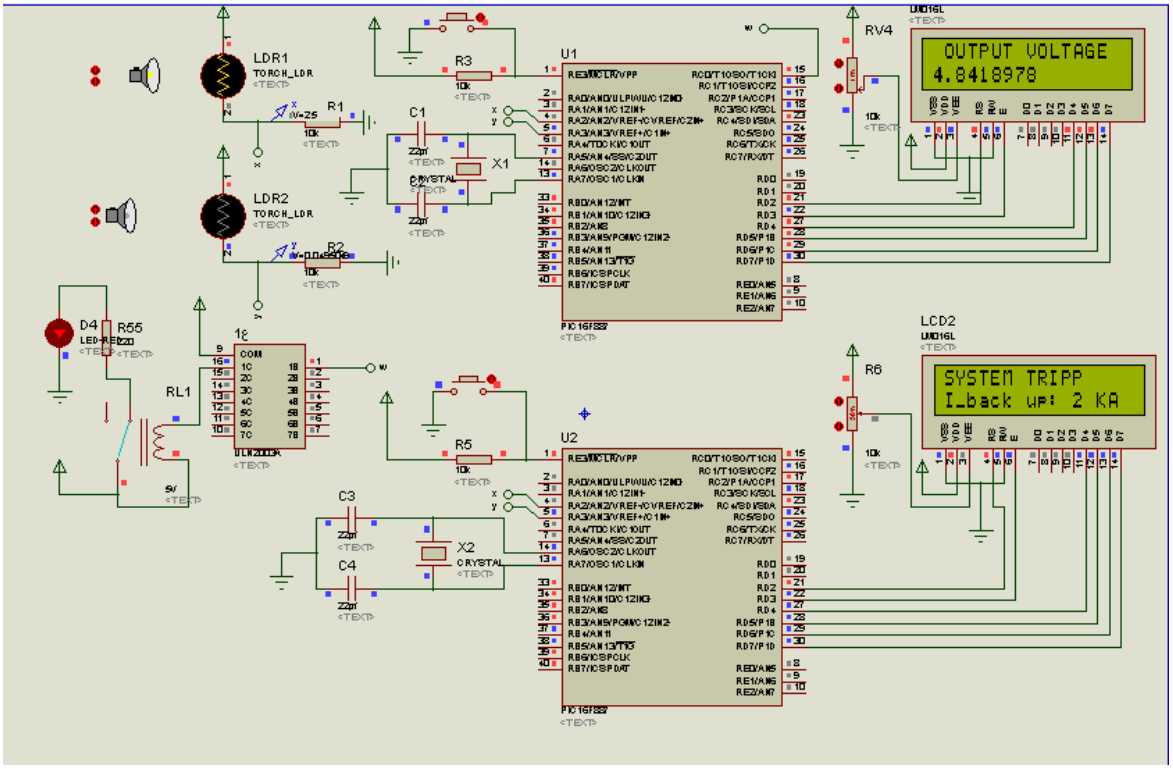

Figure 6.26 Proteus schematic of Microcontroller based relay showing the tripping status with the pickup current value

Figure 6.27 Hardware Overcurrent Relay showing the Faulty Operation

The design and the realization of Microcontroller based Overcurrent are performed in Proteus and Experimental model. The result carried out is summarized in Table 6.1. The OFCT readout and operation time obtained from the PROTEUS simulation and

hardware implementations have small variation. The experimental results carried out are satisfactory. The similar approach can also be performed in more advanced and fast microcontrollers such as Digital Signal Processors (DSP's) for both applications. It is found that this prototype can also be adopted to sense the current in the entire high voltage environment. In addition, this prototype can be used as a frequency relay by sensing the frequency of the operating voltage.

Table 6.1 Experimental model of Overcurrent based OFCT Results

Applied Current [A]	OFCT read out [V]	System status (Tripping operation)	Trip Signal Time [Sce.]
50	0.183	stable	--
350	1.550	Stable	--
770	3.004	Tripped	0.123
1300	3.635	Tripped	0.074
2000	4.841	Tripped	0.052

6.7 Summary

This chapter has given a brief introduction and description of the hardware and software setup necessary to conduct both the optical fiber current transformer and the numerical overcurrent relay test experimentally. The MEGGER PCITS2000/2 Primary Current Injection, He Ne Laser, Polarizer, Single Mode optical fiber sensing element with their accessories have been described and circuit block diagrams of the electronic signal processing circuits for the OFCT are presented. The relevant features of the PIC16F877A microcontroller and the analog-to-digital converter (ADC) are introduced. The overcurrent relay hardware is briefly described. A software flow chart for conducting the proposed monitoring and protection system is detailed and presented for the PIC16F877A microcontroller programmed using the PROTEUS® Software and the mikroC® Software development environments. Experimental set-up for the Optical Fiber Current Transformer is provided and tested. Experimental set-up for the OFCT based overcurrent protection is investigated. The experimental results obtained are presented. The C code for practical implementation of PIC16F877A microcontroller based overcurrent relay is presented in Appendix C. Photographs of the hardware setup are presented in appendix C.

Chapter Seven
Conclusions and Future Work

7.1 Conclusions

The research work presented in this thesis has particularly been concentrated on the model development of a novel optical fiber current transformer for power system protection and monitoring.

A complete model of OFCT and OVT is modeled using the Jones calculus method. These developed mathematical models of optical sensing parts are incorporated with the second part of the transformers, the electronic signal processing. The final model combines the two parts, the optical and electrical models. Different simulation scenarios are used to evaluate of the performance of novel optical instrument transformers.

The frequency response characteristic of the OFCT shows that, the sensitivity of OFCT depends upon the wavelength of the light source, Verdet constant of magneto-optic material, and the number of fiber loop around the current carrying conductor. Therefore, higher performance of OFCT can be achieved by precisely designing fiber loop of the sensing head using reflection configuration to eliminate linear birefringence retardations and all possible disturbances in sensing fiber.

The OFCT with higher number of turns makes possible to use OFCTs with lower Verdet constant. In addition, OFCT exhibit a linear responsivity over a wide detection bandwidth. This allows them to detect transient electrical faults, inspect noise on direct current (DC) lines for the monitoring of partial discharges during automatic control, and protect high power equipment and vital electrical components.

According to the results obtained, the OFCTs are capable to measure current with very high accuracy over wide dynamic range with acceptable errors that match the IEC 0.2 class accuracy requirements.

The novel Optical instrument transformer have a lot of advantages over the conventional instrument transformers which results in accurate harmonic and transient-state measurements due to wider bandwidth. In addition, OFCT provide gain in space and simplicity in design. In addition, the novel optical instrument

transformers has excellent better transient characteristics than the conventional one and competent for the control and protection uses of power equipment. It can be used both in measurement and in protection relays as its well linearity, rapid response, broad dynamic range, wide frequency band, no magnetic saturation, small in volume, light in weight, and safe in insulation.

The performance evaluation of numerical protection schemes based on OFCT has been simulated and discussed. The results show that, developed model successfully evaluated the performance power system protection based optical fiber current transformer (OFCT) and optical voltage transformer (OVT) for different operational conditions.

For the over-current protection scheme there is a significant improvement in performance with respect to trip decision and average tripping time. The system operated successfully and cleared the faults with proper delay. The DC offset current does not affect the tripping time adversely. Performance of the novel system used OFCT can be regarded as excellent when considering the results obtained for the directional over-current protection function.

From simulation results, it is clear that developed model successfully evaluated the performance of distance protection scheme using the optical OFCT and OVT for different operational conditions. It has been shown that the system could provide an enhancement, or an alternative to conventional distance protection method used that conventional CT may cause both under-reaching and overreaching. Meanwhile, OFCT may cause under-reaching only, and it is easier to prevent OFCT current clipping than CT saturation, indicate that the novel OFCT can provide the distance protection better security than the conventional CT and more accurate discrimination of fault location could be achieved; this could be to modify conventional zone settings. For example, the need for an 80% zone 1 setting could be eliminated; zone 1 could be extended to cover 100% of the line without need for communication. According to simulation results, relay model is able to accurately detect internal zone faults and differentiate them with mentioned other states that may be misleading.

Numerical protection system using optical fiber instrument transformers and numerical relays are exhibit benefit higher accuracy and selectivity from this superior performance of new sensing technologies. Additional benefits that can be anticipating

by the novel implementation are: lower sensors and wiring costs by means of a digital process bus with high speed communication that allows the data exchange between devices and reduced times and cost associated with deployment of new devices via a standardized object models and device configuration files.

The main attraction of this novel protection scheme is that both currents and voltages can be acquired passively from widely-spaced locations and made available simultaneously at an interrogation point. This presents possibilities for extremely fast (and possibly single-relay), differential, distance protection schemes without the need for additional dedicated communications channels for data transfer and/or to enhance the speed of operation.

6.2 Future Work

The developed optical fiber current transformer and their practical applications in power system protection and monitoring have made noticeable progress. Continuing efforts will be necessary to demonstrate the long-term reliability and further improve the acceptance and confidence in the new technology of optical instrument transformers. Another critical challenge is novel optical instrument transformers interfaced to digital relays via an IEC 61850-9-2 digital process bus, in the case of performance evaluation, as the output signals of the novel optical instrument transformer are vastly different from the outputs of conventional instruments transformer.

For further development of numerical protection based OFCTs, to achieve more stable measurement characteristics, following can be suggested for more research study:

1. Usage of the special low birefringence sensing fiber, reflection type system for stable optical characteristics, simple signal processing for stable electronic characteristics, and compact sensing head of simple structure.
2. Future research should address the harmonics effect at the OFCT response, mal-function, and noise based on different OFCTs structure and configuration.
3. The possibility to connect OFCTs in series to conventional CTs, this may be helpful for end-users with either existing or newly constructed substations. In an intermediate step, it is possible to compare both technologies and gain

practical experience with novel instrument transformers (NITs) and process bus applications.

4. Studying SMART substation architecture proposal with seamless integration and utilization of novel optical instrument transformer, numerical protection relays, and digital communication based on IEC 61850 utility and industry standard.
5. The development of Merging Unit (MU), which performs the signal processing necessary to make available through the process bus communications the sampled values of the currents based secondary protection for the large mesh distribution system using novel optical instrument transformer.
6. The optimal location of PMU placement for back up protection in the SMART GRID system.

References:

[1] F. Rahmatian, “High-voltage current and voltage sensors for a smarter transmission grid and their use in live-line testing and calibration”, presented at Power and Energy Society General Meeting IEEE, Minneapolis, Minnesota, USA, July 24–29, 2010.

[2] Horak, John, and J. Hrabliuk. "Current transformer errors and transformer inrush as measured by magnetic, optical and other unconventional CTs", Proc. 55th Texas A&M Conf. Protective Relaying Engineers. 2002.

[3] A. VÁZQUEZ "Novel piezoelectric transducers for high voltage measurements", Thesis of Ph.D ,E.T.S.E.I. “Universitat Politècnica de Catalunya” (U.P.C) Barcelona January, 2000.

[4] Lenz, James E. "A review of Magnetic Sensors", Proceedings of the IEEE 78.6, 1990.

[5] Sun, Lei, Shibin Jiang, and John Marciante. "All-fiber optical magnetic field sensor based on Faraday rotation", Optical Fiber Communication Conference. Optical Society of America, 2010.

[6] T. Sawa et al ," Development of Optical Instrument Transformer ", IEEE Trans. Power Del, Vol. 5, No. 2, April 1990.

[7] K. Bohnert, P. Gabus, and H. Brändle," Fiber-Optic Current and Voltage Sensors for High-Voltage Substations" **,** 16th International Conf. on Optical Fiber Sensors, Nara, Japan, Technical Digest, pp 752-754. Oct, 2003.

[8] Steer, A. P., et al. "Application of An Optical Fibre Current Sensor To Electricity Supply Protection." Fibre Optics' 89. International Society for Optics and Photonics, 1989.

[9] Frankie Y.C. Leung et al," Fiber-optic Current Sensor Developed for Power System Measurement ", IEE International Conf on Advances in Power System Control, Operation and Management, Hong Kong , November 1991.

[10] Silva, Ricardo M., et al. "Optical current sensors for high power systems: a review." Applied sciences 2.3, 2012.

[11] Leung, Frankie YC, et al. "Fiber-optic current sensor developed for power system measurement." Advances in Power System Control, Operation and Management, 1991. APSCOM-91.,1991 International Conference on. IET, 1991.

[12] J. Blake, “Fiber optic current sensor calibration,” Proc. IEEE Transm. Distrib. Conf. Expo., Atlanta, GA, pp. 127–130, 2001.

[13] T. Bosselmann, “Electric and magnetic field sensing for high voltage applications,” Tech. Proc. SPIE Europe Series, FL, 1997, pp. 305–316.

[14] T. Sawa, K. Kurosawa, T. Kaminishi, and T. Yokota, “Development of optical instrument transformers,” IEEE Trans. Power Del., vol. 5, no.2, Apr. 1990.

[15] T. W. Cease, et al, “Optical voltage and current sensors used in revenue metering system,” IEEE Trans. Power8Del., vol. 6, no. 4, Oct. 1991.

[16] J. D. P. Hrabliuk, “Interfacing optical current sensors in a substation,” Proc. IEEE Power Eng. Soc. Summer Meeting, Vancouver, BC, Canada, 2001.

[17] J. D. P. Hrabliuk, “Optical current sensors eliminate CT saturation,” in Proc. IEEE Power Eng. Soc. Winter Meeting, New York, vol. 2, pp. 1478–1481, Jan. 2002,

[18] Z. Qian, N. Tan, and J. E. Lu, “The design and improvement of high voltage side circuit in electronic current transformer,” Proc. IEEE8th Int. Conf. Properties and Applications of Dielectric Materials, Indonesia, Jun. 2006.

[19] A. Cruden et al “Current measurement device based on the Faraday Effect,” Proc. IEEE 5th Int. Conf. Devel in Power System Protection,York,U.K., 1993.

[20] Y. Nie, X. Yin, and Z. Zhang, “Optical current transducer used in high voltage power system,” Proc. IEEE/Power Eng. Soc.Transmission and Distribution Conf. Exhibit., Yokohama, Japan, pp. 1849–1853, 2002.

[21] J. Blake et al, “An optical current transducer having linearity better than 0.4% from 4 to 108,000 A,” Proc. Optical Fiber Sensors Conf., Portland, OR, pp. 545–548. 2002,

[22] C. Jinling, et al, “A novel optical current transformer based on comparative measurement,” Proc. IEEE 41st Int. Conf. Universities Power Engineering, Newcastle, U.K. pp. 837–840, 2006.

[23] P. Mihailovic et al, “Development of a portable fiber-optic current sensor for power systems monitoring,” IEEE Trans. Instrum. Meas., vol.53, no.1, Feb. 2004.

[24] J. G. Werthen et al “Current measurements using optical power,” Proc. IEEE Transmission and Distribution Conf., Los Angeles, CA, 1996, pp.213–218.

[25] H. J. El-Khozondar, et al, “Magnetic Field Inhomogeneity Induced on the Magneto-optical Current Sensors,” in Information Photonics 2011 ICO International Conference, Ottawa Convention Center, Canada, , pp.1–2, 2011.

[26] Q. Chen et al, “Research on improvements of using electronic current transformer on distance protection,” Proc. 2007 42nd Int. Univ. Power Eng. Conf., Brighton, U.K., Sep. 2007.

[27] E. F. Donaldson et al," Hybrid optical current transformer with optical and power-line energisation,” Proc. Inst. Elect. Eng. Gen., Transm. Distrib., 2000.

[28] K. Kurosawa, et al, “Development of optical fiber current sensors and their applications,” Proc. IEEE Transmission and Distribution Conf. Exhibit., Dalian, China, 2005.

[29] Y. Yamagata et al, “Development of Optical Current Transformers and Application to Fault location Systems for Substations,” IEEE Trans. Power Del., vol. 3, no. 3, Jul. 1993.

[30] F. Rahmatian and J. N. Blake, “Applications of high-voltage fiber Optic Current Sensors,” Proc. IEEE Power Eng. Soc. General Meeting, Montreal, QC, Canada, pp.1–6, 2006.

[31] López-Higuera, J. M., ed. "Handbook of Optical Fibre Sensing Technology." Chichester, UK: John Wiley, 2002.

[32] Uilian,et al, "Quasi-Distributed Optical Fiber Transducer for Simultaneous Temperature and Vibration Sensing in High-Power Generators", SENSORS JOURNAL IEEE, vol. 18, pp. 1547-1554, 2018.

[33] Hotate, K.; Thai, B.T.; Saida, T. "Comparison between Flint Glass Fiber and Twisted/Bent Single-Mode Fiber as a Faraday Element in an Interferometric Fiber Optic Current Sensor". In European Workshop on Optical Fibre Sensors, Scotland, pp. 233–237, 8 July 1998.

[34] C. Jinling, et al, “A novel Optical Current Transformer based on Comparative Measurement,” in Proc. IEEE 41st International Conf. Universities Power Engineering, Newcastle, 2006.

[35] Barczak, K.; Pustelny, T.; Dorosz, D.; Dorosz, J. "New Optical Glasses with High Refractive Indices for Applications in Optical Current Sensors". Acta Phys. Pol. vol.116, pp.247–249, 2009.

[36] T. W. Cease and P. Johnston, "A magneto-optic Current Transducer," IEEE Transactions on Power Delivery, vo1.5 **(2),** pp. 548-555, October 1990.

[37] T. W. MacDougall, D. R. Lutz, and R. A. Wandmacher, "Development of a fibre Optical Current Sensor", IEEE Transactions on Power Delivery, vo1.7 (2), pp.848–852, April 1992.

[38] Drexler, P., Fiala, P. "Utilization of Faraday mirror in Fiber Optic Current Sensors". Radioengineering, vol. 17, pp 101–107, 2008.

[39] Zhou, S.; Zhang, X. "Simulation of Linear Birefringence Reduction in Fiber Optical Current Sensor." IEEE Photon. Technol. Lett, pp.1568–1570 2007.

[40] Rose, A.H.; Ren, Z.B.; Day, G.W. "Twisting and Annealing Optical Fiber for Current Sensors". J. Lightwave Technol ,vol.14, pp. 2492–2498 1996.

[41] Laming, R.I.; Payne, D.N. "Electric-current Sensors Employing Spun Highly Birefringent Optical Fibers". J. Lightwave Technol. vol.7, pp 2084–2094, 1989.

[42] Bohnert, K.; Gabus, P.; Brandle, H. Towards "Commercial use of Optical Fiber Current Sensors". In Conference on Lasers and Electro-Optics (CLEO 2000), San Francisco, CA, USA, pp. 303–304, 7–12 May 2000.

[43] Tang, D.; Rose, A.H.; Day, G.W.; Etzel, S.M. "Annealing of Linear Birefringence in Single-mode Fiber Coils—Application to Optical Fiber Current Sensors". J. Lightwave Technol. vol. 9, pp 1031–1037, 1991.

[44] Rose, A.H.; Etzel, S.M.; Wang, C.M. "Verdet constant Dispersion in Annealed Optical Fiber Current Sensors". J. Lightwave Technol. vol.15, pp 803–807, 1997.

[45] Moghadas, Amin A., et al. "Fiber Bragg Grating Sensor for Fault Detection in Radial and Network Transmission Lines." Sensors 10.10 , 2010.

[46] Slobodan J. Petricevic,"Practical Application of Fiber-Optic Current Sensor in Power System Harmonic Measurement" IEEE Trans. on Instrumentation and Measurement, vol. 55, No.3, June 2006.

[47] F. Rahmatian and A. Ortega, “Applications of optical current and voltage sensors in high-voltage systems,” Proc. IEEE/Power Eng. Soc. Transmission Distribution Conf. Expo., Latin America, Venezuela, Aug. 2006.

[48] M. Takahashi et al, “Optical current transformer for 245 kV integrated air insulated switchgear”, Proc. IEEE Tran. and Distrib. Conf. Expo., Dallas, TX, 2003.

[49] Y. Hasegawa et al, “Development of a new type of optical transducer for measuring fault current,” IEEE Trans. Power Del., vol. 3, no. 3, Jul. 1994.

[50] Bull, Jeffrey David," An integrated-optic current sensor for relaying and metering in high-voltage power systems". Diss. University of British Columbia, 2003.

[51] Blake, J. N., and A. H. Rose. "Interfacing optical CTs and VTs to relays and meters." Proceedings of IEEE Conference on Transmission and Distribution Conference and Exhibition. 2006.

[52] Kucuksari, Sadik. "Development of Models for Optical Instrument Transformers". Diss. Arizona State University, 2010.

[53] Rahmatian, Farnoosh, Patrick P. Chavez, and Nicolas AF Jaeger. "230 kV optical voltage transducers using multiple electric field sensors." IEEE transactions on power delivery 17.2, 2002.

[54] K. Bohnert, P. Gabus, and H. Brändle, “Fiber-optic Current and Voltage Sensors for High Voltage Substations,” invited paper at 16th International Conference on Optical Fiber Sensors, 2003.

[55] ABB, "MOCT Optical Current Transformer System for Metering," http://www.tdproducts.com/files/36371861.pdf.

[56] F. Rahmatian and J. N. Blake, "Applications of High-voltage Fiber optic Current Sensors," in Power Engineering Society General Meeting IEEE, pp. 1–6, 2006.

[57] "Arteche SDO OCT," www.arteche.com.

[58] C. Li, X. Cui, T. Yoshino, “Measurement of AC Electric Power Based on Dual Transverse Pockels Effect,” IEEE Trans. on Instrumentation and Measurement, vol. 50, October 2001.

[59] T. W. Cease, J. G. Driggans, S. J. Weikel, “Optical voltage and current sensors used in revenue metering system,” IEEE Trans. on Power Delivery, vol. 6, October 1991.

[60] T. W. Cease, P. M. Johnston, “A magneto-optic Current Transducer,” IEEE Trans. on Power Delivery, vol. 5, April, 1990.

[61] Sun Ning et al**,** "The Development and Application of Non-conventional Current and Voltage Transformer." 16th International Conference on Electrical Engineering, Busan Korea July 11-14, 2010.

[62] K. Kurosawa, S. Yoshida, E. Mori, G. Takahashi, S. Saito, " Development of an optical instrument transformer for DC voltage measurement," IEEE Trans. on Power Delivery, vol.8, October 1993.

[63] C. Li, X. Cui, "An Optical Voltage and Current Sensor with Electrically Switchable Quarter Waveplate," Trans. Sensors and Actuators A: Physical, vol. 126, January 2006.

[64] H. J. El-Khozondar, et al, "Magnetic Field Inhomogeneity Induced on the Magneto-optical Current Sensors," in Information Photonics 2011 ICO International Conference, Ottawa Convention Center, Canada, pp. 1–2, May 2011.

[65] F. Rahmatian, "High-voltage Current and Voltage Sensors for A Smarter Transmission Grid and their use in Live-line Testing and Calibration," presented at Power and Energy Society General Meeting IEEE, Minneapolis, Minnesota, USA, July 24–29, 2010.

[66] Z. P. Wang and X. Y. Liu, "Effects of Linear Birefringence inside Sensing Head upon Bulk glass Current Sensors Sensitivity," Optics & Laser Technology, vol. 38, no. 3, pp. 177–182, 2006.

[67] G. Li and M. Kong, "Sensitivity Improvement of an Optical Current Sensor with Enhance Faraday Rotation," Journal of Lightwave Technology, vol. 15, no. 12, pp. 2246–2252, 1997.

[68] Papp, A., and Harms, H., "Magneto-optical Current Transformer." Applied Optics, 19(22): pp 3729-3745, 1980.

[69] R. Kondo and K. Kurosawa, "A method for Improving Temperature Dependence of an Optical Fiber Current Sensor," IEEJ Transactions on Power and Energy, 130(4): 414–420 (in Japanese), 2010.

[70] K. Kurosawa, "Present Status of Application of Optical Fiber Current Sensors," Them Journal of The Institute of Electrical Engineers of Japan, 130(10): 672–675 (in Japanese). 2010.

[71] Adolfsson, M., Einvall, et al, "EHV Series Capacitor Banks. A new Approach to Platform to Ground Signalling, Relay Protection and Supervision". IEEE Trans. Pwr. Delivery, 4(2): pp. 1369-1378, 1989.

[72] Brojboiv, M., Virginia Ivanov, and Silvia Maria Diga. "Implementation of The Optical Current and Voltage Transducers in The Power Systems." In 7th International conference on electromechanically and power systems. 2009.

[73] Maf Fetone, T.D. and McClelland, T.M., "345kV Substation Optical Current Measurement System". IEEE Trans. Pwr. Delivery, 6(4): p. 1430-1437,1991.

[74] Mladen, Kezunovic, et al "Impact of Optical Instrument Transformer Characteristics on the Performance of Protective Relays and Power Quality Meters." In Transmission & Distribution Conference and Exposition: Latin America, 2006. TDC'06. IEEE/PES, pp. 1-7. IEEE, 2006.

[75] M. Kezunovic, et al, "Digital Protective Relaying Algorithm Sensitivity Study and Evaluation", IEEE Transactions on Power Delivery, Vol. 3, No. 3, pp. 912-922, July 1998.

[76] E.A. Udren, J.A. Zipp, "Proposed Statistical Performance Measures for Microprocessor-based Transmission Line Protective Relays, Part 1: "Explanation of the Statistics", IEEE Transactions on Power Delivery, Vol. 12, No. 1, pp. 134-143, January 1997.

[77] E.A. Udren, J.A. Zipp, "Proposed Statistical Performance Measures for Microprocessor-based Transmission Line Protective Relays, Part 2: "Collection and uses of data", IEEE Transactions on Power Delivery, Vol. 12, No. 1, pp. 144-156, January 1997.

[78] Stanley H. Horowitz and Arun G. Phadke. "Power System Relaying", Research Studies Press Limited, 3rd edition, 2008.

[79] E. M. dos Santos, G. Cardoso, et al," CT Saturation Detection Based on the Distance Between Consecutive Points in the Plans Formed by the Secondary Current Samples and Their Difference-Functions", IEEE Transactions on Power Delivery, vol. 28, no. 1, January 2013.

[80] Bruno M. Schettino, et al. "Current-Transformer Saturation Detection Using Savitzky-Golay Filter", IEEE Transactions on Power Delivery, vol. 31, no. 3, June 2016.

[81] Bruno M. Schettino, et al "A New Method of Current-Transformer Saturation Detection in the Presence of Noise", IEEE Transactions on Power Delivery, vol. 29, no. 4, August 2014.

[82] Ali Hooshyar, Majid Sanaye-Pasand. "CT Saturation Detection Based on Waveform Analysis Using a Variable-Length Window", IEEE Transactions on Power Delivery, vol. 26, no. 3, July 2011.

[83] Hongxing Wang, Yuanpeng Guan. "Study on Long-term Operation Stability of Fiber Optical Current Transformer", IEEE International Conference on Intelligent Trans- portation, Big Data and Smart City, December 2015.

[84] I. M. El-amin and N. H. Al-abbas, "Saturation of Current Transformers and its Impact on Digital Overcurrent Relays," 2006 IEEE/PES Transmission & Distribution Conference and Exposition: Latin America, Caracas, 2006, pp. 1-6.

[85] S. Nasukawa, et al, "Application of optical fiber current sensors to underground cables," in 7th JICABLE Conf., Session A.5, Diagnostics, vol. 2, no. A5.5, 2007.

[86] M. Kayaki, T. Hirata, et al, "Development of Fault Detection System using Wave Division Multiplexing Transmission of Optical Fiber Current Sensor," IEEJ Transactions on Power and Energy, 2010, 130(1): 49–54 (in Japanese).

[87] Nasukawa, S. "Application of Optical Fiber Current Sensor to Underground Cables." In Proc. 7^< th> JICABLE Conference, Paris (2007-6). 2007.

[88] K. Kurosawa "Development of Fiber-Optic Current Sensing Technique and Its Applications in Electric Power Systems" PHOTONIC SENSORS / Vol. 4, No. 1, 2014.

[89] P. Orr et al., "Flexible Protection Architectures using Distributed Optical Sensors," in Proc. 11th Int. Conf. Develop. Power Syst. Protection (DPSP), Apr. 2012, p. 155.

[90] Edachali, Dhilju Prakashan. "Detection and signaling of High Impedance Faults in Transmission line using Fiber Optic Sensing Network and PLC/SCADA technology." In 20th International Conference on Electricity Distribution. June 2009.

[91] AREVA T&D, "Network Protection and Automation Guide". 1st Ed., Cayfosa, Barcelona, ISBN 2-9518589-0-6, July 2002.

[92] U. N. Khan and T. S. Sidhu, "A Phase-Shifting Transformer Protection Technique Based on Directional Comparison Approach," in IEEE TRANSACTIONS ON POWER DELIVERY, vol. 29, no. 5, pp. 2315-2323, Oct. 2014

[93] M. Nasir, A. Dyśko, P. Niewczas, C. Booth, P. Orr and G. Fusiek, "Development of Power system Differential Protection based on Optical Current Measurement," POWER ENGINEERING CONFERENCE (UPEC), 2013 48TH INTERNATIONAL UNIVERSITIES', Dublin, pp. 1 4, 2013,

[94] H. Y. Li, et al, "A New Type of Differential Feeder Protection Relay Using the Global Positioning System for Data Synchronization", IEEE PES Summer Meeting, , Denver, Colorado. July 1996.

[95] H.Y. Li et al,"Application of Fiber Optical Current Transducer to Protection " .1997

[96] A. Moghadas, R. Barnes, M. Shadaram, "An innovative Fiber Bragg Grating Sensor Capable of Fault Detection in Radial Power Systems," Systems Conference, 2010 4th Annual IEEE , pp.165-168, 5-8 April 2010.

[97] P. Orr et al., "Distributed Photonic Instrumentation for Smart Grids," in Proc. IEEE Int. Workshop Appl. Meas. Power Syst. (AMPS), Aachen, Germany, pp. 63–67 Sep. 2013.

[98] X. Tang, K. Kobayashi, et al, "Development of 765kV Transformer Protection Relay," Proc. Advanced Power System Automation and Protection, 2011.

[99] A. D. Kersey et al, "Fiber Grating Sensors," J. Lightwave Tech., vol. 15, no. 8, pp. 1442-1463, August 1997.

[100] P. Orr and P. Niewczas, "FBG-based Fibre-optic Current Sensors for Power Systems Protection: Laboratory evaluation," IEEE/OSA Journal of Lightwave Technology 29(22):3387–3392, Nov 2011.

[101] Alstom, Network Protection and Automation Guide. Available online at http://www.alstom.com/grid/NPAG/.

[102] Stanley H. Horowitz, Arun G. Phadke, "Power System Relaying", John Wiley & Sons Ltd, ISBN: 978-0-470-05712-4, Third Edition, 2008.

[103] Ashish S. Paramane, Avinash N. et al, "Rogowski Coil - A Novel Transducer for Current Measurement", 6th International Conference on Power System

Protection and Automation, CBIP, New Delhi, India, pp. 80-88 27- 28 February 2014,

[104] Avinash N. Sarwade, et al, “Optimum Setting of Distance Protection Scheme for HV Transmission Line”, Journal of Power Electronics and Power Systems, STM, Volume 3, Issue 2, , pp 23-30, 2013.

[105] Piotr Sawko, “Impact of Secondary Burden and X/R Ratio on CT Saturation” Wroclaw University of Technology, Faculty of Electrical Engineering, pp 1-3, 2008.

[106] Joe Mooney, “ Distance Element Performance Under Conditions of CT Saturation” 11th Annual Georgia Tech Fault and Disturbance Analysis Conference as an alternate, Atlanta, Georgia, pp 1-7, 19-20 May 2008.

[107] Sarwade, A. N., P. K. Katti, and J. G. Ghodekar. "Use of Rogowski Coil for accurate measurement of secondary current contaminated with CT saturation in distance protection scheme." In Power Systems (ICPS), 2016 IEEE 6th International Conference on, pp. 1-6. IEEE, 2016.

[108] R. Barnes, A. Moghadas, M. Shadaram, "An Innovative Fiber Bragg Grating Sensor Capable of Fault Detection in Radial Power Systems," Systems Conference, 2010 4th Annual IEEE , vol., no., pp.165-168, 5-8 April 2010

[109] L. Dziuda, P. Niewczas, et al, “Hybrid Fiber- Optic Voltage Sensor for Remote Monitoring of Electrical submersible Pump Motors”, Optical Engineering, Vol. 44, No. 6, pp 64401-1-6, June 2005.

[110] Niewczas, A. Dysko, C. Booth, P. Orr, P. "FBG-Based Fiber-optic Current Sensors for Power Systems Protection: Laboratory evaluation," Universities Power Engineering Conference (UPEC), 2009 Proceedings of the 44th International, pp.1-5, 1-4 Sept. 2009.

[111] Orr, P., G. Fusiek, P. et al. "Distributed Optical Distance Protection using FBG-based Voltage and Current Transducers." In Power and Energy Society General Meeting, 2011 IEEE, pp. 1-5. IEEE, 2011.

[112] I. Hall, P. G. Beaumont, et al, “New Line Current Differential Relay using GPS Synchronization,” Proc. IEEE Power Tech Conference, Bologna, p. 8, June 2003

[113] A. Carta, N. Locci, C. Muscas, “A PMU for the Measurement of Synchronized Harmonic Phasors in Three-Phase Distribution Networks,” IEEE Trans. Instr. and Meas., vol. 58, no. 10, pp. 3723–3730, Oct 2009.

[114] M. Shadaram, A. Moghadas, R. Barnes, “An innovative Fiber Bragg Grating sensor capable of fault detection in radial power systems,” Systems Conference, 2010 4th Annual IEEE, pp.165-168, 5-8 April 2010.

[115] P. Niewczas, P. Orr, A. Dysko, C. Booth, "FBG-based fiber-optic Current Sensors for Power systems Protection: Laboratory evaluation," Universities Power Engineering Conference (UPEC), 2009 Proceedings of the 44th International , pp.1-5, 1-4 Sept. 2009.

[116] Ferry A., Viawan, Jianping Wang, et al "Effect of Current Sensor Technology on Distance Protection." In Power Systems Conference and Exposition, 2009. PSCE'09. IEEE/PES, pp. 1-7. IEEE, 2009.

[117] W. Chen," The Electrical Engineering Handbook". Burlington, MA: Elsevier Academic Press, 2005.

[118] B. Naodovic, "Influence of Instrument Transformers on Power System Protection," Master's thesis, Texas A&M University, May 2005.

[119] IEC, Communication Networks and Systems in Substation Communication Requirements for Functions and Device Models, IEC Std., 2013. [Online]. http://webstore.iec.ch/webstore/webstore.

[120] Tziouvaras, Demetrios A., et al. "Mathematical Models for Current, Voltage, and Coupling Capacitor Voltage Transformers." IEEE Transactions on Power Delivery 15.1, 2000.

[121] Carazo, Alfredo Vázquez. "New Requirements for Instrument Transformers." NOVEL PIEZOELECTRIC TRANSDUCERS FOR HIGH VOLTAGE MEASUREMENTS .2000.

[122] Morais, Bruno Tiago Pires. "Emerging Technologies and Future Trends in Substation Automation Systems for The Protection, Monitoring and Control of Electrical Substations", 2014.

[123] K. Bohnert, P. Gabus, et al, "Optical fiber sensors for the electric power industry," Opt. Lasers Eng. 43, 511–526 2005.

[124] K. Bohnert, H. Brändle, et al, "Highly Accurate Fiber-optic dc Current Sensor for The Electrowinning Industry," IEEE Trans. Ind. Appl. vol. 43, pp. 180–187, 2007.

[125] ABB, "MOCT Optical Current Transformer System for Metering," http://www.tdproducts.com/files/36371861.pdf.

[126] F. Rahmatian and J. N. Blake, "Applications of High-voltage Fiber Optic Current Sensors," in Power Engineering Society General Meeting (IEE, 2006), pp. 1–6.

[127] "Arteche SDO OCT," www.arteche.com.

[128] Ning, Y.N.; Wang, Z.P. "Recent Progress in Optical Current Sensing Techniques", Rev. Sci. Instrum,1995.

[129] Perciante, C.D.; Ferrari, J.A. "Magnetic Crosstalk Minimization in Optical Current Sensors". IEEE Trans. Instrum. Meas, 2008.

[130] Chakraborty, S., and S. C. Bera. "Magneto-optic Over-current Detection with null optical tuning." Sensors & Transducers Journal 87.1, 2008.

[131] Silva, Ricardo M., et al, "Optical Current Sensors for High power systems: a review." Applied sciences 2.3 , 2012.

[132] Blake, J.; Tantaswadi, P.; Carvalho, R." In-line sagnac interferometer current sensor", IEEE Trans.Power Delivery, 1996.

[133] Tao, Shen, et al. "A Novel Reflective Fiber Optic Current Sensor and Error Characteristics in the Key Optical Components." International Journal of Control and Automation 8.6 , 2015.

[134] El Adawy, Mohamed I., et al. "Failure accommodation of optical fiber current sensors using integrated adaptive neuro-fuzzy inference scheme." Alexandria Engineering Journal 44.4, 2005.

[135] Nascimento, Ivo Maciel. "Optical fiber sensors technology for supervision, control and protection of high power systems." , 2016.

[136] Coldren, Larry A., Scott W. et al. "Diode lasers and photonic integrated circuits". Vol. 218. John Wiley & Sons, 2012.

[137] Schaer, Toby, et al. "A dynamic simulation model for semiconductor laser diodes." Electrical and Computer Engineering, 2003. IEEE CCECE 2003. Canadian Conference on. Vol. 1. IEEE, 2003.

[138] Henry, Charles. "Theory of the linewidth of semiconductor lasers." IEEE Journal of Quantum Electronics 18.2 ,1982.

[139] L. Bjerkan, A. Røyset, L. Hafskjaer, and D.Myhre, "Measurement of Laser Parameters for Simulation of High-Speed Fibre Optic Systems," Journal of Lightwave Technology, vol.14, No.5, pp.839-850, May 1996.

[140] Park, B. Hyle, et al. "Jones matrix analysis for a polarization-sensitive optical coherence tomography system using fiber-optic components." Optics letters 29.21 , 2004.

[141] BŁAŻEJCZYK, Tomasz, Henryk SIBILSKI, and Krzysztof KRASUSKI. "Experimental Comparison of Two Various Optical Fibre Current Sensors Dedicated to High Current Applications." Przegląd Elektrotechniczny 90.10 , 2014.

[142] Park, B. Hyle, et al. "Jones matrix analysis for a polarization-sensitive optical coherence tomography system using fiber-optic components." Optics letters 29.21 ,2004.

[143] Bass, Michael, et al., eds. "Handbook of optics". Vol. 2. New York: McGraw-Hill, 2001.

[144] Zalewski, Edward F., and J. Geist. "Silicon photodiode absolute spectral response self-calibration." Applied Optics 19.8 ,1980.

[145] Ristova, M., Y. Kuo, and S. Lee. "Influence of the roughness of molybdenum back electrode on the photodiode characteristics under He–Ne illumination." Semiconductor science and technology 18.8 , 2003.

[146] Noda, Juichi, Katsunari Okamoto, and Yutaka Sasaki. "Polarization-maintaining Fibers and Their Applications." Journal of Lightwave Technology 4.8 ,1986.

[147] Lee, Byoungho. "Review of The Present Status of Optical Fiber Sensors." Optical fiber technology 9.2, 2003.

[148] Ripka, P., "Magnetic Sensors and Magnetometers", IEEE, Artech House, London, 2001.

[149] Drexler, P, P. Fiala, and R. Kadlec. "Utilization of faraday mirror in fiber optic current sensors and experiments." PIERS Proceedings. 2009.

[150] Yuan, Duan Lei, et al. "Theoretical Modeling and Error Analysis for Reflection Structure Fiber Optical Current Transformer." Applied Mechanics and Materials. Vol. 511. Trans Tech Publications, 2014.

[151] Drexler, Petr, and Pavel Fiala. "Utilization of Faraday mirror in fiber optic current sensors." Radioengineering , 2008.

[152] Proakis, J.G.; Nanolakis, D.G. "Digital Signal Processing", 4th ed.; Prentice Hall: Upper Saddle River, NJ, USA, 2007.

[153] Zubia, Joseba, et al. "Design and development of a low-cost Optical Current Sensor." Sensors 13.10, 2013.

[154] LIN, SHIH-CHUN, and TG GIALLORENZI. "Sensitivity Analysis of the Sagnac-effect Optical-fiber Ring Interferometer." SPIE milestone series 28, 1991.

[155] MacDougall, et al, "Development of a fiber optic current sensor for power systems." Transmission and Distribution Conference, Proceedings of the 1991 IEEE Power Engineering Society. IEEE, 1991.

[156] Nguyen, Truong X., Jay J. Ely, and George N. Szatkowski. "A fiber-Optic Current Sensor for Lightning Measurement Applications." SPIE Sensing Technology+ Applications. International Society for Optics and Photonics, 2015.

[157] Karri, Avinash. "Employment of dual frequency excitation method to improve the accuracy of an optical current sensor, by measuring both current and temperature." (2008).

[158] Santos, Josemir Coelho, et al. "Pockels high-voltage measurement system." High Voltage Engineering, 1999. Eleventh International Symposium. Vol. 1. IET, 1999.

[159] E. Collett, “Polarized Light in Fiber Optics,” SPIE Press, 2003.

[160] Pan, Feng, et al. "An optical AC voltage sensor based on the transverse pockels effect." Sensors 11.7, 2011.

[161] Griffin, Barry, and Michael J. Connelly. "Digital signal processing of interferometric fiber optic sensors." Lightwave Technologies in Instrumentation and Measurement Conference, 2004. Proceedings of the. IEEE, 2004.

[162] Kuliš, Ivan Goran, et al. "Protection relay software models in interaction with power system simulators." MIPRO, 2012 Proceedings of the 35th International Convention. IEEE, 2012.

[163] Wakhare, Kalyani, and Nandkumar Wagh. "Discrete Fourier Transform Algorithm Based Digital Multifunction Relay for Transmission Line Protection."

[164] Terzija, Vladimir, et al. "Wide-area monitoring, protection, and control of future electric power networks." Proceedings of the IEEE 99.1, 2011.

[165] Sachdev, M. S., and T. S. Sidhu. "Modelling relays for use in power system protection studies." , 2001.

[166] Kezunovic, Mladen. "Smart Fault location for Smart grids." IEEE transactions on smart grid 2.1 , 2011.

[167] Wang, Yifan, and Venkata Dinavahi. "Low-latency distance protective relay on FPGA." IEEE Transactions on Smart Grid 5.2, 2014.

[168] Sherwali, Hamid H., and Eng Abdlmnam A. Abdlrahem. "Simulation of numerical distance relays." SCIYO. COM, 2010.

[169] Abdlrahem, Abdlmnam A., et al. "Modelling of Numerical Distance Relays using MATLAB." Industrial Electronics & Applications, 2009. ISIEA 2009. IEEE Symposium on. Vol. 1. IEEE, 2009.

[170] Zhang, Peichao, et al. "Compatibility and Interoperability Evaluation for All-digital Protection System Through Automatic Application Test." Power Engineering Society General Meeting, IEEE, 2006.

[171] De La Ree, Jaime, et al. "Synchronized Phasor Measurement Applications in Power Systems." IEEE Transactions on Smart Grid 1.1, 2010.

[172] Phadke, Arun G., and John Samuel Thorp. "Synchronized Phasor Measurements and their Applications." Springer Science & Business Media, 2008.

[173] Uma, Uma U., and I. K. Onwuka. "Overcurrent Relay Setting Model for Effective Substation Relay Coordination." IOSR Journal of Engineering 4.5, 2014.

[174] Almas, et al. "Over-current Relay model implementation for real time simulation & Hardware-in-the-Loop (HIL) validation." IECON 2012-38th Annual Conference on IEEE Industrial Electronics Society. IEEE, 2012.

[175] Chopra, et al. "Performance assessment of a digital overcurrent relay in distribution system using Matlab/Simulink.", International Journal of Enhanced Research in Science Technology & Engineering,vol.3, 2014.

[176] Mahat, Pukar, et al. "A simple adaptive Overcurrent Protection of Distribution Systems with Distributed Generation." IEEE Transactions on Smart Grid 2.3, 2011.

[177] Sivov, et al. "Adaptive Setting of Distance Relay for MOV-protected Series Compensated Line Considering wind Power." Electric Power Systems Research 137, 2016.

[178] Magnago, Fernando H., and Ali Abur. "Fault Location using Wavelets." IEEE Transactions on Power Delivery 13.4, 1998.

[179] Wang, Hualei. "The Protection of Transmission Networks Containing AC and DC Circuits". Diss. University of Bath, 2014.

[180] Anamika Yadav, A.S. Thoke, "Transmission Line Fault Distance and Direction Estimation using Artificial Neural Network,",International Journal of Engineering, Science and Technology Vol. 3, No. 8, 2011.

[181] Gu, Jyh-Cherng, and Sun-Li Yu. "Removal of DC Offset in Current and Voltage Signals using A novel Fourier Filter Algorithm." IEEE Transactions on Power Delivery 15.1, 2000.

[182] Kang, Sang-Hee, et al. "Fourier Transform-based Modified Phasor estimation Method Immune to the effect of the DC offsets." IEEE Transactions on Power Delivery 24.3, 2009.

Appendix A

This appendix presents the Simulink models and its parameter for Laser source and numerical relays

A.1 The Laser Source Model Parameters

Table A.1 the laser model parameters

Symbol	Value	Dimension	Description
i(t)	-	[mA]	Laser Current
$S(t)$	-	[m^{-3}]	Photon Density
Γ	0.44	-	optical confinement factor
g_o	3×10^{6}	[cm^{-3}/s]	slope gain
N(t)	-	[m^{-3}]	carrier density
N_o	1.2×10^{18}	[cm^{-3}]	carrier density at transparency
ε	3.4×10^{-17}	[cm^{3}]	gain saturation parameter
τ_p	1.0×10^{-12}	[s]	photon lifetime
β	4.0×10^{4}		spontaneous emission factor
τ_n	3.0×10^{-9}	[s]	carrier lifetime
V_a	9.0×10^{-11}	[cm^{3}]	volume of the active region
α_L	-	-	line width enhancement factor
q	1.062×10^{-17}	[F]	electron charge
$\phi(t)$	-	-	phase of the laser electric field
$P(t)$	-	[W]	Laser optical output power
η	0.1	-	total quantum efficiency
υ	-	[s^{-1}]	frequency of the laser
h	6.624×10^{-34}	[J.s]	phase of the laser electric field

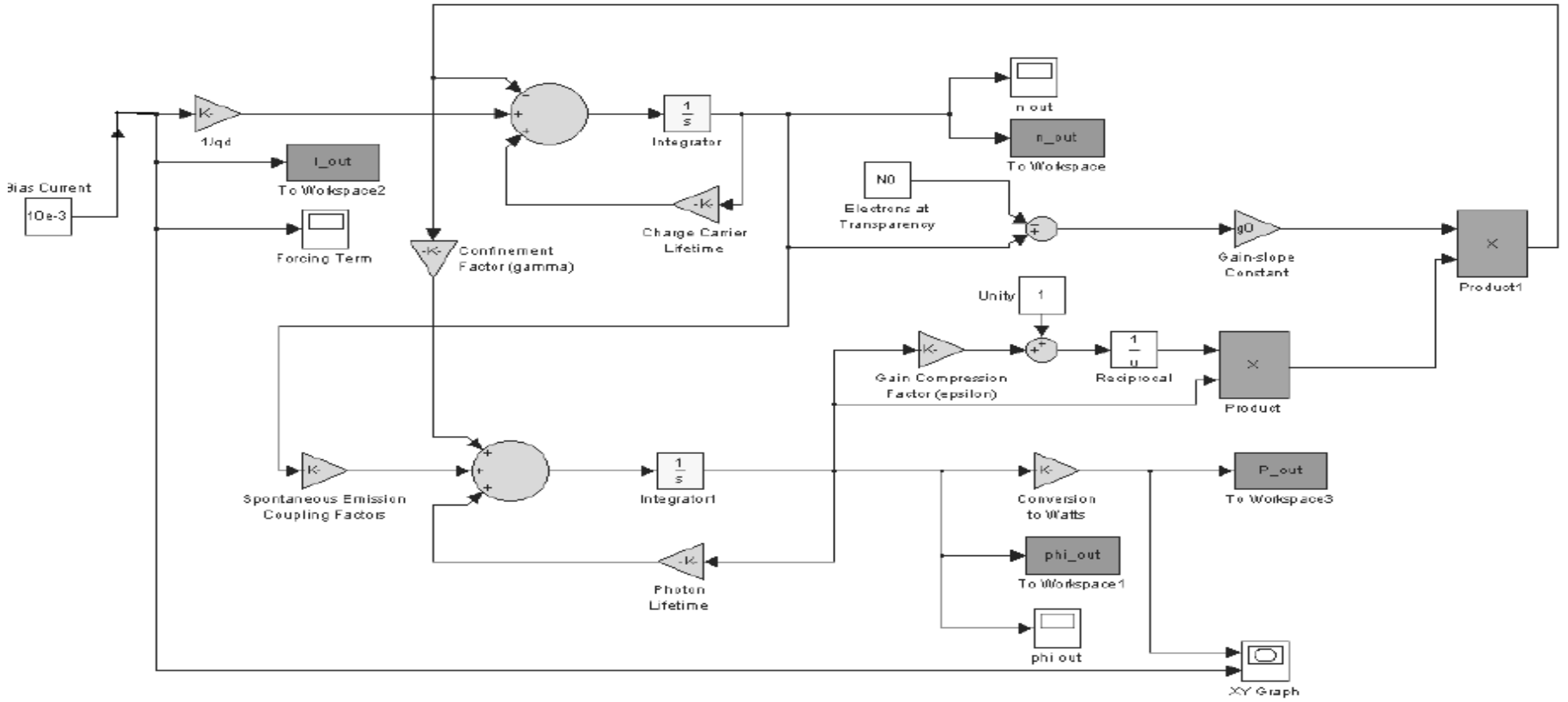

Figure A.1 Complete Laser Simulink model

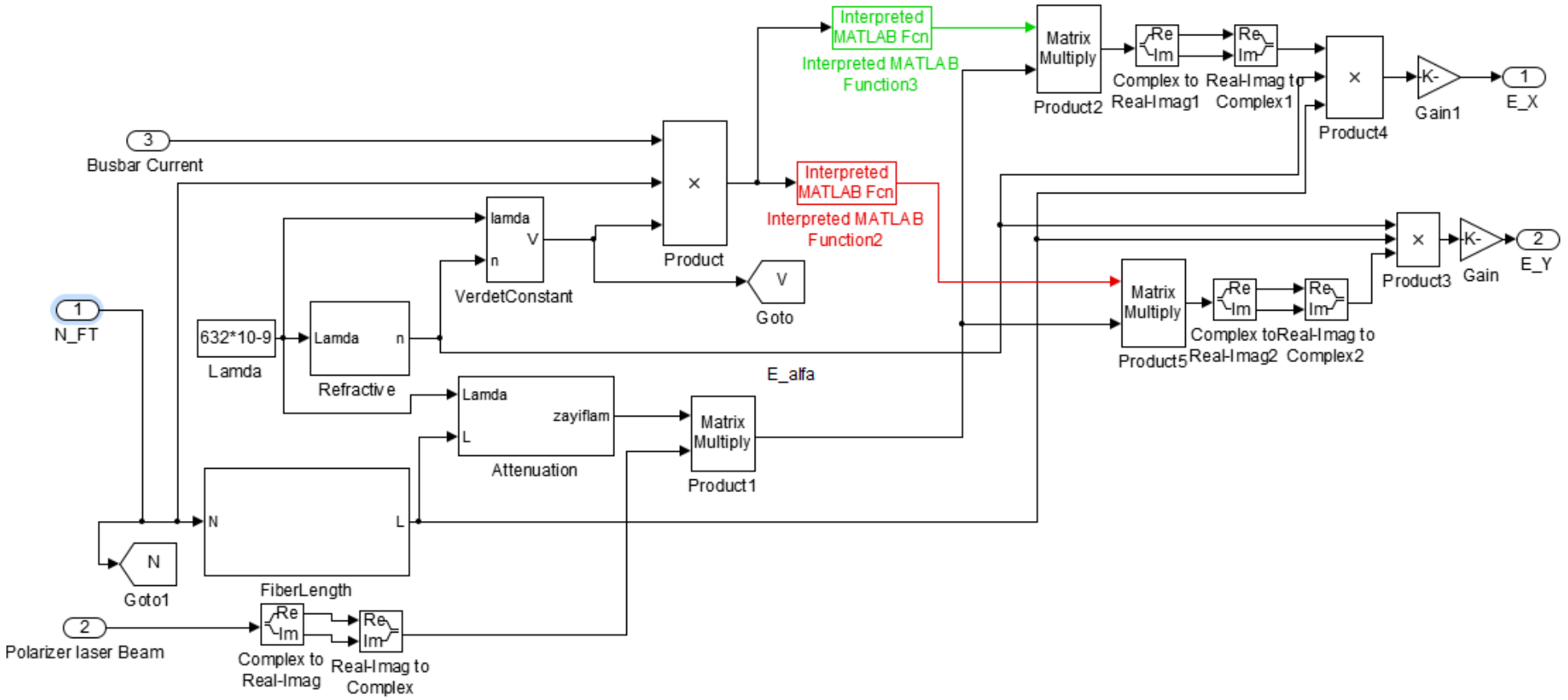

Figure A.2 Optical Fiber Current Transformer Simulink model

A.3 Overcurrent numerical relay simulink model

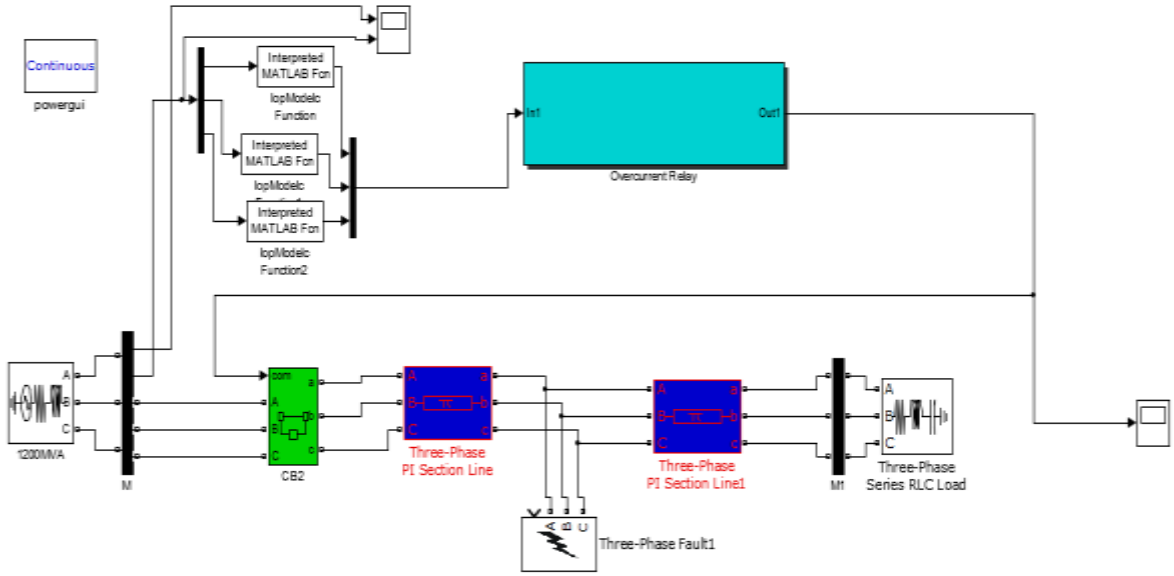

Figure A.2 Test Case Model developed in SimPowerSystems

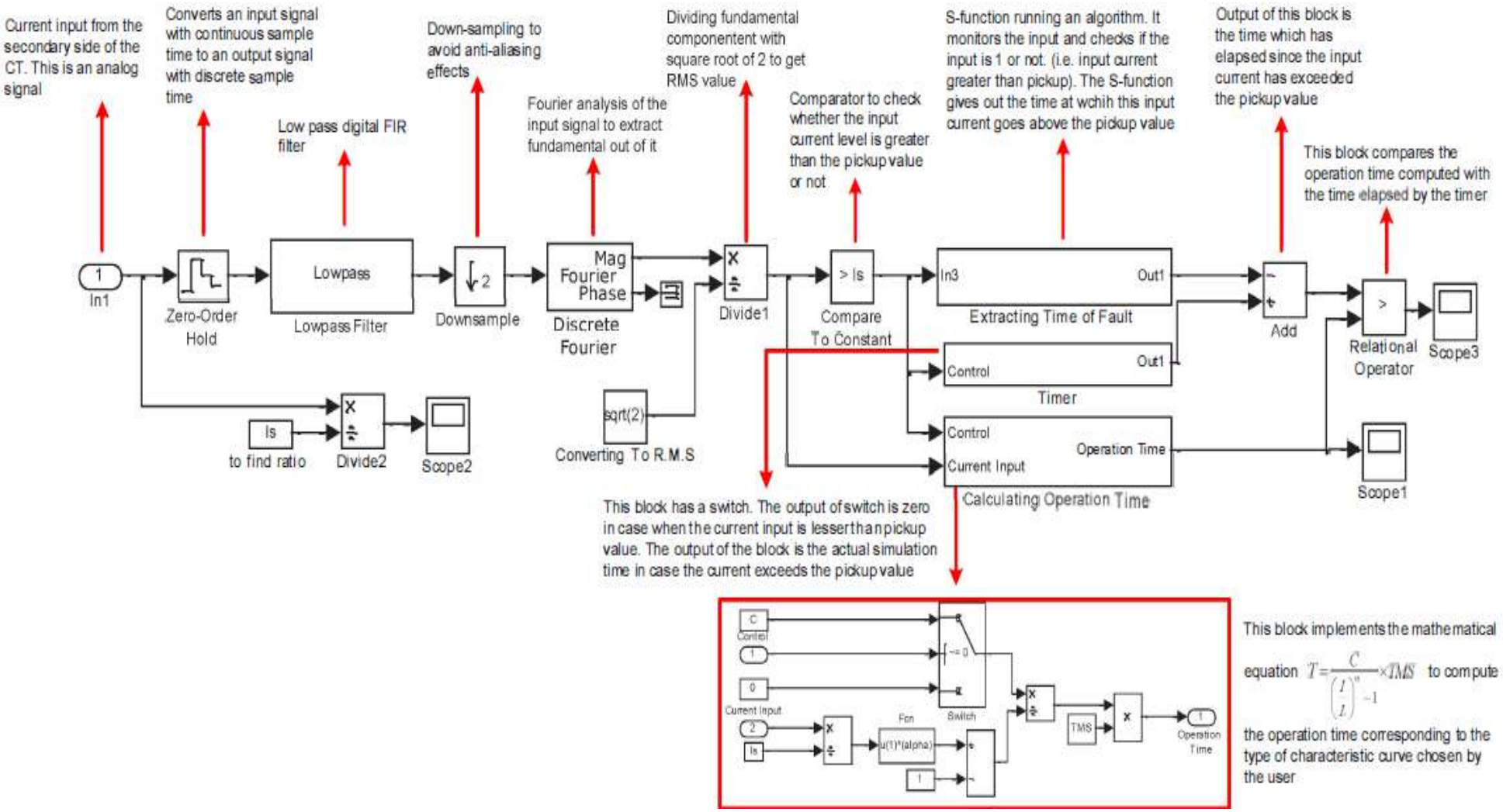

Figure A.2 Detailed Model of Overcurrent Relay Implemented in MATLAB/Simulink

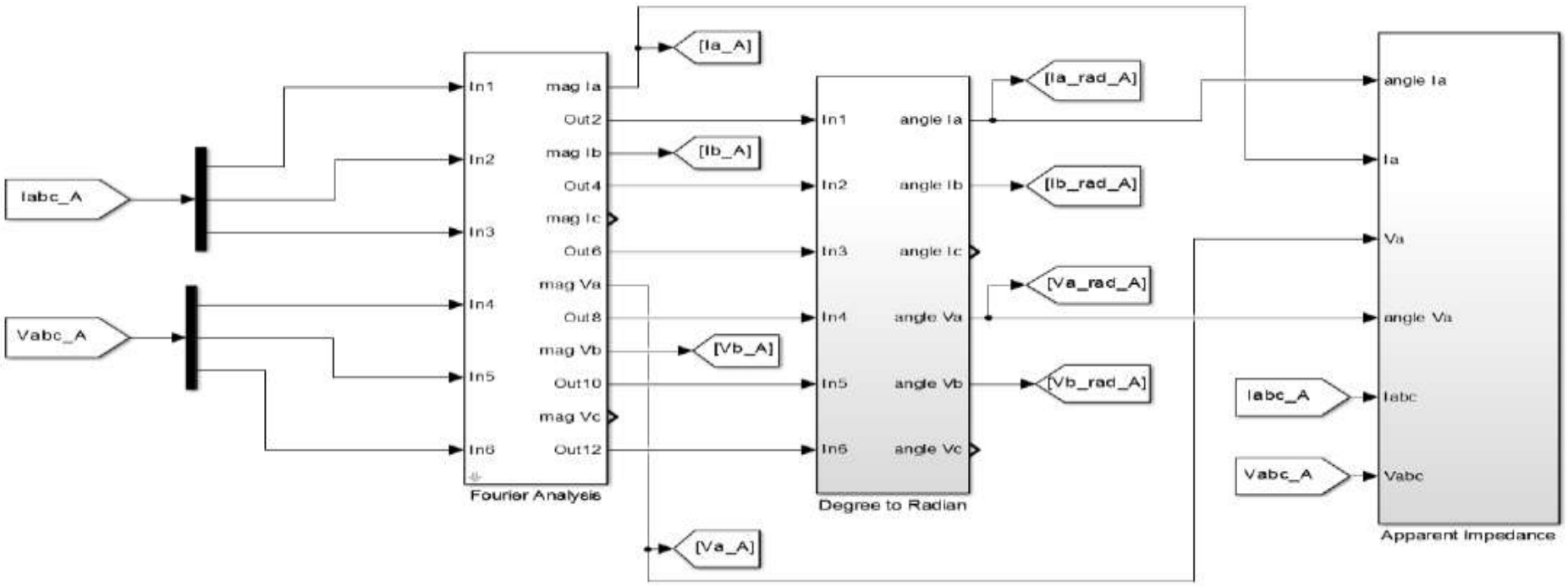

Figure A.3 Detailed Model of Distance Relay Implemented in MATLAB/Simulink

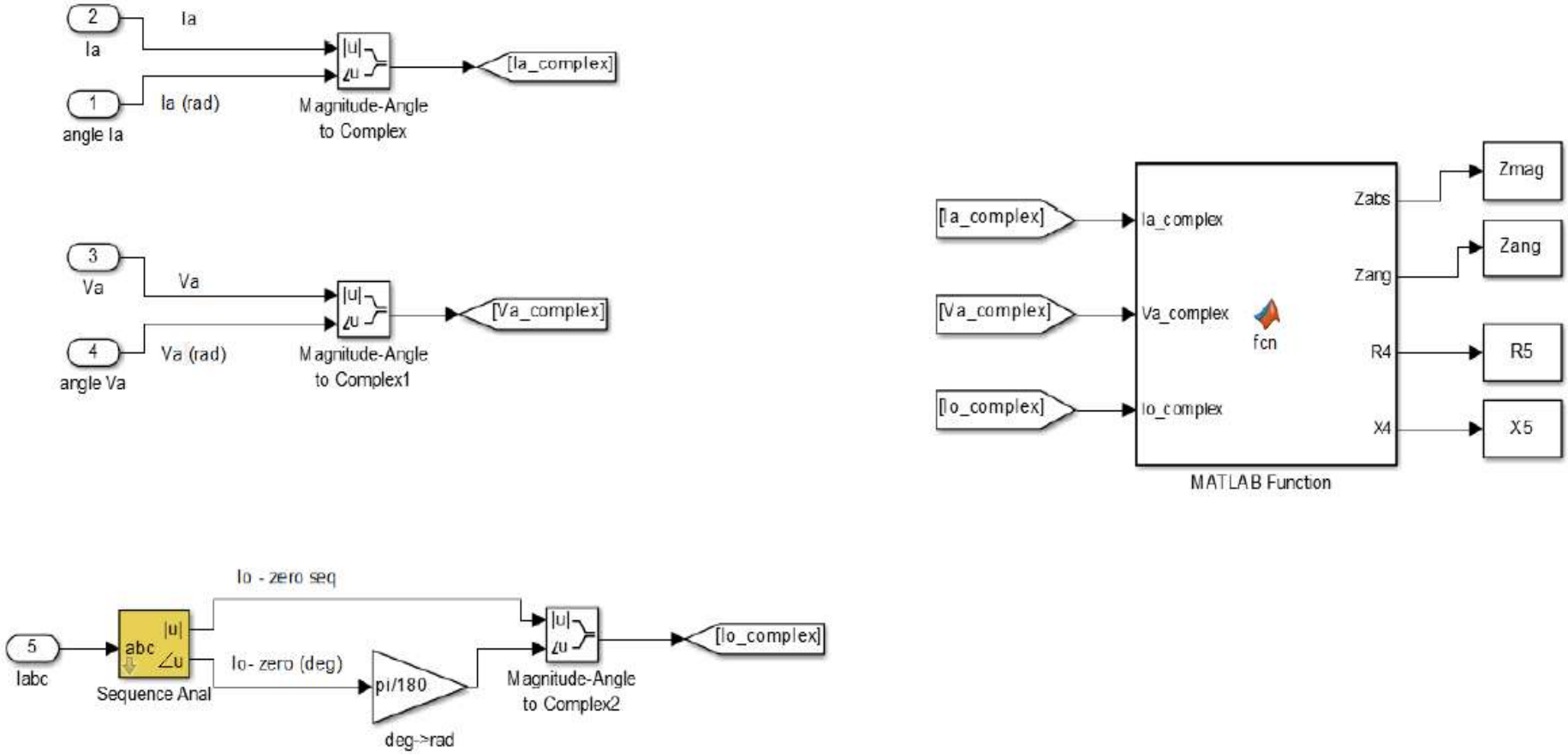

Figure A.4 Impedance Calculation for phase-A SLGF

APPENDIX B

This appendix presents the MATLAB codes of the matlab functions that used to simulate OFCT ,OVT and numerical relay fault detection algorithm**.**

B.1 OFCT using FRM MATLAB Code

```
function P = OFCTmodel(I)
% codegen
% Jones vector
Ex=[1 0]'; % x polarized light
Ey=[0 1]'; % y polarized light
%Faraday rotation angle
V=4.68*10^-6; % Verdet constant of fiber optic cable [rad/A]
N=2; % number of fiber optic cable turns around conductor
Theta=1/2*4*V*N*I; % rotation angle
%Jones matrices
Mq_f=1/sqrt(2)*[1 -1i;-1i 1]*exp(1i*pi/2); % Forward quarter wave plate
Mcoil_f=[cos(Theta) -sin(Theta...ؚ(
sin(Theta) cos(Theta)]; % Forward Faraday rotator
Mm=[-1 0; 0 1]; % Mirror
Mcoil_b=[cos(Theta) sin(Theta...ؚ)
-sin(Theta) cos(Theta)]; % Back Faraday rotator
Mq_b=1/sqrt(2)*[1 1i;1i 1]*exp(1i*pi/2); % Back quarter wave plate
Mp_y=[0 1]; % Linear polarizer, y
Mp_x=[1 0];% Linear polarizer, y
%Final states of lights
Eyy=Mp_y*Mq_b*Mcoil_b*Mm*Mcoil_f*Mq_f*Ex; % Final state of x polarized light
Exx=Mp_x*Mq_b*Mcoil_b*Mm*Mcoil_f*Mq_f*Ey; % Final state of y polarized light
P1=angle(Eyy)-angle(Exx); %angle between the two final states of the lights
P=(I/P1)*1/0.3183; %Normalization (0.4183 is the maximum of P1)
end
```

B.2 OVT MATLAB Code

The following Matlab M-files where used to study the application of evolution algorithms for optical voltage transformer.

```
function P = opModelvt_E(V)
%Jones vector of circular polarized light
Ec=1/sqrt(2)*[1;i];
%Volategs accross the crystals based on their locations
V1=V*1.232/1.525;
V2=V*0.748/1.525;
V3=V*0.206/1.525;
%rotation in Poeckels cell
alpha1=1/(240)*pi*V1*10^-4;
alpha2=1/(240)*pi*V2*10^-4;
alpha3=1/(240)*pi*V3*10^-4;
%Jones matrices of Pockels cells
Mpockel1=[cos(alpha1/2) i*sin(alpha1/2);...
i*sin(alpha1/2) cos(alpha1/2)];
Mpockel2=[cos(alpha2/2) i*sin(alpha2/2);...
i*sin(alpha2/2) cos(alpha2/2)];
```

```
Mpockel3=[cos(alpha3/2) i*sin(alpha3/2);...
i*sin(alpha3/2) cos(alpha3/2)];
%Final states of three lights
E1=Mpockel1*Ec;
E2=Mpockel2*Ec;
E3=Mpockel3*Ec;
%Intensities of each light
E1oxH=transpose(conj(E1(1,:)));
E1oyH=transpose(conj(E1(2,:)));
U1=(E1oxH-E1oyH)/(E1oxH+E1oyH);
E2oxH=transpose(conj(E2(1,:)));
E2oyH=transpose(conj(E2(2,:)));
U2=(E2oxH-E2oyH)/(E2oxH+E2oyH);
E3oxH=transpose(conj(E3(1,:)));
E3oyH=transpose(conj(E3(2,:)));
U3=(E3oxH-E3oyH)/(E3oxH+E3oyH);
%Final intensity
P1=-(U1+U2+U3);
%Normalization
P=P1/(1.8756*10^-6); %1.8756*10^-6 is the maximum of P1
end
```

B.3 impedance calculation

```
function [Zabs,Zang,R5,X5] = fcn(Ia_complex,Va_complex,Io_complex)
freq=50; %Hz
length=300; %km
Roo=0.1055*length; %zero-sequence resistance
R11=0.038806*length; %pos-sequence resistance
Loo=(0.7389/377)*length; %zero-sequence inductance
L11=(0.377416/377)*length; %pos-sequence inductance
Z00=Roo+1i*2*pi*freq*Loo; %zero-sequence impedance
Z11=R11+1i*2*pi*freq*L11; %pos-sequence impedance
m=(Z00-Z11)/Z11; %fixed zero-sequence comp. factor "m"
%Apparent impedance with fixed zero-sequence compensation factor "m"
Ztotal=(Va_complex)/(Ia_complex+m*Io_complex);
Zabs=abs(Ztotal);
Zang=angle(Ztotal)*180/pi;
R5=real(Ztotal);
X5=imag(Ztotal);
```

B.4 Mho Relay Apparent Impedance Plots

```
function Plot_ApparentImpedance(R6,X6)
theta = 0:.01:(2*pi);
p=0;
q=-100:0.6:550;
r=-300:0.3:300;
s=0;
%-------------------- Transmission Line Impedance ----------------
line_length = 300;
R1 = 0.038806;
X1 = 0.377416; %Xl1=2*pi*f*L
Xc = 1.15922e-8*377; %Xc1=2*pi*f*C
%-----------Distributed Parameters Compensation--------------------
```

```
Zt = R1+1i*X1; %line impedance
Yt = 1i*Xc; %admittance
zc = sqrt(Zt/Yt); %characteristic impedance
gam = sqrt(Zt*Yt); %propagation constant
Lset = 300; %relay reach
%-----------------------------------------------------------------
Zset1 = zc*tanh(gam*Lset*0.8); %protection zone 1 80% reach
Zset2 = zc*tanh(gam*Lset*1.2); %protection zone 2 120% reach
%-----------------------------------------------------------------
%Zone 1
Req1=real(Zset1);
Xeq1=imag(Zset1);
Zangle1=atan(Xeq1/Req1);
%Zone 2
Req2=real(Zset2);
Xeq2=imag(Zset2);
Zangle2=atan(Xeq2/Req2);
% radius of zone 1 circle
R_zone1 = sqrt((Req1)^2+(Xeq1)^2)/2;
%center of zone 1 circle (a,b)
a=R_zone1*(cos(Zangle1));
b=R_zone1*(sin(Zangle1));
%circle of radius Zone 1 centred at (a,b)
c = R_zone1*cos(theta)+a;
d = R_zone1*sin(theta)+b;
% radius of Zone 2 circle
R_zone2 = sqrt((Req2)^2+(Xeq2)^2)/2;
%center of zone 2 circle (f,e)
f=R_zone2*(cos(Zangle2));
e=R_zone2*(sin(Zangle2));
%circle of radius zone 2 centred at (f,e)
g = R_zone2*cos(theta)+f;
h = R_zone2*sin(theta)+e;
%impedance line
t=0:0.1:250;
u=t*(b/a);
plot1 = figure('position',[455 200 350 300]);
set(gca,'fontsize',13)
plot2=plot(t,u,'b',c,d,'g',g,h,'m','LineWidth',2);
hold on
plot3=plot(p,q,'k--',r,s,'k--','LineWidth',0.4);
plot4=plot(R6,X6,'r+');
ymax=1.11*max(h);
ymin=-22;
xmax=1.15*max(g);
xmin=1.34*min(g);
axis([xmin xmax ymin ymax]);
xlabel('Resistance (R)');
ylabel('Reactance (X)');
hold off
grid off
end
```

Appendix C

This appendix presents the C codes of for PIC based OFCT signal processing and PIC based overcurrent relay fault detection algorithm**.**

C.1 C code for Signal Processing of OFCT

```
_main:
;measurement .c,25 ::           void main() {
;measurement .c,26 ::           ANSEL  = 0x06;              //
Configure AN2 pin as analog
      MOVLW      6
      MOVWF      ANSEL+0
;measurement .c,27 ::           ANSELH = 0;                 //
Configure other AN pins as digital I/O
      CLRF       ANSELH+0
;measurement .c,28 ::           C1ON_bit = 0;               //
Disable comparators
      BCF        C1ON_bit+0, 7
;measurement .c,29 ::           C2ON_bit = 0;
      BCF        C2ON_bit+0, 7
;measurement .c,31 ::           TRISA  = 0xFF;              //
PORTA is input
      MOVLW      255
      MOVWF      TRISA+0
;measurement .c,32 ::           TRISC  = 0;                 //
PORTC is output
      CLRF       TRISC+0
;measurement .c,33 ::           TRISB  = 0;                 //
PORTB is output
      CLRF       TRISB+0
;measurement .c,35 ::           Lcd_Init();
// Initialize LCD
      CALL       _Lcd_Init+0
;measurement .c,37 ::           Lcd_Cmd(_LCD_CLEAR);
// Clear display
      MOVLW      1
      MOVWF      FARG_Lcd_Cmd_out_char+0
      CALL       _Lcd_Cmd+0
;measurement .c,38 ::           Lcd_Cmd(_LCD_CURSOR_OFF);
// Cursor off
      MOVLW      12
      MOVWF      FARG_Lcd_Cmd_out_char+0
      CALL       _Lcd_Cmd+0
;measurement .c,43 ::           do {
L_main0:
;measurement .c,44 ::           result = ADC_Read(1);   // Get
10-bit results of AD conversion
      MOVLW      1
      MOVWF      FARG_ADC_Read_channel+0
      CALL       _ADC_Read+0
      MOVF       R0+0, 0
      MOVWF      _result+0
      MOVF       R0+1, 0
      MOVWF      _result+1
;measurement .c,45 ::           volt=result*4.88;
```

```
      CALL        _Word2Double+0
      MOVLW       246
      MOVWF       R4+0
      MOVLW       40
      MOVWF       R4+1
      MOVLW       28
      MOVWF       R4+2
      MOVLW       129
      MOVWF       R4+3
      CALL        _Mul_32x32_FP+0
      CALL        _Double2Int+0
      MOVF        R0+0, 0
      MOVWF       _volt+0
      MOVF        R0+1, 0
      MOVWF       _volt+1
;measurement .c,46 ::            temp=volt/10;
      MOVLW       10
      MOVWF       R4+0
      MOVLW       0
      MOVWF       R4+1
      CALL        _Div_16x16_S+0
      MOVF        R0+0, 0
      MOVWF       _temp+0
      MOVF        R0+1, 0
      MOVWF       _temp+1
;measurement .c,48 ::            inttostr(temp,display);
      MOVF        R0+0, 0
      MOVWF       FARG_IntToStr_input+0
      MOVF        R0+1, 0
      MOVWF       FARG_IntToStr_input+1
      MOVLW       _display+0
      MOVWF       FARG_IntToStr_output+0
      CALL        _IntToStr+0
;measurement .c,49 ::            lcd_out(1,1,display);
      MOVLW       1
      MOVWF       FARG_Lcd_Out_row+0
      MOVLW       1
      MOVWF       FARG_Lcd_Out_column+0
      MOVLW       _display+0
      MOVWF       FARG_Lcd_Out_text+0
      CALL        _Lcd_Out+0
;measurement .c,51 ::            result2 = ADC_Read(2);   // Get
10-bit results of AD conversion
      MOVLW       2
      MOVWF       FARG_ADC_Read_channel+0
      CALL        _ADC_Read+0
      MOVF        R0+0, 0
      MOVWF       _result2+0
      MOVF        R0+1, 0
      MOVWF       _result2+1
;measurement .c,52 ::            volt2=result2*4.88;
      CALL        _Word2Double+0
      MOVLW       246
      MOVWF       R4+0
      MOVLW       40
      MOVWF       R4+1
      MOVLW       28
      MOVWF       R4+2
```

```
      MOVLW      129
      MOVWF      R4+3
      CALL       _Mul_32x32_FP+0
      CALL       _Double2Int+0
      MOVF       R0+0, 0
      MOVWF      _volt2+0
      MOVF       R0+1, 0
      MOVWF      _volt2+1
;measurement .c,53 ::            temp2=volt2/10;
      MOVLW      10
      MOVWF      R4+0
      MOVLW      0
      MOVWF      R4+1
      CALL       _Div_16x16_S+0
      MOVF       R0+0, 0
      MOVWF      _temp2+0
      MOVF       R0+1, 0
      MOVWF      _temp2+1
;measurement .c,55 ::            inttostr(temp2,display2);
      MOVF       R0+0, 0
      MOVWF      FARG_IntToStr_input+0
      MOVF       R0+1, 0
      MOVWF      FARG_IntToStr_input+1
      MOVLW      _display2+0
      MOVWF      FARG_IntToStr_output+0
      CALL       _IntToStr+0
;measurement .c,56 ::            lcd_out(2,1,display2);
      MOVLW      2
      MOVWF      FARG_Lcd_Out_row+0
      MOVLW      1
      MOVWF      FARG_Lcd_Out_column+0
      MOVLW      _display2+0
      MOVWF      FARG_Lcd_Out_text+0
      CALL       _Lcd_Out+0
;measurement .c,57 ::            } while(1);
      GOTO       L_main0
;measurement .c,58 ::            }
L_end_main:
      GOTO       $+0
; end of _main
```

C.2 C code for Overcurrent Protection

```
_main:
;relay.c,31 ::        void main() {
;relay.c,32 ::        ANSEL  = 0x06;              // Configure AN2
pin as analog
      MOVLW      6
      MOVWF      ANSEL+0
;relay.c,33 ::        ANSELH = 0;                 // Configure
other AN pins as digital I/O
      CLRF       ANSELH+0
;relay.c,34 ::        C1ON_bit = 0;               // Disable
comparators
      BCF        C1ON_bit+0, BitPos(C1ON_bit+0)
;relay.c,35 ::        C2ON_bit = 0;
      BCF        C2ON_bit+0, BitPos(C2ON_bit+0)
```

```
;relay.c,37 ::         TRISA  = 0xFF;              // PORTA is
input
      MOVLW      255
      MOVWF      TRISA+0
;relay.c,38 ::         TRISC  = 0;                 // PORTC is
output
      CLRF       TRISC+0
;relay.c,39 ::         TRISB  = 0;                 // PORTB is
output
      CLRF       TRISB+0
;relay.c,40 ::         portb = 0;
      CLRF       PORTB+0
;relay.c,43 ::         Lcd_Init();                      //
Initialize LCD
      CALL       _Lcd_Init+0
;relay.c,45 ::         Lcd_Cmd(_LCD_CLEAR);             // Clear
display
      MOVLW      1
      MOVWF      FARG_Lcd_Cmd_out_char+0
      CALL       _Lcd_Cmd+0
;relay.c,46 ::         Lcd_Cmd(_LCD_CURSOR_OFF);           // Cursor
off
      MOVLW      12
      MOVWF      FARG_Lcd_Cmd_out_char+0
      CALL       _Lcd_Cmd+0
;relay.c,51 ::         do {
L_main0:
;relay.c,52 ::         result = ADC_Read(1);   // Get 10-bit
results of AD conversion
      MOVLW      1
      MOVWF      FARG_ADC_Read_channel+0
      CALL       _ADC_Read+0
      MOVF       R0+0, 0
      MOVWF      _result+0
      MOVF       R0+1, 0
      MOVWF      _result+1
;relay.c,53 ::         volt=result*4.88;
      CALL       _word2double+0
      MOVLW      246
      MOVWF      R4+0
      MOVLW      40
      MOVWF      R4+1
      MOVLW      28
      MOVWF      R4+2
      MOVLW      129
      MOVWF      R4+3
      CALL       _Mul_32x32_FP+0
      CALL       _double2int+0
      MOVF       R0+0, 0
      MOVWF      _volt+0
      MOVF       R0+1, 0
      MOVWF      _volt+1
;relay.c,54 ::         temp=volt/10;
      MOVLW      10
      MOVWF      R4+0
      MOVLW      0
      MOVWF      R4+1
      CALL       _Div_16x16_S+0
```

```
      MOVF       R0+0, 0
      MOVWF      _temp+0
      MOVF       R0+1, 0
      MOVWF      _temp+1
;relay.c,56 ::         inttostr(temp,display);
      MOVF       R0+0, 0
      MOVWF      FARG_IntToStr_input+0
      MOVF       R0+1, 0
      MOVWF      FARG_IntToStr_input+1
      MOVLW      _display+0
      MOVWF      FARG_IntToStr_output+0
      CALL       _IntToStr+0
;relay.c,57 ::         lcd_out(1,1,display);
      MOVLW      1
      MOVWF      FARG_Lcd_Out_row+0
      MOVLW      1
      MOVWF      FARG_Lcd_Out_column+0
      MOVLW      _display+0
      MOVWF      FARG_Lcd_Out_text+0
      CALL       _Lcd_Out+0
;relay.c,59 ::         result2 = ADC_Read(2);   // Get 10-bit
results of AD conversion
      MOVLW      2
      MOVWF      FARG_ADC_Read_channel+0
      CALL       _ADC_Read+0
      MOVF       R0+0, 0
      MOVWF      _result2+0
      MOVF       R0+1, 0
      MOVWF      _result2+1
;relay.c,60 ::         volt2=result2*4.88;
      CALL       _word2double+0
      MOVLW      246
      MOVWF      R4+0
      MOVLW      40
      MOVWF      R4+1
      MOVLW      28
      MOVWF      R4+2
      MOVLW      129
      MOVWF      R4+3
      CALL       _Mul_32x32_FP+0
      CALL       _double2int+0
      MOVF       R0+0, 0
      MOVWF      _volt2+0
      MOVF       R0+1, 0
      MOVWF      _volt2+1
;relay.c,61 ::         temp2= volt2/10;
      MOVLW      10
      MOVWF      R4+0
      MOVLW      0
      MOVWF      R4+1
      CALL       _Div_16x16_S+0
      MOVF       R0+0, 0
      MOVWF      _temp2+0
      MOVF       R0+1, 0
      MOVWF      _temp2+1
;relay.c,62 ::         inttostr(temp2,display2);
      MOVF       R0+0, 0
      MOVWF      FARG_IntToStr_input+0
```

```
      MOVF        R0+1, 0
      MOVWF       FARG_IntToStr_input+1
      MOVLW       _display2+0
      MOVWF       FARG_IntToStr_output+0
      CALL        _IntToStr+0
;relay.c,63 ::         lcd_out(1,9,display2);
      MOVLW       1
      MOVWF       FARG_Lcd_Out_row+0
      MOVLW       9
      MOVWF       FARG_Lcd_Out_column+0
      MOVLW       _display2+0
      MOVWF       FARG_Lcd_Out_text+0
      CALL        _Lcd_Out+0
;relay.c,65 ::         x = (temp - temp2);
      MOVF        _temp2+0, 0
      SUBWF       _temp+0, 0
      MOVWF       R0+0
      MOVF        _temp2+1, 0
      BTFSS       STATUS+0, 0
      ADDLW       1
      SUBWF       _temp+1, 0
      MOVWF       R0+1
      CALL        _int2double+0
      MOVF        R0+0, 0
      MOVWF       FLOC__main+0
      MOVF        R0+1, 0
      MOVWF       FLOC__main+1
      MOVF        R0+2, 0
      MOVWF       FLOC__main+2
      MOVF        R0+3, 0
      MOVWF       FLOC__main+3
      MOVF        FLOC__main+0, 0
      MOVWF       _x+0
      MOVF        FLOC__main+1, 0
      MOVWF       _x+1
      MOVF        FLOC__main+2, 0
      MOVWF       _x+2
      MOVF        FLOC__main+3, 0
      MOVWF       _x+3
;relay.c,66 ::         y = (temp + temp2);
      MOVF        _temp2+0, 0
      ADDWF       _temp+0, 0
      MOVWF       R0+0
      MOVF        _temp+1, 0
      BTFSC       STATUS+0, 0
      ADDLW       1
      ADDWF       _temp2+1, 0
      MOVWF       R0+1
      CALL        _int2double+0
      MOVF        R0+0, 0
      MOVWF       _y+0
      MOVF        R0+1, 0
      MOVWF       _y+1
      MOVF        R0+2, 0
      MOVWF       _y+2
      MOVF        R0+3, 0
      MOVWF       _y+3
;relay.c,67 ::         u = 0.5*asin (x / y);
```

```
        MOVF        R0+0, 0
        MOVWF       R4+0
        MOVF        R0+1, 0
        MOVWF       R4+1
        MOVF        R0+2, 0
        MOVWF       R4+2
        MOVF        R0+3, 0
        MOVWF       R4+3
        MOVF        FLOC__main+0, 0
        MOVWF       R0+0
        MOVF        FLOC__main+1, 0
        MOVWF       R0+1
        MOVF        FLOC__main+2, 0
        MOVWF       R0+2
        MOVF        FLOC__main+3, 0
        MOVWF       R0+3
        CALL        _Div_32x32_FP+0
        MOVF        R0+0, 0
        MOVWF       FARG_asin_x+0
        MOVF        R0+1, 0
        MOVWF       FARG_asin_x+1
        MOVF        R0+2, 0
        MOVWF       FARG_asin_x+2
        MOVF        R0+3, 0
        MOVWF       FARG_asin_x+3
        CALL        _asin+0
        MOVLW       0
        MOVWF       R4+0
        MOVLW       0
        MOVWF       R4+1
        MOVLW       0
        MOVWF       R4+2
        MOVLW       126
        MOVWF       R4+3
        CALL        _Mul_32x32_FP+0
        MOVF        R0+0, 0
        MOVWF       _u+0
        MOVF        R0+1, 0
        MOVWF       _u+1
        MOVF        R0+2, 0
        MOVWF       _u+2
        MOVF        R0+3, 0
        MOVWF       _u+3
;relay.c,68 ::          a = (u/42)     ;
        MOVLW       0
        MOVWF       R4+0
        MOVLW       0
        MOVWF       R4+1
        MOVLW       40
        MOVWF       R4+2
        MOVLW       132
        MOVWF       R4+3
        CALL        _Div_32x32_FP+0
        MOVF        R0+0, 0
        MOVWF       _a+0
        MOVF        R0+1, 0
        MOVWF       _a+1
        MOVF        R0+2, 0
```

```
      MOVWF       _a+2
      MOVF        R0+3, 0
      MOVWF       _a+3
;relay.c,69 ::         floattostr(a,display3);
      MOVF        R0+0, 0
      MOVWF       FARG_FloatToStr_fnum+0
      MOVF        R0+1, 0
      MOVWF       FARG_FloatToStr_fnum+1
      MOVF        R0+2, 0
      MOVWF       FARG_FloatToStr_fnum+2
      MOVF        R0+3, 0
      MOVWF       FARG_FloatToStr_fnum+3
      MOVLW       _display3+0
      MOVWF       FARG_FloatToStr_str+0
      CALL        _FloatToStr+0
;relay.c,70 ::         lcd_out(2,1,display3);
      MOVLW       2
      MOVWF       FARG_Lcd_Out_row+0
      MOVLW       1
      MOVWF       FARG_Lcd_Out_column+0
      MOVLW       _display3+0
      MOVWF       FARG_Lcd_Out_text+0
      CALL        _Lcd_Out+0
;relay.c,72 ::         if(a >= 4){
      MOVLW       0
      MOVWF       R4+0
      MOVLW       0
      MOVWF       R4+1
      MOVLW       0
      MOVWF       R4+2
      MOVLW       129
      MOVWF       R4+3
      MOVF        _a+0, 0
      MOVWF       R0+0
      MOVF        _a+1, 0
      MOVWF       R0+1
      MOVF        _a+2, 0
      MOVWF       R0+2
      MOVF        _a+3, 0
      MOVWF       R0+3
      CALL        _Compare_Double+0
      MOVLW       1
      BTFSS       STATUS+0, 0
      MOVLW       0
      MOVWF       R0+0
      MOVF        R0+0, 0
      BTFSC       STATUS+0, 2
      GOTO        L_main3
;relay.c,73 ::         portb.f4 = 1;
      BSF         PORTB+0, 4 ;relay.c,74 ::       }
      GOTO        L_main4
L_main3: ;relay.c,76 ::          portb.f4 = 0;
      BCF         PORTB+0, 4
L_main4: ;relay.c,79 ::          } while(1);
      GOTO        L_main0 ;relay.c,80 ::          }
L_end_main:
      GOTO        $+0
; end of _main
```

Appendix D

List of Author's Publications

1. Sulieman Eldoud, Yousif HA Rahim, Abdelaziz Y M Abbas, Giddani Kalcon, "Design of Modern Optical Fiber Current Transformer" EUROPEAN ACADEMIC RESEARCH, Vol. 5, Issue 5, August 2018, pp2222-223.
2. Sulieman Eldoud, Yousif HA Rahim, Abdelaziz Y M Abbas, " Performance Evaluation of Optical Fiber Current Transformer based Over-current Protection " FES Journal of Engineering Sciences,vol.14, Issue 6, Oct 2018.